

**Investigating the Effect of Mechanical Loading in
a Total Reversed Shoulder Implant**

**A Thesis Submitted for the
Degree of Doctor of Philosophy
By**

Nesreen Abulkhair

**School of Engineering and Design
Mechanical Engineering
Brunel University**

March 2012

Acknowledgment

This thesis could not have been written without Professor. Ibrahim Esat, who encouraged and challenged me through my academic program, he never accepted less than my best efforts. I thank him for his invaluable inspiration, notable contribution, guidance and support throughout the preparation and execution of this research. Thank you.

I would like also to thank Dr. Mahmoud Chizari, Francis Popham, Mohamad Rahman, Keith Withers and the Biomet, UK team who has supported me and helped me throughout my research to complete and rectify the core of this project. Without you, this thesis would have not been completed.

I would like also to express my gratitude to Prof. Ofer Levy and Mr. Stephen Copeland at Reading Shoulder Unit for their help and assistance in the beginning of this project.

Most especially to my family, friends and my husband, and daughters words alone cannot express what I owe them for their encouragement and whose patient love enabled me to complete this thesis.

And especially to God, who made all things possible.

ABSTRACT

The shoulder joint is a multi-axis synovial ball and socket joint, by having a loose connection it provides a wide degree of freedom; however this means the joint lacks robustness and is prone to damage most commonly from shoulder dislocations. A rotator cuff tear causes major problems in allowing the arm to be lifted beyond a 90° abduction position. It is common that this insufficiency aggravates arthritis problems that may have occurred due the rotator cuff tear problem. The study focuses on investigating, describing and quantifying the implant geometric properties to evaluate the joint contact characteristics and use the outcome in redesign the implant.

The investigation presents results of finite element analysis on a heavy loading condition on a Verso (reverse) shoulder implant which is validated using experimental data on the same prosthesis. The results are validated within a 5% error margin.

A Verso implant is modelled using MIMICS (materialise) and imported into ABAQUS (Simulia, Providence, USA) to analyse the distribution of stress, strain and displacement across the Humerus and Scapula. Details of interaction, boundary conditions, loads and material properties are all obtained from research and applied to the model to portray realistic behaviour.

The resulting stress, strain and displacement from this simulation are indicated to show the magnitude and distribution across the entire bone region. This validates the benefits of a Verso implant compared to conventional and long stemmed reverse shoulder implants, as well as provide a basis from which improved designs can be built upon and allow further accurate methods to be developed in analysing shoulder implants effectively.

Table of Contents

Chapter 1. Introduction and Preliminary information.....	1
1.1 Introduction	1
1.2 Shoulder Anatomy.....	1
1.2.1 Bones	2
1.2.2 Joints of the Shoulder Girdle.....	3
1.2.3 Shoulder joint	5
1.2.4 Muscles, tendons and ligaments	5
1.2.5 Articular cartilage	8
1.3 Kinematics of shoulder.....	9
1.3.1 Movements of the Shoulder Girdle:	9
1.3.2 Movements of the Shoulder Joint:.....	10
1.4 Kinetic of shoulder	12
1.4.1 Shoulder joint forces.....	12
1.4.2 Shoulder joint stabilisers	12
1.5 Prospective problems in shoulder.....	14
1.6 Surgical cure	15
1.7 Research Hypothesis	15
1.8 Purpose and aim of the study.....	16
1.9 Summary.....	17
1.10 Summary of Thesis Chapters:.....	18
Chapter 2. Literature Review of Total Reverse Shoulder Implants	20
2.1 Introduction	20
2.2 Shoulder problems.....	20
2.3 Shoulder Surgical treatment	20
2.3.1 Hemi-arthroplasty.....	20
2.3.2 Total shoulder arthroplasty.....	21
2.3.3 Reverse shoulder arthroplasty	22
2.4 Complications in surgical treatment.....	33
2.4.1 Glenoid Implant Loosening	34
2.4.2 Causes of Loosening- Area of failure.....	35
2.4.3 Causes of Loosening - Interface strength and material strength	37
2.4.4 Causes of Loosening- osteolysis	37
2.4.5 Notching of the inferior scapula	38

2.4.6	Dislocation of prosthesis	39
2.4.7	Dislodgement of the base plat	40
2.4.8	Acromial fractures	40
2.4.9	Humeral side complications	41
2.5	Finite Element Analysis (FEA) of shoulder implants	41
2.6	Conclusion	46
Chapter 3.	Verso Shoulder Implant	48
3.1	Introduction	48
3.2	Reverse Shoulder Arthropathy:	48
3.2.1	Symptoms and Methods of Treatment.....	48
3.2.2	The Diagnosis	51
3.3	Verso Shoulder Implant.....	51
3.4	Verso Implant Complications.....	53
3.5	Range of Motion Comparison:	53
3.6	Summary.....	55
Chapter 4.	Data Collection and Methodology.....	57
4.1	Introduction	57
4.2	Data Collection	57
4.3	Body Planes	58
4.4	Methodology:	59
4.5	Geomagic Software	60
4.6	MIMICS Software:	60
4.6.1	Import CT scan images.....	61
4.6.2	Thresholding.....	63
4.6.3	Region Growing	66
4.6.4	Filling	67
4.6.5	Remeshing	69
4.6.6	Exporting to ABAQUS:	71
4.7	ABAQUS Software:	72
4.7.1	Model creation.....	73
4.8	Experimental analysis.....	73
4.9	Summary.....	75
Chapter 5.	Mechanical Testing, Methods and Results	76
5.1	Introduction:	76

5.2	Mechanical Testing Preparations and Materials:.....	76
5.3	Tensile Testing (Load to Failure Test using Pulling out Test)	79
5.3.1	Test 1&2&3 (0) (Pulling test without screws):	80
5.3.2	Tensile testing Test (1) T4&T5&T6 (+ 1 side screw):	92
5.3.3	Tensile testing Test(2)(GBP + 2 side screws) T7, T8 and T9 :	99
5.4	Cyclic Testing:.....	107
5.4.1	Pulling out T(0) (GBP without screws) after Cyclic Testing	108
5.4.2	Pulling out test T(1) (GBP+ 1side screw) after Cyclic Testing:	110
5.4.3	Cyclic Testing T(2) T16, T17 and T18 (GBP+2 side screws):	112
5.5	Conclusion:.....	118
Chapter 6.	Modelling, Simulation and Results	120
6.1	Introduction	120
6.2	Objective of FEA.....	121
6.3	ABAQUS/CAE Introduction:.....	121
6.3.1	Finite Element Analysis Technique:	122
6.3.2	ABAQUS Dynamic Explicit/Implicit:	123
6.4	Methodology.....	125
6.4.1	Modelling Process:	125
6.4.2	Units System within ABAQUS Software:	143
6.4.3	Final Step - Finite Element Analysis Method	143
6.5	Modelling and Simulation of a Foam Block as a bone:	144
6.5.2	Simplified Foam Block Modelling	147
6.5.3	Results and Discussion for Block Model	148
6.6	Humeral Interaction.....	160
6.6.1	CANCELLOUS BONE.....	160
6.6.2	CORTICAL BONE	164
6.7	Scapula Interaction	168
6.7.1	CANCELLOUS BONE.....	168
6.7.2	CORTICAL BONE	171
6.8	Discussion Summary	174
6.9	Conclusion.....	176
6.9.1	Simulated Foam Block Model.....	176
6.9.2	Humerus Model	178
6.9.3	Scapula Model	179

Chapter 7.	Discussion.....	182
7.1	Introduction	182
7.2	Mechanical tests	182
7.2.1	Visual observation for pull-out test	183
7.2.2	Maximum tolerated load on the interface between GBP and foam block.....	183
7.2.3	Stiffness	184
7.2.4	Cyclic test as a measure of fatigue of the joint.....	185
7.2.5	Pull out test at different loading rate	185
7.3	Finite element analysis	185
7.3.1	Simulated Block Model	186
7.3.2	Humerus Model	186
7.3.3	Scapula Model	187
7.4	Comparison between the Mechanical tests and FEA	188
7.5	Error analysis	189
7.5.1	Random errors	189
7.5.2	Systematic Errors.....	189
7.5.3	Manufacturing errors	190
7.5.4	Measurement errors	190
7.5.5	Reading errors	190
7.5.6	Calculating and definition errors	190
7.6	Summary.....	191
Chapter 8.	Conclusion and Future Work.....	192
8.1	Research Findings:	192
8.2	Future Suggestions:	195
Appendices		
Appendix A.....		203
Appendix B.....		206
Appendix C.....		214
Appendix D.....		215

Table of Figures

Figure 1-1: Shoulder Anatomy – right front view and left back view.	2
Figure 1-2: Anterior and posterior view of the scapula.....	3
Figure 1-3: Sternoclavicular articulation - Anterior view	4
Figure 1-4: The left shoulder and acromioclavicular joints, and the proper ligaments of the scapula	4
Figure 1-5: Shoulder joint	5
Figure 1-6: Glenohumeral Ligaments.....	6
Figure 1-7: Shoulder muscles and tendons (short muscles)	7
Figure 1-8: Shoulder muscles and tendons (rotator cuff muscles)	7
Figure 1-9: Lateral CT of transverse section of glenoid and cartilage tissue (top) and schematic of the glenoid cross-section (bottom) demonstrating the conforming cartilage structures.	8
Figure 1-10: Shoulder Range of Motion.....	11
Figure 1-11: Resultant forces of neutral (N), external rotation (X) and internal rotation (I) vectors.....	12
Figure 1-12: Subluxation and dislocation definitions where arrows denote resultant joint force.	13
Figure 1-13: Glenoid depth and perpendicular compressive force (F_y) are both proportional to the transverse force (F_x).	13
Figure 2-1: a) In the shoulder of patients with no rotator-cuff tendons. b) In the reverse prosthesis, the deltoid muscle lever arm is restored.	21
Figure 2-2: Left: A 70-year-old woman who underwent a left total shoulder arthroplasty. Right: A 79-year-old woman who underwent hemi-arthroplasty of the left.	22
Figure 2-3: Left: Neer’s Mark I design with larger spherical component. Right: Neer’s Mark III system incorporated axial rotation of the prosthetic stem.	24
Figure 2-4: Left: The Reverse Total Shoulder System, Right: Components of the shoulder prosthesis	25
Figure 2-5: Left: The prosthesis designed by John M. Fenlin, Jr. Right : Liverpool shoulder. ..	27
Figure 2-6: Left: The Bickel shoulder prosthesis. Right :The Stanmore total shoulder prosthesis	28
Figure 2-7: Left: The first model of the Grammont reverse prosthesis. Right: Current design of the Grammont reverse prosthesis. The Delta III prosthesis.....	30
Figure 2-8: left: Universelle Arrow System, right: Inbuilt medial notch on humeral cup	32
Figure 2-9: Before implantation (left) & retrieved threaded implant (right) showing partially intact cement at the pegs.....	36

Figure 2-10: Revision surgery showing cement intact with the glenoid bone (left) & retrieved glenoid showing failure occurring at the implant/cement interface (right).....	36
Figure 2-11: Nerot classification of progressive scapular notching. a Grade 0: no notch, b grade 1: small notch, c grade 2: notch with condensation (stable), d grade 3: evolutive notch (erosion of inferior screw), e grade 4: first glenoid loosening	39
Figure 2-12: left: An 82-year-old woman who underwent reverse shoulder arthroplasty (Tornier System). Right-a: Anteroposterior radiograph of the right shoulder. Right-b: Axillary radiograph in the same patient showing the dislocated prosthesis (Tornier System).....	40
Figure 2-13: Left: Anteroposterior radiograph of the right shoulder. Right: A 65-year-old man who underwent reverse shoulder prosthesis placement (Tornier System) due to rotator-cuff arthropathy.....	40
Figure 2-14: A: Postoperative radiograph of a keeled glenoid component (grade 0 lucency). B: Twelve-month follow-up radiograph of the same keeled component demonstrating grade 3 lucency. C, D: Postoperative radiograph of a pegged glenoid component (grade 0 lucency).....	42
Figure 2-15: Finite element models of the (A) the Reverse Shoulder Prosthesis (32-mm neutral) and (B) the Delta III.....	45
Figure 2-16: FE models of the reversed-anatomy glenoid components (with screws) tested in this study: (a) Anatomical (Zimmer); (b) Bayley–Walker(Stanmore); (c) Delta III (Depuy); (d) RSPneutral (Encore); (e) RSP-reduced (Encore); (f) Verso (Biomet)	46
Figure 3-1: Humeral head damaged and degenerative by Arthritis.....	49
Figure 3-2 : Traditional Reverse Shoulder Implant [Delta]. Verso Shoulder Implant by Biomet	49
Figure 3-3 : Traditional reverse shoulder implant.....	50
Figure 3-4: Verso shoulder implant parts	52
Figure 3-5 : X-Ray of Verso Shoulder Implant.....	52
Figure 4-1 : Flowchart for Softwares Methodology	58
Figure 4-2 : Different Body Planes.....	59
Figure 4-3 : Verso Implant parts in .step and .sat files in CAD model	60
Figure 4-4 : Overview of the modules of Mimics	61
Figure 4-5: Axial (top right), sagittal (bottom left) and coronal (top left) views of the pathological Shoulder joint.....	63
Figure 4-6 : The interface in Mimics. Note the icon for the thresholding function. Dialogue box for setting the thresholding	64
Figure 4-7: Segmentation of bones from the soft tissues	65
Figure 4-8: Different colour masks assigned to the Scapula and Humerus.....	65

Figure 4-9 : Interface in Mimics; note the icon for region growing function.	66
Figure 4-10: Removing excess and void density.....	67
Figure 4-11: Interface in Mimics. Note the icon for the multiple slice edit function for filling cavities within the bone.	67
Figure 4-12: Interface for filling. Density masks of both humerus and scapula after filling.	68
Figure 4-13: 3D Model of the Shoulder Joint	68
Figure 4-14 : Side bar for MIMICS after Wrapping and Remeshing 3D.....	69
Figure 4-15 : Remeshed Humerus and Scapula	70
Figure 4-16 : the final look to the remeshed parts Scapula and Humerus.....	71
Figure 4-17 : Export the mesh to ABAQUS	71
Figure 4-18 : Export step to ABAQUS	72
Figure 4-19 : Imported Models into ABAQUS.....	73
Figure 5-1: Glenoid Base Plate pre-testing preparation	77
Figure 5-2: The Implant parts used in the mechanical testing; Glenoid Head, Peripheral Screw and Glenoid Base Plate, respectively from left to right.....	77
Figure 5-3: Foam Block from Saw Bone with 20 pcf, 13cm x 18cm x 4cm.....	79
Figure 5-4: Instron machine 8501 used to apply pulling force on the foam block. (Upgraded to 8800).....	79
Figure 5-5: Drilling 22mm in depth into the foam block	81
Figure 5-6: Conical Shape drill head.....	81
Figure 5-7: Drilling Process of Conical head shape	82
Figure 5-8: Foam Block Preparations.....	82
Figure 5-9: Screwing the Glenoid Base Plate into the foam block using a torque wrench	83
Figure 5-10: Securing the Specimen on the Load cell on Instron 8800 and attaching it to the cylindrical actuator	83
Figure 5-11: Blue Hill2 Software used to measure the load, displacement, strain and stress.....	84
Figure 5-12: Method set up on Blue Hill2 software.....	84
Figure 5-13: Test (0) T1 Pulling out test (tensile) for the GBP without screws	85
Figure 5-14: Test (0) T1 Pulling out test for GBP without screws (debris)	86
Figure 5-15: Test (0) T1 Pulling out test for GBP.....	86
Figure 5-16: Test (0) T1 GBP pulled out from the foam block.....	86
Figure 5-17: Mode of failure for Test (0) T1&T2&T3	87
Figure 5-18: The conical shape threads of the GBP	87
Figure 5-19: Test (0) T1(red)&T2(blue)&T3(purple) (No Peripheral screw) tensile test results	88

Figure 5-20: Average Curve for Test (0) 1&2&3 No screws.....	88
Figure 5-21: Stiffness of the GBP for the Test (0) 1&2&3 No screws	89
Figure 5-22: Strain mm/mm VS Stress MPa for test 1 no screws.....	90
Figure 5-23: Stain mm/mm VS Stress MPa for test 2 no screws	90
Figure 5-24: Strain mm/mm VS Stress MPa for test 3 no screws.....	90
Figure 5-25: preparation of foam block for T(1) +1 screw set of tests	92
Figure 5-26: metal rod attached to the support plate with two long brass screws.....	93
Figure 5-27: Torque wrench used to screw the side screw in 10° angle.....	93
Figure 5-28: the specimen is ready to be tested with GBP and one side screw	94
Figure 5-29: T(1) T4(first repeat) GBP + 1 side screw in tensile testing.....	94
Figure 5-30: T(1) T5(second repeat)GBP +1 side screw tensile testing	94
Figure 5-31: T(1) T6(Third repeat) GBP +1 side screw tensile testing	95
Figure 5-32: Mode of failure in T(1) +1 side screw tensile testing for T4, T5 and T6.....	95
Figure 5-33: Load, displacement figure for the case with one peripheral screw, Test(1) T4(Blue line), T5(Red line) and T6(Green line) +1 screw Load, displacement.....	96
Figure 5-34: Average load and displacement figure for three repeat of Test(1) +1 screw for tests T4,T5 and T6.....	96
Figure 5-35: Stiffness for average results of the Test (1) +1 screw in the limits of allowable micro motion	97
Figure 5-36: Stress and Strain Test (1)+1 screw (T4)	98
Figure 5-37: Stress and Strain Test(1) +1 screw (T5)	98
Figure 5-38: Stress and Strain Test(1) +1 screw (T6)	98
Figure 5-39: redesign the metal rod to give extra strength during testing.....	100
Figure 5-40: Tensile testing T(2) T7 + 2 side screws.....	100
Figure 5-41: Test(2) (GBP+ 2 side screws) T7 cracked foam block.....	101
Figure 5-42: Test (2) (GBP+ 2 side screws) T8 cracked foam block.....	102
Figure 5-43: Test (2) (GBP+ 2 side screws) T9 Fractured foam block.....	102
Figure 5-44: T(2) (GBP+ 2 side screws) T8 complete breakage to the foam block in tensile testing.	102
Figure 5-45: Load and displacement T(2)(GBP+ 2 side screws) T7.....	103
Figure 5-46: Load and displacement T(2)(GBP+ 2 side screws) T8.....	103
Figure 5-47: Load and displacement T(2)(GBP+ 2 side screws) T9.....	103
Figure 5-48: Load, displacement Test(2) (GBP+ 2 side screws) T7(Red line), T8(Green line) and T9(Blue line).....	104

Figure 5-49: Average Load and average Displacement T(2) (GBP+ 2 side screws) T7, T8,T9.	104
Figure 5-50: Stiffness for T(2) (GBP+ 2 side screws) in the allowable limits.....	104
Figure 5-51: Stress and Strain for T(2) (GBP+ 2 side screws) T7	105
Figure 5-52: Stress and Strain for T(2) (GBP+ 2 side screws) T8	106
Figure 5-53: Stress and Strain for T(2)(GBP+ 2 side screws) T9	106
Figure 5-54: Wave matrix software used in the analysis of GBP cyclic testing	107
Figure 5-55: Failure after cyclic and load to failure test in a with no side screw specimen	108
Figure 5-56: Load to failure test at the rate of 20mm/min (GBP +no side screw) following a cyclic loading on a foam block.....	109
Figure 5-57: T(0) (GBP with no screw)Pulling out test, Load-Displacement at rate 5mm/min .	109
Figure 5-58: T(0) (GBP with no screw)Pulling out test, Load-Displacement at 10mm/min	109
Figure 5-59: T(0) (GBP with no screw)Pulling out test, Load-Displacement at 20mm/min	110
Figure 5-60: GBP with +1 side screw after applying 20 mm/min failure loading	111
Figure 5-61: GBP with 1 screw tensile testing at 5mm/min and 10mm/min	111
Figure 5-62: Load-Displacement of GBP with 1 side screw at 5mm/min	112
Figure 5-63: Load-Displacement of GBP with 1 side screw at 10mm/min.	112
Figure 5-64: Load-Displacement of GBP with 1 side screw at 20mm/min	112
Figure 5-65: GBP with 2 side screws tensile testing at 10mm/min and 20mm/min	113
Figure 5-66: GBP with 2 side screws tensile testing at 5mm/min	113
Figure 5-67: Load-Displacement of GBP with 2 side screws at 5mm/min.....	114
Figure 5-68: Load-Displacement of GBP with 2 side screws at 10mm/min.....	114
Figure 5-69: Load-Displacement of GBP with 2 side screws at 20mm/min.....	114
Figure 5-70: Trend of increasing the mean of micro motion in a cyclic loading (Preconditioning) at 10 cycles.	116
Figure 5-71: Trend of increasing the mean of micro motion in a cyclic loading at 500 cycles ..	116
Figure 5-72: Load-Displacement at preconditioning.....	117
Figure 5-73: Load-Displacement at Cyclic Loading	117
Figure 6-1: ABAQUS/CAE (ABAQUS 6.9 user manual 2009)	122
Figure 6-2: Flowchart of Dynamic Explicit Finite Element Method	124
Figure 6-3: a: Full shoulder model, b: Scapula model, c: Humerus model.....	125
Figure 6-4: ABAQUS Model Tree	126
Figure 6-5: Importing Parts into ABAQUS.....	126
Figure 6-6: Geometry repair tool.....	127
Figure 6-7: Results after Geometry repair	127

Figure 6-8: Converting parts into Solid part.....	128
Figure 6-9: Apply Material Properties to the parts.....	128
Figure 6-10: Material Assignment.....	129
Figure 6-11: Assign sections	129
Figure 6-12: Instance and Constraint menu.....	131
Figure 6-13: Merge/Cut Instance Menu	131
Figure 6-14: Parts after merging and cutting.....	132
Figure 6-15: Function cut-extrude to remove extra nodes from parts.....	132
Figure 6-16: Edit the cut extrusion in the required part	133
Figure 6-17: Mesh Controls.....	134
Figure 6-18: Global Seed menu.....	134
Figure 6-19: Resulting Mesh Parts	135
Figure 6-20: Create Step Menu	136
Figure 6-21: Create Interaction Function	136
Figure 6-22: Create interaction property	137
Figure 6-23: Edit Contact Properties	138
Figure 6-24: Exploded view of an FE model of a glenoid implant inserted into a polyurethane block. Loadings are displayed.	138
Figure 6-25: Create Load to apply it on the model	139
Figure 6-26: Apply and edit load on the Implant	139
Figure 6-27: Set the boundary condition to the Model.....	140
Figure 6-28: Apply the BC to the model	140
Figure 6-29: Final Model after Assembly	141
Figure 6-30: Assembled shoulder with meshing	142
Figure 6-31: Create Job step in the Model	142
Figure 6-32: Edit Job step.....	142
Figure 6-33: Foam Block model configurations	147
Figure 6-34: Block Model	148
Figure 6-35: Block Model Von Mises Stress GBP without screws Full Assembly (Average Loading 1130N).....	149
Figure 6-36: Block Model Von Mises Stress GBP without screws Artificial Bone (Average Loading1130N).....	150
Figure 6-37: Block Model Von Mises Stress GBP without screws Glenoid Base (Average Loading1130N).....	151

Figure 6-38: Block Model Von Mises Stress 1 Screws Full Assembly (Average Loading 1469N)	152
Figure 6-39: Block Model Von Mises Stress 1 Screw Artificial Bone (Average Loading 1469N). <i>*This is a mirror image of the same model result; there was no change of screw position</i>	152
Figure 6-40: Block Model Von Mises Stress 1 Screw Glenoid Base (Average Loading 1469N) shows a mirror image of the one screw model.	153
Figure 6-41: Block Model Von Mises Stress 1 Screw Peripheral Screw (Average Loading 1469N)	154
Figure 6-42: Block Model Von Mises Stress 2 Screw Full Assembly (Average Loading 2396N)	154
Figure 6-43: Block Model Von Mises Stress 2 Screw Artificial Bone (Average Loading 2396N)	155
Figure 6-45: Block Model Von Mises Stress 2 Screw Peripheral Screws (Average Loading 2396N)	156
Figure 6-44: Block Model Von Mises Stress 2 Screw Glenoid Base (Average Loading 2396N)	156
Figure 6-46: Block Model Micro-motion No Screws Artificial Bone (Average Loading 1130N)	157
Figure 6-47: Block Model Micro motion 1 Screw Artificial Bone (Average Loading 1469N)	157
Figure 6-48: Block Model Micro-motion 2 Screws Artificial Bone (Average Loading 2396N)	158
Figure 6-49: Block Model Maximum Principal Strain No Screws Artificial Bone (Average Loading 1130N)	159
Figure 6-50: Block Model Maximum Principal Strain 1 Screw Artificial Bone (Average Loading 1469N)	159
Figure 6-51: Block Model Maximum Principal Strain 2 Screws Artificial Bone (Average Loading 2396N)	159
Figure 6-52: Humeral Implant Model Von mises stress full assembly (1070N Magnitude)	160
Figure 6-53: Humeral Implant Model Von mises stress Artificial Bone side view (1070N Magnitude)	161
Figure 6-54: Humeral Implant Model Von mises stress Artificial Bone top view (1070N Magnitude)	162
Figure 6-55: Humeral Implant Model Von mises stress Implant (1070N Magnitude)	162

Figure 6-56: Humeral Implant Model Micro-motion of Artificial Bone (side view, 1070N Magnitude)	163
Figure 6-57: Humeral Implant Model Micro-motion of Artificial Bone (top view, 1070N Magnitude)	163
Figure 6-58: Humeral Implant Model Maximum Principal Strain Artificial Bone (side view, 1070N magnitude)	164
Figure 6-59: Humeral Implant Model Maximum Principal Strain Artificial Bone (top view, 1070N magnitude)	164
Figure 6-60: Humeral Implant Model Von mises stress full assembly (side view, 1070N)	165
Figure 6-61: Humeral Implant Model Von mises stress bone (side view, 1070N Magnitude)	165
Figure 6-62: Humeral Implant Model Von mises stress bone (top view, 1070N Magnitude)	166
Figure 6-63: Humeral Implant Model Von mises stress implant (top view, 1070N Magnitude)	166
Figure 6-64: Humeral Implant Model micro-motion bone (side view, 1070N Magnitude)	167
Figure 6-65: Humeral Implant Model micro-motion bone (top view, 1070N Magnitude)	167
Figure 6-66: Concentrated force on the implant head	168
Figure 6-67: Scapula Implant Model Von Mises stress full assembly (1070N Magnitude)	169
Figure 6-68: Scapula Implant Model Von Mises stress Artificial Bone (1070N Magnitude)	169
Figure 6-69: Implant Model Von Mises stress Glenoid Base (1070N Magnitude)	170
Figure 6-70: Implant Model Von Mises stress Peripheral Screws (1070N Magnitude)	170
Figure 6-71: Scapula Implant Model Micro-motion Artificial Bone (1070N Magnitude)	171
Figure 6-72: Scapula Implant Model Maximum principal strain Artificial Bone (1070N Magnitude)	171
Figure 6-73: Scapula Implant Model Von Mises stress full assembly (1070N Magnitude)	172
Figure 6-74: Scapula Implant Model Von Mises stress Artificial Bone (1070N Magnitude)	172
Figure 6-75: Implant Model Von Mises stress Glenoid Base (1070N Magnitude)	173
Figure 6-76: Implant Model Von Mises stress Peripheral Screws (1070N Magnitude)	173
Figure 6-77: Scapula Implant Model Micro-motion Artificial Bone (1070N Magnitude)	174

List of Tables

Table 3-1: Outcome for patients who had reverse shoulder replacement and Verso shoulder replacement.....	55
Table 4-1 : Properties of the medical image data generated from CT scan	62

Table 5-1: Foam Block Material Properties. Saw Bone website. “Coefficient of Thermal Expansion (CTE) = $6.3 \times 10^{-5} \text{ K}^{-1}$ (from -46 to +93 °C). Water absorption ranges from 0.301 to 0.0 kg/m ² . Material property data parallel to rise of foam using test methods ASTM D-16. (www.sawbone.com).....	78
Table 5-2: summary of the protocols used in cyclic testing for the GBP + 0, 1 and 2 side screws	115
Table 6-1 : Material Properties of each model part (Cortical bone+ implant parts)	130
Table 6-2: Unit Systems within ABAQUS /CAE	143
Table 6-3: Material properties in the FEA (Foam Block (Cancellous) + Cortical bone+ implant parts).....	145
Table 6-4: Average loads for the three set of tests carried out with no screws, with one screw and two screws attached to the GBP (Glenoid Base Plate).....	148
Table 6-5: Summary of the model’s material and conditions of the FEA.....	175
Table 6-6: Summary of applied load and achieved micro motion	176

Chapter 1. Introduction and Preliminary information

The clinical nature of this study has necessitated the use of medical terms and descriptions throughout this text. To assist the reader, a glossary of terms has been included as Appendices A.

1.1 Introduction

Human motion analysis is one of the most pioneering research fields in today's research areas. The results of human motion analysis are used to determine the best course of treatment or rehabilitative therapy that is given to these subjects. The results also facilitate in designing better orthotic and prosthetic devices. This analysis is also used in the field of sports for strength training and athletic purposes.

Human motion mostly takes place through the joints structures. There are various joints in a human body like hip, elbow, knee and shoulder and each of them facilitate parts of a body motion. Consequently, if any of body joints did not operate properly due to injury, this will cause limitation in the body movements and intolerable pain.

The shoulder joint plays a very important role in the mobility of the arm, the most unrestrained part in a body. Also many daily activities hugely dependant on the mobility and dexterity of the arms which means, any problem that occurs with the function of the shoulder can cause great distress, both mentally and physically.

This Chapter will focus on Shoulder Anatomy in brief description to its different parts and joints. The Shoulder Kinematics, movement and explain different range of motion of the normal shoulder joints. Then the problems associated with Shoulder joints and the surgical procedures suggested were briefly mentioned. Research hypothesis and aim of this study were discussed to give an idea to the reader to this research topic. In this study, it is important to understand the previous mentioned points as they could influence the output of the research.

1.2 Shoulder Anatomy

The anatomy of the shoulder girdle consists of several bony joints, or "articulations", which connect the upper limbs to the rest of the skeleton and provide a large range of movement. The

most important aspect of the shoulder is the large range of movement that it permits, which is essential to many activities of daily living.

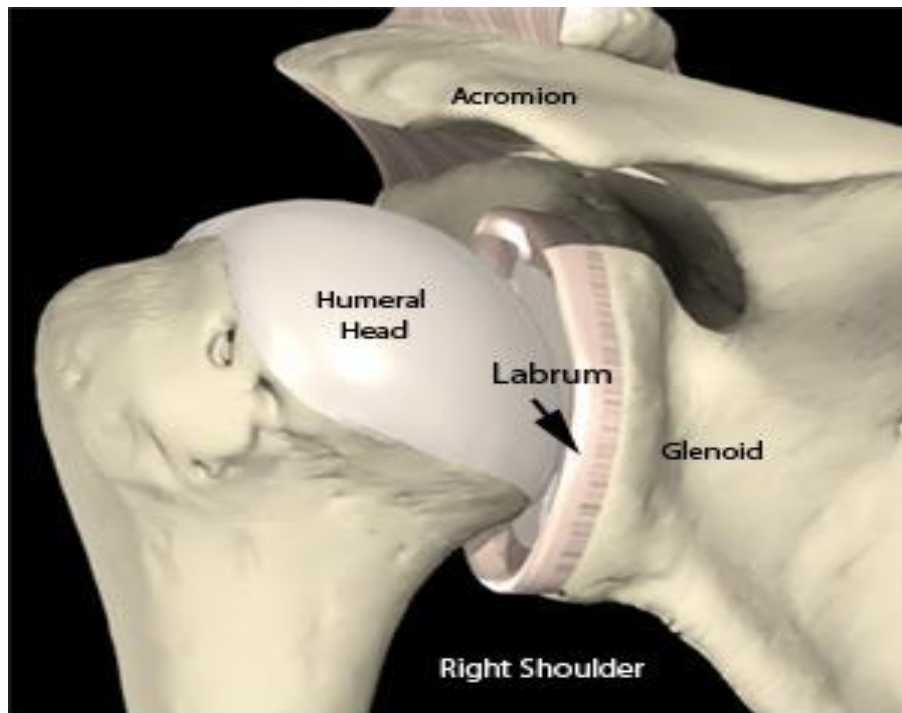


Figure 1-: Shoulder Anatomy – right front view and left back view; v1.0© Primal pictures Ltd. (http://www.kneesource.com/shldr_dislocation.aspx)

1.2.1 Bones

The two bones which form the shoulder girdle are the Clavicle (Collarbone), the Scapula (Shoulder Blade). Also the scapula and the Humerus (upper arm bone) create shoulder joint.

1.2.1.1 The Clavicle:

The clavicle has the appearance of an elongated “S” and it articulates with the acromion process of the scapula on the lateral side (Acromioclavicular Joint) and on the medial side with the sternum (Sternoclavicular Joint). The medial half of the bone is anteriorly convex and the lateral side is concave (Hay & Reid, 1999; Roetert, 2003).

1.2.1.2 The Scapula:

The scapula is a flat bone that is roughly triangular in shape with a medial, lateral and superior border (Hey & Reid, 1988). It consists of three angles that are superior, lateral and inferior. The scapula extends up and around the shoulder joint at the rear to form a roof called the acromion, and around the shoulder joint at the front to form the coracoid process. The end of the scapula,

called the glenoid, meets the head of the humerus to form a glenohumeral cavity that acts as a flexible ball-and-socket joint.

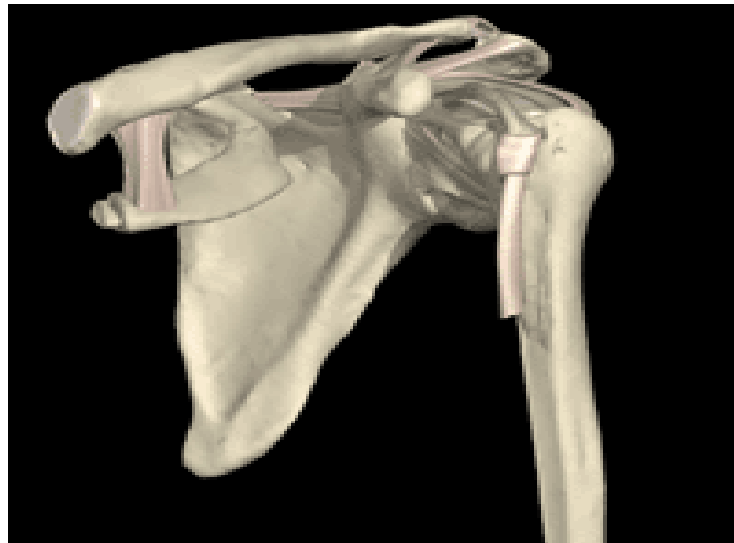


Figure 1-: Anterior and posterior view of the scapula (Sawchuk and Padiak © 2003)<http://reel.utsc.utoronto.ca/mboyer/Sawchuk/images>

1.2.1.3 Humerus:

The humerus is a long asymmetrical bone which makes up the arm skeleton. It articulates with the shoulder blade at the proximal part (glenohumeral joint) and with the radius and ulna at the distal part (elbow joint). The head of the humerus and face of the glenoid create the joint cavity which is covered by articular cartilage.

1.2.2 Joints of the Shoulder Girdle

The shoulder girdle consists of two joints, which on each lateral side has a glenoid fossa for articulation with the head of the humerus (glenohumeral joint):

1.2.2.1 The Sternoclavicular Joint:

This joint is a synovial joint between the medial end of the clavicle and the superior lateral corner of the manubrium of the sternum and the cartilage of the first rib. A fibrous capsule covers the articulation and provides strength to the joint by an:

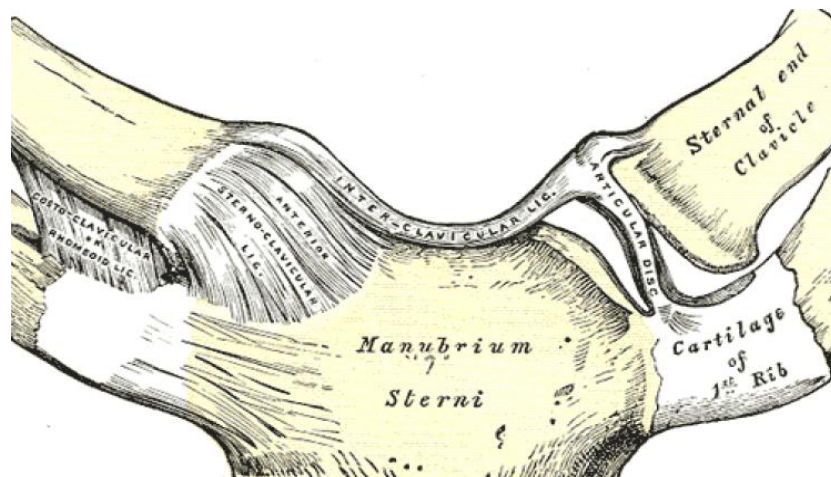


Figure 1-: Sternoclavicular articulation - Anterior view (<http://www.bartleby.com/107/illus325.html>)

- anterior and posterior sternoclavicular ligament;
- interclavicular ligament; and a
- costoclavicular ligament (Marieb, 1995; Hay & Reid, 1999).

The sternoclavicular joint is a very strong joint and dislocation is uncommon. If the acromion of the scapula is struck or when a force is transmitted from an outstretched arm when the hand strikes the ground on falling, it is likely that the clavicle may break, but the joint will rarely dislocate (Hay & Reid, 1999; Martini et al., 2001).

1.2.2.2 The Acromioclavicular Joint:

The acromioclavicular joint, which is also an arthrodiar joint, forms the union between the lateral end of the clavicle and the acromion process of the scapula.

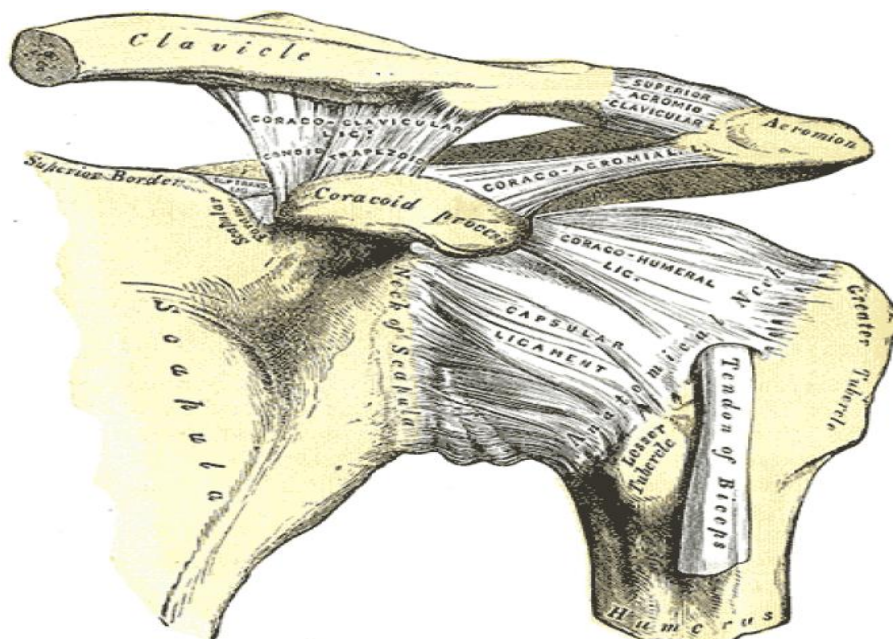


Figure 1-: The left shoulder and acromioclavicular joints, and the proper ligaments of the scapula (<http://www.bartleby.com/107/illus326.html>)

The superior and the inferior acromioclavicular ligaments aid in supporting the joint (Marieb, 1995; Hay & Reid, 1999). The coracoclavicular ligament, which is not part of the joint, helps to maintain the integrity of the joint. Dislocation of this joint is common in contact sports when the athlete falls on his shoulder and this condition is often incorrectly referred to as a “shoulder separation” (Hamill & Knutzen, 1995; Hay & Reid, 1999; Martini et al., 2001).

1.2.3 Shoulder joint

The shoulder joint (glenohumeral joint), itself is a ball-and-socket, formed by the small, shallow, pear-shaped glenoid cavity of the scapula and the head of the humerus (Figure 1-) (Marieb, 1995). In ball-and-socket joints, the hemispherical or spherical head of one bone articulates with the concave socket of another bone. These joints are multi-axial with universal movement in all axes and planes.

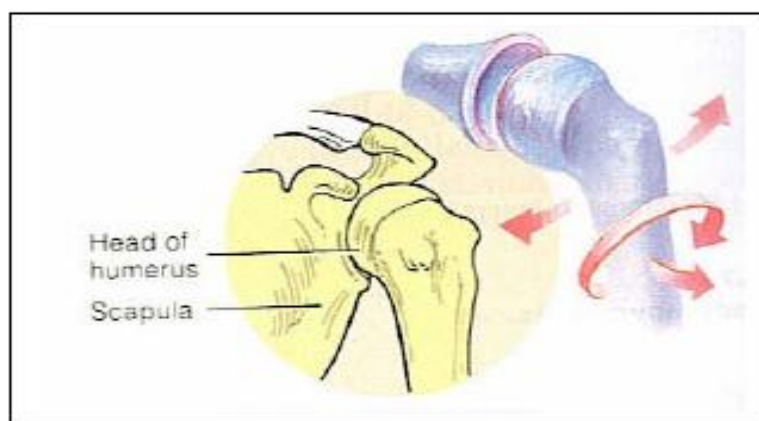


Figure 1-: Shoulder joint - Marieb, 1995; Hay & Reid, 1999

1.2.4 Muscles, tendons and ligaments

The bones of the shoulder are held together by muscles, tendons, and ligaments. Tendons (tough cords of tissue that attach the shoulder muscles to bone) and ligaments (attach bones to bones) provide additional strength and stability.

The **biceps tendon** attaches the biceps muscle to the shoulder and helps to stabilize the joint.

The Glenohumeral ligaments (Figure 1-) arise from folds of the anterior portion of the capsule and reinforce the joint. These ligaments provide the stability and prevent translation of the head of the humerus from the glenoid fossa.

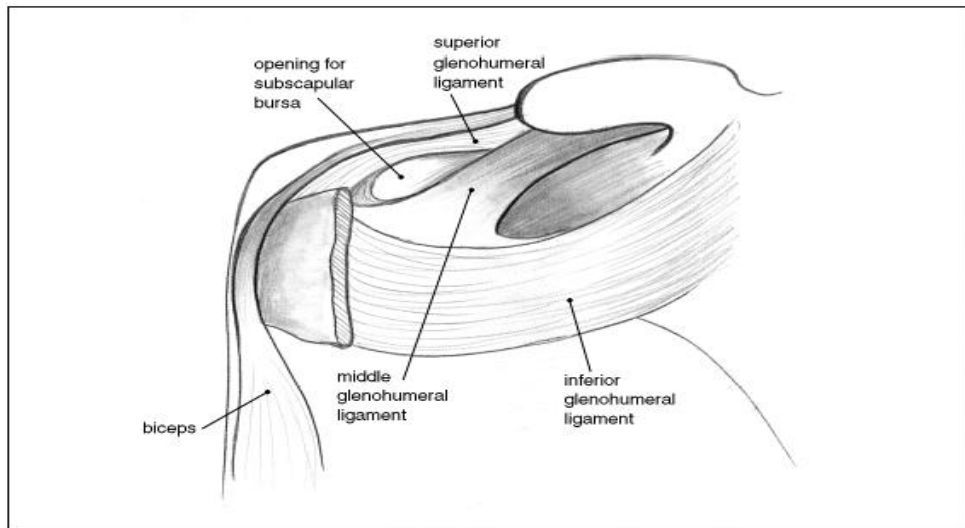


Figure 1-: Glenohumeral Ligaments (Hay & Reid, 1999)

Shoulder joint stability is gained by its Muscles and Tendons which called the Shoulder Dynamic Stabilizers as shown in Figure 1-. They surround the humeral head and help to approximate it into the glenoid fossa. The muscles of the shoulder complex provide stability and movement. During shoulder movements such as lifting, certain muscle groups help to move the shoulder, while other muscle groups help to stabilize the shoulder complex. Much of the stability in the shoulder complex is provided by this muscular coordination. The rotator cuff muscles are: Supraspinatus, Infraspinatus, Teres minor, Subscapularis. And the other dynamic muscle stabilisers are the long head of the biceps tendons, deltoid, and teres major.

Dynamic support of the shoulder joint occurs primarily in the midrange of motion and is provided by the muscles as they contract in a coordinated pattern to compress the humeral head in the glenoid cavity. The posterior rotator cuff muscles provide significant posterior stability, the subscapularis muscle provides anterior stability, and the long head of the biceps brachii prevents anterior and superior humeral head translation, and the deltoid and the other scapulothoracic muscles position the scapula to provide maximum glenohumeral stability. When all of the rotator cuff muscles contract, the humeral head is compressed into the joint, and with an asymmetric contraction of the rotator cuff, the humeral head is steered to the correct position. This muscle group also rotates and depresses the humeral head during arm elevation to keep the humeral head in position.

The articular anatomy, the capsule, ligaments, and glenoid labrum provides the shoulder with static stability. The shoulder static stabilisers are acting together to give smooth yet complex motion. In Figure 1- the rotator cuff muscles are shown to give an overview of the static and dynamic stabilisers. They define the shoulder state and range of motion. The ball and socket articulation is delicate yet reliable to give this wide range of motion in the shoulder.

However, because there is minimal contact between the glenoid fossa and the head of the humerus, the shoulder joint largely depends on the ligamentous and muscular structures for stability. Stability is provided by both static and dynamic components, which provide restraint and guide and maintain the head of the humerus in the glenoid fossa.

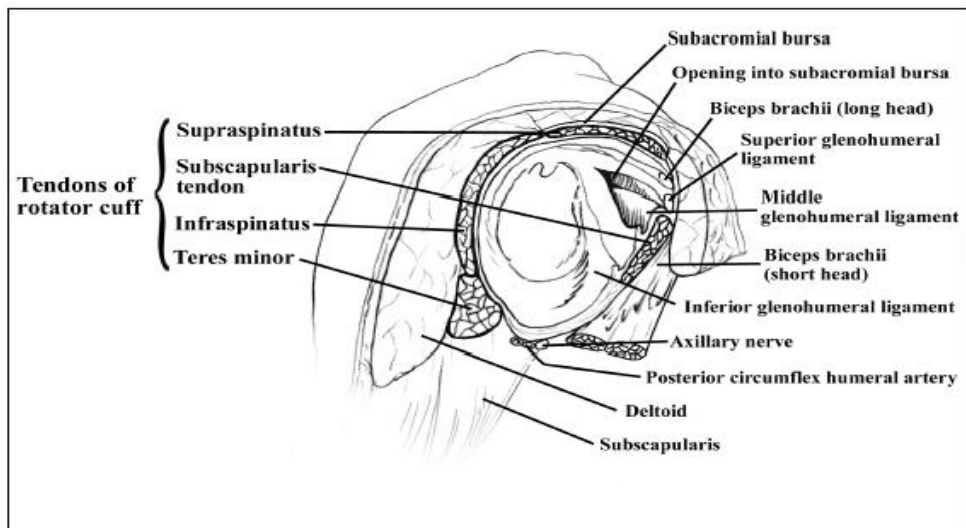


Figure 1-: Shoulder muscles and tendons (short muscles) (Hay & Reid, 1999)

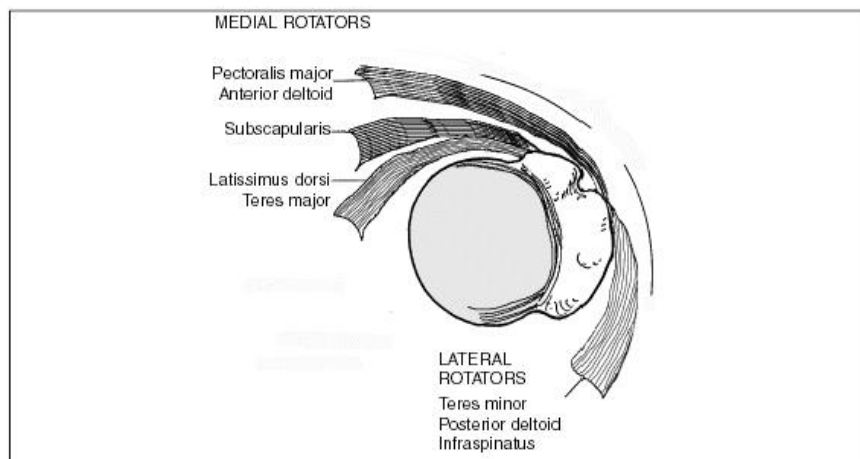


Figure 1-: Shoulder muscles and tendons (rotator cuff muscles) (Hay & Reid, 1999)

1.2.5 Articular cartilage

The joint cavity is cushioned by **articular cartilage** covering the head of the humerus and face of the glenoid. . Both articulating surfaces are lined with a layer of cartilage, where the humeral cartilage thickens in the middle of the humeral head surface, and conversely, the glenoid cartilage layer thickens at the rim, thereby increasing cohesion (Figure 1-).

The labrum is the fibrous cartilage ring of triangular cross-section found to be continuous with the articulating cartilage of the glenoid. The labrum allows the glenoid to form a deeper, more conforming socket for the head. The inner surface of the ring contacts the humeral head and the outer surface serves as attachment sites for ligaments, thus providing the perfect fit between the humeral head and glenoid fossa.

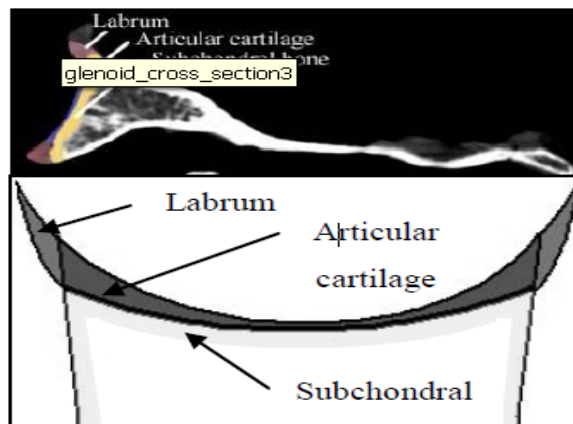


Figure 1-: Lateral CT of transverse section of glenoid and cartilage tissue (top) and schematic of the glenoid cross-section (bottom) demonstrating the conforming cartilage structures (Barnett et al. 1961).

The hyaline cartilage lining of the GH joint can vary from a thickness of 1-2 mm in smaller joints and in the aging population, to 4-7 mm in younger people and has been found to thicken with long and short-term exercise. The thickness, compressibility and the transparency of the joint cartilage has been found to decrease with age (Barnett et al. 1961).

Cartilage consists predominantly of extracellular matrix, produced by chondrocyte cells that are sparsely distributed homogeneously throughout the matrix. The matrix consists of interwoven collagenous fibrils and ground substance, forming the glue to the fibrous network. Understandably there are no nerves within the cartilage and no vascular supply except at the bone/cartilage interface where the cartilage is calcified and interface bonding is strong. Although

the matrix consists of 70% water in weight, the characteristics of the bearing material is attributed to the mucopolysaccharides¹.

1.3 Kinematics of shoulder

Kinematics is the branch of mechanics concerned with the motion of objects without reference to the forces that cause the motion (<http://en.wikipedia.org/wiki/Kinematics>). Shoulder kinematics concerned with shoulder joints movements and degree of freedom. Human body movement such as walking, bending, lifting, and grasping inherently is part of shoulder kinematics. Limited movement, such as when a person is confined to bed or elects a sedentary life style, can contribute to deleterious health effects such as cardiovascular disease, diabetes, and cancer. However, the limitation to human's movements or his inability to move may contribute, either directly or indirectly, to his susceptibility to musculoskeletal injury. The shoulder is the most movable joint in the body, and is unstable. It is easily injured by impact, simple overuse, lifting heavy objects or by belligerent exercising. In the following sections the shoulder kinematics will be reviewed and discussed.

1.3.1 Movements of the Shoulder Girdle:

All the movements of the scapula depend on the combined motion capabilities of both the sternoclavicular and the acromioclavicular joints. The sternoclavicular joint permits movement in almost all directions, including circumduction. The acromioclavicular joint permits the gliding motion of the articular end of the clavicle on the acromion, and also some rotation of the scapula both forward and backward on the clavicle (Hay & Reid, 1999). The movements of the scapula in combination with the clavicle are as follows:

1.3.1.1 Adduction and abduction:

Adduction of the scapula occurs when the medial border of the scapula moves toward the spine and abduction of the scapula when the medial border moves away from the spine. Adduction can be seen when sticking out the chest and pulling back the shoulders (Yokochi et al., 1989; Hay & Reid, 1999).

¹ Mucopolysaccharide is found in connective tissue, skin, bone and cartilage together with proteins from the intercellular cells where collagen and elastin are embedded (http://www.skincareinnovation.com/article_info.php/articles_id/3).

1.3.1.2 Elevation and depression:

Elevation is the upward movement of the scapula with no rotation, as in raising the shoulders. The downward movement of the scapula is called depression. Elevation and depression can be felt by placing the hand on the scapula and the clavicle either separately or simultaneously while first lifting the shoulders and then pushing them down again (Yokochi et al., 1989; Hay & Reid, 1999).

1.3.1.3 Rotation:

The axis of rotation can be either at the sternoclavicular or the acromioclavicular joint. Upward rotation is the outward and upward movement of the inferior angle of the scapula. Downward rotation is the inward and downward movement of the inferior angle of the scapula (Hay & Reid, 1999).

1.3.2 Movements of the Shoulder Joint:

The movements of the glenohumeral joint should not be confused with those movements of the shoulder girdle, although they usually occur together and should be considered together. Extension, flexion, a slight degree of hyperextension, abduction, adduction, circumduction, medial rotation and lateral rotation may all occur at the shoulder joint, but their range of motion is limited if there is no shoulder girdle involvement (Hay & Reid, 1999). During all flexion and abduction motions of the glenohumeral joint there are simultaneous scapulothoracic (shoulder girdle) movement. The scapula remains fixed through the first 30° to 60°, but there may be motion at the joint until a stable position is obtained, or the scapula may move on the chest wall. After 30° of abduction or 60° of forward flexion, there is a constant relationship between the humeral and the scapula movement with two degrees of humeral movement for every one degree of scapular rotation (Figure 1-) (Yokochi et al., 1989; Hay & Reid, 1999).

Taken from the anatomical position, the full range of movement in flexion of the arm above the head can only be accomplished if medial rotation of the humerus occurs, whereas full abduction is possible from this position (Yokochi et al., 1989). If abduction is attempted with the palm of the hand facing the thigh, the range of motion is limited to approximately 90°. Lateral rotation will permit further abduction from this point (Hay & Reid, 1999).

As shown in Figure 1-: Shoulder Range of Motion can be varied depending on the joint degree of freedom. There are six degrees of freedom for the shoulder movement. They can be as follows:

Flexion: 180°, Extension: 60°, Abduction: 180°, Adduction: 60°, Internal rotation: 90° (with arm abducted) and External rotation: 90° (with arm abducted).

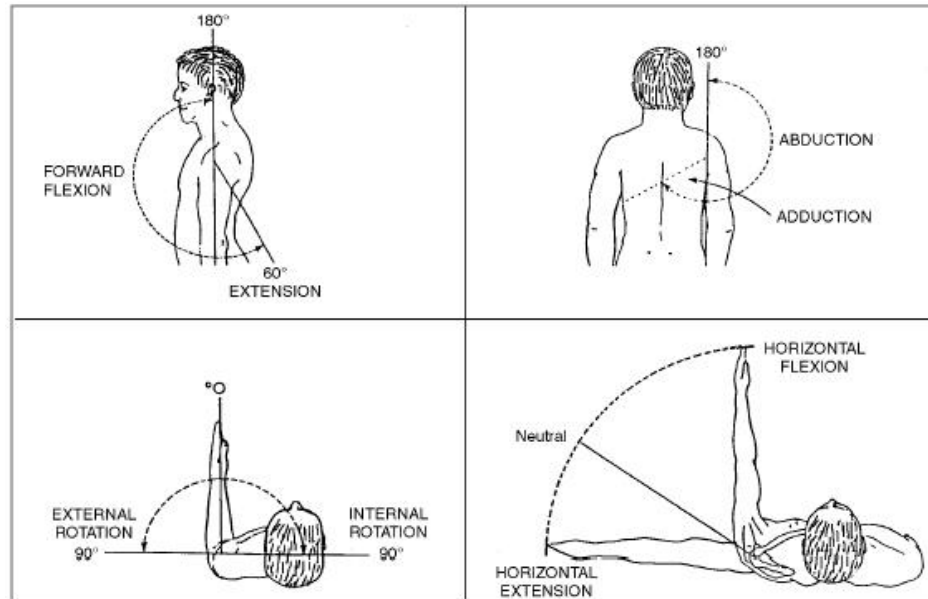


Figure 1:- Shoulder Range of Motion

It is essential to understand how bony and soft-tissue elements of the shoulder interact among each other or with an endo-prosthesis to generate movement. The movement at the glenohumeral joint requires motion at the other joints of the shoulder complex. The coordinated movement of these joints during arm movement is referred to as the scapulo-humeral rhythm. The scapulo-humeral rhythm describes movement that occurs at the glenohumeral joint compared to movement that occurs at the other shoulder complex joints, the sternoclavicular, the acromioclavicular and the scapulothoracic joints. The scapulothoracic joint is not a proper joint but it illustrates the movement of the scapula against the thoracic wall during the arm movement.

However, the scapulo-humeral rhythm allows the shoulder to move through its full range of movement and it allows the head of the humerus to be centred within the glenoid fossa. It is known that for every 15 degrees of shoulder abduction, 10 degrees occurs at the glenohumeral joint and 5 degrees occurs at the scapulothoracic joint. But for every 180 degrees of shoulder abduction, 120 degrees occurs at the glenohumeral joint and 60 degrees occurs at the scapulothoracic joint. If there are changes to the scapulo-humeral rhythm, the head of the humerus does not remain centred and it can lead to problems with the rotator cuff tendons such as tendonitis or rotator cuff impingement.

The shoulder motion in its normal cases i.e. without pain or shoulder injuries is a motion of the previous mentioned joints/muscles acting together to perform the known wide range of motion.

1.4 Kinetic of shoulder

The kinetic of shoulder joint has complex behaviour like other joints of body. In this part the forces created inside shoulder joint are categorized and mechanisms which make this joint stable are reviewed.

1.4.1 Shoulder joint forces

The shoulder muscles generating a force vector through the GH joint has been shown to be maximum at 90° abduction, where the resultant force lies superiorly in the glenoid (Figure 1-).

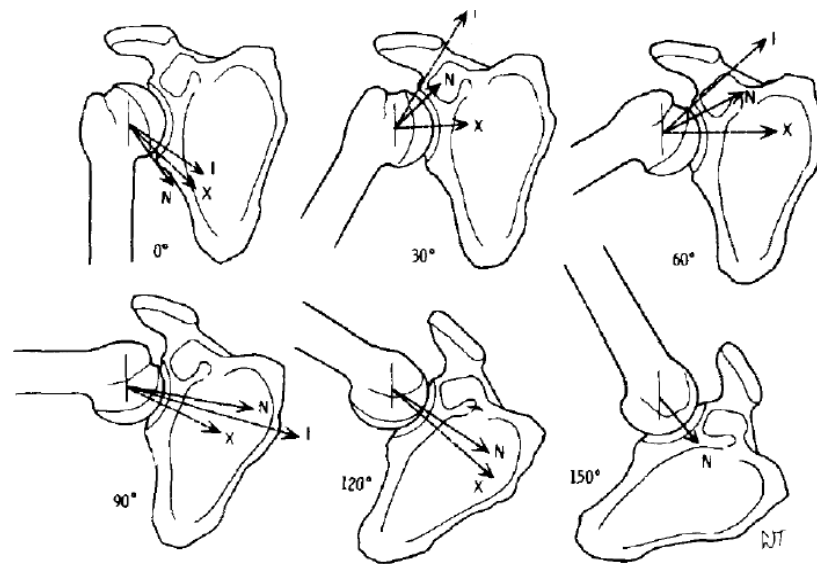


Figure 1-: Resultant forces of neutral (N), external rotation (X) and internal rotation (I) vectors. Fu et al. 1991.

1.4.2 Shoulder joint stabilisers

Several mechanisms that help stabilise the joint are categorised as static, dynamic, passive and active stabilisers (Matsen III et al. 2006). The mechanisms of stabilisation in the shoulder joint are the glenoid conformity/concavity, muscular compression, capsuloligamentous restraints, adhesion-cohesion of the articulation surfaces and suction. Instability is defined as the point when the resultant joint force falls beyond the joint rim edge and the point of instability is defined as the subluxation point. Dislocation is defined as the point when rim edge aligns with the head centre (Figure 1-).

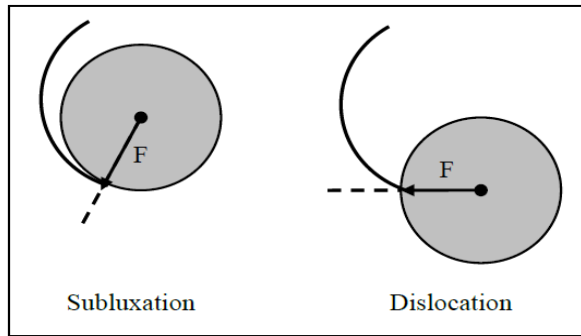


Figure 1-: Subluxation and dislocation definitions where arrows denote resultant joint force

The glenoid concavity works by creating a conforming surface in order to centre the humeral head. Joint stability is affected by the level of concavity and conformity in two ways; increasing either the glenoid conformity or depth will increase the transverse force required to subluxate or dislocate the joint (Figure 1-). Similarly, increasing the compressive perpendicular force from surrounding muscular tissues increases the transverse force needed to destabilise the joint. The flexibility of the labrum allows for small head movement in the ball and socket joint without compromising the stability (Matsen III et al. 2006).

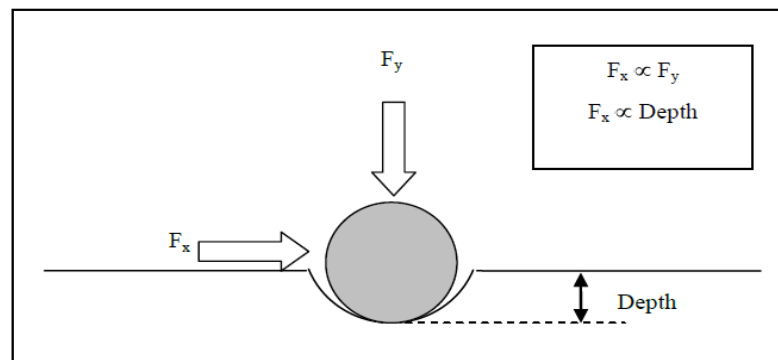


Figure 1-: Glenoid depth and perpendicular compressive force (F_y) are both proportional to the transverse force (F_x). Note: forces generated by surrounding muscles.

The joint compression (F_y) is provided primarily by the four rotator cuff muscles, each providing compression and stability around the joint both passively and actively (Figure 1-). The subscapularis is the primary stabiliser for anterior aspect of the joint. The supraspinatus is mainly the superior stabiliser and the infraspinatus and teres minor, provide the main posterior support. Other shoulder and scapula muscles help provide compression, however, their support are more effective at various positions during shoulder movement. It is the rotator cuff providing the mid-range stability of the joint and throughout all movements of the shoulder. The second purpose of the rotator cuff is to act as agonists and antagonists in shoulder motion (Chadwick et al. 2004).

The joint capsule and ligaments serve as restraints to restrict the range of motion of the humeral head, and by doing so, prevent damage to the tissues. Therefore the ligaments stay lax and unloaded during mid-range movement where the muscular forces dominate (Labriola et al. 2005; Matsen III et al. 2006; Schiffert et al. 2002). As the shoulder reaches its limit, the forces exerted by the muscles decrease and are no longer sufficient to provide stability, the ligaments and capsule become effective and stretch in tension, creating a reactionary force applied to the head, preventing further movement. This capsuloligamentous mechanism is passive and does not require energy like muscles do.

The adhesion-cohesion and suction mechanisms are also passive and work on the physical properties of water and tissues. The adhesion-cohesion is the smooth sliding of the glenohumeral joint due to the thin film of synovial fluid between the articulating tissues which allow sliding and resist separation as a drop of water does between two glass sheets. The suction is created between the head and glenoid socket as a result of the concavity and conformity (radial match) provided by the labrum, generating low pressure in the joint, which maintains the glenohumeral contact.

1.5 Prospective problems in shoulder

The normal shoulder is a ball and socket joint. The ball is called the humeral head and the socket is called the glenoid. In the Arthritic shoulder the normal cartilage (smooth surface of joint) is worn away and there is bone-on-bone without the normal smooth gliding surfaces, which are able to glide on one another with little friction and wear. The joint may also become irregular from bony growth (*osteophytes*), which is the body's attempt to "heal" the cartilage injury. Pain is usually due to the irregular joint surfaces rubbing on one another and from the inflammation of this wear and tear.

One of the most detrimental problems that arise regarding the movement of the shoulder occurs at the glenohumeral joint, where the erosion of the solid cushioning known as cartilage and the lubricated synovium causes the bones to rub together when moving. This is known as arthritis of which there are two types that prevail in the shoulder. Osteoarthritis is a common occurrence caused by constant exposure of the joint to high stresses. Rheumatoid arthritis occurs when the synovium inflames destroying the bone and cartilage it encompasses. The direct contact of the

two rough bony surfaces causes many problems including stiffness of joints and pain and therefore must be treated by surgery – although there are non intrusive methods of treatment they will not enable regrowth of the cartilage and are therefore seen more as pain management.

1.6 Surgical cure

The surgical method to cure arthritis is a specific form of orthopaedic surgery called total replacement arthroplasty, which is where the ends of the joints are cut off and replaced with a man-made imitation. In total shoulder replacement this involves replacing the head of the humerus with a metal hemisphere and the glenoid cap in the scapula with a polyethylene cup. The problem with this method is that any musculoskeletal problems the patient had prior to surgery, which were not due to the geometry of the joint but to the supportive muscles, will still be prominent with the new shoulder, specifically when that restriction is caused by a loss of strength, or tear of the rotator cuff muscles.

1.7 Research Hypothesis

One method of analysing the stresses and micro-motion within the implant is by running a finite element analysis (FEA) on a computational representation of an implant, which has previously been used to compare healthy and arthritic shoulder joints. The research carried out by Büchler et al. 2002 showed the stress distribution over the scapula with varying positions of the humeral head on a healthy and arthritic shoulder using FEA. The results showed that stresses within the scapula were more evenly distributed in the healthy shoulder with lower maximum stresses than in the arthritic shoulder, whose stresses were considerably localised. It is this effect of exponentially increased damage through increasing stress localisation that leads to surgery being the only effective method of curing osteoarthritis.

The Reverse Shoulder Replacement is a newly approved implant that has been used successfully for over ten years in Europe. It was approved by the FDA for use in the U.S.A. in March of 2004. It is designed specifically for use in shoulders that have a deficient rotator cuff and arthritis or complex fractures, as well as other difficult shoulder reconstructions. It is sometimes a very useful option for revision of a failed prior joint replacement where the rotator cuff tendons are chronically torn and cannot be repaired.

The Reverse Shoulder Replacement using Verso changes the orientation of the shoulder so that the normal socket (glenoid) now is replaced with an artificial ball, and the normal ball (humeral

head) is replaced with an implant that has a socket into which the artificial ball rests. This type of design completely changes the mechanics of the shoulder and enables the artificial joint to function when the rotator cuff is either absent or when there is significant bone loss.

1.8 Purpose and aim of the study

The thesis investigates the total shoulder arthroplasty using Verso. The Verso Shoulder (Biomet Verso) has been designed specifically for patients suffering from Osteoarthritis associated with rotator cuff insufficiency. The objective of this project is to examine the mechanical behaviour of the glenoid interface of a shoulder fitted with a Biomet Verso Shoulder implant by using finite element analysis and experimental tests when the joint is subjected to high impact loading.

This specific interface has been chosen because this is the most common area of failure in reverse shoulder implants which could be possibly due to stress levels of the screws and/or bone exceeding their material yield strengths or large displacements of any of the parts, which make up the joint, when subjected to considerable loading. What the results should show is how the design and geometry of the Verso Shoulder should react to high loads and whether its design would need to be evaluated. The finite element method will be used as it is easily accessible method and will be able to show all the mechanical behaviour that occurs within a relatively small, inaccessible area.

The interface between humeral implant and humeral bone channel was simulated and the mechanical parameters such as stress, strain and deformation were analyzed for the Verso implant. The bone channel micro-motion during the shoulder joint simple motion was analyzed and the result was discussed.

The results from finite element analysis of this thesis will help in predicting areas where the stress concentrations can cause failure to either the bone or prosthesis. Moreover, the results should show how the design and geometry of the Verso Shoulder should react to high loads and whether its design would need to be evaluated.

Biomet Ltd. has developed and manufactured Verso implant together with Reading shoulder unit, UK. This work has been done in collaboration with Biomet Ltd to investigate the current design and report the outcome of the mechanical testing and FEA results; and whether the

current design is stable and reliable. The mechanical properties for the Verso implant such as Poisson's ratio and Young's modulus were provided by Biomet.

This work forms the basis of a new method that can be used to design a bespoke total shoulder implant by using data the patient's CT scan and developing an optimised (minimum weight, high strength) implant for the patient.

The mathematical modelling phase describes all the necessary components for developing such a method. This research has provided useable method and information and is a useful basis for someone considering the redesign of similar medical implants.

The thesis developed the mathematical models and procedure for a "total reverse shoulder implant" analysis which can be used for optimization and bespoke development.

The thesis can be divided into three main sections: - background, mathematical modelling, experimental identification and validation. The first section includes the second and third chapters and covers the background and literature survey. This section concentrates on the study into total shoulder replacement surgery.

1.9 Summary

The chapter discussed the shoulder anatomy, kinematics and showed the range of normal movement of the shoulder joints. Consequently the shoulder joints proposed problems and surgical solution were highlighted.

The data used in this . In this study the geometry of the Verso has been created primarily from CT scans compiled together using MIMICS (Materialise) and the model has then been imported into ABAQUS (SIMULIA, Providence, USA). The material properties such as density, Poisons ratio and Young's modulus have been set to each part of the model including the bones and all parts of the Verso. The load and boundary conditions have been applied to the model to mimic forces exerted on the shoulder joint with complicated actions such as lifting.

Finally, this study aims to describe the mechanical behaviour of Scapula and Humerus bones at the implant sites. The study uses a finite element method to examine the mechanical parameter

such as stress and strain at the interface between the Verso implant and the bone. The study specifically focuses on the interface between the implant in humerus and scapula bones. The possible micro-motion of the bone at the interface under loading are evaluated. To achieve this aim, it is necessary to understand the shoulder anatomy to know the movements of the shoulder joints.

A total review for Shoulder joints Movements and history of current surgical and non-surgical methods used to replace the affected shoulder will be discussed in the next chapter.

1.10 Summary of Thesis Chapters:

As stated in chapter 1 earlier: The objective of this project is to examine the mechanical behaviour of the glenoid interface of a shoulder fitted with a Biomet Verso Shoulder implant by using finite element analysis when the joint is subjected to high impact loading.

Moreover, to investigate the interaction between the Verso (reverse) shoulder implant and the humeral and scapula cavities. To understand shoulder anatomy and kinematics and use ABAQUS (SIMULIA, Providence, 6.9) to create a virtual simulation of a complete assembly of the shoulder joint and Verso implant. Material properties, surface interactional behaviour, boundary conditions, and loads are assigned to portray realistic behaviour. Visual models of displacement (micro motion); Stress (principle, von mises) and Strain are required to certify benefits of the Verso implant.

Chapter 2 has stated and highlighted the previous reverse shoulder implant used in the past. A literature review has been discussed about the application of the total shoulder replacement implant available in the market. Their uses, application, operation, and the problems reported postoperative whether on a long term or short term.

Chapter 3 discussed the total shoulder replacement operation techniques used nowadays. A total reverse shoulder replacement operation using traditional implant such as Delta implant was discussed in details showing the whole operation. Likewise, a total reverse shoulder operation using the Verso implant was discussed (using the target patient data), to show the differences between both techniques (traditional reverse and Verso reverse). Postoperative rehabilitation techniques and recommendation was highlighted as well.

Chapter 4 underlined the different techniques and methods used in this research. The different types of software used such as Geomagic, MIMICS and ABACUS (SIMULIA, Providence) to perform the analysis process using the patient data obtained from chapter 3. Lastly, the mechanical testing technique used to investigate the Implant behaviour under different types of loading, also, to identify the implant strength with different settings applied to the Verso implant.

Chapter 5 draws the attention to the outcome of the mechanical testing results that were obtained when applying different settings to the Verso implant with or without side screws. This to prove the hypothesis proposed about the strength and stability of the implant under various conditions.

Chapter 6 investigates the mechanical behaviour using FEA through ABACUS software. The implant was tested through different models and different settings. However, part of the FEA has replicated the mechanical testing performed in chapter 5.

Chapter 7 highlighted the comparison of the results obtained from the finite element analysis in chapter 6 and the mechanical testing results obtained from chapter 5.

Chapter 8 underline the research topic conclusion, findings and the future work suggestions.

Chapter 2. Literature Review of Total Reverse Shoulder Implants

2.1 Introduction

This Chapter will highlight the shoulder problems, surgical treatments in brief description. The chapter reviews the mechanical analysis previously been done in total reverse shoulder implants.

2.2 Shoulder problems

The most common shoulder problems are:

- Dislocation
- Separation
- Rotator cuff disease
- Rotator cuff tear
- Frozen shoulder
- Fracture
- Arthritis.

The symptoms and treatment of shoulder problems vary, depending on the type of problem.

2.3 Shoulder Surgical treatment

Shoulder replacement surgery is an option for treatment of severe arthritis of the shoulder joint. Arthritis is a condition that affects the cartilage of the joints. As the cartilage lining wears away, the protective lining between the bones is lost. When this happens, painful bone-on-bone arthritis develops. Severe shoulder arthritis is quite painful, and can cause restriction of motion. While this may be tolerated with some medications and lifestyle adjustments, there may come a time when surgical treatment is necessary. The surgical method could be divided on three methods.

2.3.1 Hemi-arthroplasty

A hemi-arthroplasty involves replacing the humeral head and not replacing the glenoid (socket) which might be the best option if the glenoid does not have any arthritis or if there is some concern that the glenoid component might fail if it is replaced. In patients with no rotator cuff, the humeral head tends to subluxate superiorly when the deltoid muscle contracts (Figure 2-a). This vector is not corrected by a standard hemi-arthroplasty in patients with no rotator cuff. The reverse prosthesis corrects this abnormal vector by moving the centre of rotation of the arm

laterally and by redirecting the pull of the deltoid muscle (Figure 2-b). Moving the centre of rotation with the prosthesis allows the deltoid to elevate the arm despite the shoulder joint having few or no rotator cuff tendons present. Biomechanically, the reverse prosthesis works by changing the direction of pull of the deltoid muscle (McFarland 2006).

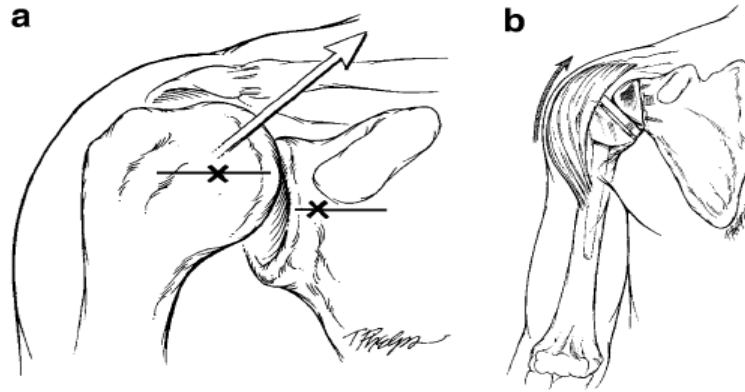


Figure 2-: a)In the shoulder of patients with no rotator-cuff tendons. b) In the reverse prosthesis, the deltoid muscle lever arm is restored (McFarland et. Al. 2006).

2.3.2 Total shoulder arthroplasty

A total shoulder involves replacing the humeral head and the glenoid. A total shoulder might be the best option if the glenoid is damaged but sufficient bone and rotator cuff remain to ensure that the glenoid component will last. A total shoulder is contra-indicated if the rotator cuff is not intact.

In shoulder replacement surgery, the painful surfaces of the damaged shoulder are resurfaced with artificial shoulder parts. The part that replaces the ball consists of a stem with a rounded metal head. The part that replaces the socket consists of a smooth plastic concave shell that matches the round head of the ball. When both sides of the joint are resurfaced, we call it a total shoulder replacement. However, the doctor may determine that only the humeral side of the joint (ball) should be resurfaced. We call this a partial shoulder replacement or Hemi-arthroplasty.

Figure 2- Left: A 70-year-old woman who underwent a left total shoulder arthroplasty due to degenerative arthrosis. Anteroposterior radiograph of the left shoulder showing a standard total shoulder arthroplasty. Right: A 79-year-old woman who underwent hemi-arthroplasty of the left shoulder for a proximal humerus fracture 6 years ago. Anteroposterior radiograph of the left shoulder shows a failed hemi-arthroplasty with superior subluxation of the humerus due to a rotator-cuff tear. (McFarland et. al. 2006).

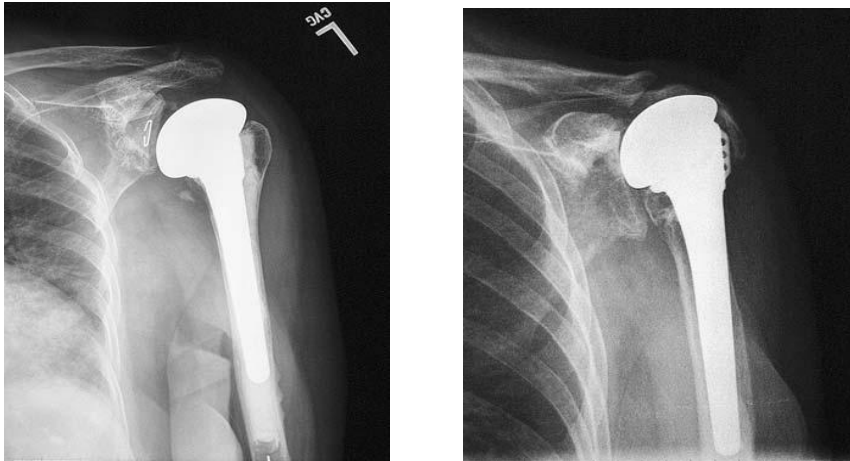


Figure 2-: Left: A 70-year-old woman who underwent a left total shoulder arthroplasty. Right: A 79-year-old woman who underwent hemi-arthroplasty of the left (McFarland et. al. 2006).

2.3.3 Reverse shoulder arthroplasty

A reverse shoulder replacement, also referred to as a reverse total shoulder replacement, is a surgical option for patients who would not be helped by a standard total shoulder replacement because they have rotator cuff damage along with shoulder osteoarthritis. The shoulder is a ball-and-socket joint. In a normal shoulder, the humerus (upper arm bone) ends in a ball shape. The ball fits into a socket formed by the scapula (shoulder blade). The ball and socket form the shoulder joint.

A reverse shoulder arthroplasty involves replacing both the humeral head and the glenoid, but the ball and socket are reversed to improve the muscle function. Because the centre of rotation is translated medially, the deltoid muscle has a longer moment arm and can generate more force. The deleterious effect of translating the centre of rotation is decreased range of motion and increased impingement. This increased impingement causes scapular notching and can undermine the glenoid component. This will be discussed latter.

The first shoulder arthroplasty, performed in 1893 was a constrained prosthesis designed by the French surgeon Jules Emile Pean. The humeral stem was made of platinum and leather and it articulated with a head made of rubber coated with paraffin. The prosthesis was used to treat a case of tuberculosis (Wirth et.all 1996), (Lugli 1978) but while the functional results were reasonable, they were also short-lived and the prosthesis was removed two years later as a result of infection. There followed half a century without any reference to shoulder prostheses in the literature before Charles Neer performed the first simple, non-constrained humeral prosthesis in

a case of fracture of the humeral head. This was a one block implant made of vitallium which reproduced the anatomy of the superior part of the humerus (Neer 1982).

Katz et al 2007 has categorized three different period of progress for shoulder implant historically as follow.

1. Pre-Grammont.
2. The period during which Professor Grammont developed his principles.
3. Post-Grammont.

2.3.3.1 Pre-Grammont: Early setbacks 1970. Neer's experiments

Neer- Averill prosthesis "Mark I" was the first Shoulder arthroplasty were designed in 1970 (Neer 1990). Difficulties in implanting a glenoid implant which was large enough to prevent proximal movement and to stabilize the prosthesis encountered the idea of reversing the implant. As this kind of problem was famous for small glenoid without adequate bone stock. To overcome this problem The Mark I model designed with a large glenosphere which did not let re-attachment of the cuff or its remnants. Charles Neer felt it very important to be able to reconstruct the cuff around the prosthesis; his philosophy preceding the Grammont concept of replacing the irreparable rotator cuff with the deltoid, the only intact muscle available for shoulder elevation. To allow for the repair of the cuff, Neer developed the Mark II prosthesis; a "three element" prosthesis (Huten 1987) with a smaller glenosphere which allowed for a better periprosthetic reconstruction. However, the smaller radius of curvature of the sphere limited the range of motion and therefore increased the constraint of the joint.

Neer then developed the Mark III prosthesis. To limit the constraint on the glenoid component he used a smaller glenosphere than in the Mark I. He also introduced an axial rotation between the humeral stem and the diaphysis to overcome the limited range of motion of the Mark II prosthesis. After this trial, Neer abandoned his constrained prosthesis experiments in 1974 concluding that constraint did not eliminate the requirement to repair the rotator cuff, particularly the supraspinatus, in order to recover a good range of motion.

Figure 2-: Left: Neer's Mark I design with larger spherical component allowed greater motion. Right: Neer's Mark III system incorporated axial rotation of the prosthetic stem, Reprinted with permission from Neer CS 2nd. Shoulder Reconstruction. Philadelphia, PA: WB Saunders; 1990.

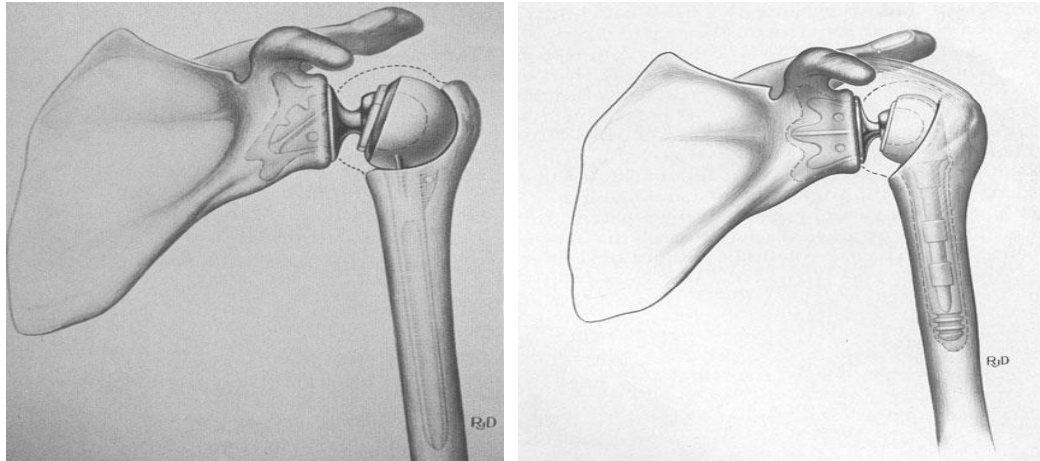


Figure 2-: Left: Neer's Mark I design with larger spherical component. Right: Neer's Mark III system incorporated axial rotation of the prosthetic stem. Philadelphia, PA: WB Saunders; 1990. Copyright _1990 Elsevier.

2.3.3.2 Reeves prosthesis 1972.

The Leeds shoulder which was designed by Reeves et al. 1972 included a divergent threaded peg glenoid component (Figure 2--Left) (Reeves 1974). This design showed higher pullout strength in compare to other designs in vitro testing condition. Although this implant did not go beyond experiment test, this system was designed in way to have an instant centre to show the normal anatomic behaviour (Evan et al. 2011).

2.3.3.3 Gerard and Lannelongue prosthesis1972

Gerard et al. 1972 & 1985 in two different papers reported 22 cases in which their model was used. In that report there were four implant breakages, three dislocations of prosthesis and two infections in the patient however they have explained that high number of problems could not be simply because of the shape of the implant. The cases were complicated and had different reasons. For instance it could be the reconstruction following tumour resection, revision surgery and post-traumatic reconstruction.

Figure 2-: Left: The Reverse Total Shoulder System designed by Reeves et al. included a divergent threaded peg glenoid component, demonstrated higher pullout strength than other designs in vitro testing, and was designed around an instant centre of rotation, which recreated the normal anatomic centre. Reprinted with permission of Professional Engineering Publishing from Reeves B, Jobbins B, Dowson D, Wright V. A total shoulder endoprosthesis. Eng Med. 1974;1:64–67. Right: Components of the shoulder prosthesis designed by Ko'lbl and

Friedebold are shown. Reprinted with permission of Georg Thieme Verlag KG from Kolbel R, Friedebold G. Shoulder joint prosthesis [in German]. Z Orthop Ihre Grenzgeb. 1975;113:452–454.

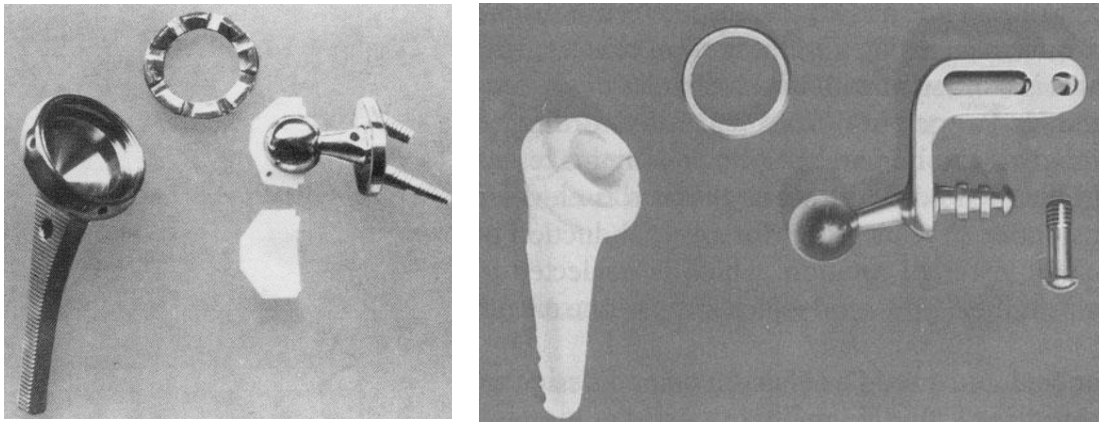


Figure 2-: Left: The Reverse Total Shoulder System designed by Reeves et al. Right: Components of the shoulder prosthesis designed by Kolbel and Friedebold Kolbel R, Friedebold G.

2.3.3.4 Kolbel prosthesis1973

Burkhead 1994 compare the prosthesis designed by Kolbel et al. 1973 & 1987 with other models. In 6 different cases the use of this model was reported. This model was a constrained prosthesis and was designed for reconstruction of bone loss after tumour resection. In this model at the beginning with a central screw the glenoid implant was fixed then with the screws directed towards the coracoids process and/or the axillary border of the scapula the two plates with (Figure 2-:Right) were installed.

2.3.3.5 Kessel prosthesis1973

Bodey and Yeoman 1983 summarised Kessel prosthesis characteristics. They mentioned that this implant was laterally placed to the glenoid by a large central screw. This implant just give 90 degrees of Abduction which is 180 degrees theoretically (although this theoretical mobility is not show able clinically), however this prosthesis allowed acceptable range of rotation which is necessary for a daily life motions. Brostrom et al.1992 reported 23 cases which Kessel prosthesis were used with rheumatoid arthritis. From these numbers 17 patients were tested regularly for 87 months. Wretenberg 1999 by checking the same patients several years later confirmed the following issues. a) Flexion was up to between 90 and 105 degrees, b) lateral rotation was between 20 and 45 degrees c) there were no improvement in abduction d) there was a trace of radiolucent lines on the glenoid screw in all cases after one year.

2.3.3.6 Bayley-Walker prosthesis1973

Bayley-walker prosthesis has the same design as Kessel implant, however the central glenoid screw was coated with hydroxyapatite. Ahir et al 2004 reported the use of this prosthesis in 81 non-tumor patients and 43 patients with malignancy since 1994. They have not seen any loosening within five years of their research. Also in a case of an amputation as a result of a sarcoma recurrence, they have reported an improvement of the centre of rotation in the case with the lowered and medialized's joints with the use of this implant.

2.3.3.7 Jefferson prosthesis of Fenlin1975

As the designing of the reverse shoulder implant improved through the years, there a greater focus to maximize deltoid function. Fenlin 1975 demonstrated the necessity of a large sphere for the glenoid implant. Fenlin believed that with a large glenosphere firstly the deltoid muscle would compensate for the absent rotator cuff secondly there will be an increase in the glenohumeral motion c) the deltoid lever arm (Figure 2-: Left) will increase. However this opinion was different from the principles of Grammont. In Fenlin implant with a so large glenosphere to lighten the total implant weight, it was made with polyethylene, while the humeral cup was metallic. Fenlin 1975 unveiled his fixed-fulcrum system. This system was designed to allow the deltoid muscles to compensate for the deficient rotator cuff, and this design was truly focused toward the patient with cuff tear arthropathy. Fenlin 1985 reported the results of implementation of this implant in five patients and concluded that the ideal application of his design was for the rotator cuff injuries. In that paper he explained some of the long term failures related to the loosening, mechanical breakage and instability of the implant.

2.3.3.8 Liverpool prosthesis of Beddow1975

Liverpool prosthesis design was similar to a Charnley hip prosthesis (Charnley 1979) and the stem of the implant was fixed into the scapula. Blauth W, Donner1979 explained that the Liverpool prosthesis was initially designed in 1969 by Beddow and Elloy similar to the design of a hip prosthesis (Figure 2-: Right). The glenoid component and stem were fixed into the scapular pillar with the polyethylene socket cemented into the proximal humerus. The results of the surgery with in five-year exist for 16 out of 19 patients. In 11 patients the pain were relieved, although four patients suffered from the loosening of the scapular component.

Figure 2- Left: The prosthesis designed by John M. Fenlin, Jr., illustrates the large glenosphere intended to maximize the deltoid function. (Reprinted with permission from Fenlin JM Jr. Total glenohumeral joint replacement). Orthop Clin North Am. 1975;6:565–583. Copyright 1975 Elsevier. Right: In the Liverpool shoulder designed by Beddow and Elloy, the glenoid component and stem were fixed into the scapular pillar with the polyethylene socket cemented into the proximal humerus. This design recreated the anatomic centre of rotation. (Reprinted with permission of Springer Science Business Media from Beddow FH, Elloy MA). Clinical experience with the Liverpool shoulder replacement. In: Bayley J, Kessel L, eds. Shoulder Surgery. Berlin, Germany: Springer-Verlag; 1982.

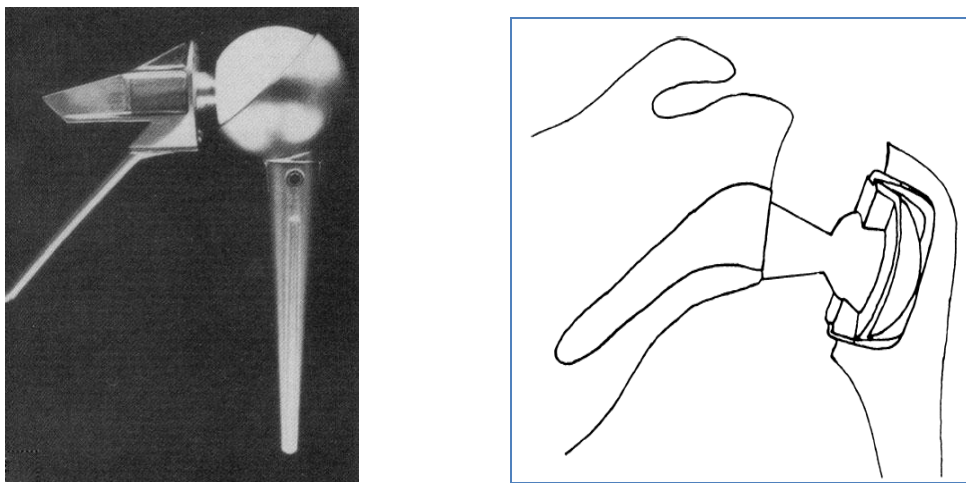


Figure 2-: Left: The prosthesis designed by John M. Fenlin, Jr. Right : Liverpool shoulder designed by Beddow and Elloy Bayley J, Kessel L, eds. Shoulder Surgery. Berlin, Germany: Springer-Verlag; 1982.

2.3.3.9 Bickel , Lettin and Scales1976 & 1977

Cofield & Stauffer 1977, Linscheid & Colfield 1976 explained that the designs by Bickel (Figure 2- left) and also Coughlin et al. 1979, Lettin et al. 1972 &1982, Post 1979 mentioned that the Stanmore implant by Lettin and Scales (Figure 2- right) were maintained the standard for ball-and-socket glenohumeral joint, although these prosthesis have increased constraint. Cofield & Stauffer 1977 reported that the Bickel implant had a small ball-shaped humeral component completely constrained within a polyethylene socket. This socket was seated within the glenoid vault and required a substantial amount of bone removal from the scapula. They have also reported that the problem rates at 18 to 39 months after the surgery were high (Loosening 9%, fracture 18%, pain 27%). Lettin et al 1982 demonstrated that the Stanmore components snapped

together after installation and the glenoid was supported by methylmethacrylate cement. They have also mentioned although there were some improvement in patient's function and ROM (Range Of Motion), this improvement was reported as "inconsistent and disappointing". Cofield & Stauffer 1977 reported that the most important problem with these models was loosening of the glenoid components which case high rates of revision.

Figure 2- Left: The Bickel shoulder prosthesis illustrates the medialized glenoid component, which required substantial bone removal for implantation.. Right :The Stanmore total shoulder prosthesis maintained the standard ball-and-socket glenohumeral articulation, although with increased constraint. The components snapped together after implantation and the glenoid was heavily supported by methylmethacrylate cement. Reprinted with permission from Cofield RH. Status of total shoulder arthroplasty. Arch Surg. 1977;112:1088–1091. Copyright 1977 American Medical Association. All rights reserved.

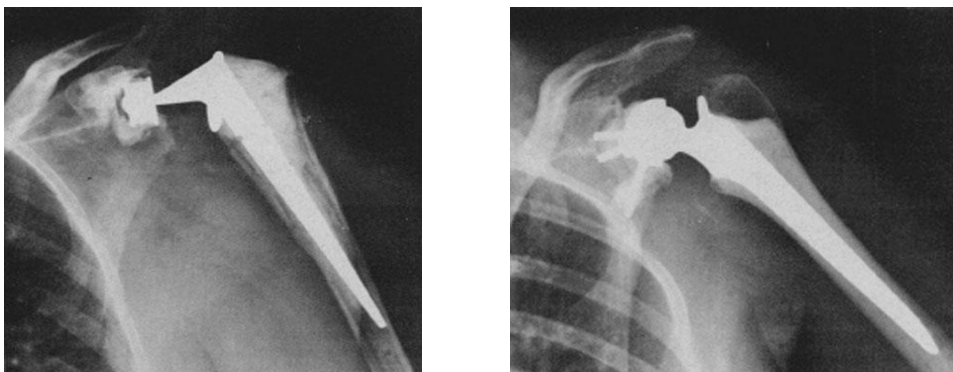


Figure 2-: Left: The Bickel shoulder prosthesis. Right :The Stanmore total shoulder prosthesis. Arch Surg. Copyright, 1977 American Medical Association

2.3.3.10 Buechel-Pappas-DePalma prosthesis1978

Buechel 1997 designed this prosthesis similar to the Neer Mark III. A small glenosphere articulates with a mobile intermediate polyethylene cup. This intercalated element also articulates with a humeral head. While not strictly speaking a reverse prosthesis; the Buechel-Pappas-DePalma prosthesis and the trispherical prosthesis of Gristina are similar in that they include a glenosphere.

2.3.3.11 Gristina - trispherical prosthesis 1978

This prosthesis named "trispherical" because it consists of three parts, a glenosphere, a spherical humeral head and a third, a sphere articulating with the other two (Ungethüm M, Bl Omer 1986).

All the implants explained so far has only marginal functional improvement or even abandoned as failures till the Grammont prosthesis that offers a more reliable design for the patients with the rotator cuff problems.

2.3.3.12 Paul Grammont's reverse shoulder prosthesis

Katz 2007 explained that there were a new concept of medialization a lowering the centre of rotation. The new concept about the reverse shoulder which introduced by Paul Grammont in 1985 was different from previous reverse shoulder implant method. Grammont 1987 explained the differences of his idea on four key features: (1) stability of the implant should be permanently; (2) the part which tolerates the load should be convex, and the other part should be concave; (3) the glenoid centre should be within the implant (glenoid) neck; and (4) the centre of rotation must be medialized and distalized. Grammont find out by moving the centre of rotation distally and medially, it is possible to increase the functionality of the deltoid muscles. Grammont et al. 1987 reported eight different cases of patients on his first design. Although in his first design the centre of rotation was medialized, the centre of rotation of the glenoid component remained lateral relative to the native glenoid surface. Grammont understood that his new model could take more forces at the glenoid bone-implant interface, and also he noted that loosening and breakage of the glenoid parts in previous reverse shoulder arthroplasty happens too often, so tried to change the glenoid component, to lower the malfunctions of implant.

Therefore Grammont design success relies on the deltoid muscles' strength. Katz 2007 predicted in Grammont model that increasing the medialization of the centre of rotation by 10 mm causes to increase the moment of the arm by 20%. Also bringing down the centre of rotation by 10mm will increase the moment of arm by 30%. Rotator cuff constrains prevented the shoulder dislocation during abduction and elevation by as the rotator cuff constrains transforms the dislocating forces into centripetal forces. The reverse orientation of the prosthesis allows the resulting forces to be directed towards the centre of the glenosphere which in turn act on the neck of the scapula. Medialization of the centre of rotation has two effects, except at the initiation of abduction,,: first it is increasing the lever arm of the deltoid muscle and secondly it is reducing the shearing forces. Therefore to stabilize the implant to the scapula two divergent screws were used.

Figure 2-: Left: The first model of the Grammont reverse prosthesis, designed by Grammont in 1985, had only 2 components: the humeral component was all-polyethylene and trumpet-shaped

and the glenoid component was a metallic or ceramic ball, initially two thirds of a sphere and 42 mm in diameter. It was designed to fit over the glenoid like a glove and fixed with cement. (Picture: Courtesy of Emmanuel Baulot, MD). Right: Current design of the Grammont reverse prosthesis. The Delta III prosthesis has 5 parts: the glenoid base plate (metaglenoid), the glenosphere, the polyethylene cup, the humeral neck, and the humeral stem.

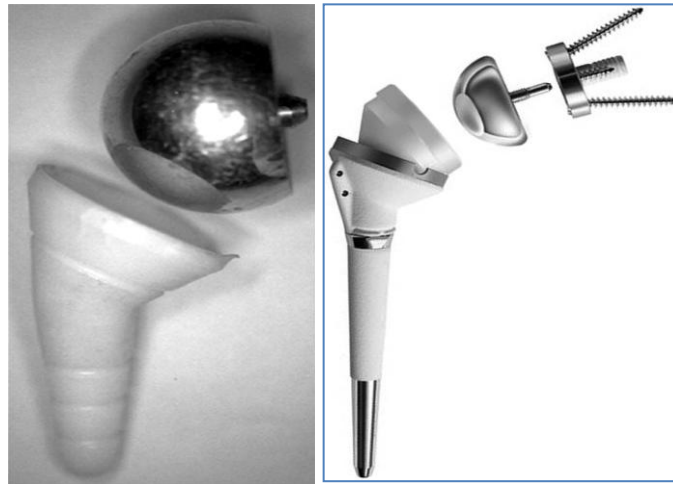


Figure 2-: Left: The first model of the Grammont reverse prosthesis. Right: Current design of the Grammont reverse prosthesis. The Delta III prosthesis.

2.3.3.13 First version of Grammont's prosthesis 1985

Katz 2007 summarized the characteristic of the first model of Grammont in two elements. The first part was the glenoid component which formed from two-thirds of a sphere and was connected to a glenoid base prepared with a bell-shaped saw. The second part was the polyethylene humeral stem which was the shape of an inverted trumpet. The articulating part had a concavity corresponding to one-third of a sphere. Grammont 1987 reported the results of this model in a series of eight patients. Increasing in shearing forces due to laterality of the position of the centre of rotation of the glenoid component related to the centre of the glenoid, led the Grammont to redesign his first model.

2.3.3.14 Second version of Grammont's prosthesis 1989.

In 1991 the DELTA III prosthesis, the second generation of the Grammont's design (DELTA for deltoid muscles, the only motor for this prosthesis) introduced to the market. In the first model, the metaglenoid was a circular plate with a central peg for push-fit impaction to resist to the shearing forces. The glenosphere was screwed directly onto the peripheral edge of the plate. The idea of peripheral screwing of the glenosphere had to be banded due to secondary loosening of

the screws. In the second generation the periphery of the metaglenoid was conical and smooth with a Morse-Taper effect. The metaglenoid was coated with hydroxyapatite on its deep surface to improve bony fixation. The centre of the metaglenoid was hollow in order to allow locking of the glenosphere with a central securing screw. The humeral component was a monobloc with a cup of standard thickness. In 1994, the third generation of Grammont prosthesis were introduced with the new features pertaining to the humeral component. In order to obtain a better fit, a diaphyseal stem was screwed on to a metaphyseo-epiphyseal block of one of three available sizes. The polyethylene cup (a third of a sphere) was fitted over the epiphyseal end. However the cup was of insufficient size and rapidly deteriorated as a result of medial impingement. The cup was therefore replaced by a lateralized cup available in two diameters of 36 mm and 42 mm. A metallic wedge is available to allow correction of length problems in the cases with loss of metaphyseal bone. A retentive cup can be used in cases of major instability.

Boileau et al. 2007, Sirveaux et al. 2004, Valenti et al. 1996, Delloye 2002 and Nyffeler 2004 discussed about the drawbacks of the reverse shoulder prosthesis: a) Medial notching of the scapula b) A passive range of motion of the prosthesis in specimens in which the glenosphere was fixed superiorly c) superior loosening on humeral d) Adjustment of the tension of the deltoid muscles as a source of stability. These problems will be discussed in the following parts.

2.3.3.15 The reverse shoulder prosthesis: Post-Grammont

De Wilde et al. 2004, Frankle 2005 and Harman 2005 explained several new models based on the experiences to date which are under improvement. The TORNIER Company has developed a reverse prosthesis which fulfils the bio-mechanical principles described by Grammont, but with certain new innovations. The metaglenoid is fixed with divergent locking screws (to add the strength to the joints the screws are fixed to the glenoid with a 20° angle instead of zero (parallel to each other) shown in figure 2-8. Wedges and polyethylene cups of varying thickness are used to correct tension of the deltoid and metaphyseal bone loss. Nyffeler et al. 2005 recommended that in the DELTA and TORNIER prostheses, the metaglenoid could be installed lower on the glenoid with a bit more inferior tilt.

Frankle 2005 reported the design of the Reverse prosthesis (ENCORE Medical, Austin-Texas, U.S.A.) in 1998. It was placed less medially than the DELTA and the centre of rotation was closer to its usual anatomical location. He has reported 60 cases follow-up for two years which there were less abduction than in the DELTA series but a better total range of rotation. However,

due to a glenosphere, with two-thirds of a sphere, increased shearing of the screwed metaglenoid has been reported. In addition a series of complications involving the glenoid component including loosening (7 cases) and breakage of the platinum and screws has been experienced. Herman 2005 from Frankle's group concluded that a concave metaglenoid was better than a flat one.

In the Duocentric prosthesis the risk of medial impingement is avoided by an inferior extension of the glenosphere. Unlike the REVERSE, this model respects Grammont principles with the centre of rotation lying at the level of the glenoid.

Katz 2007 in order to improve the range of rotation (which had been found to be poor in Grammont's design) and to eliminate the risk of medial impingement, designed the UNIVERSAL ARROW SYSTEM Figure 2- left which has been available commercially in Europe since 2002. The centre of rotation is the glenoid, but the design allows the prosthesis to be placed less medially than the Delta prosthesis. In addition, the humeral cup has an inbuilt medial notch Figure 2- right to avoid friction against the pillar of the scapula. The metaglenoid is concave, adapting to the normal curvature of the glenoid fossa. In an experimental work, DeWilde et al. 2004 has confirmed that medialization and lowering the implant affect the moment arm of the deltoid and improve the arc of rotation, which is essential in performing activities of daily life.



Figure 2-: left: Universelle Arrow System, right: Inbuilt medial notch on humeral cup- Katz 2007

Valenti 2006 presented the results of a comparative study of 40 DELTA and 40 ARROW prosthesis on a French Congress of Orthopaedic Surgery in Paris in Nov 2006. It was shown that ARROW SYSTEM allowed for less medialization but that the extent of humeral lowering was the same with both systems. With a minimum follow-up of 12 months, the ARROW series did not show any signs of scapular notching or glenoid loosening, while the Delta group showed notching in 62%.

2.4 Complications in surgical treatment

Surgical treatment always creates various problems after shoulder replacement. Some of these problems are only related to medical situation but others are directly related to our objective of study.

- **Infection.**
- **Stiffness:** Patients may experience stiffness in the shoulder joint after surgery. This stiffness usually resolves with time and physical therapy.
- **Fracture:** The humerus or glenoid can crack when preparing the bone for insertion of the components, actually inserting the components, or even years after the surgery. Fractures usually are treated with metal cables or a plate, and usually heal.
- **Component Loosening:** Occasional the bone will not grow into the implanted components. The components may loosen and change position. Component loosening can occur years after the surgery from wear debris from the plastic liner. The motion of the loose component may cause pain and require another surgery to revise the components.
- **Nerve Injury:** Although extremely rare, nerves to your shoulder, arm and hand can occasional be injured. These nerves may or may not recover by themselves. If they do not, you may be left with a weak arm.
- **Bleeding:** Rarely, the blood vessels around the shoulder are damaged by the surgery and excessive bleeding occurs after or during the surgery, requiring additional surgery. Occasionally, blood gathers in the shoulder even if no major blood vessel is damaged and further surgery (or observation) is required to correct the problem.
- **Blood Clots:** Blood clots in your arm veins are possible after any surgery on the upper extremities. The occurrence of blood clots can be minimized with blood thinners and early mobilization. The main danger of blood clots is if they dislodge and travel to your veins in your lungs. This phenomenon is called a pulmonary embolus and can result in

respiratory difficulty, chest pain, or even death. Blood clots may or may not hurt or cause swelling in your arm.

- **Osteolysis:** Polyethylene bearings can wear over many years and cause osteolysis which is the body's response to the plastic wear debris from the shoulder replacement. The body tends to attack the tiny plastic particles and inadvertently causes the bone around the shoulder joint to weaken. The weakened bone can lead to fractures or component loosening.
- **Dislocation:** The humeral head rarely can dislocate from the glenoid component. Occasionally, unstable shoulder replacements need to be revised to correct this condition if it keeps occurring.
- **Need for Further Surgery:** Though uncommon, shoulder replacements occasionally fail sooner than expected. Some other problems can also make further surgery necessary, including: bone forming where it should not, breaking of the bone around the prosthesis (during or after surgery), and irritation of the soft tissues by wire or sutures.
- **Death:** Though very rarely, patients have died following shoulder replacements. This can be due to underlying medical or heart problems that arise or worsen after the surgery. It can also be due to blood clots travelling to the lungs as mentioned above, or from the stress placed on the body by more than the usual amount of bleeding.

In the list above only some of complications are directly related to our aim of study and the rest of them is related to medical part but indirectly could affect our research. Here the biomechanical complications of the shoulder surgery will be discussed briefly.

2.4.1 Glenoid Implant Loosening

The short term to mid-term outcomes (postoperative to 5 years) of TSA have shown excellent to good clinical results as shown by Neer and Morrison 1988 where out of 19 patients 89% showed excellent to good results. Similarly Gill et al. (1999) found 88% of patients (15 out of 17) had excellent or better pain relief. Collins et al. (2004) found in 25 TSA shoulders, all subjects experience better pain relief and function. Cofield (1984) publicised a mid-term study (2-6 years) of 73 shoulders showing 92% of patients found an improvement to pain, Torchia et al. (1997) showed 81% of the 89 patients had improved with regards to pain after 5-17 years follow-up. It is clear that the short-term outcomes of TSA are very good.

However more mid-term results reveal some of the problems in TSA as shown by Hill and Norris (2001) who investigated the follow up of 14 patients after an average of 5.8 years showing 9 patients (64%) with good to satisfactory outcome whereas 5 (36%) were unsatisfactory with 2 (21%) failing due to glenoid loosening, requiring re-surgery. Instability and loosening accounted for the majority of the complications. Martin et al. (2005) show TSA failure occurred in 16 out of 140 shoulders (11%) from which 5 were due to loosening of the glenoid implant. Comparatively in a paper by Wallace et al. (1999), out of 86 shoulders, 14 showed complications (16%) with 8 (9%) requiring revision, however loosening was not a cause for re-surgery. A retrieval study by Scarlat and Matsen (2001) investigated 37 retrieved implants. The authors found the cause for re-surgery for 95% (18/19) of the glenoid were due to instability and loosening.

2.4.2 Causes of Loosening- Area of failure

Information on loosened glenoid and retrieved glenoid are few. However some papers have touched on this, such as Wirth et al. (1999) who investigated the wear particles of UHMWPE in three cases of retrieved glenoid 10 to 16 years postoperatively due to aseptic loosening. The conditions of the loosened keel glenoid (the fixation site) were described as “the cement was mainly attached to the keel of the glenoid component although some cement was recovered from the glenoid trough”. This indicates the glenoid fixation detached mainly from the cement/bone interface at the keel but also partially from the implant/cement interface. However it is still not clear which of the two interfaces are more resistant to failure and which interface fails first in-vivo. Similarly, photos of a retrieved glenoid in a paper by Yian et al. 2005 indicate the cement partially covering the glenoid back and pegs (Figure 2-). However, Nyffeler et al. 2003 demonstrated failure completely at the implant/cement interface from one retrieval case (Figure 2-). With the few retrieval studies published, most have focused on the surface wear.



Figure 2-: Before implantation (left) & retrieved threaded implant (right) showing partially intact cement at the pegs (Yian et al. 2005).

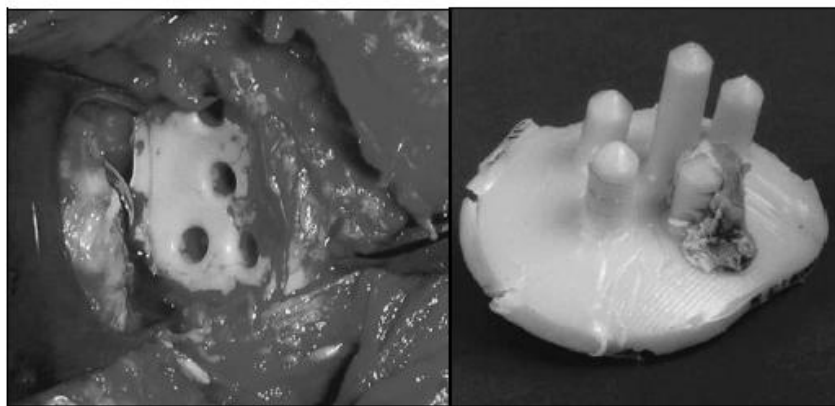


Figure 2-: Revision surgery showing cement intact with the glenoid bone (left) & retrieved glenoid showing failure occurring at the implant/cement interface (right) (Nyffeler et al. 2003)

PMMA bone cement failure is believed by some authors to contribute to fixation failure (Lacroix & Prendergast 1997). The material properties of bone cement have also been shown to be weak under tension, particularly under fatigue loading (Wixson et al. 1987). Many of these studies are FE based; however, clinically there is no mention of such failure. The variability of the cement mantle thickness is notoriously varied and cement cracks from the retrieval photos (Figure 2-) are evident. However, this may be a result of another failure elsewhere in the fixation. Thus some comments on the nature of fixation failure have not been conclusive and warrant further study.

Clinical studies, using radiolucent lines (r. lines) have associated the appearance of r. lines as a loss of fixation, either by a physical interfacial gap or by the formation of fibro-cartilage tissue, indicating glenoid loosening as a cement/bone interface problem (Bohsali et al. 2006; Matsen III et al. 2008). Despite the correlation between a complete lucent line around the glenoid implant

and loosening of the glenoid (Torchia et al. 1997), the emergence of r. lines is yet to be fully understood.

2.4.3 Causes of Loosening - Interface strength and material strength

Mann et al. 1999 tested the cement/bone interface in tension and shear in tibia bone and found the interface is weak under tensile loads (1.35 MPa and 2.25 MPa respectively). Mixed-mode failure of the cement/bone interface under tensile and shear loads showed an increase in strength compared to pure tensile loads (Mann et al. 2001). Perhaps this raises questions as to what the predominating loads are at the interfaces during loading.

However, there are no published studies on the cement/bone strength in glenoid bone and the implant/cement interface strength. A study by Sanghavi (Sanghavi et al. 2007) has shown the interface strength between PE of roughness varying from 0 m to 5.55 ± 0.37 m and cement to be 0 to 3.2 MPa respectively. The interface strength \pm SD between cadaveric glenoid bone and cement was found to be 3 ± 1.4 MPa compared to the interface between cement and bone substitute of minimum 2.32 ± 0.54 MPa.

Many studies on the tensile, compressive and fatigue properties of PMMA and other commercially available bone cements have been published (Krause & Hoffman 1989; Lewis 1997; Linden et al. 1989; Wixson et al. 1987). The considerably lower tensile fatigue strength of cement compared to the materials quasi-static tensile strength has led some to believe cement as one of the problems in fixation failure. Fatigue tests to 100,000 cycles, or the equivalent of 20 arm abductions a day for 13.5 years have shown that the tensile strength of the cement has been reduced from 27.1MPa to as low as 6MPa (Krause & Mathis 1988; Krause & Hoffman 1989), a problem that is predicted to arise at long-term results. However, it is still clear glenoid fixations are being lost at mid-term outcomes, indicating to a much earlier problem than cement fatigue. Therefore the awareness of interfacial strengths under static and fatigue loads is important when investigating fixation performance.

2.4.4 Causes of Loosening- osteolysis

Osteolysis, defined as an immune response to foreign particles, such as polymer or metallic particulates, present at the bone/cement or bone/implant interface, resulting in resorption of bone round the implant. This leads to loss of the implant fixation and eventual loosening. This phenomenon was particularly prevalent in early hip replacements where high PE wear of the

acetabular cup caused PE particulate build up at the joint, particularly at the cement/bone interface, leading to osteolysis and loosening.

Although osteolysis is a concern across all implanted PE (Polyethylene) bearing surfaces, the short term complications in TSA indicate wear is not the primary problem (loosening and osteolysis are considered primary problems). Furthermore, due to lower bearing loads at the shoulder, it is rather joint stability and loosening, which are the most common complications. The primary problem is the glenoid loosening.

2.4.5 Notching of the inferior scapula

One of the most common complications after implantation of the reverse prosthesis is notching of the inferior scapula by the humeral component (Figure 2-11). This notching is believed to be due to contact between the proximal portion of the humeral component and the inferior scapula. This notching has been classified by Nerot [Sirveaux et al. 2004 &Valenti et al. 2001] (Figure 2-11) and appears soon after implantation, usually becoming stable after 1 year in most patients [Werner 2005]. There remains controversy over whether this notching produces clinical symptoms [Werner 2005].

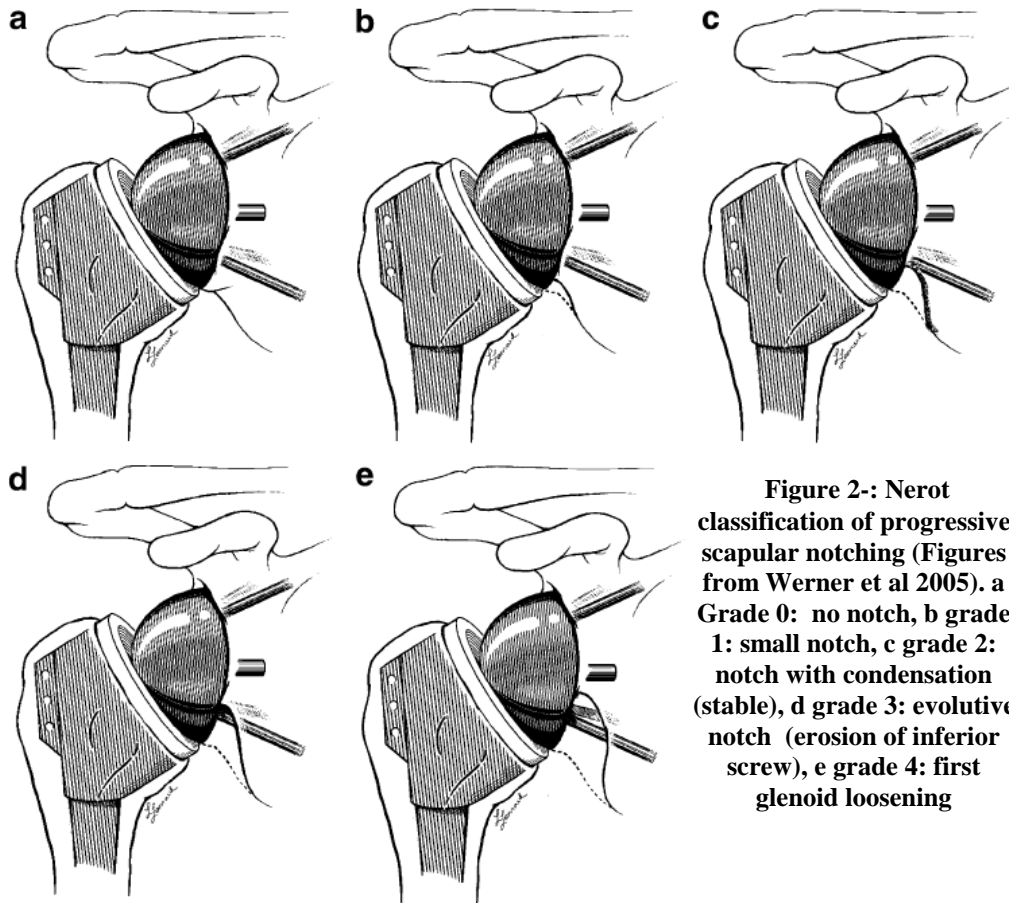


Figure 2-: Nerot classification of progressive scapular notching (Figures from Werner et al 2005). a Grade 0: no notch, b grade 1: small notch, c grade 2: notch with condensation (stable), d grade 3: evolute notch (erosion of inferior screw), e grade 4: first glenoid loosening

2.4.6 Dislocation of prosthesis

Another complication seen with the reverse prosthesis is dislocation of the prosthesis (Figure 2-). Radiographs at right angles to each other are necessary to make this diagnosis (Figure 2-). Instability of the prosthesis may be due to inadequate soft-tissue tension, malpositioning of the components or loosening of the components with movement.

Figure 2- Left: An 82-year-old woman who underwent reverse shoulder arthroplasty (Tornier System) 7 months prior. She experienced immediate onset of pain when putting lotion on her head in an abducted and externally rotated shoulder position. Oblique radiograph of the right shoulder showing a dislocation of the reverse prosthesis 493. Right-a: Anteroposterior radiograph of the right shoulder showing a different patient with dislocation of the reverse prosthesis. Right-b: Axillary radiograph in the same patient showing the dislocated prosthesis (Tornier System).

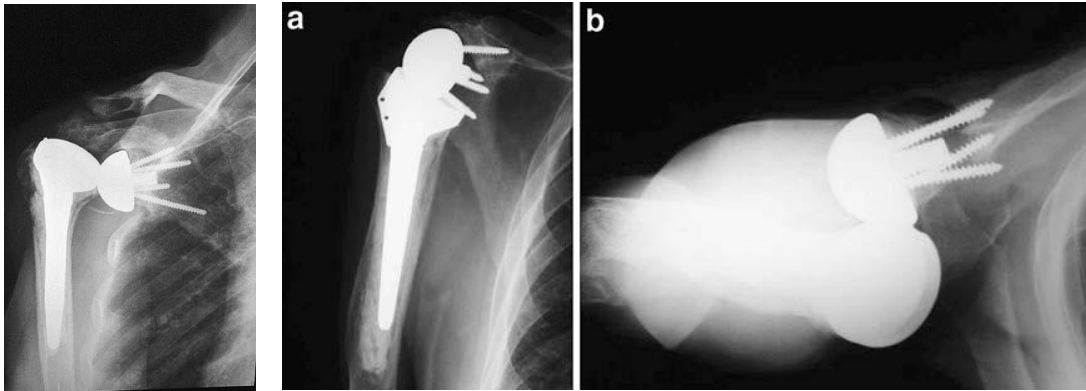


Figure 2-: left: An 82-year-old woman who underwent reverse shoulder arthroplasty (Tornier System). Right-a: Anteroposterior radiograph of the right shoulder. Right-b: Axillary radiograph in the same patient showing the dislocated prosthesis (Tornier System)

2.4.7 Dislodgement of the base plat

Dislodgement of the base plate has been seen. When the baseplate fixation fails, the glenoid plate and sphere may shift and move. Although screw failures can be seen, they may indicate impending failure of the base plate (McFarland et al. 2006) (Figure 2- Left: Antero-posterior radiograph of the right shoulder showing a fractured screw of the glenoid baseplate, which in this case is associated with superior migration of the glenoid base plate (Tornier System)).

2.4.8 Acromial fractures

Acromial stress fractures have been reported with the use of the reverse prosthesis (Figure 2- Right: A 65-year-old man who underwent reverse shoulder prosthesis placement (Tornier System) due to rotator-cuff arthropathy. Four months after surgery, he had significant pain in his shoulder, predominantly posteriorly. He denied a history of trauma. Axillary plain radiograph of the right shoulder shows an acromial stress fracture (arrow) [McFarland et al. 2006]). These are believed to be due to increased stress upon the posterior aspect of the acromion from the configuration of the prosthesis (McFarland et al. 2006).

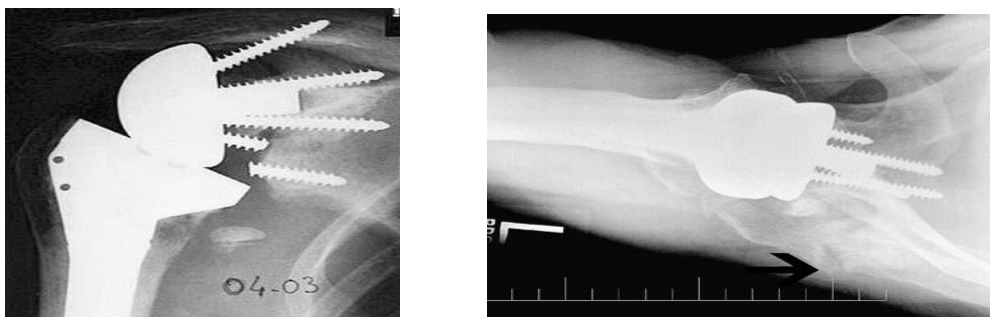


Figure 2-: Left: Anteroposterior radiograph of the right shoulder. Right: A 65-year-old man who underwent reverse shoulder prosthesis placement (Tornier System) due to rotator-cuff arthropathy (McFarland et al. 2006).

2.4.9 Humeral side complications

The humeral component stem appears much like a standard total shoulder stem except that it tends to be wider proximally near the upper end of the humerus. Humeral side complications are uncommon, but include radiolucencies, subsidence of the humeral component if uncemented (Sirveaux 2004, Werner et al. 2005), and fracture.

2.5 Finite Element Analysis (FEA) of shoulder implants

As discussed in the section 2.4 surgical treatment specially shoulder arthroplasty, could cause various problems after shoulder replacement. Some of these issues inevitable and are only related to medical situation (Infection, bleeding, blood cuts, etc). However many others could possibly be prevented by design, simulation and Finite element analysis prior a surgery such as failure and fracture, loosening and dislocation of the joints, etc. This part of the problems directly relate to our objective of study. FEA simulation would give an indication to where the most common areas of failure on both bone and implant; this to avoid bone and implant failure post-operatively and allow for an implant redesign or change the implant positioning. In addition, most of the time, the long term effect of a prosthesis could be predicted by realistic FE simulations; this could help preventing future problems. This kind of analysis potentially provides an insight into the mechanical behaviour of an implanted scapula or humerus head according to different parameters related to implantation technique.

Moreover, Glenoid component fixation can present the most difficult problem in total shoulder arthroplasty, loosening of this component remains one of the main complications in this field. It is presumed that loosening in the glenoid is caused by high stresses in the cement layer. Several anchorage systems have been designed with the aim of reducing the loosening rate, the two major categories being "keeled" fixation and "pegged" fixation (Figure 2-). Figure 2- shows A: Postoperative radiograph of a keeled glenoid component (grade 0 lucency). B: Twelve-month follow-up radiograph of the same keeled component demonstrating grade 3 lucency. C, D: Postoperative radiograph of a pegged glenoid component (grade 0 lucency). (T. Bradley Edwards et al, 2010).

Locroix et al 2000, studied the stresses level in the cement layer and surrounding bone for glenoid replacement components. A three-dimensional model of the scapula was generated using CT data for geometry and material property definition. Keeled and pegged designs were inserted

into the glenoid, surrounded by a 1-mm layer of bone cement. A 90 deg arm abduction load with a full muscle and joint load was applied, following van der Helm 1994. Deformations of the prosthesis, stresses in the cement, and stresses in the bone were calculated. Stresses were also calculated for a simulated case of rheumatoid arthritis (RA) in which bone properties were modified to reflect that condition. A maximum principal stress-based failure model was used to predict what quantity of the cement is at risk of failure at the levels of stress computed.

Loxriox et al 2000, found out 94 percent (pegged prosthesis) and 68 percent (keeled prosthesis) of the cement has a greater than 95 percent probability of survival in normal bone. In RA bone, however, the situation is reversed where 86 percent (pegged prosthesis) and 99 percent (keeled prosthesis) of the cement has a greater than 95 percent probability of survival. Bone stresses are shown to be not much affected by the prosthesis design, except at the tip of the central peg or keel. It is concluded that a "pegged" anchorage system is superior for normal bone, whereas a "keeled" anchorage system is superior for RA bone.

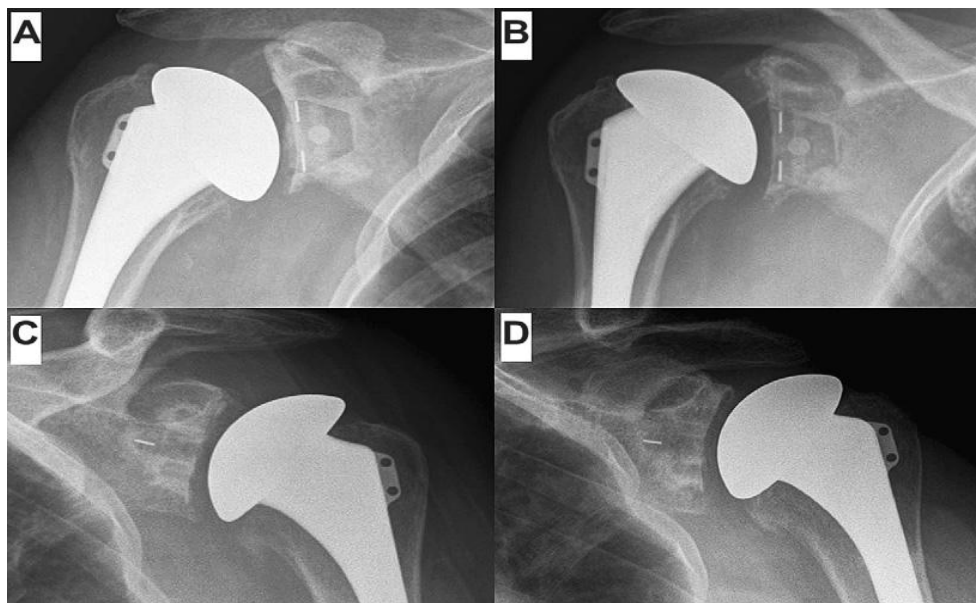


Figure 2-: A: Postoperative radiograph of a keeled glenoid component (grade 0 lucency). B: Twelve-month follow-up radiograph of the same keeled component demonstrating grade 3 lucency. C, D: Postoperative radiograph of a pegged glenoid component (grade 0 lucency). T. Bradley Edwards et al, 2010.

Couteau et. al 2001 analyzed the mechanical effect of some of the surgical variables encountered during shoulder arthroplasty using the finite element method. The effect of one eccentric load case, cement thickness and conformity has been investigated. They designed a 3D finite element model of a healthy cadaveric scapula implanted with an anatomically shaped glenoid from

computed tomography (CT) images. The 3D finite element model was first validated by comparison with experimental measurements and by fitting of the mechanical properties of the cortical bone. Then the articular pressure location, the surface contact geometry and the cement thickness have been analyzed to observe their effect on stresses and displacements at the interfaces and within the scapular bone.

Couteau et al. 2001 found out the antero-posterior bending of the scapula was a notable feature and this was accentuated when an eccentric load was applied. The gleno-humeral contact area had a major role on the stress level in the supporting structures though but not on the global displacements. Varying the cement mantle modified stresses according to the load case and it essentially changed the latero-medial displacement of the cement relatively to the bone. Conformity decreasing may involve drastic increase of stresses within structures and a thick cement mantle is not necessarily advantageous relatively to the stresses at the cement/bone interface. They demonstrated the importance of the humeral head centring in the horizontal plane. Also Results emphasized the role of some of the parameters a clinician may face.

Mansat et al 2007 creates a finite element biomechanical model of an in vivo scapula. The effect of eccentric loading was analyzed on a keel glenoid and a peg glenoid implant. Results indicated that eccentric loading greatly increases stresses in the cement mantle at the bone-cement interface, and no significant difference was predicted between keel and peg implants. The results suggested that eccentric loading is a likely cause for initiation of cracks in the cement layer especially on the posterior side. Moreover, these results, compared with other studies, indicate that geometric and bone properties of the scapula may be more important factors in the success of shoulder arthroplasty than implant design.

Gupta et al 2004, firstly determined the initial stress distributions within an un-cemented implanted glenoid during elevation of the arm and to investigate whether failure is caused by stresses generated within this implant-bone structure. And secondly Compared stress patterns between the un-cemented design and two basic models of cemented prosthesis. They developed a 3-D finite element submodel an un-cemented prosthesis was generated using CT-scan data and realistic loading conditions (humeral abduction, 30-180 degrees). The submodelling approach was based on an overall solution of a complete scapula acted upon by all muscles, ligaments and joint reaction forces.

Gupat et al found out that a high Von Mises stresses (20-70 MPa) were generated in the metal-backing during abduction. Stresses were reduced in the polyethylene cup by 17-20% as compared to the cemented designs. Stresses in the underlying bone were substantially lower than to the natural glenoid. Stress-shielding can be observed in the trabecular bone underlying the prosthesis. The implant-bone interface is secure against interface failure at moderate loads, although the implant-bone (metal-bone) interface around the superior edge of the prosthesis is subject to high stresses (normal: 11.85 MPa, shear: 6.67 MPa) as compared to the cemented prosthesis. Nevertheless, the cement-bone interface appears more likely to fail either at locations adjacent to the keel or at locations around the superior edge of the cemented design. The uncemented design therefore appeared to be a reasonable alternative to fixation with cement.

Nazeem et.al 2007 developed biomechanical and finite element models, using high-strength polyurethane foam blocks, to represent the glenoid bone/base plate junction to determine if increasing the distance between the glenoid bone and the centre of rotation of the glenosphere increases base plate motion during static loading in the reverse shoulder design. They found out, although there was a general trend toward increased base plate motion with increasing distance from the glenoid to the centre of rotation, in vitro mechanical testing revealed no significant difference between the 7 glenosphere types tested, with average base plate motion during 1000 load cycles ranging from 90 μm to 120 μm . Results from the finite element analysis strongly correlated with the in vitro mechanical testing. The magnitude of base plate motion occurring in a modelled representation of bone under simulated physiologic loading conditions was similar for the 7 reverse shoulder glenoid components tested in this study.

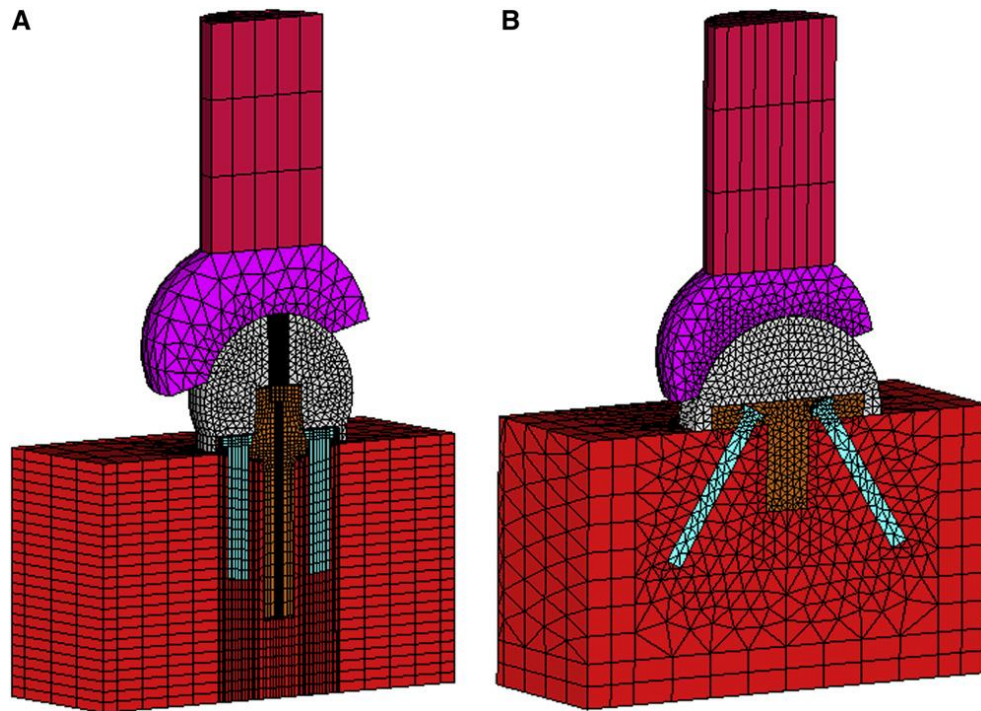


Figure 2-: Finite element models of the (A) the Reverse Shoulder Prosthesis (32-mm neutral) and (B) the Delta III. (Nazeem et al 2008).

As the literature shows most of the problem arise from fixation and the loosening of the implant in the glenoid section. In this section we discussed how finite element could help surgeon to choose appropriate implant and compare their functionality before using in a real case which probably causes irreversible problems for the patient. In the chapter 6 it will be shown how finite element and 3D simulation has been used to study the micro motion of the Verso joint in a body.

A FEA study by Hopkins and Hansen, 2009, on a group of reverse shoulder implants including Delta III, Zimmer, Bayley-Walker, RSP-neutral, RSP-reduced and Verso has shown that two out of six existing reverse shoulder implants were stable and reliable. The study has aimed to determine the capability of six existing glenoid devices to resist interface motions under loading (Figure 2-). The predicted extent of bony on-growth was dependent on the maximum permitted interface micro-motion, and in some instances an additional 30 per cent of the interface was predicted to promote bone on-growth when the threshold was raised from 20mm to 50mm. When the maximum threshold for micro-motion that would still permit bone on-growth was set to 20mm or 30mm, the Zimmer Anatomical device was found to be the most stable of the series of the six designs tested herein, achieving up to an additional 8 per cent (by surface area) of bone on-growth above the closest peer product (Biomet Verso). When this threshold was raised to 40mm, the Biomet Verso design was most stable (3 per cent above the second-most stable

design, the Zimmer Anatomical). The Encore RSP designs showed the greatest benefit from an increased threshold for bone on-growth, where raising the threshold from 20mm to 50mm increased the area of predicted bone on-growth by approximately 40 per cent for both designs.

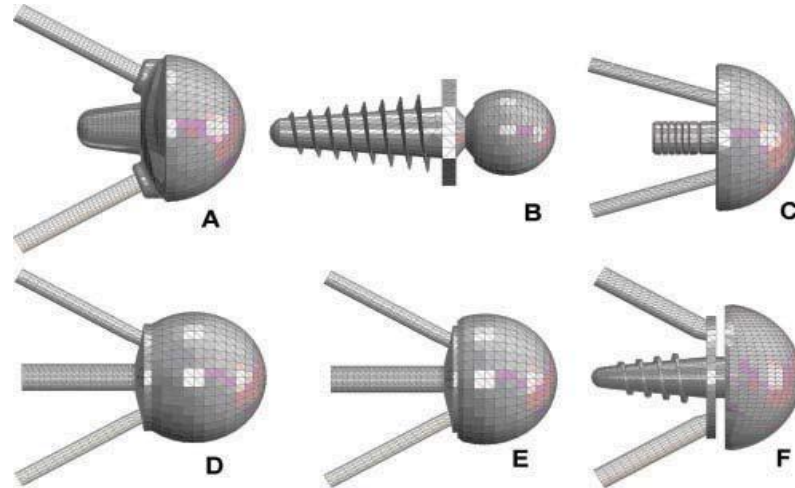


Figure 2-: FE models of the reversed-anatomy glenoid components (with screws) tested in this study: (a) Anatomical (Zimmer); (b) Bayley–Walker(Stanmore); (c) Delta III (Depuy); (d) RSPneutral (Encore); (e) RSP-reduced (Encore); (f) Verso (Biomet)

2.6 Conclusion

Cuff tears arthropathy and the cuff-deficient shoulder present unique challenges for both the patient and orthopaedic surgeon. Early unconstrained shoulder arthroplasty systems suffered high complication and implant failure rates. The evolution toward the modern reverse shoulder arthroplasty includes many variables of constrained shoulder arthroplasty designs. This review explored the development of reverse shoulder arthroplasty, specifically describing (1) the evolution of reverse shoulder arthroplasty designs, (2) the biomechanical variations in the evolution of this arthroplasty, and (3) the current issues relevant to reverse shoulder arthroplasty.

Reverse shoulder arthroplasty now presents an option for some patients with cuff tear arthropathy and a cuff-deficient shoulder. The current indications for this prosthesis generally include patients with painful cuff tear arthropathy and pseudoparalysis, proximal humerus fractures in the older patient with poor bone or cuff quality, tumor involving the proximal humerus requiring glenohumeral reconstruction, and revision arthroplasty in the setting of tuberosity nonunion or irreparable rotator cuff tear. Contraindications include axillary nerve deficit such that deltoid function is inadequate, active infection, inadequate glenoid bone stock to secure the glenoid component, and perhaps the younger patient. These indications and contraindications continue to be debated, such as how one defines pseudoparalysis and at what

age a patient is “too young” for a reverse shoulder arthroplasty; as the model geometry will differ accordingly. Guery et al. 2006, Sirveaux et al. 2004, wall et al. 2007, Werner et al. 2005 demonstrated the possible outcome improvement for reverse shoulder arthroplasty. The improvements in pain and ROM (Range Of Motion) have therefore made reverse arthroplasty an increasingly commonly selected option for patients and subject for study.

Reverse total shoulder arthroplasty prosthesis today vary in certain design details, although their intrinsic design remains based on Grammont’s principles. The variables in the current prosthesis have been developed to address concerns that have arisen with reverse shoulder arthroplasty. The persistent problems and high complication rate with this procedure have been described extensively in the current literature, with complications including hematoma formation (Werner et al. 2005), infection (Boileau et al. 2005, Frankle et al. 2005, Guery et al. 2006, Sirveaux et al. 2004, Werner et al. 2005, Wierks et al. 2009), scapular notching (Levigne et al. 2008, Simovitch et al. 2007, Sirveaux et al. 2004, Wierks et al. 2009), instability (Guery et al. 2006, Werner et al. 2005, Wierks et al. 2009), acromial insufficiency (Frankle et al. 2005, Werner et al. 2005), and glenoid component failures (Fenlin et al. 1985, Gristina et al. 1982, Reeves et al. 1972, Sirveaux et al. 2004). Additionally, complications and patient satisfaction vary among primary cuff tear arthroplasty, revision cases, and fractures (Boileau et al. 2005, Frankle et al. 2005, Guery et al. 2006, Sirveaux et al. 2004, Werner et al. 2005, Wierks et al. 2009). The followup available has demonstrated declining radiographic and clinical results after 6 to 8 years (Guery et al. 2006).

As the study of reverse shoulder arthroplasty has advanced and varying systems have developed, vibrant controversies have arisen. Debate exists over the medialization of the centre of rotation, with some proposing a more lateral offset (Frankle et al. 2005). Proponents of the more lateral centre of rotation point to a lower rate of scapular notching and an increase in impingement-free motion (Sperling et al. 1982). Others suggest notching may also be minimized with appropriate positioning of the more medial glenoid component (Simovitch et al. 2007). These issues require additional high-quality studies and must continue to be explored and debated.

Certainly the development of the modern reverse total shoulder arthroplasty is an interesting and important aspect of orthopaedic surgery. Modern designs do have a high complication rate, and this procedure remains one that must be offered judiciously. Ongoing study and advancements in design are focused at addressing the challenges of this procedure.

Chapter 3. Verso Shoulder Implant

3.1 Introduction

In retrospect the Verso has been developed from designs of the reverse shoulder implant by Dr. Paul Grammont in 1987, the design has been proven to be more effective when dealing with rotator cuff tears which are also linked to arthritis. The study did look for stress, strain and displacement distribution around the weakened cavities (Grammont et. Al, 1987).

This Chapter will discuss the reverse shoulder implant used in hospitals. Specifically the Verso shoulder implant designed by Biomet Ltd.

This chapter will introduce the reverse shoulder arthroplasty, the symptoms and methods of treatment available for patients with rotator cuff tears. The range of motion for the shoulder joint post-operative will be highlighted.

Moreover, the complications that can occur post-operation for patients will be discussed. The chapter also, gives overview to the procedure prior to discussing this project theory and analysis procedures. **The surgery of traditional reverse shoulder implant (Delta III) and Verso shoulder implant were presented in Appendix B*.*

3.2 Reverse Shoulder Arthropathy:

3.2.1 Symptoms and Methods of Treatment

The shoulder joint is a ball and socket joints, which consists of a ball and rotator cuff. The rotator cuff is the group of tendons and muscles that surround the shoulder joint. These muscles and tendons have a critical role to keep the ball of the joint at the centre of the rotator cuff. Rotator cuff tear arthropathy limits the shoulder task and performances (such as lifting the arm overhead) and cause a pain on shoulder joint. This problem is normally occurred when a patient has both shoulder arthritis and an irreparable rotator cuff tear as shown in Figure 3-.



Figure 3-: Humeral head damaged and degenerative by Arthritis

Condition of losing the rotator cuff tendons and damage of the natural joint surface of the shoulder is a very painful and devastating situation, which seriously reduce the mobility and comfort of the shoulder joint. And as these parts cannot be restored, the shoulder most of the time become weaker and more unstable. Also this situation will be very painful, especially when we are moving the shoulder around (Seebauer, Walter, Keyl, 2005).

Reversed total shoulder arthroplasty design as shown in Figure 3- and using special techniques enable qualified surgeons to improve the stability and domain of the movement of the shoulder. And also this method of surgery increases the power of the deltoid muscle, even in the absence of a normal rotator cuff and cases to reduce or to eliminate the joints pain.



Figure 3- : Traditional Reverse Shoulder Implant [Delta]. Verso Shoulder Implant by Biomet

The reverse total shoulder replacement arthroplasty create a new way for incurable conditions in shoulder joint diseases and enable the experienced surgeons to treat their patients with rotator cuff tear with a nearly reliable method. Although the reverse shoulder replacement was specifically designed for the rotator cuff tear arthropathy, these days surgeon uses this method in various shoulder problems. These problems include rotator cuff tear arthropathy, instability with

anterosuperior escape, pseudoparalysis, and failures of surgery for arthritis and fracture management. Figure 3- shows the traditional reverse shoulder implant in a patient's shoulder (Grammont, Baulot, 1993), (Matsen, III, Boileau, Walch, 2007).

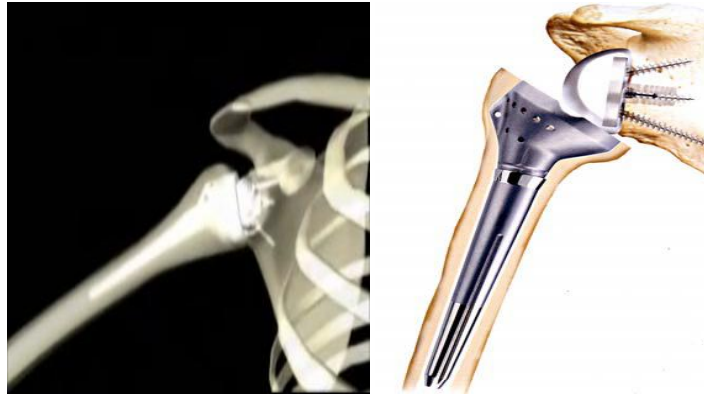


Figure 3- : Traditional reverse shoulder implant

However, as reported in that in a traditional shoulder replacement, the ball of the top of the arm bone (the humerus) is resurfaced or replaced with a metal ball. The socket of the shoulder blade (scapula) may be retained or replaced with a plastic socket. The absence of a rotator cuff causes the implant to move abnormally resulting in unusual forces on the artificial joint. This leads to a poor functional result and early failure of the replaced joint (Guery, Favard, Sirveaux, Oudet, Mole, Walch, 2006).

In the reverse shoulder replacement, although surgeon uses a ball-and-socket joint like in the previous method, the ball is placed on the shoulder blade, and the socket is placed on top of the arm bone. This method is the reverse of the natural anatomy of the shoulder joint, and for that reason, the name "reverse shoulder replacement" is chosen. Of course the method of reverse shoulder replacement is designed for patients who do not have a functioning rotator cuff, and therefore do not have "normal" shoulder anatomy. By reversing the ball and the socket of the joint, the large deltoid muscle which forms the contour of the shoulder becomes more efficient mechanically and is able to lift the arm up overhead, to compensate for the torn rotator cuff. In addition using this method causes to change the centre of rotation in the shoulder joint, which facilitate movements of the hand.

3.2.2 The Diagnosis

The doctor can diagnose degenerative changes in the shoulder by conducting a physical examination. Patient informs the doctor about his/her symptoms and level of pain. The examination will include performing simple arm and shoulder movements to help the doctor assess patient's muscle strength, joint motion, and joint stability.

X-rays help determine the condition of patient's shoulder bones and show abnormal bone growths (bone spurs), as well as loss of joint cartilage. Advanced imaging tests, such as a computed tomography (CT) scan or magnetic resonance imaging (MRI)² scan may be ordered for a more detailed view (Boulaia, Edwards, Walch, Baratta, 2002).

3.3 Verso Shoulder Implant

The Verso implant has been first clinically in use in 2005 and since then there were no lucencies (bone fracture is visible) or glenoid notching was reported. It uses Stemless Prosthesis which means no distal humeral canal reaming unlike the traditional reverse shoulder implant. The Verso Implant from Biomet Company is used for the same grounds of using the reverse shoulder implant. The Verso implant (Modular system) is consists of 5 parts as shown in Figure 3- (Biomet Ltd, UK, 2010).

1. HA and Titanium Porous Coated Stemless Humeral Component – to promote bony in-growth and provide rotational stability, with minimal bone resection. The Stemmed Humeral Component for patients whose bone quality requires additional stability.
2. A 'Dial-able Arcom Poly Liner with proven Ringloc Liner Fixation technology – provides a low medial edge, reducing potential of notching.
3. Glenoid Head with Reverse Morse Taper – provides an easy introduction of the Glenoid Head onto the Glenoid Screw, creating a strong union of components.
4. HA Coated Glenoid Base Plate with anti-rotational screws – provides a strong fixation into bone, promoting bony in-growth and increasing rotational stability.
5. High profile titanium peripheral screw(s).

² Cat scans are a specialized type of x-ray. The patient lies down on a couch which slides into a large circular opening. The x-ray tube rotates around the patient and a computer collects the results. These results are translated into images that look like a "slice" of the person. MRI is a completely different! Unlike CT it uses magnets and radio waves to create the images. No x-rays are used in an MRI scanner.

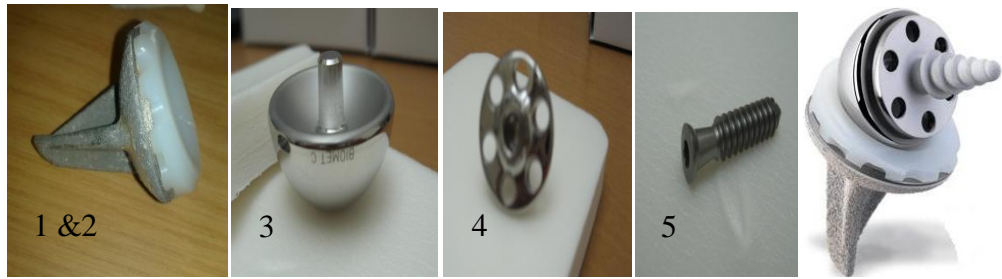


Figure 3:- Verso shoulder implant parts

This is a special bone preserving technique in a reverse shoulder replacement surgery. It follows the basic principles of reverse replacements, but is bone preserving and causes less bone erosion over the longer period. It was developed at the Reading Shoulder Unit, over a period of 10 years. The prosthesis uses special coating called hydroxyapatite that allows the bone to bond onto the prosthesis over 12 weeks, thus avoiding the use of bone cement with its problems. It has a special screw-in base plate and ball for the shoulder blade, and a short finned socket for the top of the arm bone as shown in the x-ray Figure 3- (Biomet Ltd, UK, 2010).



Figure 3- : X-Ray of Verso Shoulder Implant

The Verso shoulder joint replacement prosthesis (Biomet Ltd, UK, 2010) is used when there is:

- 1- Deficient rotator cuff with severe arthropathy.
2. Previously failed shoulder joint replacement with a deficient rotator cuff.
3. Functional deltoid muscle.
4. Primary, fracture, or revision total shoulder replacement for the relief of pain and significant disability due to gross rotator cuff deficiency. All components of Verso shoulder are indicated for cementless fixation. The glenoid base plate components are intended for cementless application with the addition of screw fixation.

3.4 Verso Implant Complications

As with all surgery there is a risk of some complications. These are rare, but you should be aware of them before your operation. They include: Complications relating to the anaesthetic (Copeland, Levy, Sforza, 2010).

1. Infection
2. Dislocation
3. Fracture of the arm bone or the acromion
4. Unwanted prolonged pain and/or stiffness
5. Damage to the nerves or blood vessels around the shoulder.
6. Loosening and Wear
7. A need to redo the surgery.
8. Infection, sepsis and osteomyelitis.
9. Absolute contraindications include:

Relative contraindications include:

1. Osteoporosis.
2. Metabolic disorders.
3. Vascular insufficiency, muscular atrophy or neuromuscular disease.
4. Uncooperative patient or patient unwilling or unable to follow instructions.
5. Incompetent or deficient soft tissue surrounding the bone.
6. Obesity.
7. Foreign body sensitivity. Where material sensitivity is suspected, tests are to be made prior to implantation.
8. Osteomalacia.
9. Distant foci of infections which may spread to the implant site.
10. Rapid joint destruction, marked bone loss or bone restoration apparent on roentgenogram.

3.5 Range of Motion Comparison:

It's important to know the normal range of motion for each joint. This can help to determine if patient have limited or abnormal range of motion. Patients who have joint surgery must also go through extensive rehabilitation to get back to normal range of motion in the affected joint. The normal range of motion is as follows (shown previously in Figure 1- in chapter 1):

- Shoulder flexion 0°-180°
- Shoulder extension 0°-60°
- Shoulder abduction 0°-180°
- Shoulder adduction 60°-0°
- Shoulder internal rotation 0°-90°
- Shoulder external rotation 0°-90°

Using reverse shoulder enhance and change the domain of movement in the shoulder joint as in the the Reverse Shoulder Arthroplasty prosthesis reverses the orientation of the shoulder joint by replacing the glenoid fossa with a glenoid base plate and glenosphere and the humeral head with a shaft and concave cup. The direct effect of Reverse shoulder arthroplasty is that the design of this prosthesis alters the centre of rotation of the shoulder joint by moving it medially and inferiorly. However this prosthesis indirectly causes to increase the deltoid muscle tension and therefore to increase the torque produced by the deltoid (Wattanaprakornkul, Halaki, Boettcher, Cathers, Ginn, 2011).

Also the reverse shoulder changes the line of pull / action of the deltoid, which cause enhanced mechanical advantage of the deltoid compensates for the deficient Rotator Cuff (because the deltoid becomes the first elevator of the shoulder joint). These are all the results reverse shoulder arthroplasty. For instance one of the improvements is the shoulder elevation level, and often individuals are able to raise their upper extremity overhead.

There are certain guide lines the patients should follow post-operative to reach their best range of motion they can achieve. It is reported that patients with reverse shoulder arthroplasty can reach a range of motion typically 80° – 120° of elevation with functional External Rotation of about 30° (Magarey, Jones, 2003).

On the other hand, Verso shoulder arthroplasty also, is using the same concept as the reverse shoulder arthroplasty in reversing the anatomy of the shoulder. Accordingly the biomechanics of shoulder motion is changed as well. It was reported from the clinical study on a group of patients with Verso implant that range of motion varied from case to case. However, the range of movement reported is 132.5° degrees for elevation, 49.8° degrees for external rotation and 63.6° degrees internal rotation. So far no glenoid notching was reported (Magarey, Jones, 2003).

Moreover, expectation for range of motion gains should be set on a case-by-case basis depending upon underlying pathology. Normal/full active range of motion of the shoulder joint following reverse shoulder arthroplasty and Verso shoulder arthroplasty *is not expected*.

The following Table 3-summarized the normal shoulder range of motion versus the range of motion resulted from reverse shoulder and Verso shoulder replacement surgery (Wattanaprakornkul, Halaki, Boettcher, Cathers, Ginn, 2011).

Table 3-: Outcome for patients who had reverse shoulder replacement and Verso shoulder replacement. NR: not recorded; ROM*: range, 0-180, with the higher value indicating better functional status. RTSA: reverse total shoulder arthroplasty, Verso total shoulder arthroplasty.

	Number Of Shoulder(s)	Active Forward Elevation (Pre-operative/ (Post-operative/	Normal shoulder ROM* for Active Elevation
Boileau et al (2006) (RTSA)	45	55°/121°	0°-180°
Sirveaux et al (2004) (RTSA)	80	73°/138°	0°-180°
Wall et al (2007) (RTSA)	186	86°/137°	0°-180°
Levy et al (2011) (Verso TSA)	64	52°/132.5°	0°-180°

3.6 Summary

This chapter highlighted the total reverse shoulder arthroplasty (TRSA). The conditions, methods of treatment were discussed. The need to look for the correct centre of rotation to localise the implant to avoid future complication or reviewing the surgery is the main aim to design the reverse shoulder implant.

The traditional reverse shoulder arthroplasty is highly dependent on a cement fixation and long humeral stem. Nevertheless the reverse shoulder arthroplasty using Verso implant is cementless prosthesis. Both prostheses aim to reverse the normal shoulder joint anatomy to regain joint mobility.

However, the difference in the design between traditional reverse shoulder implant and Verso shoulder implant, claim to have a long term better results by using the Verso shoulder implant. The reverse shoulder implant has longer humeral stem that requires cement fixation, long screws

into the glenoid. The humeral head is fixed. In revision the complications using this technique reported a scapular notching, bone fracture, dislocation and glenoid notching.

Moreover, the Verso implant tried to overcome the design problem the traditional reverse implant had and design a short humeral stem with no need to cement fixation. Short glenoid screws were designed to overcome the bone fracture or dislocations of the screws. The Dial-able was designed 10° angled to overcome the glenoid notching.

However, it was reported in both prostheses cases of glenoid notching, fractures, parts dislocation, and disassociation of the glenoid head.

Regardless of the number of failed cases reported in both prostheses the concern remain in providing the patients permanent anatomical disorder a pain free joint. Also, regain the largest range of motion available and increase the life time of the implant.

Reverse shoulder arthroplasty has a significant role in the treatment of many disorders of the shoulder that have in common permanent anatomical or functional loss of the rotator cuff contributing to an unstable centre of rotation of the glenohumeral joint. Within the last five to 10 years, no topic in shoulder reconstruction was likely to assume greater importance or command more attention than reverse arthroplasty. One can easily anticipate that the scientific data pertinent to its design and application will exponentially increase. Many of today's challenges, a few of which are mentioned above, will be resolved; in their place will appear different challenges in need of their own solution.

The recipients of these endeavours—patients—will undoubtedly be gratefully rewarded in a manner consistent with the rewards that they have obtained from reverse shoulder arthroplasty in its current state. Pre-operative radiographs enable the effective use of implant templates. This information is extrapolated to the intra-operative placement of the guide pin, whose point of entry into the glenoid and angular orientation dictates the final position of the base plate and, subsequently, of the entire glenoid component.

Finally, it was discussed in this chapter the complication the patients might have to cope with this change.

Chapter 4. Data Collection and Methodology

4.1 Introduction

This chapter introduces the softwares used in this study such as Geomagic, Mimics and ABAQUS. The further section outlines the steps in finite element analysis (FEA), methodology involved in pre-processing the computed tomography (CT) scan of the shoulder joint of the patient, properties of the CT scan, generation of 3-D model of the Humerus and Scapula girdle, meshing and material assignment. At the end of this chapter there is a section about the method of experimental analysis of the implant.

4.2 Data Collection

The data used in this study were given by Biomet and Reading shoulder unit. The data were processed through Geomagic software at first to repair the geometry. The Data includes patient's CT scans and Verso Implant parts.

The geometry of the Verso has been created mainly from patients CT scans compiled together using MIMICS (Materialise). Three dimensional co-ordinates are gathered from CT scans and placed one above the other in layers. The points are then used to create layers of skins which are stitched together to complete a shell.

The model has been converted into in .STEP and .SAT files formats readable by ABAQUS where the dimensions, loads, boundary layers and material properties are applied to commence with the simulation.

The material properties of the implant parts were provided by Reading Shoulder Unit; taken from Biomet, Matweb³, Sawbone company and a study on ultra high molecular weight polyethylene carried out by S. Kurtz (Kurtz, Mazzucco, Rimnac, Schroeder, 2006).

³ <http://www.matweb.com/>

The data were processed using MIMICS software, and then export the processed data into a readable model by ABAQUS software to avoid getting errors. Figure 4-shows the flow chart of methodology of software process used in this project.

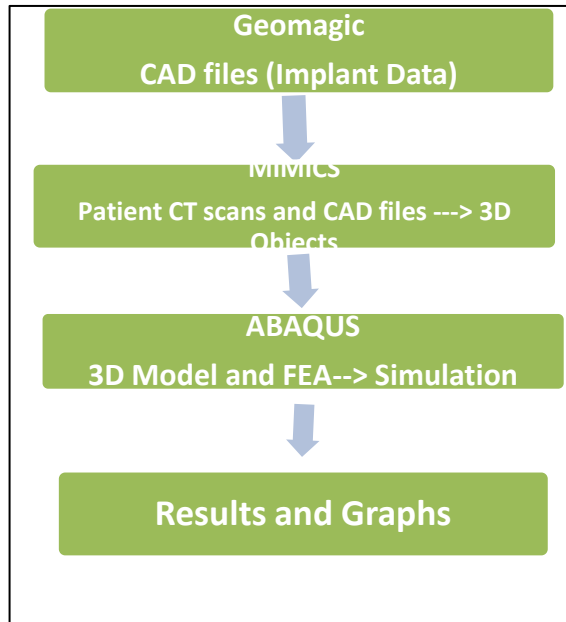


Figure 4- : Flowchart for Softwares Methodology

4.3 Body Planes

The shoulder range of movement which include Flexion and Extension, Adduction and Abduction were discussed previously in Chapter 1. It is necessary to point out the different body planes as they play an important role in using both softwares (MIMICS and ABAQUS) for the desired analysis, shown in

Figure 4-.

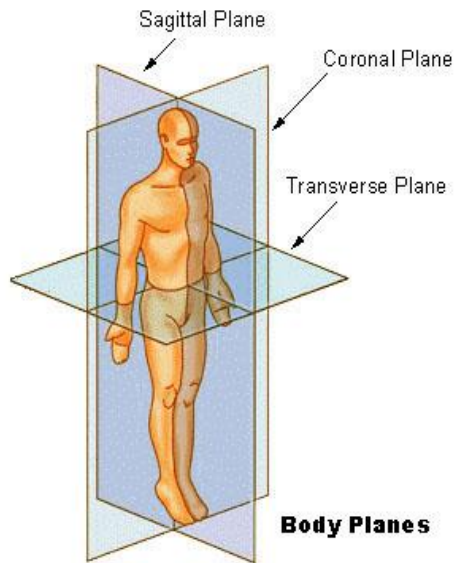


Figure 4- : Different Body Planes⁴

4.4 Methodology:

Three softwares, Geomagic studio 11, MIMICS 13.1(Materialise NV) and ABAQUS 6.9-EF1 (Simulia Daasault Systems) were used in this project.

Geomagic software repaired the surfaces of the CAD model to enable the user to get a proper geometry for the model. In addition, to make sure the number of nodes and elements can be processed by MIMICS and ABAQUS.

MIMICS is useful, in this case, for the purpose of generating 3D models of anatomical parts from medical images. The set of CT images was pre-processed within Mimics to remove artefacts and to further enhance the image quality.

The next software is ABAQUS which is commonly used to simulate the behaviour of manufacturing systems and materials. Applications include, for example, the stress, strain and loads distribution across the screws in the Verso Implant, understanding soil mechanics and predicting the effect of Verso Implant prosthesis on the Scapula and Humerus.

⁴<http://www1.apsu.edu/thompsonj/Anatomy%20&%20Physiology/2010/2010%20Exam%20Reviews/Exam%201%20Review/Ch01%20Gen%20Terms%20and%20Gen%20Anat%20Terms.htm>

4.5 Geomagic Software

The data were imported into Geomagic software as .step and .sat files. Geomagic gives the imported parts the face values used to design the implant parts. It can also be used to check the validity of the geometry of the Implant, dimensions and can separate parts from the actual model to enable the user to modify the parts before importing into MIMICS or ABAQUS. Geomagic gives an isometric view for the objects imported as shown in Figure 4-.

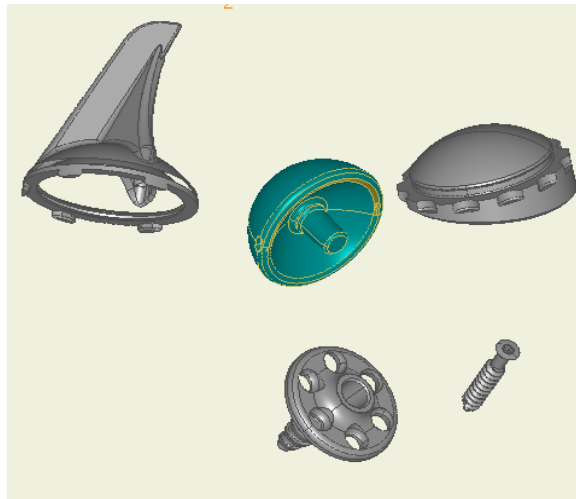


Figure 4- : Verso Implant parts in .step and .sat files in CAD model

Geomagic gives the advanced measurement assigned by Biomet and allow the user to identify the design. It gives the user a chance to adjust the dimensions to the original CAD model if needed. For example, to check the dimensions click on analysis in the menu bar and click measurement. Then identify two points in which you want to measure the part dimensions.

It gives the measurement for the peripheral screws used in this model before importing the CT scan into MIMICS as STL files. It enables modifying the sharp edges and excess number of elements which cannot be processed by ABAQUS.

4.6 MIMICS Software:

Mimics interactively read CT/MRI data in the DICOM format. Segmentation and editing tools enable the user to manipulate the data to select bone, soft tissue and skin. Once an area of interest is separated, it can be visualized in 3D. After this visualization, a file can be made to interface with STL+ or MedCAD. CAD data, imported as STL files, can be visualized in 2D and

3D for design validation based on the anatomical geometry. Mimics is made up of different modules. Figure 4.3 depicts an overview of the modules of Mimics and the links between the main program and its modules.

Mimics has the capability to do remeshing after generating the 3-D model. A volumetric mesh can also be created based on the remeshed model. The volumetric mesh, together with the material assignment can be exported to Ansys, Patran Neutral and Abaqus files and can then be used to do FE analysis on the mesh (MIMICS 13.1(Materialise NV)).

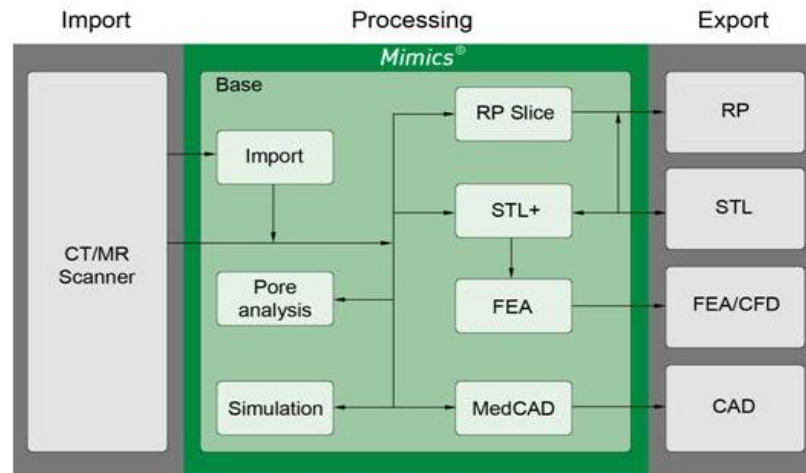


Figure 4- : Overview of the modules of Mimics

The aim of using Mimics is to generate a representative 3D surface mesh of the shoulder joint which can be exported to ABAQUS for FE analysis. In ABAQUS, the surface mesh would be converted into a volumetric mesh.

4.6.1 Import CT scan images

A CT scan was imported into MIMICS. Then segmentation for the shoulder joint only from the rest of the body was performed. This was done to create a 3D object that can be imported by ABAQUS to perform the FEA on the shoulder joint.

Import the CT scan images using automatic import wizard, since Mimics can recognise the format of the files that were used for this project. Select File -> Import Images to start the import wizard. A window will appear, containing a list of files that are automatically selected. These are the slices of the CT scan images. Click Next to continue. In the next window that appears, click on the Convert button to convert the CT images into the format required for use in Mimics.

The Change orientation dialogue box will appear. Here, define the orientation parameters by clicking on the X, indicating the missing orientation strings. Select the correct orientation of the image to the coronal and sagittal planes. Note, L and R stand for Left and Right, A and P stand for Anterior and Posterior, T and B stand for Top and Bottom. Once the orientation of the images is redefined correctly, click OK. The Mimics project opens afterwards.

The CT images loaded into Mimics can be processed to enhance the quality of the images to enable user to create a 3D model more accurately. The tools available for image processing are thresholding and region growing.

The scans were made up of 1027 cross-sectional slices with a slice distance of 0.625 mm and a field of view (FOV) of 50.00 mm. The images were exported from the CT equipment in the DICOM format with an image area of 512 x 512 pixels. The high image resolution associated with the reduced distance between slices assures a good geometrical definition and surface topography of the primary 3D models afterwards when the density segmentation operations will be performed. The actual slices that represent the Thorax (Shoulder) girdle are 81 slices.

Table 4- : Properties of the medical image data generated from CT scan

Protocol name	Thorax Shoulder
Type	CT
Pixel size	0.9766
Age	67
Tilt	0.00
Sex	Female
Resolution	512 PX
FOV	50.00 mm
Orientation	RAX
Algorithm	Bone plus 30s
Slices Distance	0.625 mm

The properties of the medical image data generated from the computed tomography scan using GE Medical systems/Light speed VCT is summarised in Table 4-shown above.

Format of files such as DICOM is known to Mimics and can be imported automatically. 1027 image slices in the DICOM format were selected and automatically imported to Mimics 13.1 (81 slices were considered representing the shoulder joint). A pixel size of 0.9766 mm was automatically computed accounting the present image resolution which was 512 x 512 pixels.

The slice distance was 0.625 mm. Indeed, the pixel size and the resolution of the image ensure the model generated is dimensionally coherent during the segmentation process. The image slices were then stacked and converted to be displayed in Coronal, Sagittal and Axial plane views. However, the orientation of each view was defined before continuing. All the images were then displayed as shown in Figure 4-

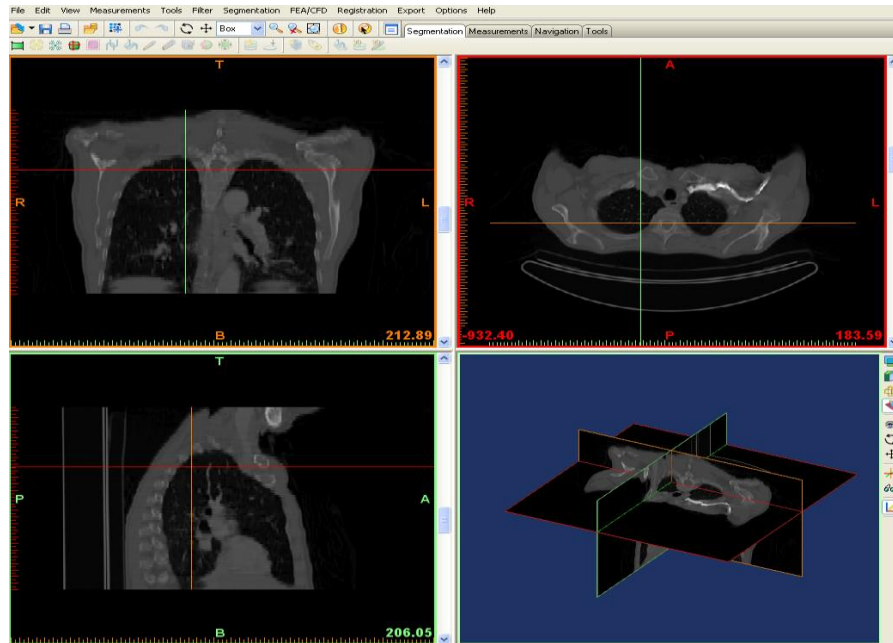


Figure 4-: Axial (top right), sagittal (bottom left) and coronal (top left) views of the pathological Shoulder joint

4.6.2 Thresholding

Thresholding is the first action performed to create a segmentation mask. The boundaries of the region of interest in that range are the lower and upper threshold value. All pixels with a grey value in that range will be highlighted in a mask.

At first a threshold for the imported CT scan images need to be set up from the tool bar. Threshold is used to create a first definition of the segmentation object. The predefined threshold allows a quick selection to a threshold for a specific tissue type. The threshold can still be adapted to the needs of the object. The threshold value can be changed by moving the sliders in the thresholding toolbar with real time visual feedback. The threshold value will be displayed in the threshold toolbar and the segmentation area is changed accordingly. There is a minimal value for the threshold and a maximum value can be set by user as shown in Figure 4-

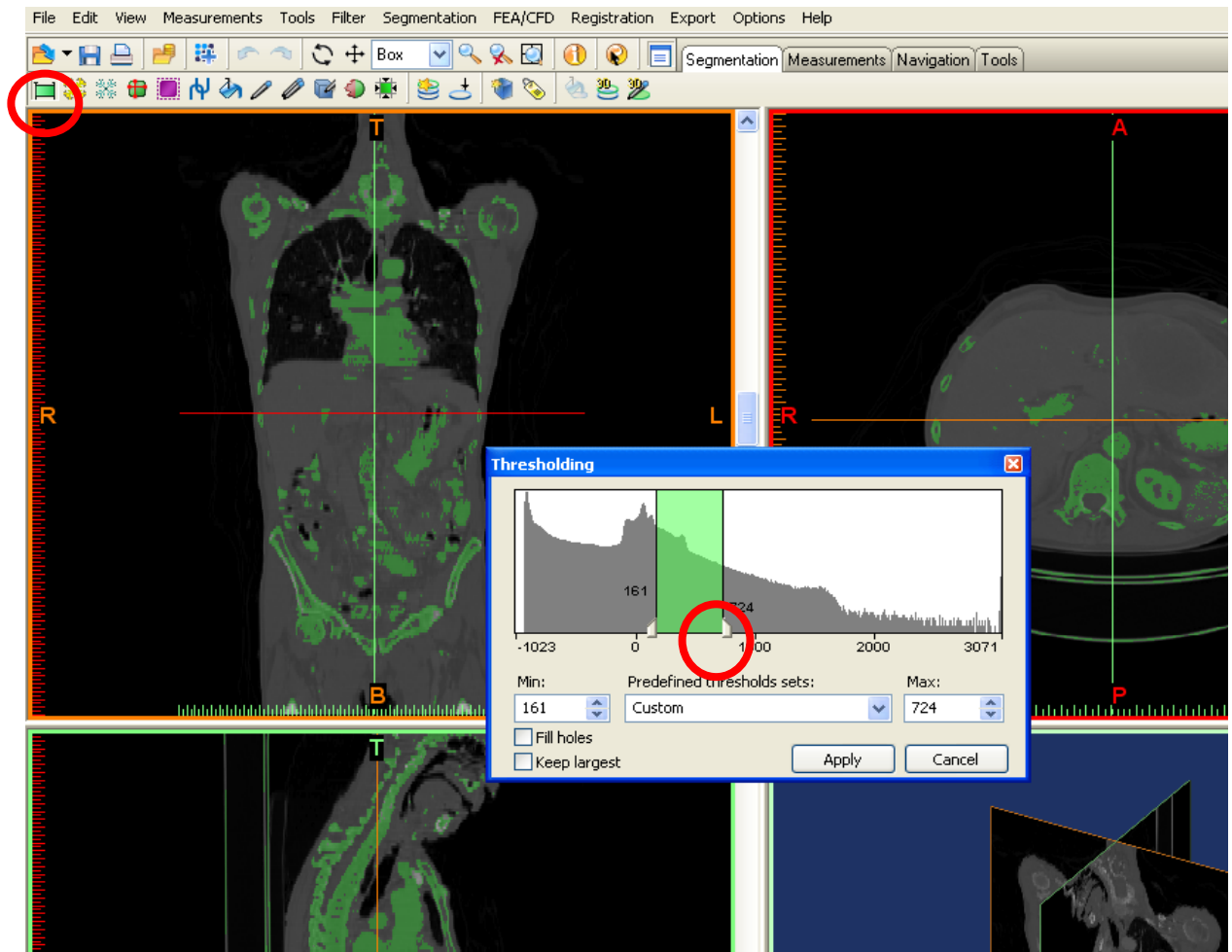


Figure 4- : The interface in Mimics. Note the icon for the thresholding function. Dialogue box for setting the thresholding

Click on the green square icon as shown in figure 4-6. In the Thresholding dialog box, adjust the slider, shown by the red circle. As the slider is adjusted, different types of materials on the CT scan image will be highlighted by a brighter colour. Adjust the slider up to a point where only the cortical bone is most brightly highlighted.

Mimics 13.1 allows changing the predefined threshold to the required threshold by choosing compact bone of an adult from a drop down menu. Therefore, a lower limit of 662 HU (Hounsfield Units) and upper limit of 1988 HU were defined in order to select only the bones from the surrounding tissues as shown in Figure 4-.

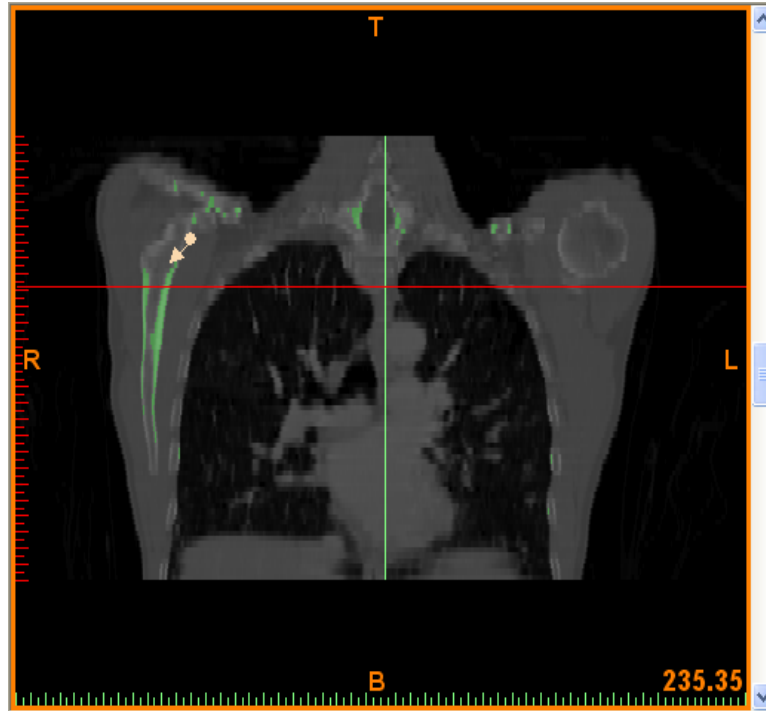


Figure 4-: Segmentation of bones from the soft tissues

The thresholding tool makes it possible to split the segmentation created by thresholding into several objects and to remove floating pixels. The Scapula and the Humerus was selected separately and assigned different masks. For instance, a point was clicked on the green area of the Humerus. Then the program started to calculate the new segmentation. That is all points on the green area of the Humerus connected to the marked point were used to form a new mask. This new segmentation is coloured yellow. Similarly, a new mask was defined for the Scapula and its corresponding colour is cyan as shown in the next Figure 4-



Figure 4-: Different colour masks assigned to the Scapula and Humerus

4.6.3 Region Growing

Once the region growing icon has been clicked, a dialogue box containing the instruction to select a boundary will appear. Draw a short line across the most prominent boundary of the cortical bone, as shown in the diagram above to ensure only the regions associated with the cortical bone will be selected.

The region growing has split the segmentation into separate entities. This enables to generate separate geometrical files and subsequently 3-D models. Noisy pixels and artefacts were eliminated manually. Cavity filling operation was performed in order to eliminate some existing voids within the density masks. This operation was done manually using the multiple slice editors as shown in Figure 4-.

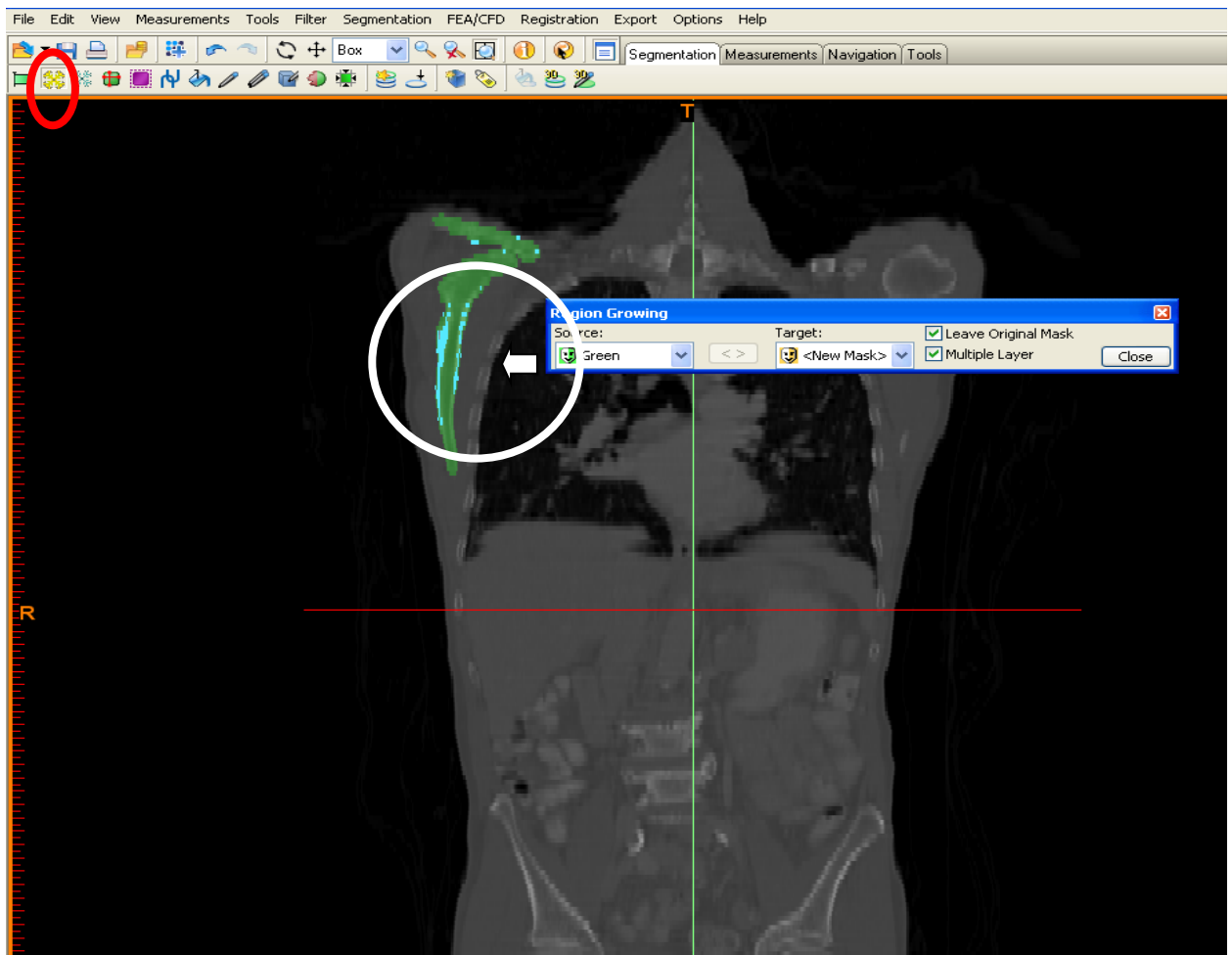


Figure 4- : Interface in Mimics; note the icon for region growing function.

It was a delicate process where each and every slice related to the scapula and humerus was filled completely. The following approach was adopted in order to make sure the accuracy and

coherency of the original slices were not affected. In fact, the slice was initially overfilled and then all the excess filling was removed by intersecting a circle with the inner boundary of the bone as shown in Figure 4-.

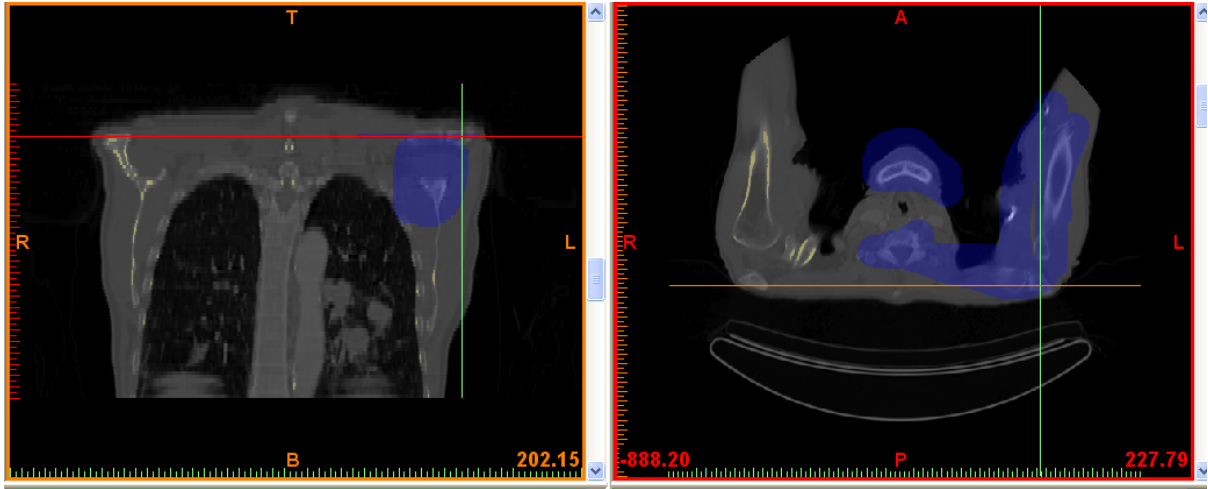


Figure 4-: Removing excess and void density

Afterwards, filling the scapula and humerus density bones took place and it is explained in the next section.

4.6.4 Filling

After region growing, select the icon with two blue pens to ‘fill the cavities of part of the Scapula and Humerus to recreate a 3D model of the Shoulder joint of a specific patient as shown in Figure 4-. In the Multiple Slice Edit dialogue box that appears, the size of the filler can be adjusted to suit the user’s preference.

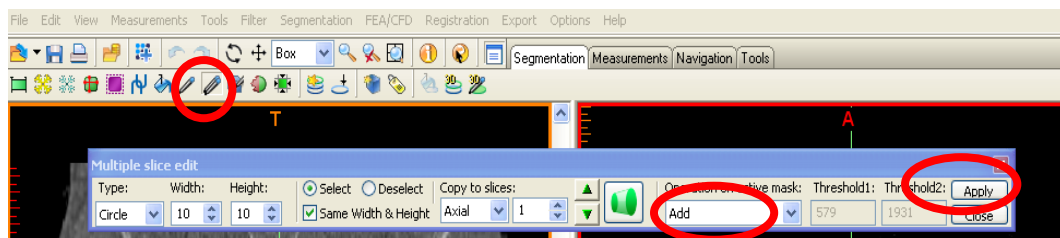


Figure 4-: Interface in Mimics. Note the icon for the multiple slice edit function for filling cavities within the bone.

The anatomical view at which filling is done can be chosen in the ‘Copy to slices’ settings. Ensure the operation of the active mask is ‘Add’ to ensure the filling operation can be achieved as shown in Figure 4-.

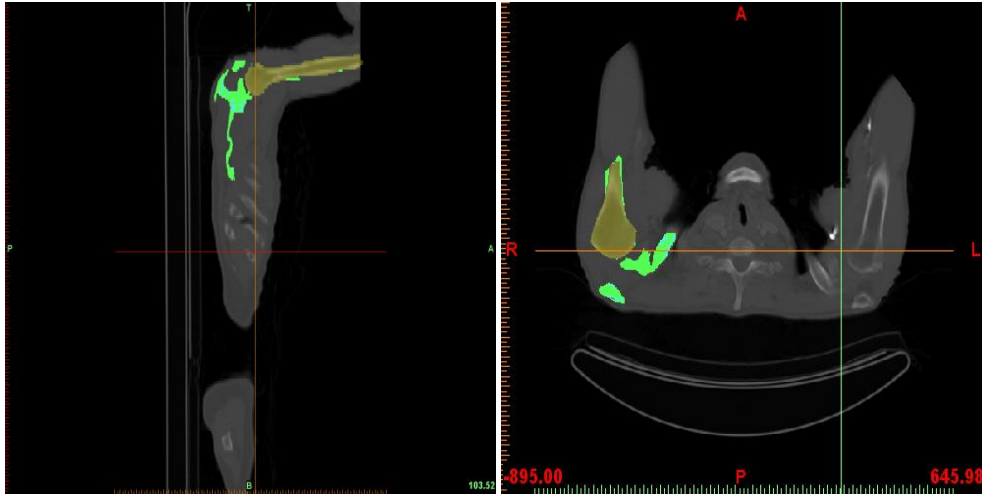


Figure 4-: Interface for filling. Density masks of both humerus and scapula after filling.

4.6.5 3D Model Creation

A 3-D computation was carried out on both the density masks generated for Scapula and Humerus. Then both the 3-D models were wrapped and conservatively smoothed using a smooth factor of 0.5 in order to have a good surface topography without affecting the anthropometrical data of the patient as shown in Figure 4-.

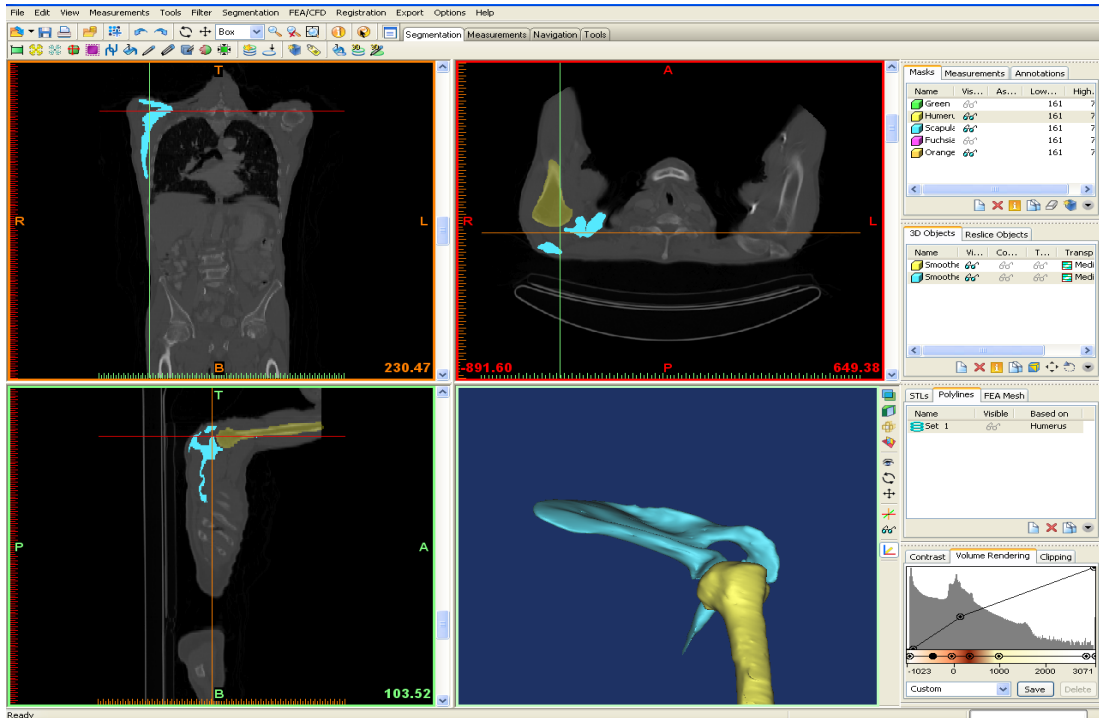


Figure 4-: 3D Model of the Shoulder Joint

Calculating 3D objects (Scapula and Humerus) will give the processed CT scan image by MIMICS the closest representation for the real bone shape and look. Then smoothing and wrapping for the surface of the 3D objects will eliminate the void and extra filled parts in the model. Thereafter a re-meshing for the surface of the 3D model will enable the software to get an optimal 3D model to export it to ABAQUS for further simulation. This helps to keep the geometry and the shape of the 3D model for bones at its minimal faults to avoid simulation errors. Figure 4- shows the side bar in MIMICS after wrapping and remeshing operation.

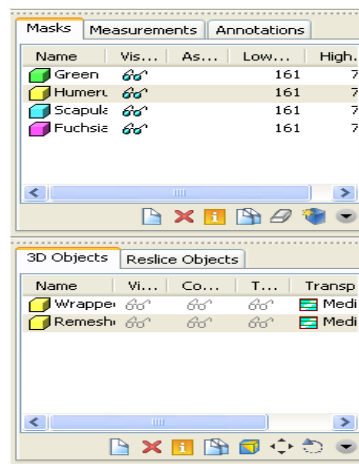


Figure 4- : Side bar for MIMICS after Wrapping and Remeshing 3D

4.6.5 Remeshing

When the remesh button was clicked, a new window will appear, with the appearance resembling that in the Figure 4- above for Scapula and Humerus. The main purposes of remeshing are: to decrease the amount of detail, to reduce the amount of triangles of the object while preserving quality, to improve the quality of the triangles of the object and to remove extra shells. Also it is possible to use the fix wizard to check there are no bad angles or edges. In addition, the fix wizard makes a full analysis including: bad edges, bad contours, shells, noise shells, overlapping triangles and intersecting triangles.

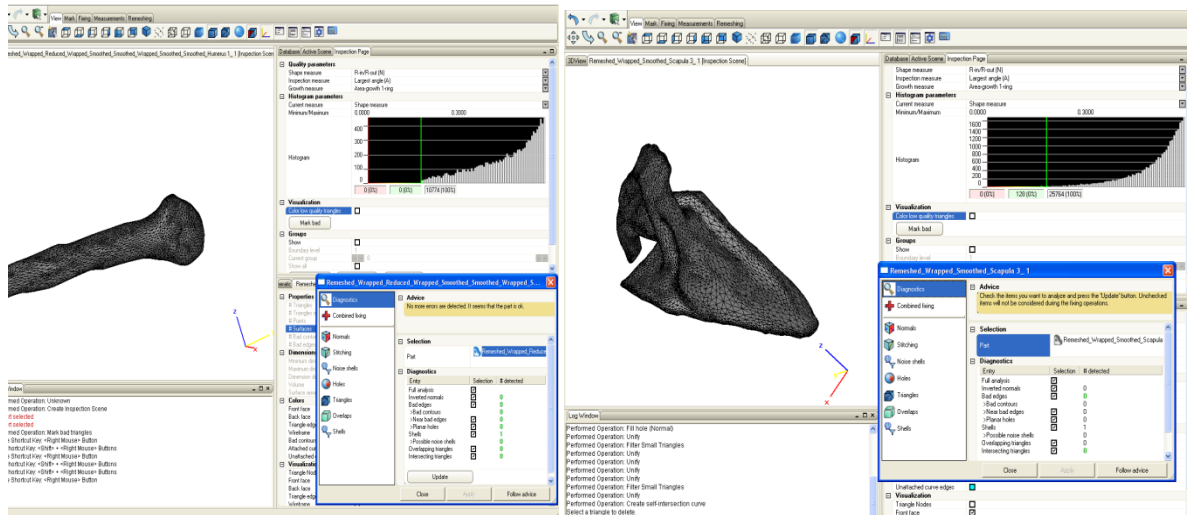


Figure 4 : Remeshed Humerus and Scapula

Applying the following steps manually will achieve the required mesh:

Step 1: Smooth 3D object.

Step 2: Fix the object and reduce the triangles.

Step 3: Remesh the object using the Auto Remeshing tool. Remove the outliers by performing the Auto Remesh function.

Step 4: Remove small triangles. Under the Remeshing Tab, select Quality preserve reduce triangles.

Step 5: Call the self-intersection test. Select Fixing -> Mark Self-intersecting triangle. No intersection should be found at this point.

Step 1 to 5 can be repeated until the histogram displayed on the right hand side of the screen is shifted to be above a certain quality parameter of 0.3 or below. Here, it has been reached nearly 0.05 of geometrical errors which enable ABAQUS to deal with it shown in Figure 4-. This is to ensure the surface mesh is suitable for FE processing in ABAQUS. ABAQUS is very sensitive to large triangles within the mesh. Figure 4- represents the final look to the remeshed 3D models before exporting to ABAQUS.

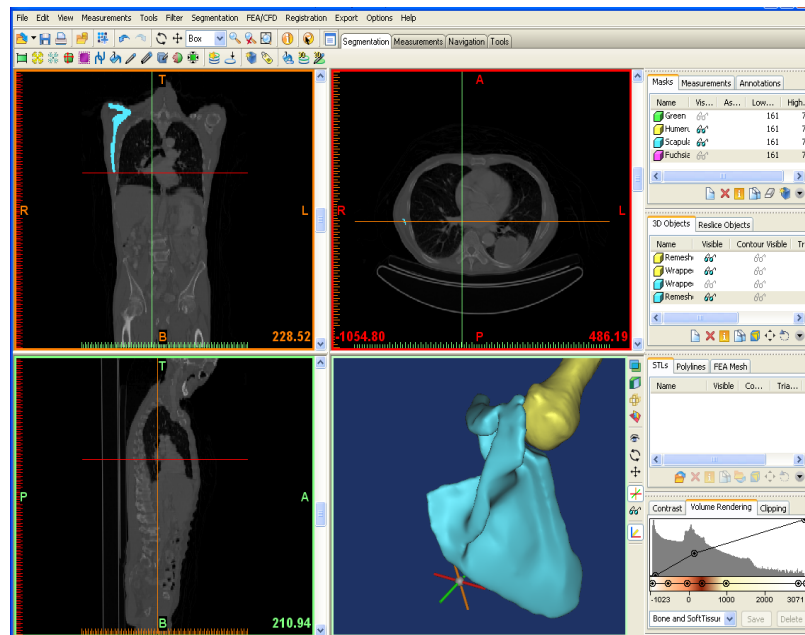


Figure 4- : the final look to the remeshed parts Scapula and Humerus

4.6.6 Exporting to ABAQUS:

The final step in MIMICS is exporting the remeshed 3D models to ABAQUS to commence the FE analysis. Figure 4- and Figure 4- respectively show the steps to export the 3D models to ABAQUS.

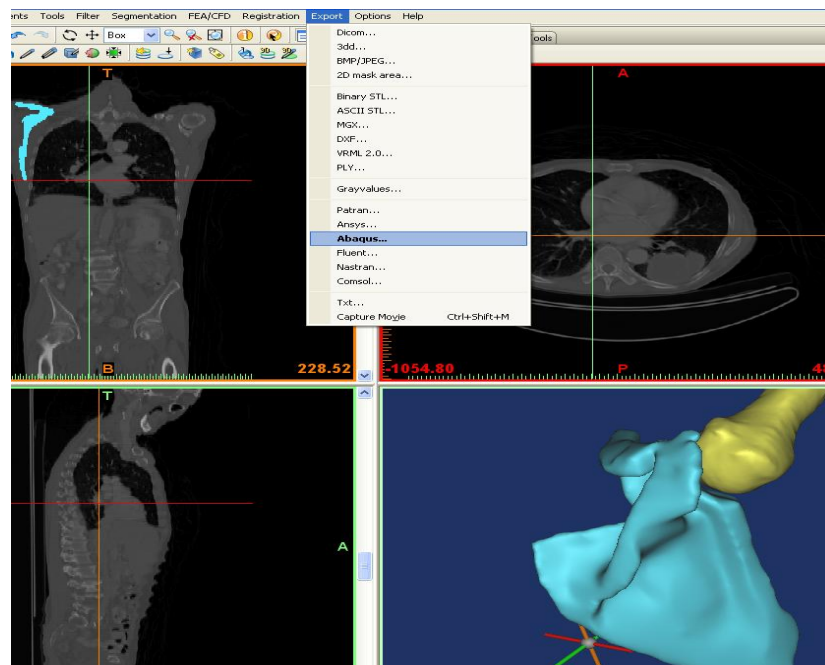


Figure 4- : Export the mesh to ABAQUS

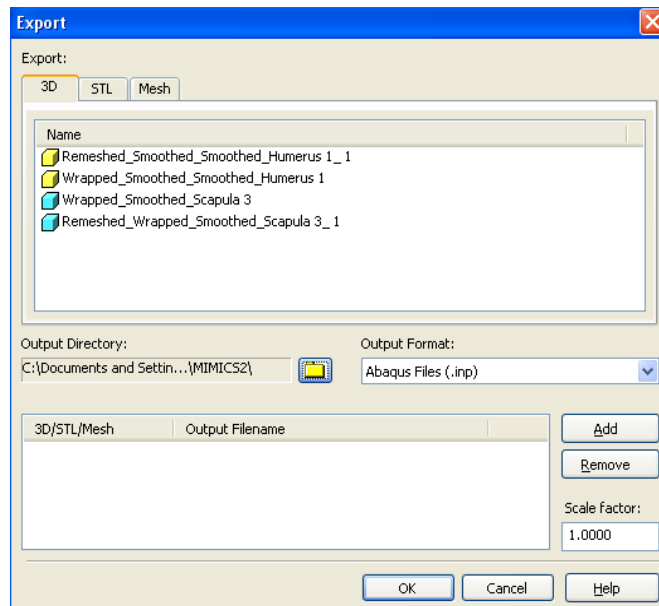


Figure 4- : Export step to ABAQUS

4.7 ABAQUS Software:

Abaqus/CAE is a sophisticated environment that is divided into different modules. This package provides a simple interface for creating, submitting, monitoring, and evaluating results from Abaqus/Standard and Abaqus/Explicit simulations. This software has all necessary tools for whole parts of modelling process, including pre-processing, processing and post-processing. For example, as pre-processing, with this interface it is possible to define the geometry and material properties; also it is possible to generate appropriate mesh with one of the modules of this environment. Each module of the Abaqus/CAE generates an input file to the Abaqus/Standard or Abaqus/Explicit analysis product (processing part). The analysis product performs the analytical process and then sends information to Abaqus/CAE to allow in monitoring the progress of the job, and generates an output database for post processing. Finally, Abaqus/Viewer performs the visualization module of Abaqus/CAE interface which has a separate license. This part provides graphical display to show the results of the analysis. Abaqus/Viewer is incorporated into Abaqus/CAE as the Visualization module.

There are three basic steps typically involved when applying FEM to any problem:

1. Model creation
2. Solution
3. Results validation and interpretation.

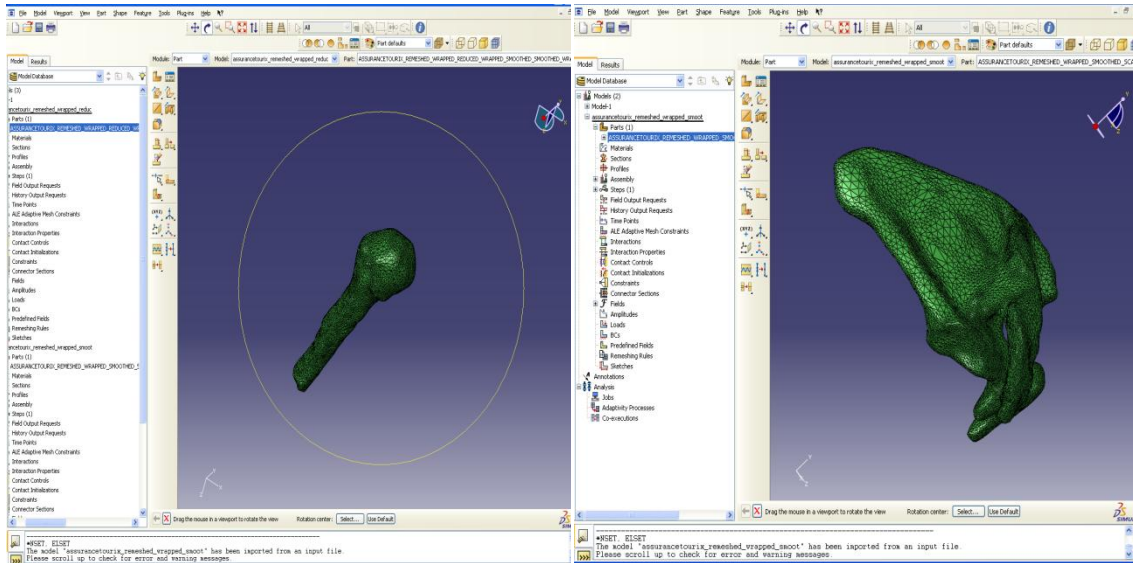


Figure 4 - : Imported Models into ABAQUS

After preparing the model through MIMICS it will be exported into ABAQUS as shown in Figure 4-. Then the model will be ready for processing and for FEA.

4.7.1 Model creation

It is often described as the pre-processing phase taking place before the solution phase. Model creation implies the mathematical description of the finite element model in term of nodes and elements, material properties, boundary and interface conditions, and applied loads. Detailed FEA techniques will be discussed in chapter 6.

4.8 Experimental analysis

Total shoulder arthroplasty (TSA) still suffers today from mid-term and long-term complications such as glenoid implant loosening and wear. With loosening being the number one reason for TSA revision, investigating methods of monitoring the glenoid implant loosening and investigate the effects of various design parameters on the loosening behaviour of the glenoid fixation is necessary to explore the problem.

Although computer simulations prove (Chapter 6) that the Verso Implant is valid for long term use for patients with no or minor problems, experimental analysis (Chapter 5) always is a necessary part to show validity of the simulations. Here to address the issue a series of mechanical lab testing has been arranged to find out the durability of this Implant under various loads (statics and dynamics) similar to the real conditions.

In this part as a method of the study, the main concern is to introduce the mechanical tests for the Verso Implant Glenoid Head, Glenoid base plate and Peripheral screws. The aim of this testing is to look at the behaviour of the glenoid base plate under certain load.

The mechanical tests were carried out at Brunel University Mechanical Lab. The machine used in the testing is inserton 8501; this machine was upgraded to 8800. Biomet, UK, Ltd provided the Glenoid base plate, Glenoid head and two Peripheral screws to enable this testing procedure to take place. A custom fixture was designed and manufactured in the workshop then attached into the glenoid base plate.

Also a foam block used to mimic the human bone and the glenoid base plate was installed inside the block. The [ASTM F-1839-08](#) "Standard Specification for Rigid Polyurethane Foam for Use as a Standard Material for Testing Orthopaedic Devices and Instruments" states that; "The uniformity and consistent properties of rigid polyurethane foam make it an ideal material for comparative testing of bones screws and other medical devices and instruments." (www.rigidbodies.com).

To mimics and simulate mechanical behaviour of the glenoid's base plate under mechanical loading a series of tests were designed. The aim of the first set of the tests which is called the load to failure test is to apply a pulling out force to the glenoid base plate from the block foam. To achieve this from one side the glenoid base plate was attached to the metal rod to enable the fixation on the machine; and from other side was installed on the block foam.

In the second set of the experiment to examine the durability of the implant; a series of cyclic loading were applied prior polling out tests. For example one set of test is: Apply loading between 10N to 50N for 10 cycles with amplitude of 20 at 1.0Hz (pre-cyclic test). It will be followed by a cyclical loading of 50N to 250N for 500 cycles with amplitude of 100. Then a single cycle load to failure tensile testing will be followed.

The entire tests were carried out in three different conditions: Implant Base plate without screw, with one screw and with two screws. Chapter 5 will illustrate the experimental test setup, tests and analysis.

4.9 Summary

This chapter describe the methodology of processing the data used in this project. Highlighting on the efficiency and application for specific software and the role they played in manipulating the data to reach to the desired model.

First, identify the objective for using the CAD software to achieve a less error with the imported parts. Then the process of removing free edges, bad triangles and sharp edges etc. will enable the more complicated software to accommodate the imported parts. In this project of study the software used were MIMICS and ABAQUS. MIMICS play an important role in segmenting the bone from other surroundings such as skin, tissues, muscles and ligaments. The parts then will be calculated as 3D models objects to prepare it for remeshing. The remeshing process will get rid of the artefacts and all bad contours surrounding the 3D object.

However, ABAQUS software can only deal with a corrected model geometry and again apply the necessary modification to enable the software to run the FE analysis on the created implant parts with the shoulder parts (humerus and scapula). Furthermore, the chapter illustrates the method each software were used and the results of each step.

In the following chapter the complete modified model that was imported into ABAQUS will use the FEA method. FEA will analyse the loads, stress, deformation and displacement of the implant at the interface with bones. In order to see how effective the reverse shoulder implant is in overcoming the problems caused by arthritis and degraded rotator cuff compared the movements used in activities of daily life of those with the Verso implant.

At the end of chapter experimental test has been introduced as an alternative method for evaluation of implant. Experimental tests have been used as a second method to analyse the behaviour of the joint implant in a short period and long duration of working situation inside the human body. Chapter 5 will cover these experiments.

Chapter 5. Mechanical Testing, Methods and Results

5.1 Introduction:

This chapter is concerned about the mechanical test for the Verso implant Glenoid Head, Glenoid base plate and peripheral screws. The aim of this testing is to look at the behaviour of the glenoid base plate under certain load.

A foam block (bone substitute) was provided by Sawbone company to carry out the experimental tests. The foam block is a standardised testing material that has been widely used in the mechanical testing procedures; and in the investigations of the implants and bone mechanical behaviour under different testing settings.

The chapter will introduce the mechanical testing procedure in details. There were three initial experimental pull out tests carried out in three configurations (0 screw, +1 side screw and +2 side screws). The results of the first set of tests were used as a reference to the cyclic testing afterwards. Then, full analysis to the results and the extracted parameters were investigated further.

The same configurations (0, +1, +2 side screw(s)) were used in cyclic testing, and then a series of pull out tests were carried out at different speed rates 5mm/min, 10mm/min and 20mm/min. the test for each configuration were repeated three times respectively to maintain steady testing process as well as check accuracy.

5.2 Mechanical Testing Preparations and Materials:

The mechanical test were carried out at Brunel University Mechanical Lab. Biomet, UK, Ltd provided the Glenoid base plate, Glenoid head and two Peripheral screws to enable this testing procedure to take place.

To mimics and simulate mechanical behaviour of the glenoid's base plate under mechanical loading a series of test was set up. A custom fixture was designed and manufactured in the

workshop then attached into the glenoid base plate. Figure 5- displays the designed fixture used to control the base plate.

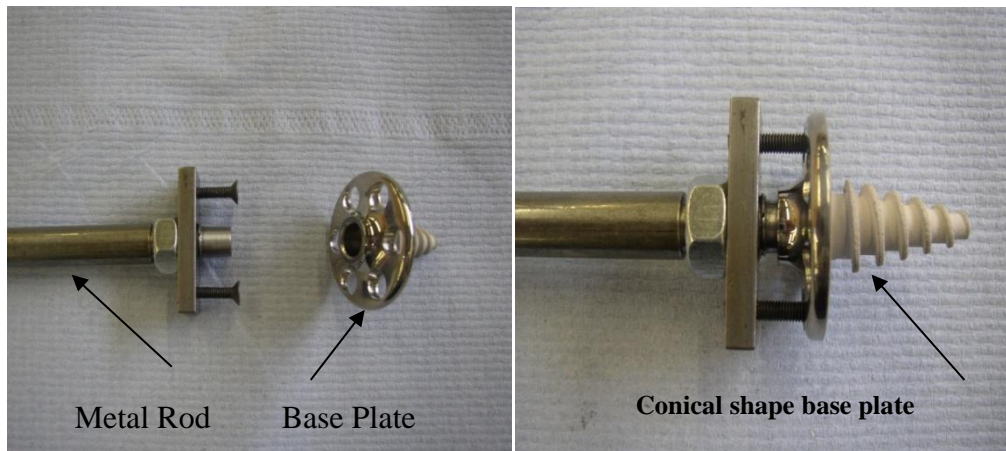


Figure 5-: Glenoid Base Plate pre-testing preparation

The metal rod used in this study was 10mm in diameter and the attached support plate for the implant was rectangle with 12mm width by 30mm long. The glenoid base plate dimensions are standard, which means they do not change in size like other implant parts. The one used in this test is measured from the top head of the glenoid base plate to the bottom 22mm (conical shape head) as shown above in Figure 5-. The peripheral screws used in the test were titanium low profile 5mm x 30mm. The glenoid head can come in different sizes according to the shoulder size will operated on. The glenoid head provided by Biomet for this test was 36mm. Figure 5- below displays the Implant parts used in the mechanical testing.



Figure 5-: The Implant parts used in the mechanical testing; Glenoid Head, Peripheral Screw and Glenoid Base Plate, respectively from left to right.

The foam block used in the mechanical testing has the material properties as shown in Table 5- taken from Saw bone website. The foam block was Standard block size measures 13cm x 18cm x 4cm with the density of 20 pcf.

Table 5-: Foam Block Material Properties. Saw Bone website. “Coefficient of Thermal Expansion (CTE) = $6.3 \times 10^{-5} \text{ K}^{-1}$ (from -46 to +93 °C). Water absorption ranges from 0.301 to 0.0 kg/m². Material property data parallel to rise of foam using test methods ASTM D-16. (www.sawbone.com)

		COMPRESSIVE		TENSILE		SHEAR	
DENSITY		STRENGTH	MODULUS	STRENGTH	MODULUS	STRENGTH	MODULUS
pcf	g/cc	MPa	MPa	MPa	MPa	MPa	MPa
5	0.08	0.60	16	1.0	32	0.59	7.1
10	0.16	2.2	58	2.1	86	1.6	19
15	0.24	4.9	123	3.7	173	2.8	33
20	0.32	8.4	210	5.6	284	4.3	49
30	0.48	18	445	12	592	7.6	87
40	0.64	31	759	19	1000	11	130
50	0.80	48	1148	27	1469	16	178

Solid rigid polyurethane foam is primarily used as an alternative test medium for human cancellous bone (www.sawbone.com). These products aren't intended to replicate the mechanical properties of human bone; however, it does provide consistent and uniform material with properties in the range of human cancellous bone. Relevant mechanical properties for comparison to human cancellous bone may depend on the particular test method that is being developed. The nature of cancellous bone composed of bony trabecular struts and marrow-filled cavities can be described in terms of structural and material properties (Ashman et. Al., 1988). *Structural* properties are defined as the extrinsic properties of both trabeculae and pores, whereas *material* properties are defined as the intrinsic properties of the trabecular struts only. Structural properties are important for global stress analyses, while material properties are important for characterizing various bone pathologies, micro-level stress analyses, and bone adaptation around implants. Micro-level stress analyses may provide valuable information about loosening and bone resorption at the implant bone interface.

The [ASTM F-1839-08](#) " American Standard Specification for Rigid Polyurethane Foam for Use as a Standard Material for Testing Orthopaedic Devices and Instruments" states that; "The uniformity and consistent properties of rigid polyurethane foam make it an ideal material for comparative testing of bones screws and other medical devices and instruments." Figure 5- shows the foam block used in the mechanical testing with Standard block size: 13cm x 18cm x 4cm measurement.

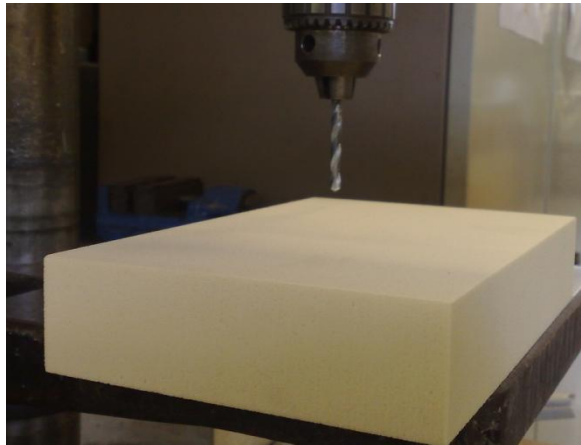


Figure 5-: Foam Block from Saw Bone with 20 pcf, 13cm x 18cm x 4cm

5.3 Tensile Testing (Load to Failure Test using Pulling out Test)

The aim of the first test which is called the load to failure test is to apply a pulling out force to the glenoid base plate. To achieve this as explained in the previous section the glenoid base plate was attached to the metal rod to enable the fixation on the machine. The machine used in the testing is Instron 8501 as shown in Figure 5- below. The Instron machine was upgraded to 8800.

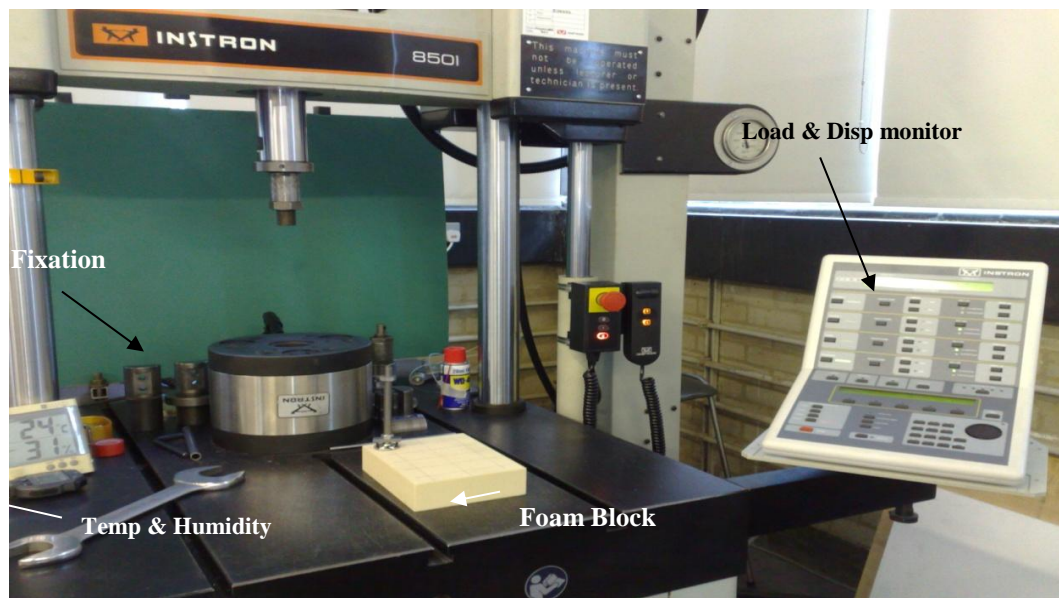


Figure 5-: Instron machine 8501 used to apply pulling force on the foam block. (Upgraded to 8800)

The pulling out series of tests was applied in three different conditions, glenoid base plate without screw, with one then with two screws respectively, and each condition repeated at least

three times. The number of screws advised by the surgeons is no more than 2 screws and no less than 1 screw to secure the glenoid base plate in place.

Each test will be includes a set of the following steps:

- 1- Preparation.
- 2- Process.
- 3- Results and Analysis.
- 4- Discussion.

The ability to resist breaking under tensile stress is one of the most important and widely measured properties of materials used in structural applications. The force per unit area (MPa or psi) required to break a material in such a manner is the ultimate tensile strength. The tensile testing is a standard test that has been used in previous studies to examine maximum load and micro-motion on a specimen during testing. Pull out mechanical tests are performed to increase the sample size. The same test load stresses and durations are applied. The loads applied are recorded but only record of movement is any failure of the fixing itself. Conducting a larger scale pull out test then gives on-site engineers the data needed to seek further rectification of the problem⁵.

5.3.1 Test 1&2&3 (0) (Pulling test without screws):

The first set of tests which will be referred to as (Test 0) indicates there were no extra peripheral screws to fixate the glenoid base plate to the foam block. Test (0) was carried out three times. The test was carried out under a room temperature of 24°C and 30% humidity. The standard unit system, SI, used by the Instron machine (SI stands for: Standard International units).

5.3.1.1 Preparation

Figure 5- shows the process of drilling the Glenoid Base Plate (GBP) into the foam block to prepare the block for testing. At first, the block was prepared to be drilled with 5 mm in diameter and 22mm in depth. These were the advised drilling measurements found in the Surgical Techniques Manual (Biomet UK, Ltd, 2010) a surgeon would follow to screw the glenoid base plate into the glenoid part of the scapula. The conical shape which simulates the conical shape of the glenoid base plate (GBP) was manufactured (at Brunel University Engineering lab) to enable the drilling process of a conical shape into the foam block. The conical head drill was designed to screw the GBP into the foam block to replicate and ensure the accuracy of the actual drilling

⁵ http://www.instron.us/wa/applications/test_types/tension/default.aspx

process and to enable us to get accurate results. Figure 5- shows the conical drill head manufactured.

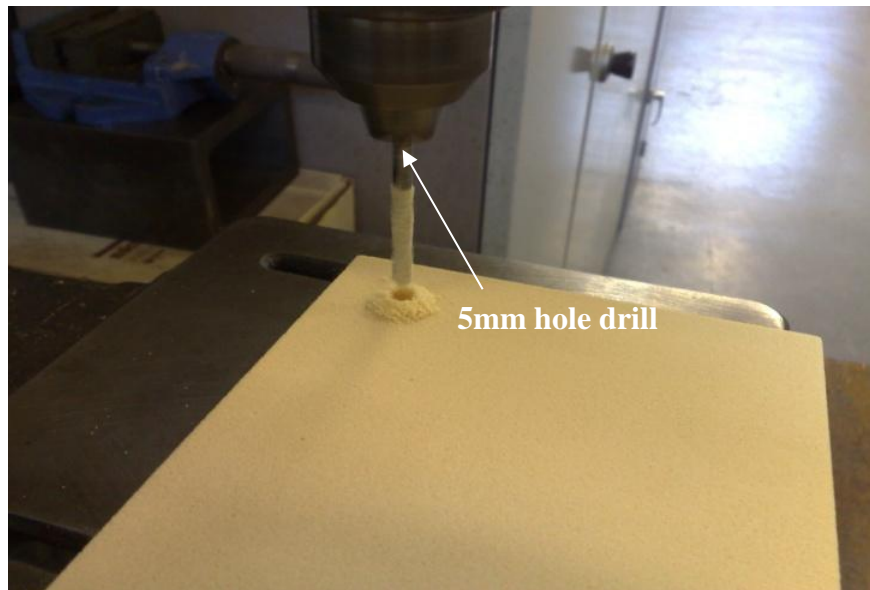


Figure 5-: Drilling 22mm in depth into the foam block

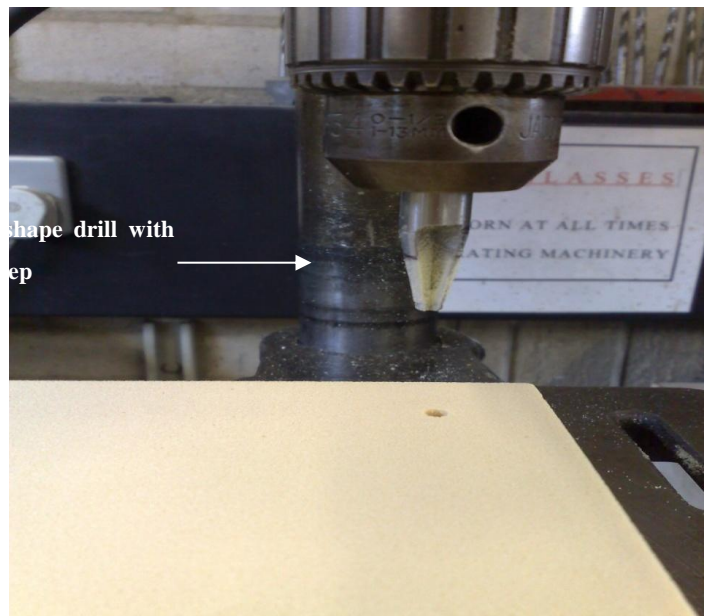


Figure 5-: Conical Shape drill head.

After creating the first holes (5mm diameter and 22 mm depth) in the foam block, then it is ready to be drilled with the conical shape head as shown in Figure 5-.

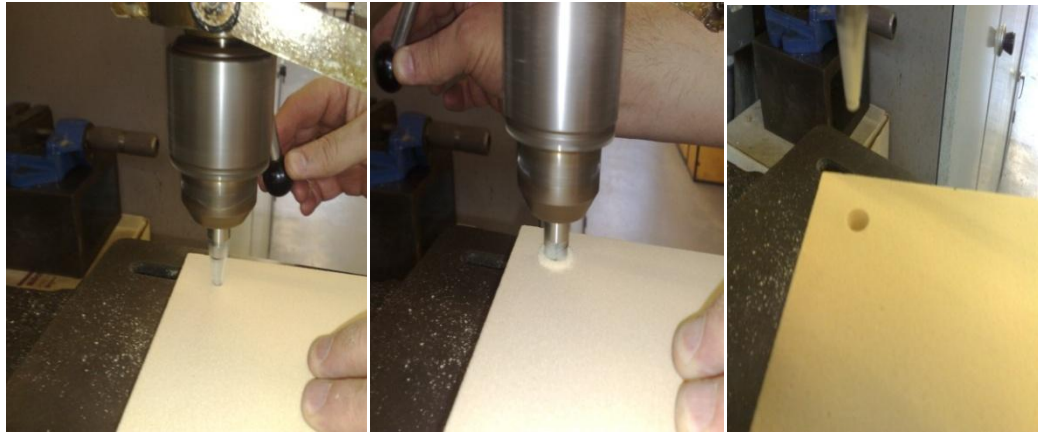


Figure 5-: Drilling Process of Conical head shape



Figure 5-: Foam Block Preparations

To enable a multiple use of the foam block during the testing, the block was divided into several sections with 42mm apart from each drilled hole and 22mm from the edges of the foam block as shown in Figure 5-.

The final hole that was drilled into the block was 22mm in depth and 11mm in diameter at top position to simulate the same dimensions used in the Surgical Techniques Manual used by Biomet, UK.

The surgical tools used in surgery were not available; hence manufactured tools at Brunel Engineering lab were used instead. Such as the T-handle rod which was replaced by the metal rod of 15cm long and 10mm diameter fixed with two screws of high tensile 3mm in diameter. The metal rod used was purposely long to give a clear view to observe the testing results.

Figure 5- shows the metal rod used in this testing. A torque wrench was used to apply force of 6Nm to ensure the GBP is fitted and secured into the foam block. The metal rod was attached to a support plate to simulate the T-handle rod used in surgery as advised by Biomet surgical techniques guide.

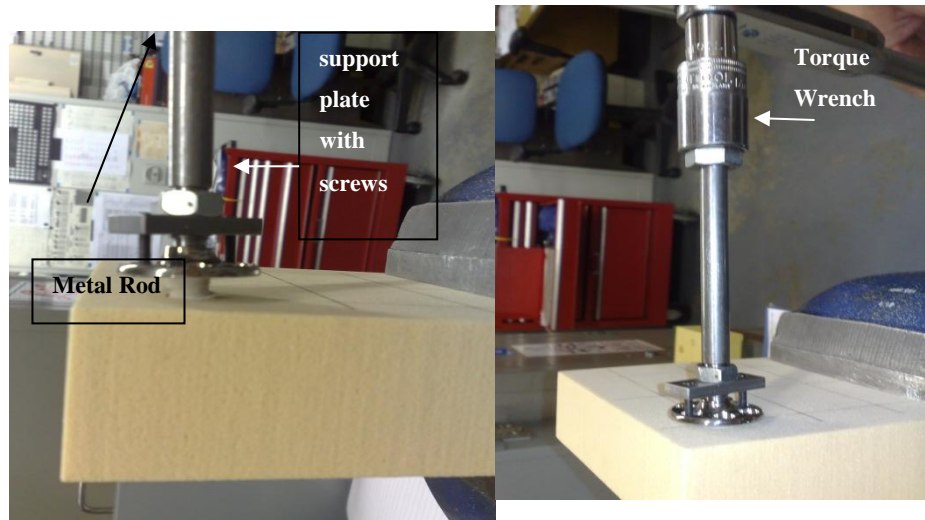


Figure 5-: Screwing the Glenoid Base Plate into the foam block using a torque wrench

5.3.1.2 Process

Now that the foam block is ready and the GBP is screwed in the block, the block is ready for the first pull out test. The block was placed on the load cell as shown in Figure 5- and two clamped and studs were used to hold the block in position onto the load cell. The metal rod was attached to the cylindrical crosshead actuator to secure the position of the specimen as shown in Figure 5-.

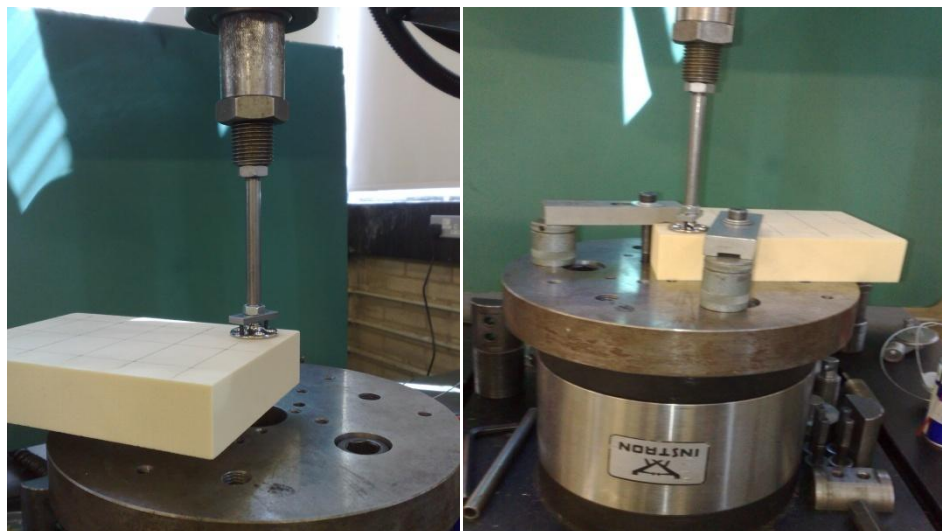


Figure 5-: Securing the Specimen on the Load cell on Instron 8800 and attaching it to the cylindrical actuator

As stated before the first set of tests were load to failure tests which uses the Blue hill2 software run by Instron to measure the pull out force (load), displacement, strain and stress as shown in Figure 5-.

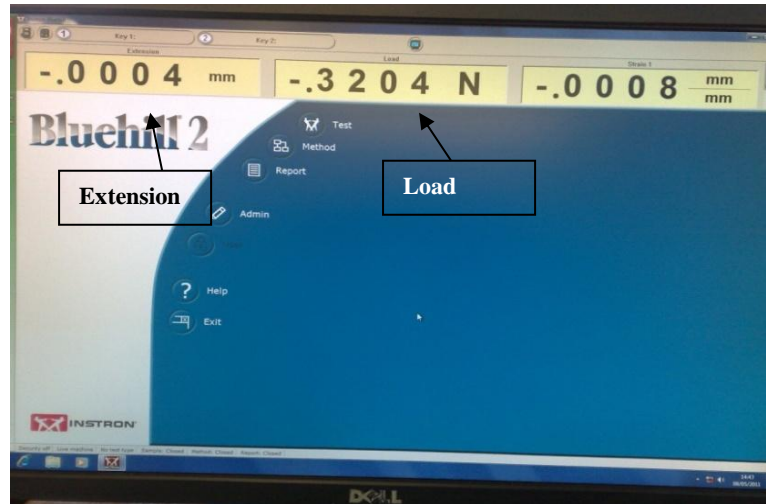


Figure 5-: Blue Hill2 Software used to measure the load, displacement, strain and stress

The method was set to specify the required parameters to be measured such as load, displacement, stress and strain. Figure 5- displays the set up of method with SI (Standard International) system units which measures in Nm and the type of the method is tension.

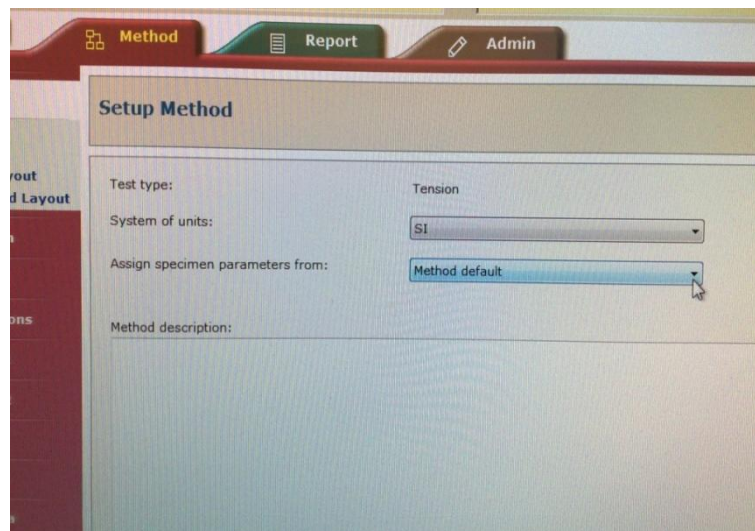


Figure 5-: Method set up on Blue Hill2 software

The test was carried out until failure occurs. The test was repeated 3 times and the failure loads were 1109N, 1172N and 1110N respectively for three specimens.

5.3.1.3 Results and Analysis:

The three pulling-out results has shown neither irregular or unexpected mechanical behaviour; nor any failure in the GBP without peripheral screw. The mean of the three tests was 1130.33N (i.e. 113kg). Figure 5- show the foam block after applying the pull out test.

From Figure 5- it can be seen the debris around the conical screw of the GBP which indicates how was it attached into the foam block (shows the mode of failure). The debris demonstrates how strong the GBP was attached to the foam block (bone substitute). Figure 5- to Figure 5- showed the result for the first trial of pulling out test of the implant without the peripheral screws (Test (0) T1). The other two tests were done similarly.

Firstly, the GBP was screwed into the foam block using the torque wrench illustrated in Figure 5- with a force of 6Nm. The foam block then would be attached to the cross head in Instron 8800 machine; then placed over the load cell as shown in Figure 5-. After securing the foam block with the side clamps, the pulling-test then starts with applying loads till the failure occurs.

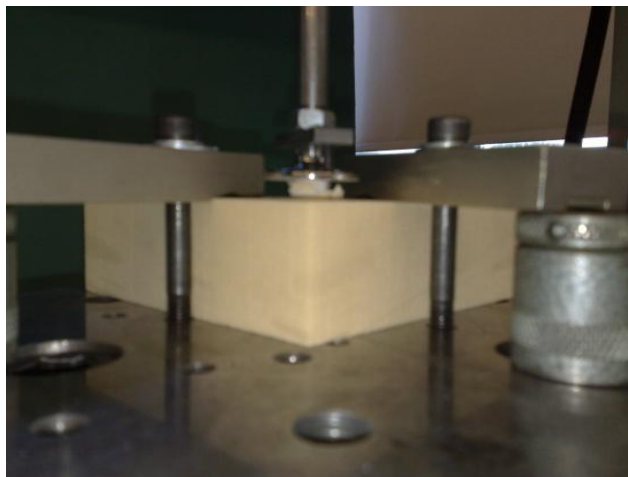


Figure 5-: Test (0) T1 Pulling out test (tensile) for the GBP without screws

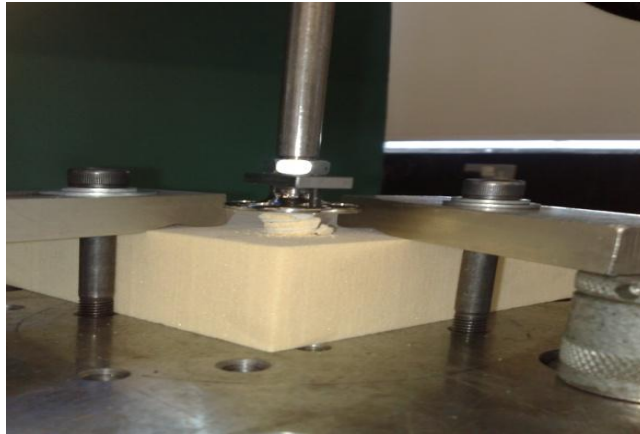


Figure 5-: Test (0) T1 Pulling out test for GBP without screws (debris)

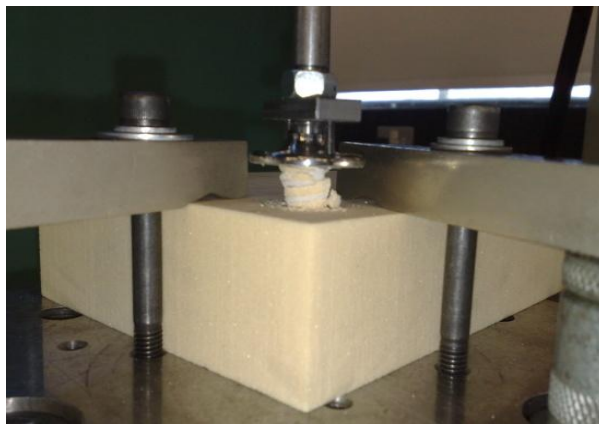


Figure 5-: Test (0) T1 Pulling out test for GBP



Figure 5-: Test (0) T1 GBP pulled out from the foam block

It can be seen from Figure 5- to Figure 5- the process of applying the load until the failure occurs and implant pulled out from the foam block. It can be seen the debris around the implant when it was pulled out as well.

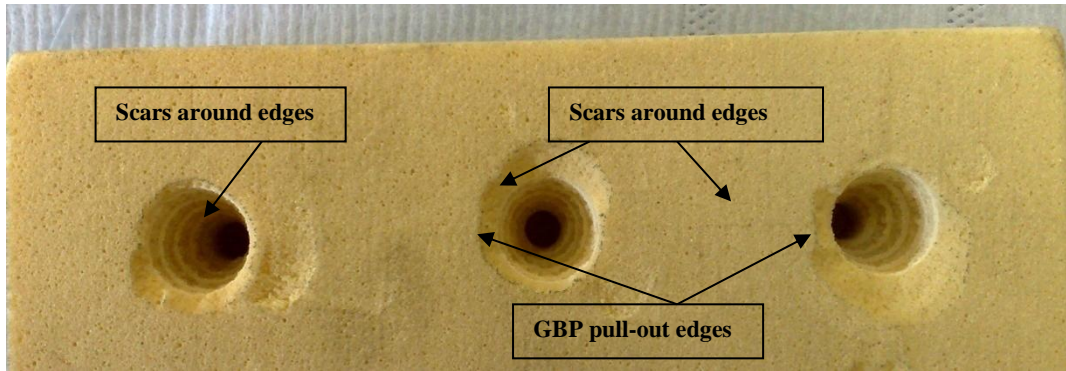


Figure 5-: Mode of failure for Test (0) T1&T2&T3

It can be seen from Figure 5- Test (0) (no screws), that the three tests have shown similar results where the implant were pulled out of the foam block leaving scars around the edges where it was fitted. Figure 5- shows the edges of the GBP where it was drilled into the foam block and cause the scars when pulled out. The tensile testing load was applied vertically and constantly on (GBP) specimen until maximum loading is reached.

It can be seen from Figure 5- the mode of failure for each test. The scars on the surface of the foam block are either due to the fixture or the design and shape of the GBP. The irregularity of the edges in Figure 5- of the GBP which were pulled-out can be due to the conical shape threads or fins of the GBP conical screw as shown in Figure 5-.

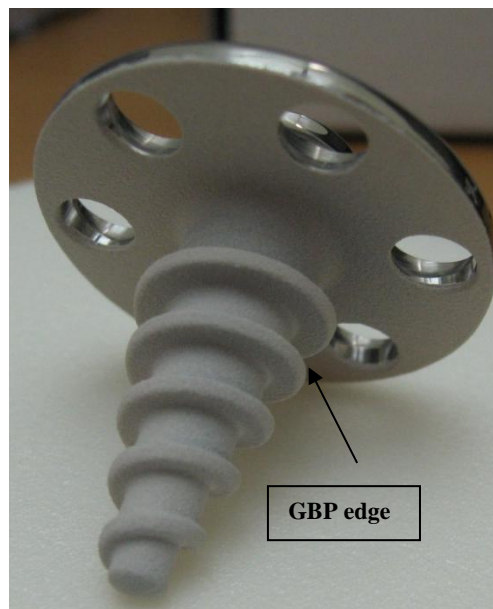


Figure 5-: The conical shape threads of the GBP

Instron 8800 machine is using Blue Hill2 software to record the predefined parameters required for the analysis process after a load to failure test is completed. The data chosen to be analysed by Blue Hill2 software were: Load, Displacement, Stress and Strain. Then the recorded raw data by Blue hill2 software were processed by MS Excel to enable figures plotting shown in next section. The following figures show the consistency of pulling out test results. It can be seen that the three pulling-out tests were approximately in the same range. Figure 5- shows the three different tests done without peripheral screws T(0). It shows the behaviour (interaction) of the GBP and foam block when the load was applied till the failure occurred. The peak of the slope shows the maximum load the GBP endured during the testing. The curve shows the failure over the displacement after a maximum load is reached. From Figure 5- it can be seen that the implant could tolerate till yield forces with specific displacement.

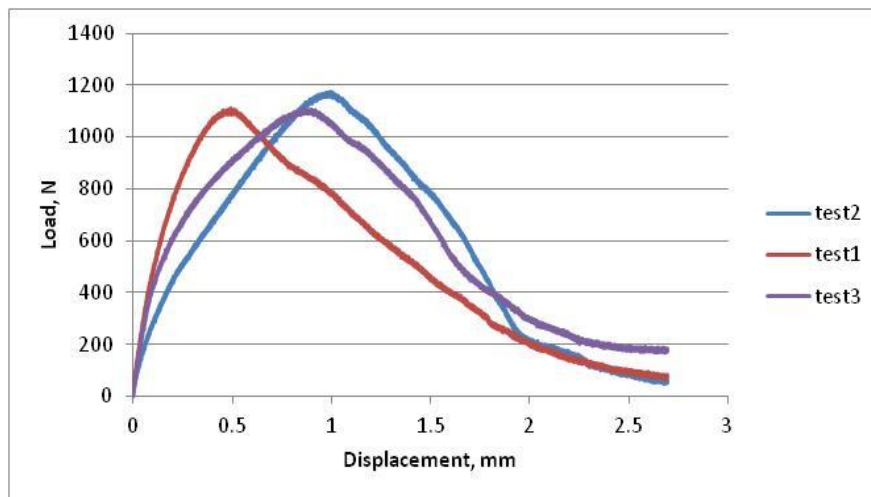


Figure 5-: Test (0) T1(red)&T2(blue)&T3(purple) (No Peripheral screw) tensile test results

Figure 5- shows the average result of the first set of tests:

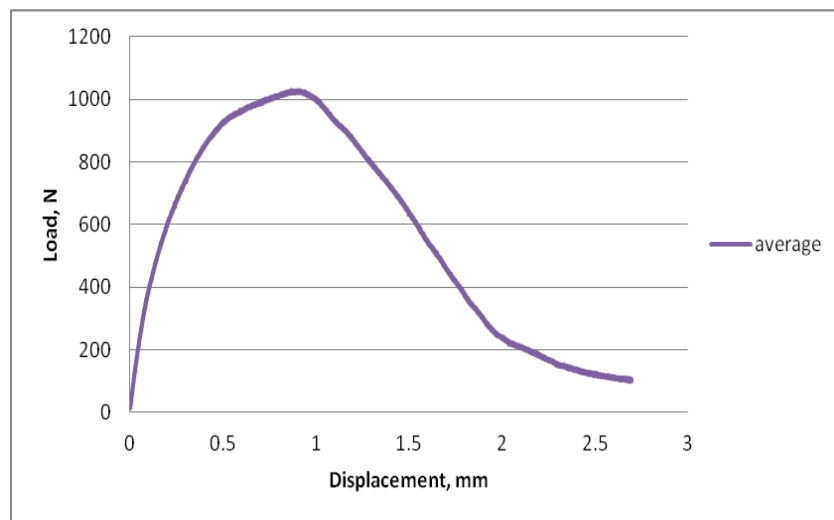


Figure 5-: Average Curve for Test (0) 1&2&3 No screws

Stiffness is the ratio of the force required to create a specified deflection or movement of a part. Stiffness is Force/Deflection⁶. Stiffness is another parameter which can be extracted from the interaction between the implant/foam block (bone substitute material). Stiffness is only valid within the limits of micro motion, and is the gradient of the linear part of the force displacement line. Figure 5- shows the stiffness, slope of the linear part of the figure within the limits of 50 to 150 μm , 2800N/mm or 2.8×10^6 N/m. This number shows the stiffness is high; however this number could have better meaning compared to other cases.

Where Stiffness equation is as follows:

$$k = \frac{F}{\delta}$$

$$\text{Gradient of a line} = \frac{Y_2 - Y_1}{X_2 - X_1} = \frac{500 - 220}{0.15 - 0.05} = 2800$$

And if we continue the black line in Figure 5-, it will cut the Y axis at 86.66

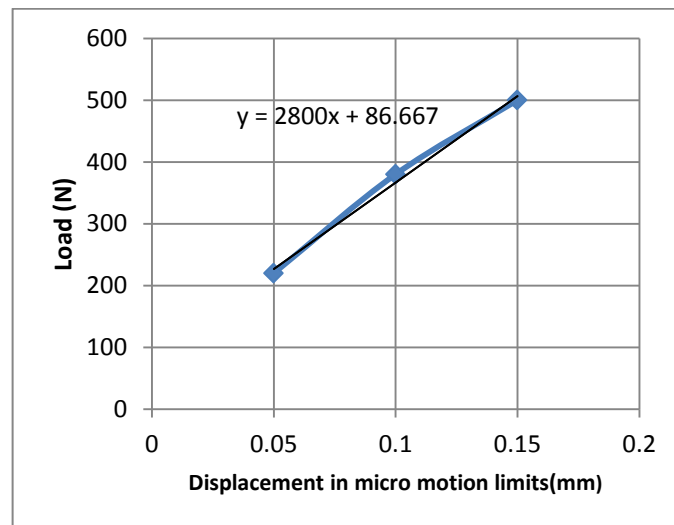


Figure 5-: Stiffness of the GBP for the Test (0) 1&2&3 No screws

The Strain and the Stress for the test 1 can be illustrated in the following figure:

⁶ <http://en.wikipedia.org/wiki/Stiffness>

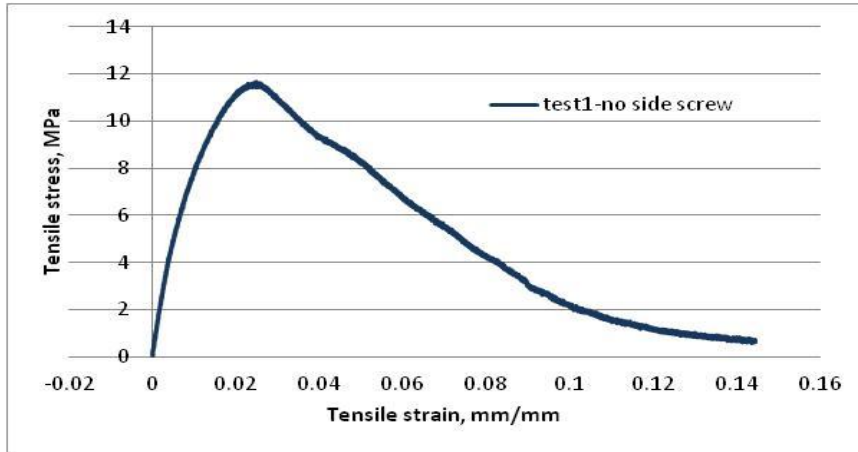


Figure 5-: Strain mm/mm VS Stress MPa for test 1 no screws

The Strain and the Stress for the test 2 can be illustrated in the following figure:

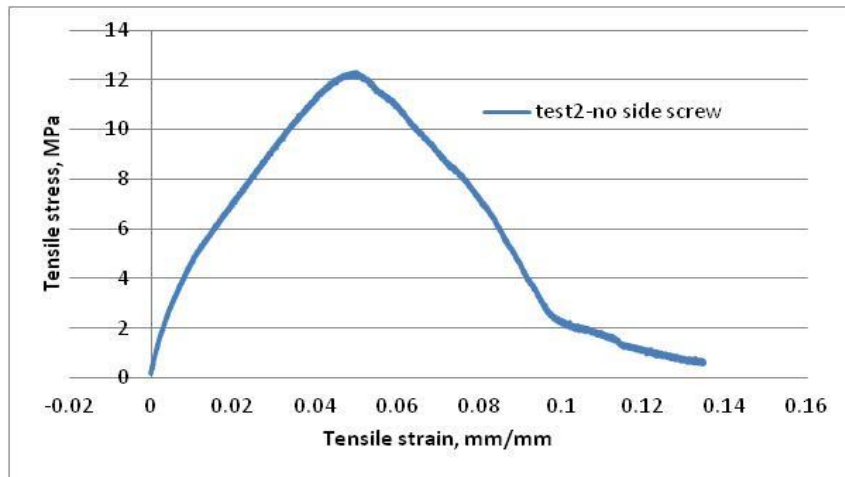


Figure 5-: Stain mm/mm VS Stress MPa for test 2 no screws

The Strain and the Stress for the test 3 can be illustrated in the following figures as recorded by Instron 8800 machine:

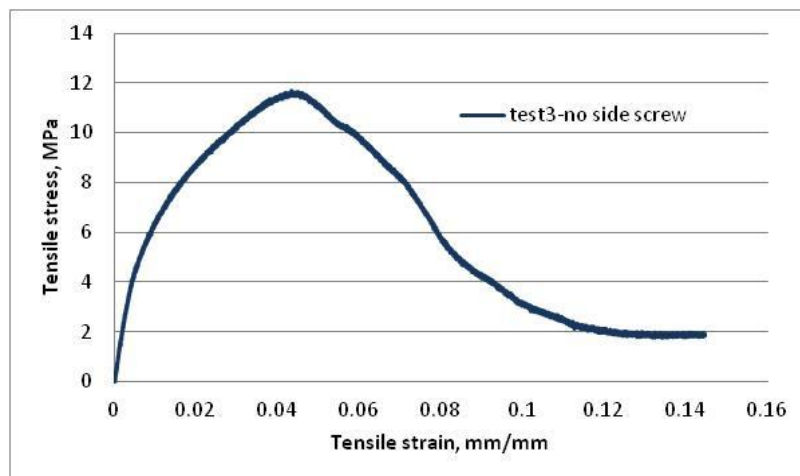


Figure 5-: Strain mm/mm VS Stress MPa for test 3 no screws

In Tensile Testing, the test specimen is deformed, usually until complete rupture or fracture occurs, with a gradually applied increasing tensile load that is applied uniaxially along the longitudinal axis of the specimen. During testing, deformation is confined to the narrow centre region which has a uniform cross section along its length. The load-displacement data is converted to engineering stress-strain data.

5.3.1.4 Discussion:

Test (0) was performed sequentially three times without screws and the result showed a consistent behaviour throughout the testing process. The mean value of loading was 1130.33N and it suggests that the implant without peripheral screws can tolerate up to the mean value of loading reached without failing. (The maximum load in this case to remain within the limits of micro motion (50-150 μ m) is 450N. However if the errors in measuring displacement compensated, the force will be about 800N for the allowable displacement of 150 μ m).

Figure 5- shows the behaviour of load-displacement for the first three tests without the screws. There are no major differences in the loading-displacement slopes in Figure 5-. Failure has occurred in the foam block when the maximum loading reached.

Stress and strain are measured internally by Istron 8800 and the raw data were then exported to excel files to produce the previous stress-strain figures. It is useful to define the stress and strain to illustrate their use in this study. Stress is a measure of the average amount of force exerted per unit area of a surface within a deformable body on which internal forces act. (Mase, George E, 1999).

Strain is the geometrical measure of deformation representing the relative displacement between particles in the material body, i.e. a measure of how much a given displacement differs locally from a rigid-body displacement (Lubliner J., 2008). Strain defines the amount of stretch or compression along a material line elements or fibers, i.e. normal strain.

However, in this experiment, where there is an interaction between GBP implant and foam block (bone substitute), the strain will be evaluated in a different way. In the linear part of the deformation, micro-motion limits, the strain is defined as the relative motion between the implant and foam block over the original length interaction.

Following tensile loading on the interface between GBP and foam block (bone substitute), the stress and strain were internally calculated by Bluehill2 software for each test. The value of stress at the maximum load in T(0) T1 was 11.67MPa, T2 was 12.33MPa and T3 was 11.68. The strain value at the maximum load in T(0) T1 was 0.24 mm/mm, T2 was 0.49 mm/mm, and T3 was 0.43 mm/mm. With an average load of 1130N applied on the GBP on T(0) average stress is 11.89MPa and the average strain is 0.38mm/mm.

The stress-strain reached their maximum values when the implant was pulled out. The stress and strain were steady as shown in Figure 5- to Figure 5- until the peak value was reached when the failure occurred on the foam block side. It was visually observed that the implant did not break or fail throughout the testing process.

From the Figure 5- and Figure 5- a value between 450N to 800N is suggested as a maximum loading the foam block (bone substitute) can tolerate where the displacement between the foam block and implant remain in the acceptable range, before failure occur. Furthermore, the yield force and elastic area can be introduced in the liner part of the force displacement line shown in Figure 5- .

5.3.2 Tensile testing Test (1) T4&T5&T6 (+ 1 side screw):

5.3.2.1 Preparation:

The second set of tests was the GBP pull out test with one peripheral screw. The same procedure as the test (0) was carried out, however one peripheral screw was added to the GBP to reinforce the connection between the glenoid and foam block. This test repeated three times (T4&T5&T6).

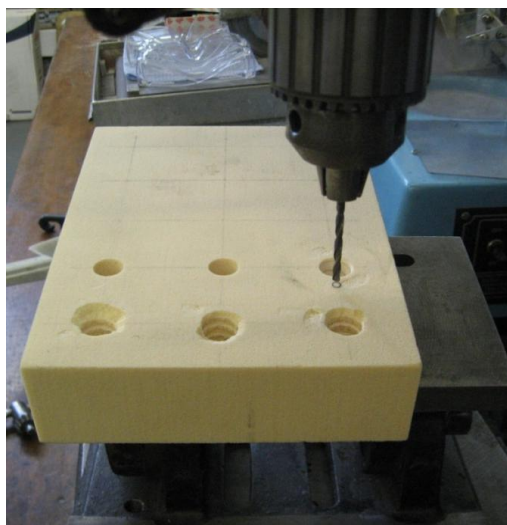


Figure 5-: preparation of foam block for T(1) +1 screw set of tests

The drilling techniques used to drill the conical shape hole into the foam block were same as described before. However, to make a one screw hole, an adjustable angle plate was used to reach the 10° angle diverge from the central axis of the conical screw to drill one side screw as advised by Biomet Surgical Technique Guide. The metal rod design had to be slightly modified to enable the side screw drilling with the required 10° angle. As result the metal rod was maintained the same but the support plate attached to the screws had to be attached to 3 mm two long brass screws instead of steel screws as shown in Figure 5-.

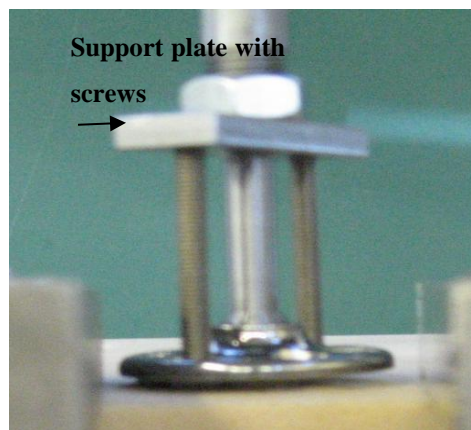


Figure 5-: metal rod attached to the support plate with two long brass screws

First the side screw hole was drilled using the drilling head of 5mm in diameter and 22mm deep. Then a torque wrench with 1Nm (Newton meter) moment used to screw the side screw with 10° angle into the GBP as shown in Figure 5-.



Figure 5-: Torque wrench used to screw the side screw in 10° angle

5.3.2.2 Process:

The specimen of GBP with one side screw is attached to the foam block is ready to be tested. In Figure 5- the specimen was attached to the load cell at the Instron 8800 with clamps attached to the foam block to secure it during tensile testing. Using bluehill2 software as before the test was commenced.

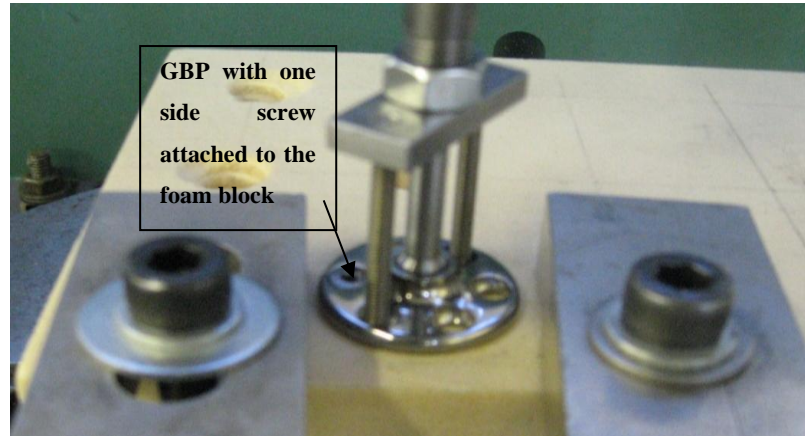


Figure 5-: the specimen is ready to be tested with GBP and one side screw

Figure 5- shows Test (1) T4, the failure when maximum load was applied in tensile testing on the glenoid base plate with one side screw attached.



Figure 5-: T(1) T4(first repeat) GBP + 1 side screw in tensile testing



Figure 5-: T(1) T5(second repeat)GBP +1 side screw tensile testing

Figure 5- shows the mode of failure when the implant was pulled out from the foam block. It can be seen from figures Figure 5- to Figure 5- the failure on the foam block with debris and scars. Again it can be due the fixture of the implant and/or the conical shape of the GBP. However, the screw did show the same effect when it was pulled out, it left scars and in Figure 5- the area surrounding the screw on the foam block was broken. The fact that the screw has 10° inclination from the vertical direction may have caused the scar formation.

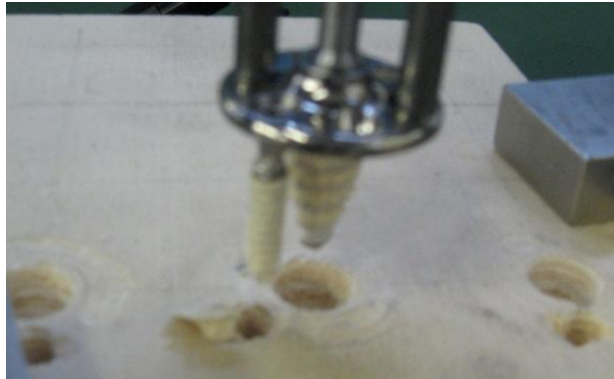


Figure 5-: T(1) T6(Third repeat) GBP +1 side screw tensile testing

5.3.2.3 Results and Analysis:

Bluehill2 software was used to record the maximum load-displacement and stress and strain relation as before. The mode of failure is shown in Figure 5- on the foam block. There were scars around both the GBP and side screw. The mode of failure was determined visually on the foam block. The GBP and side screw were fully integrated with the foam block and there were no breakage on them during tensile testing and after.

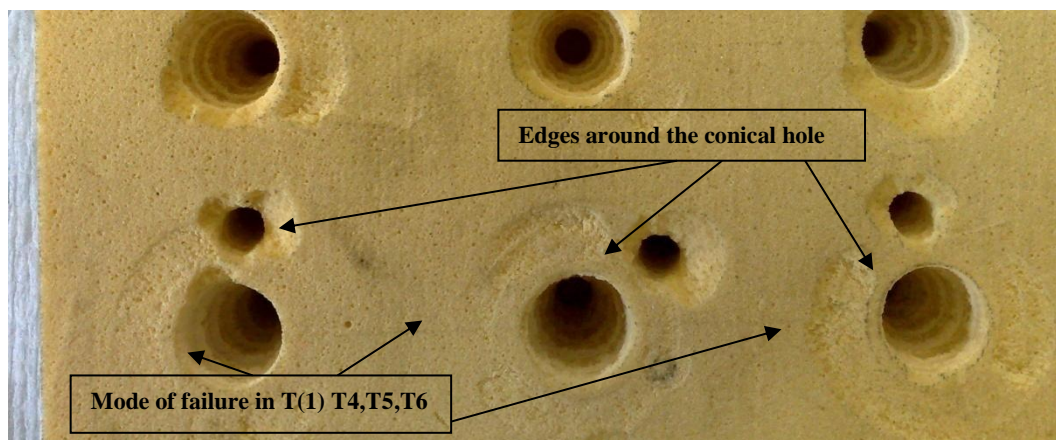


Figure 5-: Mode of failure in T(1) +1 side screw tensile testing for T4, T5 and T6

The ultimate failure of the GBP and the side screw strength specimen was measured, and load and displacement figures were recorded. The scars on the foam block surface can be due the design and shape of the implant or/and the fixture of the implant on the foam block. The edges on the foam block of both GBP and screw can be due to the GBP conical screw and peripheral screw shape and fins. The mode of failure is slightly different for each test specimen, the mode of failure in Figure 5- show the amount of scar and debris caused by pulling out the implant when the maximum loading was reached.

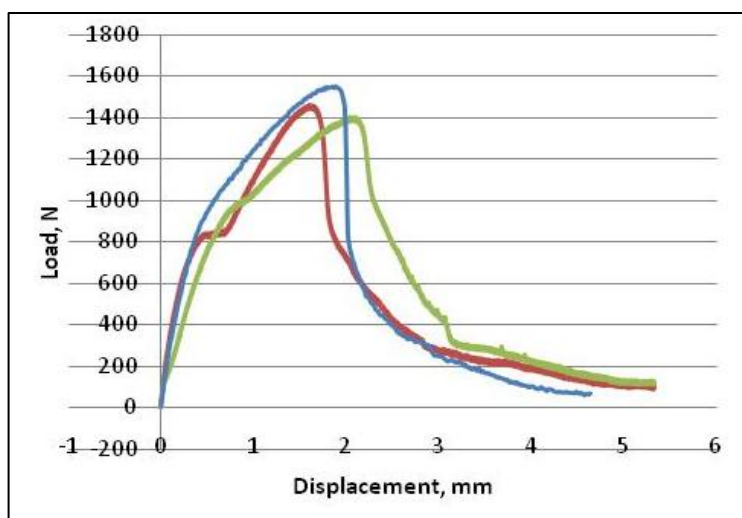


Figure 5-: Load, displacement figure for the case with one peripheral screw, Test(1) T4(Blue line), T5(Red line) and T6(Green line) +1 screw Load, displacement

The tensile testing using one side screw defiantly showed a higher maximum loading tolerability than without screws attached to the GBP. The maximum loading reached for each test was T4(1461N), T5 (1400N), and T6 (1548N).

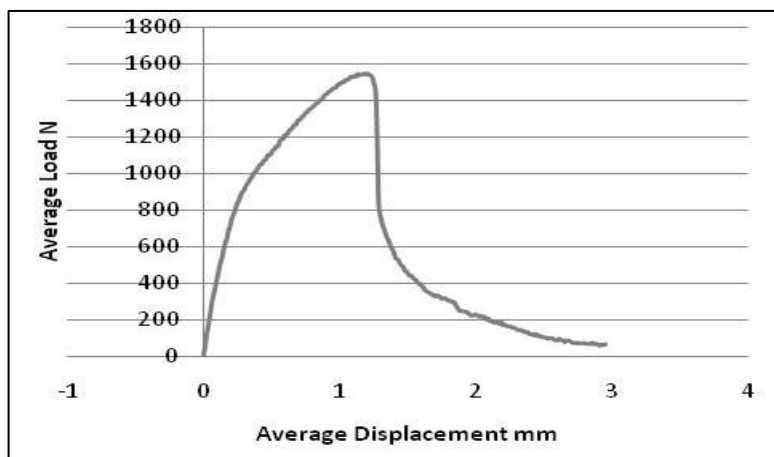


Figure 5-: Average load and displacement figure for three repeat of Test(1) +1 screw for tests T4,T5 and T6

Figure 5- shows the load- displacement relation in the three tensile tests. The curve shows the maximum load the GBP with one screw can tolerate before it fails. Figure 5- shows the average loading vs. the displacement of the three tests which was 1469.9N and that equals to 146.9kg.

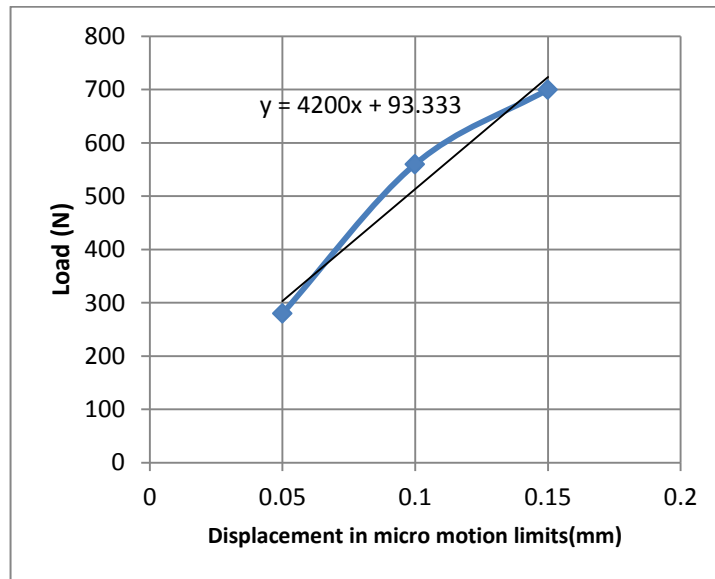


Figure 5-: Stiffness for average results of the Test (1) +1 screw in the limits of allowable micro motion

$$\text{Gradient of a line} = \frac{Y_2 - Y_1}{X_2 - X_1} = \frac{700 - 280}{0.15 - 0.05} = 4200$$

And if we continue the black line in Figure 5-, it will cut the Y axis at 93.33

As mentioned earlier stiffness is only valid in the limits of micro motion, and is defined as the gradient of the linear part of the force displacement line in this domain. Figure 5- shows the stiffness, slope of the linear part of the figure in the limits of 50 to 150 μm , 4200N/mm or 4.2×10^6 N/m. This number (4200N/mm) shows as expected the stiffness in the interface between the GBP and the foam block (bone substitute) increased by adding a peripheral screw. However defining the same allowable limits of micro motion is important in this comparison. The figure shows the stability of the implant throughout the testing procedure over the displacement. Figure 5- to Figure 5- shows the stress-strain relation recorded during the testing process based on the implant and screw geometry by Bluehill2 software.

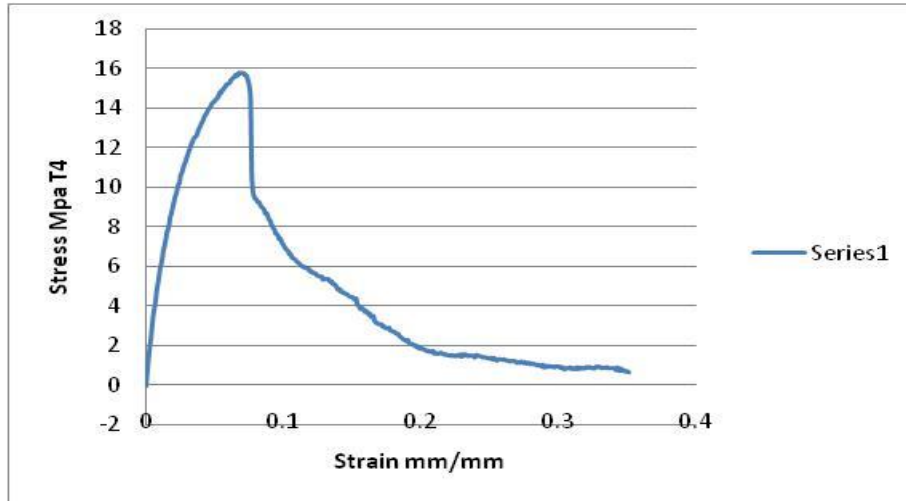


Figure 5-: Stress and Strain Test (1)+1 screw (T4)

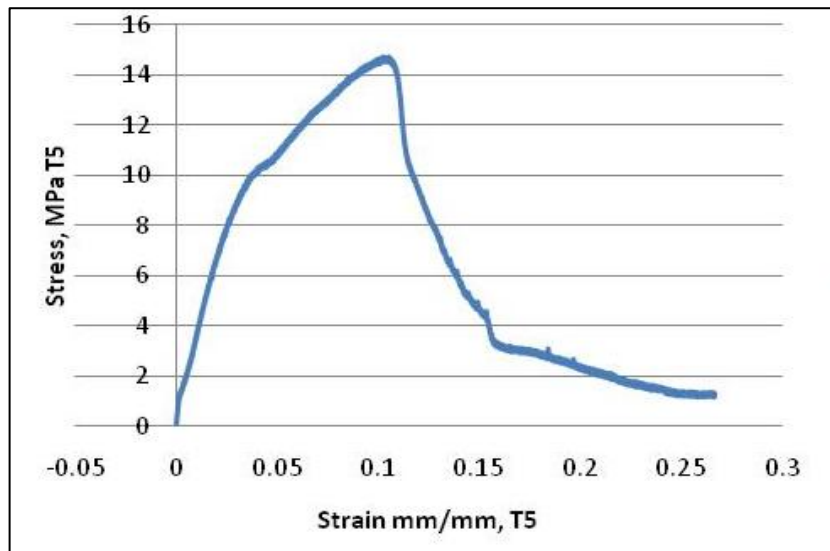


Figure 5-: Stress and Strain Test(1) +1 screw (T5)

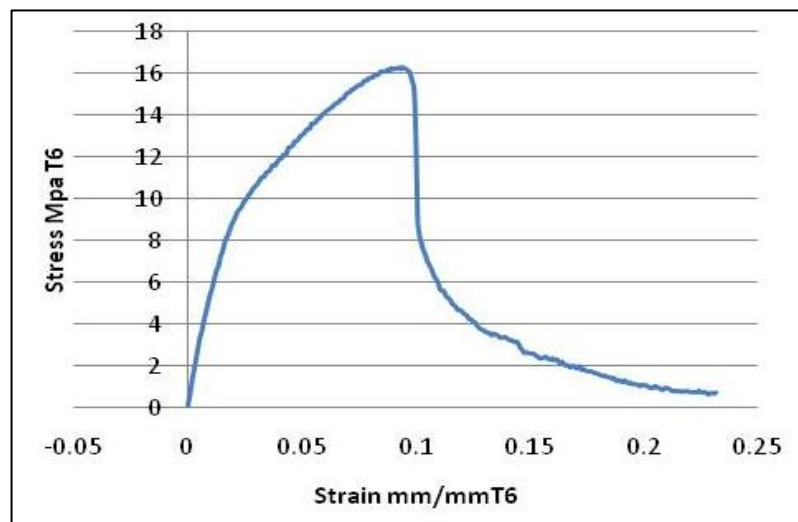


Figure 5-: Stress and Strain Test(1) +1 screw (T6)

5.3.2.4 Discussion:

The tensile testing results for the GBP with one side screw have shown similar results to the GBP tensile testing without any screws. However, as expected the average pull out load was higher compared to no screw tensile testing. The maximum load of average result as shown in Figure 5- was 1149.9N which equals 149.9kg of pulling force or weight. The one side screw has given better results and applied an extra strength to the GBP to tolerate a higher loading.

From Figure 5- to Figure 5- the results of the tensile testing with one side screw were produced and showed the average load, displacement, stiffness, stress and strain for T(1) T4,T5 and T6. It was visually observed that the GBP and the peripheral screw did not break or fail throughout the testing process.

From the Figure 5- and Figure 5- a value between 780N to 1000N is suggested as a maximum loading the GBP with one side screw can tolerate without failing. Furthermore, the yield force and elastic area can be introduced in the liner part in Figure 5-.

5.3.3 Tensile testing Test(2)(GBP + 2 side screws) T7, T8 and T9 :

5.3.3.1 Preparation:

A tensile testing was carried out using GBP with two peripheral screws attached to the foam block. Firstly, drilling the same conical shape into the foam block as before, and drill two angled holes for 2 side screws each with 10° angle inclined from the GBP conical shape screw. The metal rod design again was changed to enable extra strength during the tensile testing and to avoid breakage or loosening. Figure 5- shows the metal rod design with two high tensile steel screws attached to the support plate. As the distance between the GBP and the support plate has increased the metal rod got weaker. Therefore, to avoid this defect the high tensile steel screws were added to the support plate with maintaining the same length between the GBP and support plate. Also the change in design was aimed to facilitate the process of adding the two side screws with 10° angle. In addition, the brass screws used in the previous tensile testing (T(1)) showed a sign of possible breakage to the brass screws as they were not strong enough to tolerate two side screws hence the change in the metal rod design.

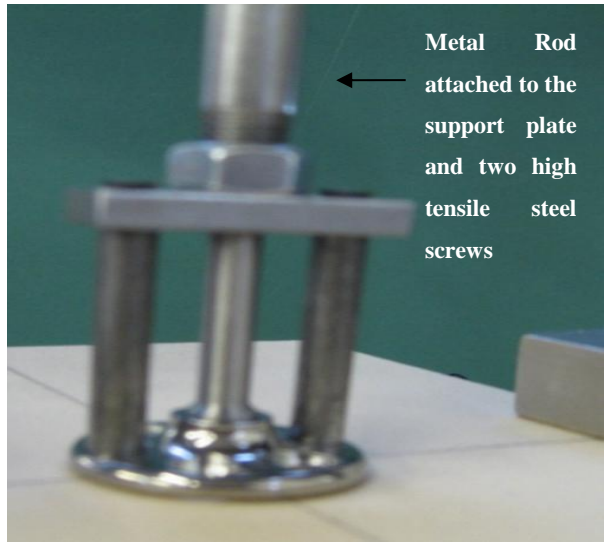


Figure 5-: redesign the metal rod to give extra strength during testing

5.3.3.2 Processing:

The tensile testing started same as before by placing the foam block, after screwing the GBP and two side screws with 10° angle inclined from the main GBP screw, on the load cell on Instron 8800 machine. As shown in Figure 5- the GBP was screwed in the foam block using the torque wrench with 6Nm to secure it on the foam block. Then the side screws were screwed with same torque wrench with 1Nm force at 10° angle on a far side of the GBP. Figure 5- shows the fixture of the first tensile testing using two side screws. The foam block then would be placed on the load cell with clamps to secure the foam block during the testing and the metal rod attached to the crosshead on Instron 8800 machine.

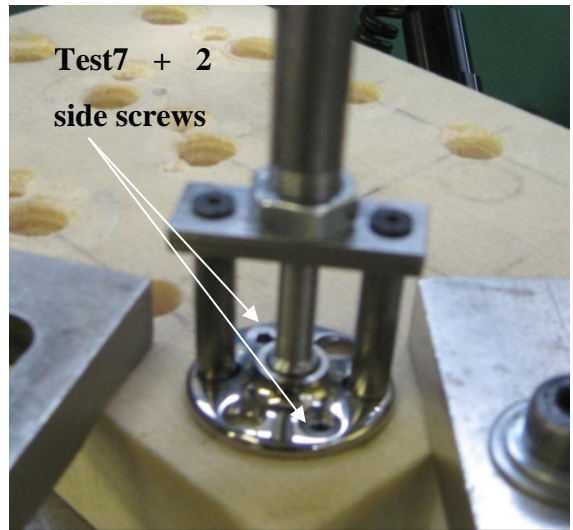


Figure 5-: Tensile testing T(2) T7 + 2 side screws

Similar fixation was applied for the three tests with an exception to the position of the GBP and side screws. The fixation of the side screws were carefully chosen to be on a far side to each other on the foam block.

The tensile testing using two side screws have resulted in higher loading that reached up to 2396N that equals to 239.6kg. The failure mode was observed on the foam block with breakage after applying maximum loading in each pull-out test. It was observed from the three tests that when the maximum loading is applied on the implant with two side screws the foam block breaks every time or fracture on the sides.

The testes were carried out on two different foam blocks to avoid overlapping and to keep enough distant with the 10° angle of the two side screws. Nonetheless, two tests were carried out on the same foam block and the third one was on the centre of the second foam block and the results were the same. Every time the foam block was splintered except the third time which was carried out on the edge of the foam block and that lead to a complete fracture in the foam block as in Figure 5-. Figure 5- to Figure 5- show the position and the fixture of the GBP and the two side screws in each test and the resulted fracture.

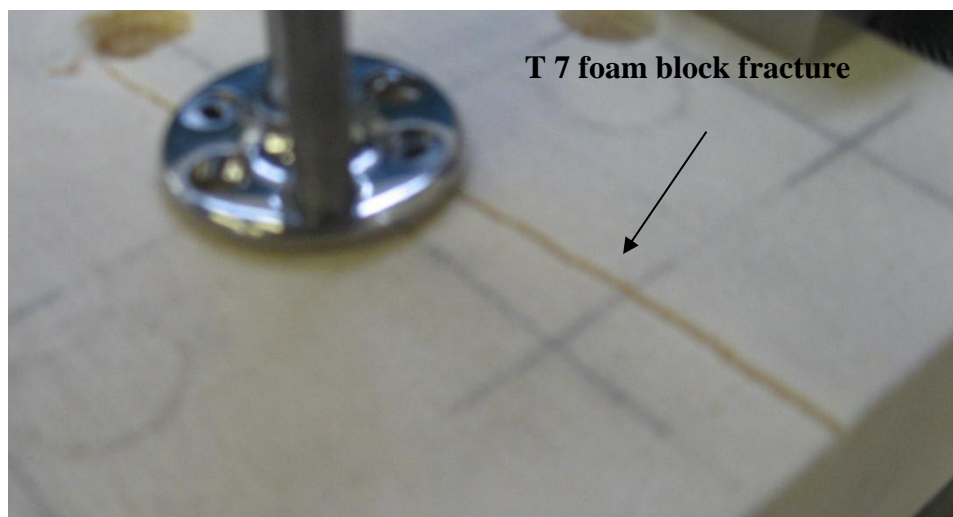


Figure 5-: Test(2) (GBP+ 2 side screws) T7 cracked foam block

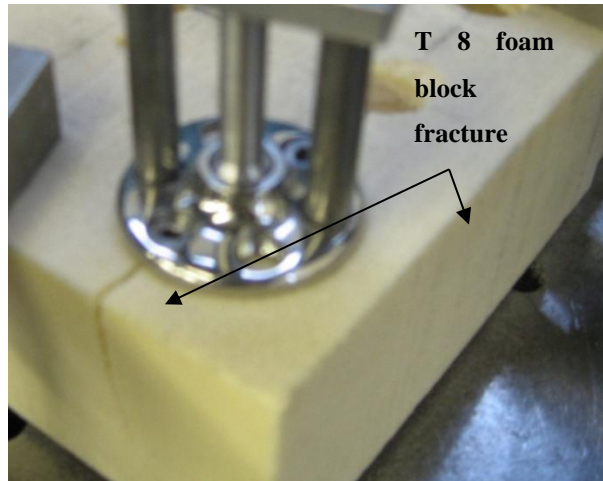


Figure 5-: Test (2) (GBP+ 2 side screws) T8 cracked foam block

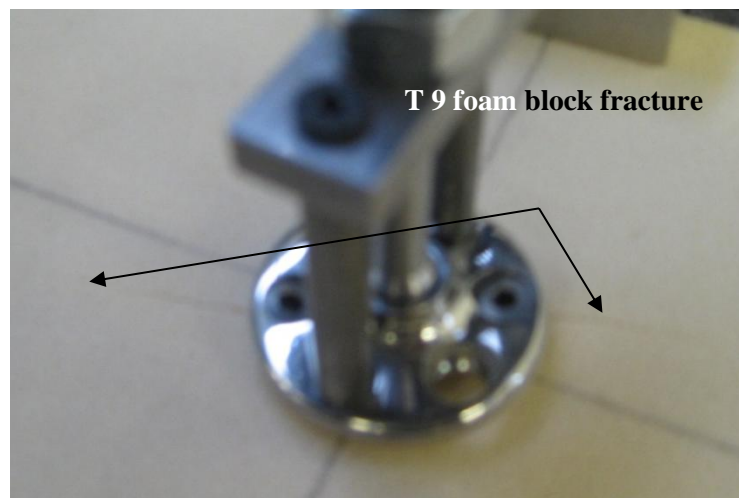


Figure 5-: Test (2) (GBP+ 2 side screws) T9 Fractured foam block

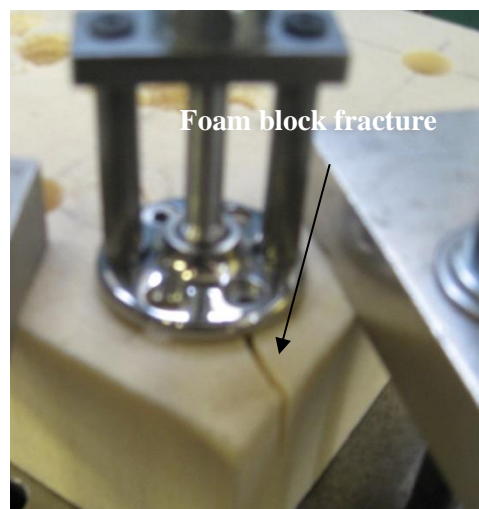


Figure 5-: T(2) (GBP+ 2 side screws) T8 complete breakage to the foam block in tensile testing.

Figure 5- displayed the fracture in the foam block after applying the tensile testing to the GBP with two side screws with a load of 2250N.

The following figures show the results of the pull-out-test for the GBP with two peripheral screws. Figure 5- to Figure 5- show the Load displacement figures for the three tests of the GBP with two peripheral screws. Figure 5- shows the consistency of the result for the three tests. The average loading result is displayed in Figure 5- and it can be seen the GBP with two screws has tolerated a higher loading compared to the two previous cases T(0) and T(1).

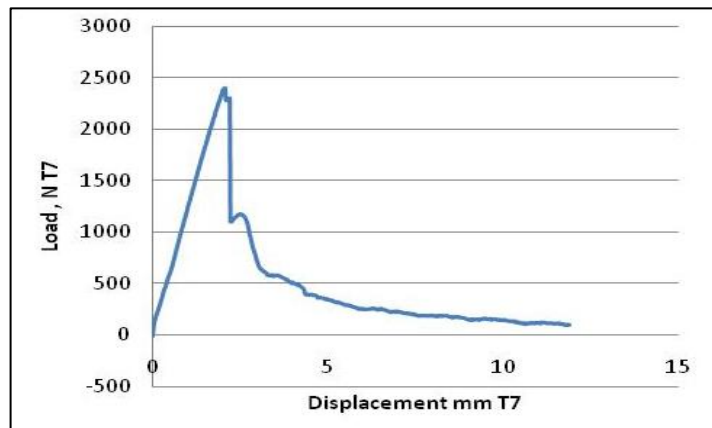


Figure 5-: Load and displacement T(2)(GBP+ 2 side screws) T7

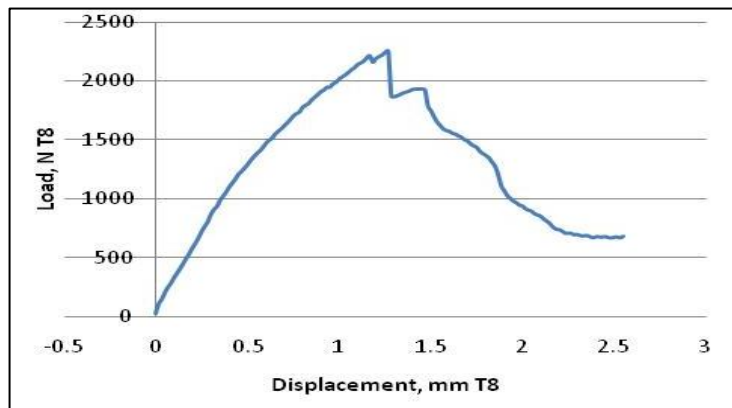


Figure 5-: Load and displacement T(2)(GBP+ 2 side screws) T8

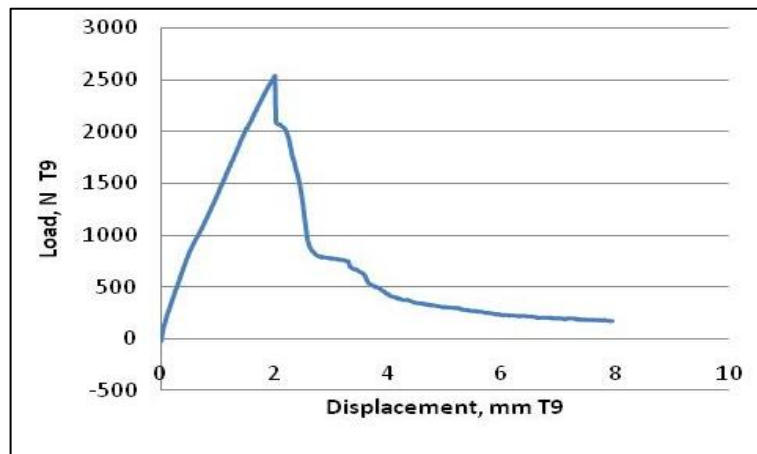


Figure 5-: Load and displacement T(2)(GBP+ 2 side screws) T9

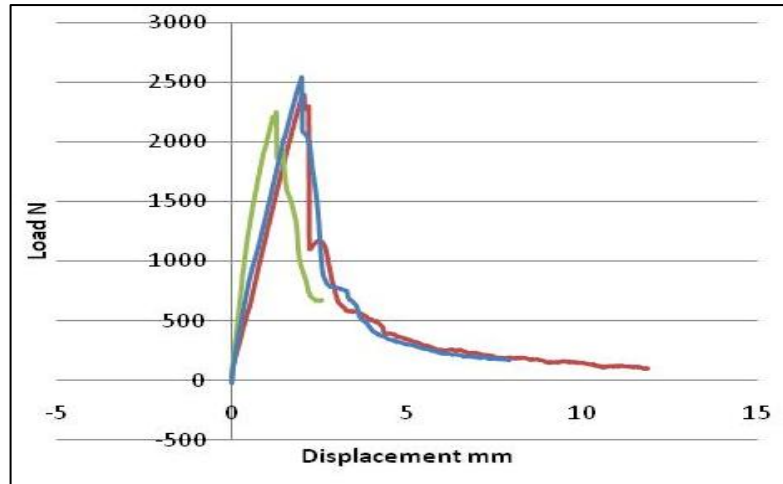


Figure 5-: Load, displacement Test(2) (GBP+ 2 side screws) T7(Red line), T8(Green line) and T9(Blue line)

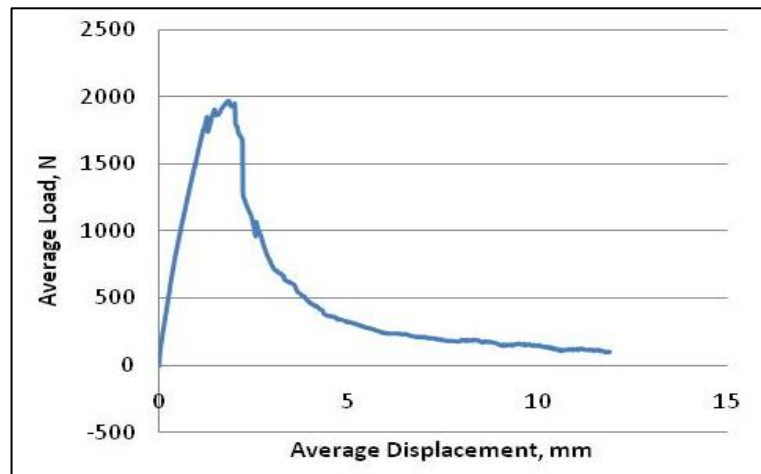


Figure 5-: Average Load and average Displacement T(2) (GBP+ 2 side screws) T7, T8,T9

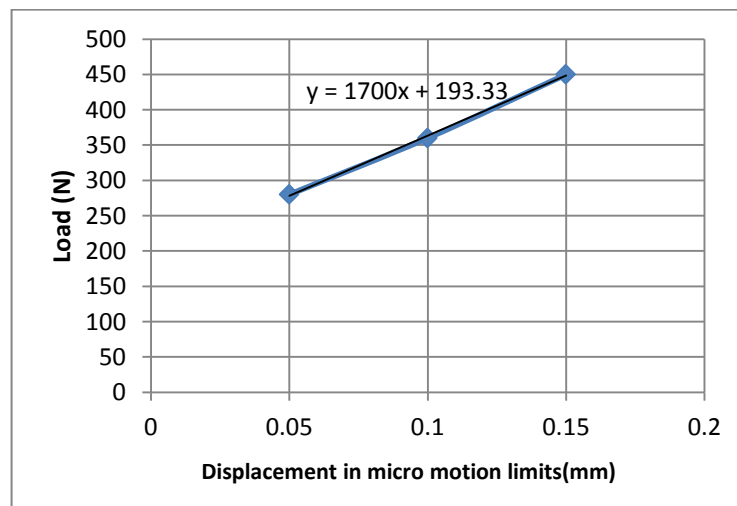


Figure 5-: Stiffness for T(2) (GBP+ 2 side screws) in the allowable limits

Again, stiffness is only valid in the limits of micro motion, and it is defined as the gradient of the linear part of the force displacement line in this domain. Figure 5- shows the stiffness, slope of

the linear part of the figure within the allowable limits of 50 to 150 μm , 1700N/mm or 1.7×10^6 N/m. This number (1700N/mm) shows the stiffness has decreased when adding two peripheral screws to the GBP. This can be due to the fact that the deflection has increased (i.e. the time for the GBP with two screws to be pulled out from the foam has increased).

$$\text{Gradient of a line} = \frac{Y_2 - Y_1}{X_2 - X_1} = \frac{450 - 280}{0.15 - 0.05} = 1700$$

And if we continue the black line in Figure 5-, it will cut the Y axis at 193.33

Adding two screws to the GBP indeed has increased the strength of the composite. On the other hand, it has developed more resistance of a higher value that led to an increase in the time required for the composite to be pulled out completely from the foam block (bone substitute). As it is explained before the fracture is by the shear forces and by having more screws, automatically the area supporting the force has been increased, hence stress reduces in the bone with the same force.

Nevertheless, the two fitted peripheral screws with 10° angle inclined from the GBP conical shape screw, has played a role in increasing the time required for the composite to be pulled out. In addition, the conical shape GBP screw might have moved sideways when pulled out with the two side screws attached, and that led to an increase in the resistance and time taken to reach the maximum loading. Therefore, the deflection has increased causing the stiffness of the composite to decrease.

Figure 5- to Figure 5- shows the stress-strain relation recorded during the testing process based on the GBP and screw geometry by Bluehill2 software.

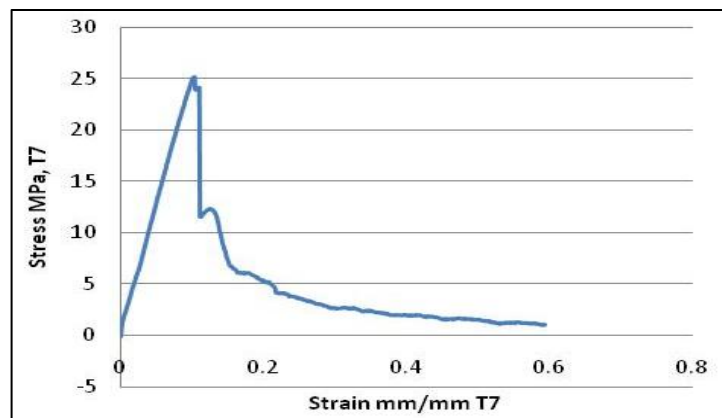


Figure 5-: Stress and Strain for T(2) (GBP+ 2 side screws) T7

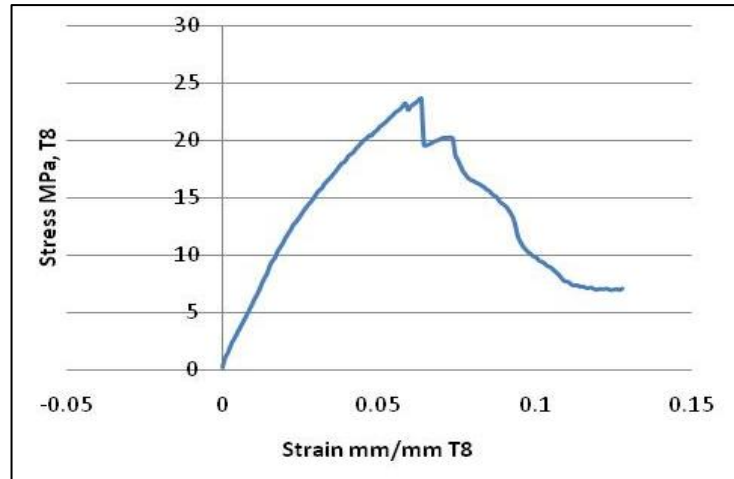


Figure 5-: Stress and Strain for T(2) (GBP+ 2 side screws) T8

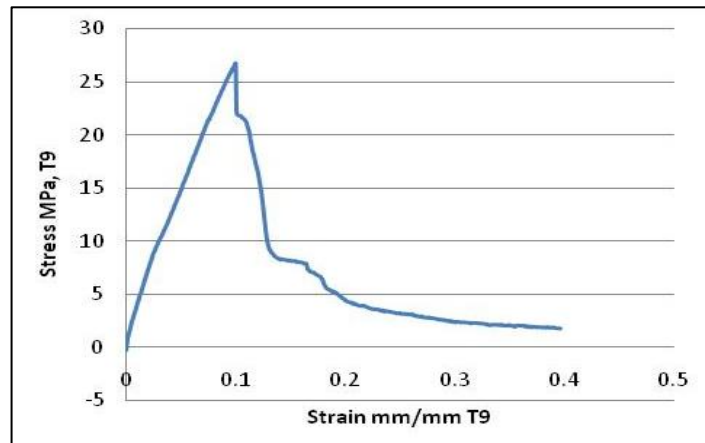


Figure 5-: Stress and Strain for T(2)(GBP+ 2 side screws) T9

5.3.3.3 Discussion:

It was observed during the pull-out test for the GBP with 2 side screws that the mode of failure was at the foam block and at each test the foam block was cracked and fractured. The GBP was pulled out at 5mm/min rate and the load has reached 2540.6N which equals 254.3kg of pulling out force. The GBP with the screws did not show any sign of failing (i.e. no fractures or breakage) throughout the tensile testing.

Indeed the GBP with two side screws composite have tolerated a higher maximum loading without failing during testing; however, it led to irreversible damage on the foam block (bone substitute). Also, the stiffness of the composite has decreased.

5.4 Cyclic Testing:

To investigate the durability of the interface between the GBP and the foam block (bone substitute) a series of cyclic testing were designed before applying the load-to-failure tests (pull out test) which has been summarized in

Table 5-.

The specimens were prepared as described previously in this chapter. Either without side screw, one side screw or two side screws. Instron 8800 machine uses Wave matrix software to produce cyclic testing raw data recorded during testing as shown in Figure 5-.



Figure 5-: Wave matrix software used in the analysis of GBP cyclic testing

The methodology was defined as the following for the no screw cyclic testing:

Apply loading between 10N to 50N with amplitude of 20 ($30N \pm 20N$) for 10 cycles at 1.0Hz as preconditioning to check the connection. It will be followed by a cyclical loading of 50N to 250N with amplitude of 100 ($150N \pm 100N$) for 500 cycles. Then a single cycle load to failure tensile testing will be followed. The failure load was repeated at different loading rate of 5, 10, 20mm/min. The protocol used in the cyclic testing was obtained from a previous study (Chizari, et. al, 2010).

5.4.1 Pulling out T(0) (GBP without screws) after Cyclic Testing

The experimental set up for the pull out test for the GBP was the same as the tensile testing. However, there were pre-conditioning of cycling at 1.0 Hz from 10N to 50N for 10 cycles followed by cyclic loading from 50 to 250 N at 1.0Hz for 500 cycles. Then, a load to failure test should be carried out. The failure load was applied at different rate to examine the effect of loading rate on failure as well. Test number T10, T11 and T12 performed at Loading rate of 5, 10, 20 mm/min were tested on the specimens respectively.



Figure 5-: Failure after cyclic and load to failure test in a with no side screw specimen

The cyclic loading test was carried out for the first specimen of the GBP without any side screw according to the predefined protocol stated previously and shown in Table 5-. After cycling test, the pull to failure test was performed similar to the previous settings as reported in section 5.3, However pull to failure tests carried out at different sample rates of 5, 10, 20mm/min. Figure 5- shows the pull out test of GBP without peripheral screw after the cyclic testing.

Figure 5- shows the failure on the foam block when a pull out test was carried out at a sample rate of 20mm/min, post cyclic loading test. Despite the fact that there was no micro motion recorded post cyclic testing as the load applied to the specimen was small, it was observed that increasing the loading sample rate will increase the possibility of foam block fracture. The pull out test was carried out at different sample rates 5, 10, 20mm/min.

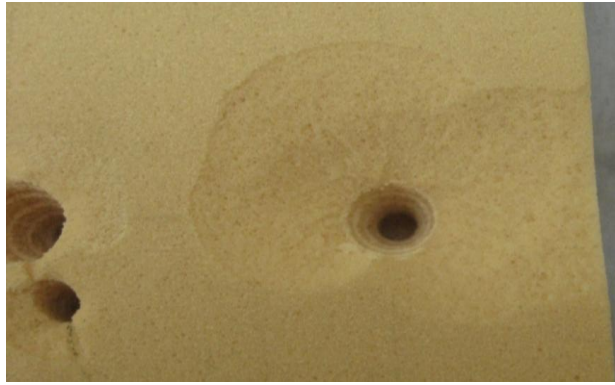


Figure 5-: Load to failure test at the rate of 20mm/min (GBP +no side screw) following a cyclic loading on a foam block

Pull out results at different loading rate of 5, 10, 20mm/min for GBP without side screw (after cyclic loading) are shown in Figure 5- to Figure 5-. The ultimate failure load of the specimen with 5mm/min loading rate is shown to be slightly more than those with 10 and 20 mm/min. It can be explained that faster loading rate increases the risk of fracture in the foam block.

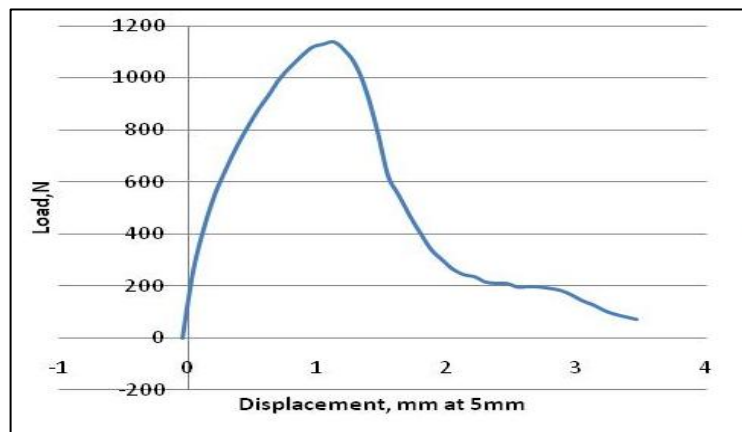


Figure 5-: T(0) (GBP with no screw) Pulling out test, Load-Displacement at rate 5mm/min

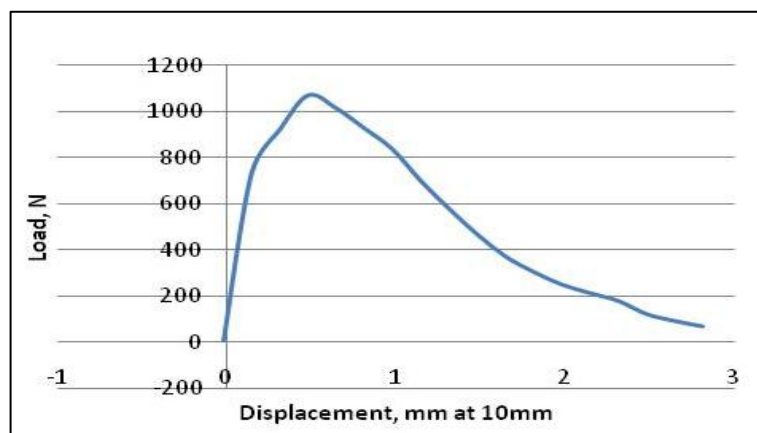


Figure 5-: T(0) (GBP with no screw) Pulling out test, Load-Displacement at 10mm/min

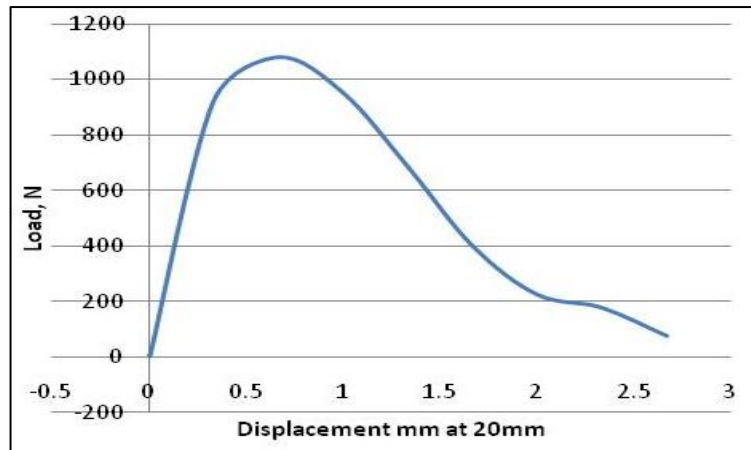


Figure 5-: T(0) (GBP with no screw) Pulling out test, Load-Displacement at 20mm/min

Also it is important to notice from the figures above that the stiffness of the interface between GBP and foam block did change significantly after a cyclic loading.

5.4.2 Pulling out test T(1) (GBP+ 1side screw) after Cyclic Testing:

In the previous test, when the cyclic load was applied, the micro motion was small and not visible. Therefore, it was decided to modify the preconditioning of the GBP with one side screw specimen. Applying a higher loading may facilitate to determine and detect any result failure from the cyclic testing. Consequently a new set up has been laid down. The preconditioning was between 50N to 250N applied at 1.0Hz for 10 cycles. Then, the loading applied of 50N to 500N for 500 cycles at 1.0 Hz. This was followed by load-to-failure test at three different loading rate of 5-10- 20mm/ minute.

Figure 5- shows the tensile testing for the specimen with one side screw attached at the loading rate of 20mm/min. There were no fractures recorded at 5mm/min or at 10mm/min. However, at 20mm/min loading rate, there was a rapid fracture and a micro-motion recorded of 0.16 mm. The test was repeated three times to verify the results and it was observed at a higher loading rate of (20mm/min) the foam block broke at both positions of the GBP conical shape screw and the side screw.



Figure 5-: GBP with +1 side screw after applying 20 mm/min failure loading

On the other hand, the location of the GBP with one side screw on the foam block did not show different results. Except when the tensile testing was carried out at 20mm/min, the foam block did break every time this condition was applied even at different location on the foam block. The higher the sample (loading) rate the higher the risk of foam blocks (bone substitute) fractures.



Figure 5-: GBP with 1 screw tensile testing at 5mm/min and 10mm/min

Comparing scars on foam block post testing as shown in Figure 5-, may relate to the GBP fitting position, shape and design. The other reason considered is the cyclic loading prior to the pull out test. The three tests showed similar results and similar mode of failure at the GBP conical shape screw and side screw positions.

Pull out test result at different loading rate of 5, 10, 20 mm/min for the three specimens after a cyclic loading are shown in Figure 5- to Figure 5-. The failure load of the specimen with 20 mm/min loading rate is shown to be less than those with 5 and 10 mm/min which shows the higher loading rate increase the risk of fracture.

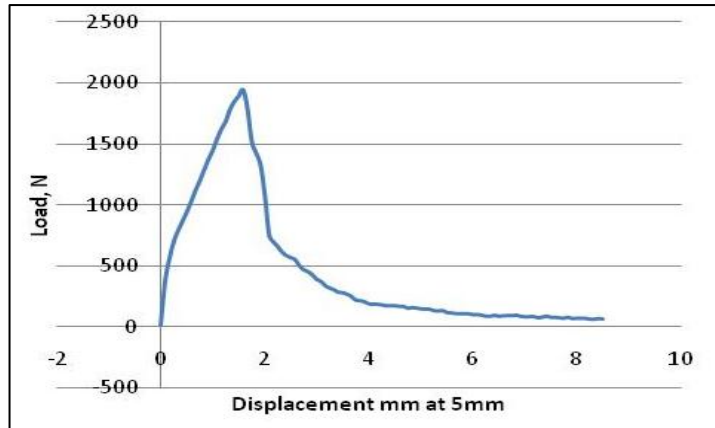


Figure 5-: Load-Displacement of GBP with 1 side screw at 5mm/min

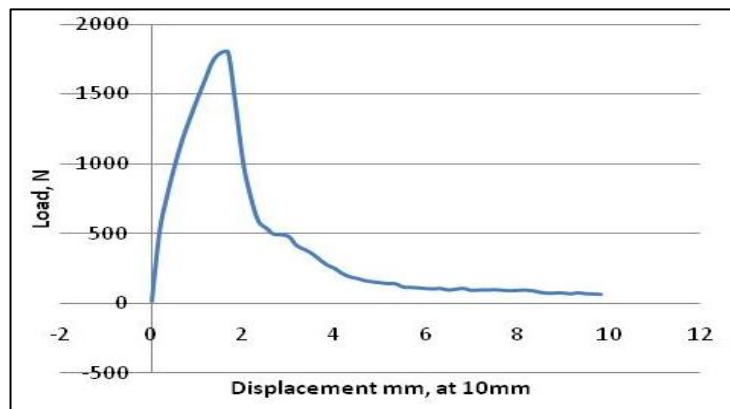


Figure 5-: Load-Displacement of GBP with 1 side screw at 10mm/min.

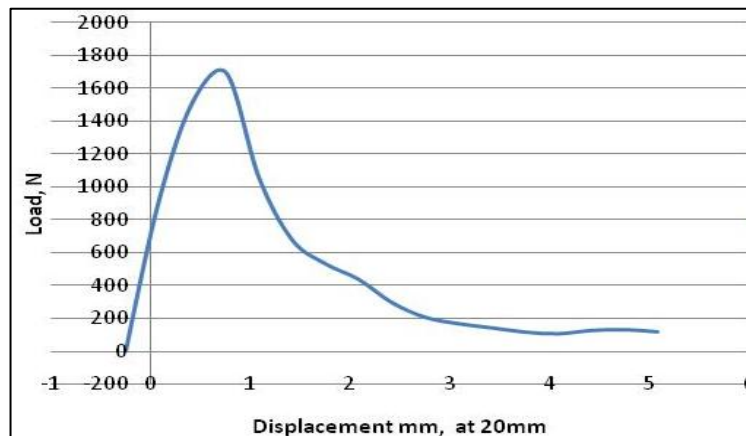


Figure 5-: Load-Displacement of GBP with 1 side screw at 20mm/min

5.4.3 Cyclic Testing T(2) T16, T17 and T18 (GBP+2 side screws):

The same settings and preconditioning used for the cyclic testing with one side screw were used for the cyclic testing with 2 side screws. The preconditioning: cycling at 1.0Hz from 50 to 250 N for 10 cycles. Then apply cyclic loading from 50N to 500N at 1.0Hz for 500 cycles. Followed by

a tensile testing should be carried out at 5-10-20 mm/min. The foam block was moved by 0.5mm when the cyclic testing was applied at 50N to 500N for 500 cycles.

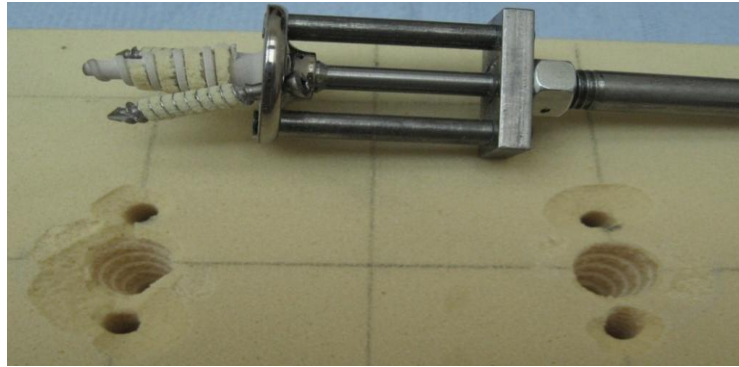


Figure 5-: GBP with 2 side screws tensile testing at 10mm/min and 20mm/min

Pull out test result at loading rates of 5, 10, 20 mm/min of the specimens after cyclic loading are shown in Figure 5- to Figure 5-. As it was expected the failure load of the specimen with 20 mm/min loading rate was less than the loading rate of 10 mm/min.



Figure 5-: GBP with 2 side screws tensile testing at 5mm/min

The specimen with loading rate of 5mm/min did not show the expected result as the foam block was totally broken at the side. The test was redone again at later stage with loading rate of 5mm/min and it showed similar results to the loading rate of 10mm/min (i.e. no breakage in the foam block). The next figure shows the loading and displacement after the foam block fractured completely at the side.

The result of the broken foam block specimen at 5mm/min loading rate was intentionally included to emphasise on the importance of the positioning on the foam block where the GBP will be screwed. Figure 5-shows the load and displacement for the 2 side screws specimen at 5

mm/min, where the foam block was totally broken as shown in Figure 5-. There are many reasons to why this could have occurred; one of which is the positioning of the GBP and the screws on the side of the foam block. Another reason is the speed of the pulling-out test and/or the fixture of the implant on the foam block.

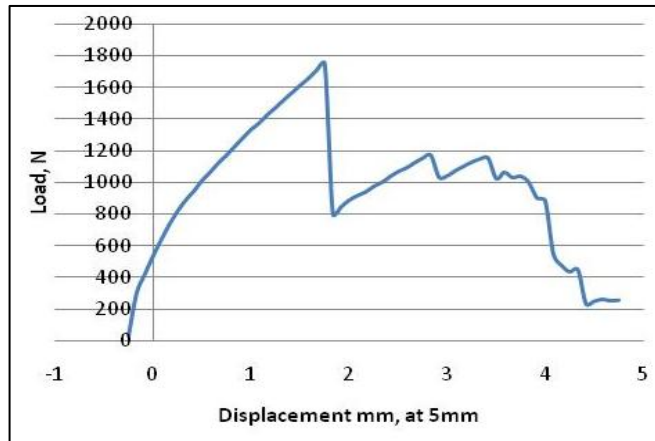


Figure 5-: Load-Displacement of GBP with 2 side screws at 5mm/min.

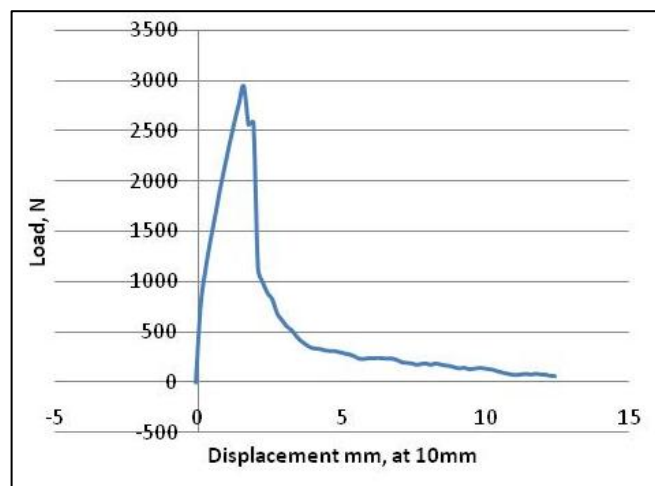


Figure 5-: Load-Displacement of GBP with 2 side screws at 10mm/min

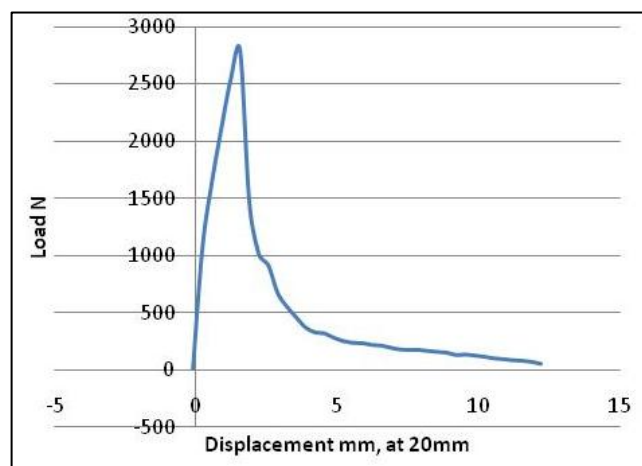


Figure 5-: Load-Displacement of GBP with 2 side screws at 20mm/min

Table 5-: summary of the protocols used in cyclic testing for the GBP + 0, 1 and 2 side screws

Specimen	File name	10-cycle test (1.0 Hz)	500-cycle test (1.0 Hz)	Failure test
0-screw	Test 13, no screw	10cycles, 10-50N		
	Test 14, no screw		500cycles, 50-250N	Test 14, no screw at 5mm/min
0-screw	Test 15, no screw	10 cycles, 10-50N		
	Test 16, no screw		500cycles, 50-250N	Test 19 no screw at 10 mm/min
0-screw	Test 1, no screw	10 cycles, 10-50N		
	Test 2(1), no screw		500cycles, 50-250N	Test 19, no screw at 10 mm/min
0-screw	Test 2(2), no screw	10cycles, 10-50N		
	Test 3, no screw		500cycles, 50-250N	Test 20, no screw at 20 mm/min
+1screw	Test 5 +1screw	10cycles, 50-250N		
	Test 6 +1screw		500cycles, 50-500N	Test 16, +1screw at 5mm/min
+1screw	Test 9 +1screw	10cycles, 50-250N		
	Test 10 +1screw		500cycles, 50-500N (Foam block moved 0.16mm)	Test 17 +1screw at 10 mm/min
+1screw	Test 12 +1screw	10cycles, 50-250N		
	Test 13 +1screw		500cycles, 50-500N	Test 18 +1screw at 20 mm/min
+2screws	Test 17, +2screws	10 cycles, 50-250N		
	Test 18, +2screws		500cycles, 50-500N (Foam block moved 0.5mm)	Test 21, +2 screws at 5mm/min
+2screws	Test 19, +2screws	10cycles, 50-250N		
	Test 20, +2 screws		500cycles, 50-500N	Test22, +2 screws at 10mm/min(Foam block Partially broken)
+2screws	Test 21, +2screws	10cycles, 50-250N		
	Test 22, +2screws		500cycles, 50-500N	Test 23, +2screws at 20 mm/min

The following Figures represent a sample of the cyclic testing results for two cyclic testing with one side screw and a displacement of 0.004mm/min after 10 cycles and 0.045mm/min after 500 cyclic testing. The rest of the results are much similar to this one.

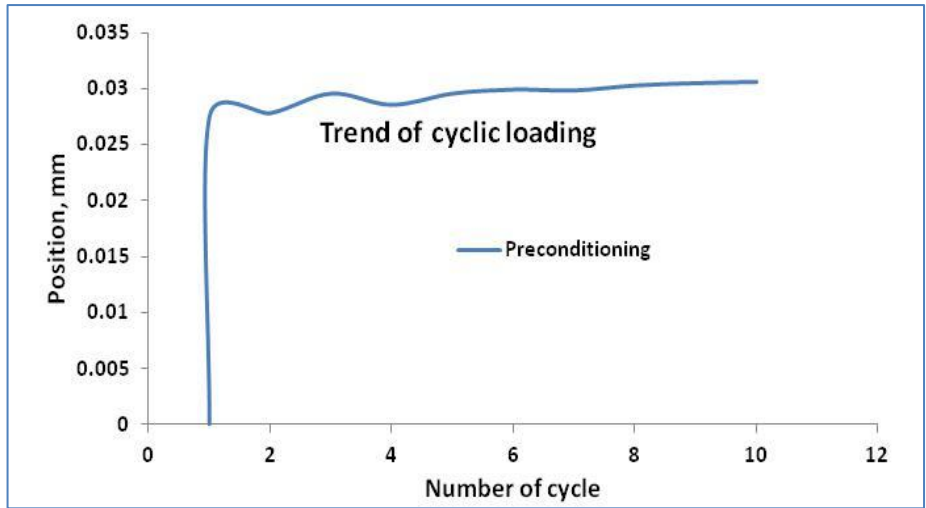


Figure 5-: Trend of increasing the mean of micro motion in a cyclic loading (Preconditioning) at 10 cycles.

Figure 5- shows the trends of micro motion in a cyclic loading at preconditioning (50N – 250N) at 10 cycles. It can be seen from the figure the behaviour of the implant which was linear and steady except for the first 3 – 4 cycles. This is considered to be a positive point in the implant performance.

In cyclic loading the force varies from 50N to 250N which causes changing in micro motion between specific limits, but the mean of the micro motion between the implant and the foam block, increasing slightly.

Figure 5- and Figure 5- show that the micro motion will slightly increase by the time and this could cause Implant loosening , which is one the most important problems.

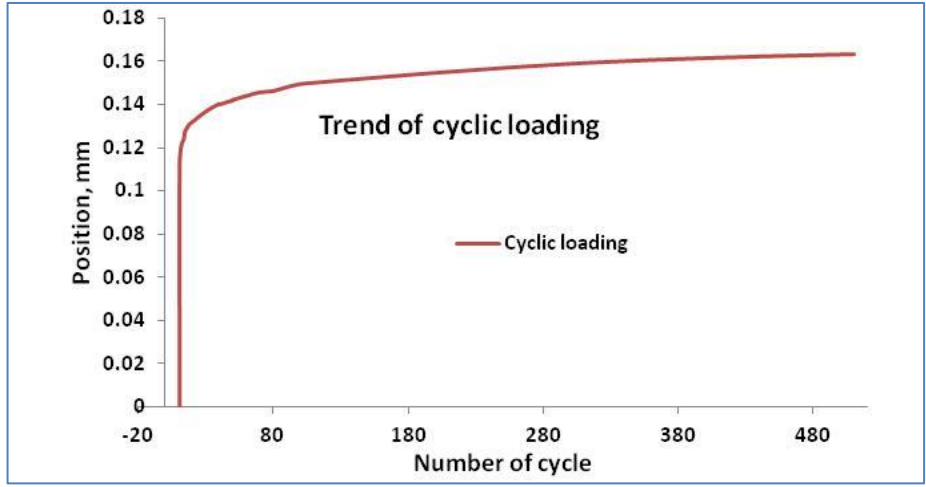


Figure 5-: Trend of increasing the mean of micro motion in a cyclic loading at 500 cycles

Figure 5- shows the trend of increasing the mean of micro motion value in a cyclic loading, within the first 80 cycles the increasing in the mean of micro motion was considerably sharp. Thereafter, the displacement showed a steady and linear curve and performance.

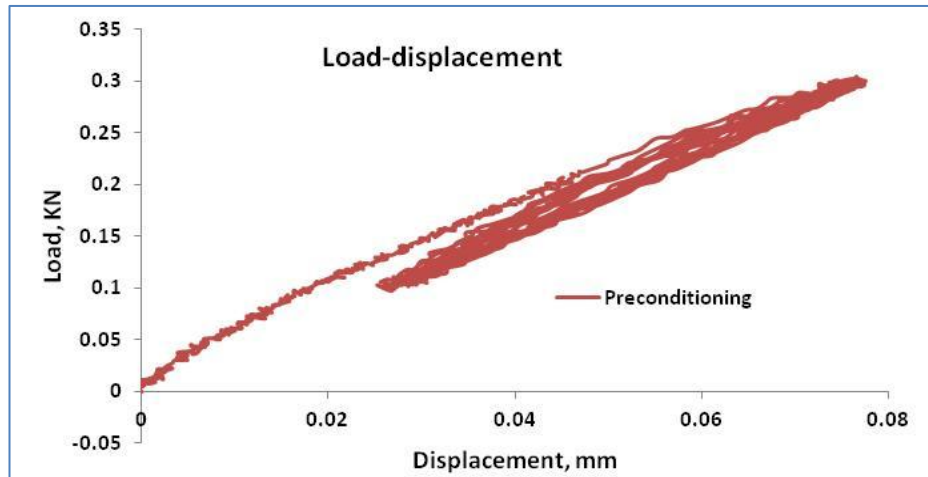


Figure 5-: Load-Displacement at preconditioning.

Figure 5-displays the loading- displacement relationship and it can be seen that when applying the 10 cycles (preconditioning 50N – 250N) there was a displacement of 0.004 mm recorded shown in the figure above (0.01 - 0.3). This is a minimal displacement that does not affect the implant performance in general.

It can be seen from the Figure 5-, the test performed was in the border of the acceptable range of micro motion. However Figure 5- is clearly shows this phenomenon, which means the load, is higher than elastic behaviour of interface between the GBP and the foam block. In other words the composite will fail if the cyclic load was repeated.

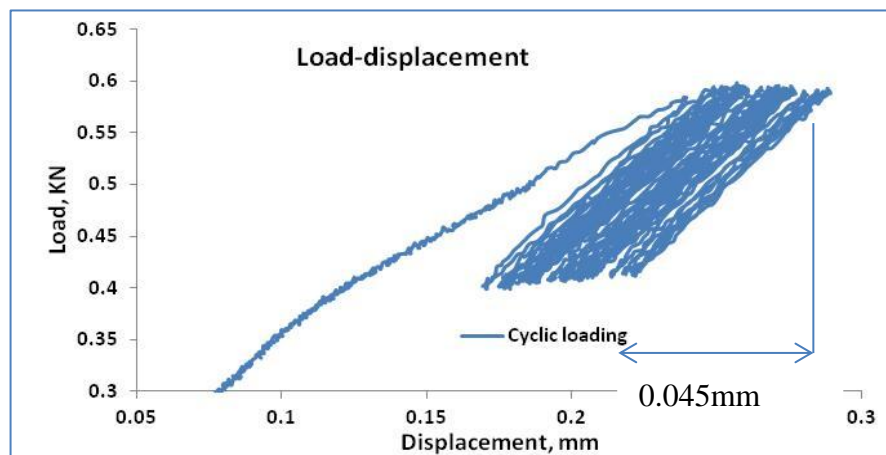


Figure 5-: Load-Displacement at Cyclic Loading

Figure 5- shows the load-displacement relationship when applying 400-600N in a 500 cyclic testing and it can be seen the displacement recorded was 0.045mm. Again, this displacement of 0.045mm is a minimal displacement that proves the stability and strength of the implant.

5.5 Conclusion:

This chapter was dedicated to investigate the importance of the fixture of the implant (GBP) with or without the screws. It investigates the mechanical behaviour of the implant when maximum loading applied/reached. The Load, displacement, stiffness, stress and strain measures were calculated using Bluehill2 software.

A foam block with cancellous bone properties was used for the mechanical testing aim. The tests were carried out using Instron 8800 machine with crosshead and load cell to carry on the pull-out test at different set ups.

Firstly, without using any screws at 5mm/min loading rate the test was done three times respectively. The results shown were similar and the failure was observed on the foam block with debris and scars around the tested area and threads marks on the edges. Secondly, the mechanical testing was carried out on a specimen of GBP with one screw at 5mm/min loading rate; the test repeated three times respectively.

The results of the pull-out tests with one screw attached to the GBP have shown once again similar results. The maximum loading was higher than those without screws attached to the GBP. Thirdly, the pull-out test was carried out on a specimen with GBP and two far side screws with an angle of 10° three times respectively. The results for these tests at 5mm/min loading rate have shown again similar results to each other except that the value of the maximum loading reached was higher. Also, the foam block has fractured from the sides where the tests were carried out on the three tests.

Consequently, it has been found contrary to the expectation the following:”increasing the number of screws will not necessarily increase the stability of the foam block (bone); it might jeopardize the strength and/or the structure of the foam block (bone) where the GBP will be implanted”.

Furthermore, cyclic testing was carried out with different settings and preconditioning to be applied on the GBP with/without screws using Wave matrix software. The first set of tests were applied on the foam block without screws, then a set of load to failure tests (pull-out) were carried out at different loading rate of 5, 10, 20 mm/min. The results were not the same for the three different loading rates. Similarly, the followed cyclic tests for the GBP with one and two screws have shown different results and a micro-motion was recorded. The micro-motion was observed mainly when a loading rate of 20mm/min was applied after a cyclic testing carried out for 500 cycles. The results and the micro-motion were explained in more details in the cyclic testing table.

Finally, this chapter has shown that more mechanical testing might be needed to investigate the mechanical behaviour of the GBP in other aspects such as the effect of loading rate on the stiffness of the composite.

Chapter 6. Modelling, Simulation and Results

6.1 Introduction

This chapter will introduce the model simulation and results using ABAQUS software. In chapter 4 an introduction to the methodology of how ABAQUS software works was introduced. However, it will be explained in much greater detail in this chapter.

The integration of FEA in commercially available software's has provided a base from which a simulation is created to portray realistic behaviour; with given material properties, boundary conditions and interaction behaviour are known.

During an arthroplasty the bone ends are excavated to make room for the implant. This significantly weakens the bone which can result in failure in which can lead to bone fractures, fracture can propagate, reduced bone growth if the micro motion is not within 50-150µm, reduced bone growth can lead to weakened adhesion to implant. Previous studies and a group of surgeons have identified the allowable range of micro-motion is between 50-150µm which help bone growth around the Implant and keep the Implant from loosening (Levy et. al. 2007). Bone growth is also an issue, as the micro-motion of the implant relative to the bone in bone-prosthesis interface is known to inhibit the bone ingrowths for micro-motion between 28-150µm. Minimising micro-motion will significantly improve adhesion to the bone (Favre et al 2011). However, the bone itself must undergo micro-motion or compression in order to grow. The study investigates the micro-motion, stress and maximum principal strain measurements using ABAQUS.

There are 5 models that have been analysed in this chapter. The first three simulations consist of the glenoid base on a foam block with 0 screw, 1 screw and 2 screws configurations under tensile loading. These three models mimic the mechanical tests in order to validate the results and indicate the initial failure regions in the simulated bone substitute material. The load used will be the average failure load obtained from the mechanical testing for each configuration. The simulations also compare the performance of each configuration.

The 4th model analyses the Humerus-Implant interface. The simulated bone substitute (foam block) has been replaced with actual bone material properties (i.e. cancellous bone and cortical bones). The 5th model analyses the scapula-implant interactions also using cancellous and cortical bone material properties.

For all models the stress, strain and displacement are analysed.

Results will indicate the performance of the Verso at high loads; part must be over engineered to withstand high stresses from everyday life activities. The results will help in redesign the Verso in order to reduce stress concentrations, i.e. round edges and increase or reduce contact surface area. Simulation results can also help in changing materials, i.e. to absorb impacts better, encourage bone growth and improve adhesion. The results will show the possible regions of failure. Also, the results may provide support for surgeons in inserting peripheral screws.

6.2 Objective of FEA

The objectives of using FEA method are to investigate the interaction between the Verso (reverse) shoulder implant and the humeral and scapula cavities. To understand shoulder anatomy and kinematics and use ABAQUS (SIMULIA, Providence, USA) to create a virtual simulation of a complete assembly of the shoulder joint and Verso implant.

However, the FEA process requires the material properties, surface interactional behaviour, boundary conditions, and loads to be assigned to the created model to portray realistic behaviour of the interaction of the implant and bone. The user is then required to utilise finite element analysis method in ABAQUS to obtain results under a specified heavy loading condition. Visual models of displacement (micro motion); Stress (Principle, Von Mises) and Strain are required to certify benefits of the Verso implant.

6.3 ABAQUS/CAE Introduction:

A complete ABAQUS analysis usually consists of three distinct stages: pre-processing, simulation, and post-processing. These three stages are linked together by files as shown below in Figure 6-:

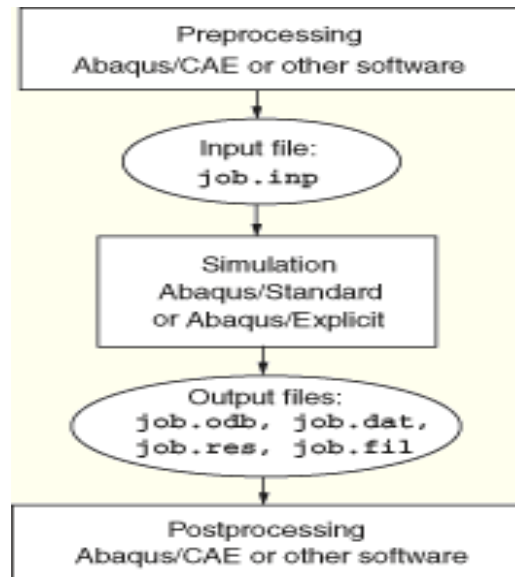


Figure 6-: ABAQUS/CAE (ABAQUS 6.9 user manual 2009)

Stage 1: Define the model of the physical problem and create an ABAQUS input file.

Stage 2: The simulation, which normally is run as a background process, is the stage in which ABAQUS /Standard or ABAQUS /Explicit solves the numerical problem defined in the model.

Examples of output from a stress analysis include displacements and stresses that are stored in binary files ready for post-processing.

Stage 3: evaluate the results once the simulation has been completed and the displacements, stresses, or other fundamental variables have been calculated. The evaluation is generally done interactively using the Visualization module of ABAQUS/CAE or another postprocessor (ABAQUS 6.9 user manual, 2009).

6.3.1 Finite Element Analysis Technique:

As stated before in chapter 4 that ABAQUS software relies on FEA. Finite Element Analysis (FEA) is a numerical method which provides solutions to problems that would otherwise be difficult to obtain. In terms of fracture, FEA most often involves the determination of stress intensity factors. FEA, however, has applications in a much broader range of areas; for example, fluid flow and heat transfer. While this range is growing, one thing will remain the same: the theory of how the method works (ABAQUS 6.9 user manual, 2009).

The process of finite element analysis begins with dividing the solution domain into discrete regions, termed finite elements that are interconnected at nodal points. The basic assumption in

the displacement based finite element approach is to establish a set of functions that are chosen so that they uniquely define the state of displacement within each element in terms of its nodal values. In this way the number of degrees of freedom becomes finite, and any other displacement within an element can be interpolated using these so called shape functions and the known nodal values (ABAQUS 6.9 user manual, 2009).

Finite Element Analysis works by the discretization of a shape into smaller elements which connect at nodes. In software packages this is known as meshing. The elements are usually triangular or rectangular and the nodes can sit at the corners alone (first order) or at the corners and along the link (second order). A brief explanation was introduced in Appendix C.

6.3.2 ABAQUS Dynamic Explicit/Implicit:

This study uses ABAQUS Dynamic Explicit method in analysing the 3D model created. However, the concept of dynamic explicit and implicit will be explained in the following section. This is to illustrate the difference and why this study chooses dynamic explicit method. An illustration of ABAQUS nodal structure was presented in Appendix C.

Dynamic solutions are derived from assessing the problem over a period of time and relate to Newton's Second Law. The initial displacements will be used to find the latter velocities and accelerations needed for the Second Law in conjunction with the mass matrix created by using the material density properties. *Implicit* works by assuming constant acceleration during time period $t_n - t_{n+1}$ and finds the forces with the mass matrix before applying the changes to the stiffness matrix. The displacements of the nodes can then be found by inverting the matrix. *Dynamic explicit* will assume linear displacement over $t_n - t_{n+1}$ and will then calculate the strains, stresses and forces before working out the acceleration. The benefit of doing this is that it requires no manipulation of the stiffness matrix and is therefore simpler to compute with each iteration. However the system does become unstable if the time periods are too great leading to a huge number of iterations. Below in Figure 6- (Wu S., Qiu W., 2008) is the flow chart of dynamic explicit finite element analysis method used in this study .

$$\text{Newton's Second Law: } \mathbf{F} = m\mathbf{a}$$

Where F = Force, m = mass, a = acceleration.

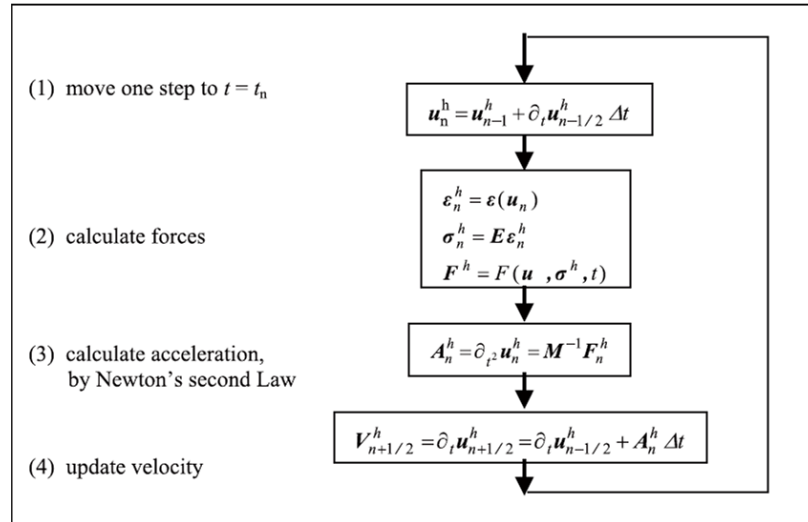


Figure 6-: Flowchart of Dynamic Explicit Finite Element Method

Where $\varepsilon = \text{Strain}$, $\sigma = \text{Stress}$, $A = \text{Acceleration}$, $F = \text{Force}$, $E = \text{Youngus Modulus}$, $V = \text{Velocity}$, $\Delta t = \text{increment of total time}$, $M = \text{Mass Matrices}$ and $u = \text{the displacement component}$.

The unconditionally stable implicit method will encounter some difficulties when a complicated three dimensional model is considered. The reasons are as follows:

- As the reduction of the time increment continues, the computational cost in the tangent stiffness matrix is dramatically increased and even causes divergence;
- (ii) Local instabilities cause force equilibrium to be difficult to achieve.

The explicit techniques are thus introduced to overcome the disadvantages of the implicit method. For the explicit method, the CPU (central processing unit) cost is approximately proportional to the size of the finite element model and does not change as dramatically as the implicit method. The drawback of the explicit method is that it is conditionally stable. The stability limit for an explicit operator is that the maximum time increment must be less than a critical value of the smallest transition times for a dilatational wave to cross any element in the mesh. Secondly, the nature of the explicit method limits it to the analysis of short transient problems. If this method is used for quasi-static problems, the inertia effects must be small enough to be neglected. One way to assure this is to set the limit on the kinematic energy to be less than 5% of the strain energy (ABAQUS 6.9 user manual, 2009).

6.4 Methodology

There are 5 models that are analysed in this research. The first 2 examine the scapula and humerus interactions with the associated implant part respectively. The latter 3 models examine the performance of the glenoid base implant under 3 configurations. These results will show the behaviour more clearly but most importantly the results are used in comparison to mechanical testing for validation of all results obtained from ABAQUS. Figure 6- shows the scapula and humerus models generated in ABAQUS.

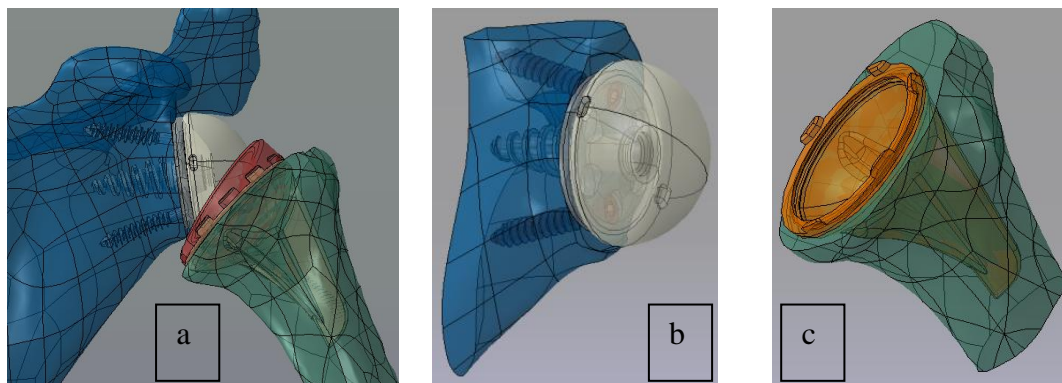


Figure 6-: a: Full shoulder model, b: Scapula model, c: Humerus model

6.4.1 Modelling Process:

As stated before in Chapter 4, in order to run FEA a 3D model must be created. In this study the model was created in ABAQUS after assembling all parts from Geomagic and MIMICS software to create a whole model includes both the Implant and bone parts.

To perform an analysis in ABAQUS the list of setting as shown in Figure 6- was completed. This list is found on panel on the left hand side of the program and indicates all the possible setting required to complete the analysis. Clearly, without an accurate setting of the parameters it is impossible to get real simulation and reliable results. Although, most of the time it is impossible to create exactly similar conditions as in the real situation, the better and more accurate definition for the setting and variables included in the analysis the more accurate and practical the results will be. Obtaining all variables is a difficult task as this alters from application to application and requires extensive experimentation to achieve. However from previous research and similar applications we can deduce the variables and settings.

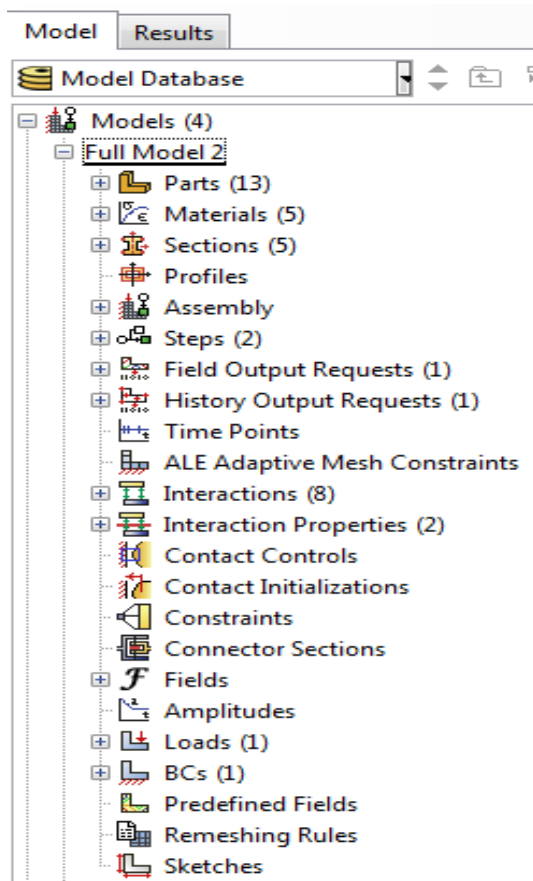


Figure 6-: ABAQUS Model Tree

The first step of the modelling was to import the scanned parts from MIMICS into ABAQUS as shown in Figure 6-. After all parts were imported they required 3D reconstruction as they were not representing the parts accurately. This may have been due to the format change in the program, or the inaccurate model geometry imported from GEOMAGIC.

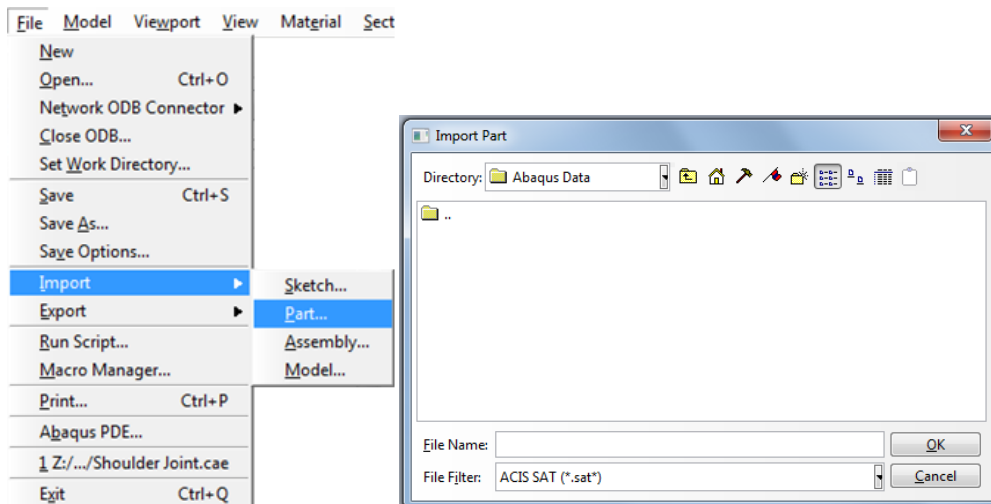


Figure 6-: Importing Parts into ABAQUS

The parts were not solid, had incomplete edges and had points outside the original part region. To overcome this problem the “Geometry repair tool” function is used as shown in Figure 6-. Selecting “part” in category and then “convert to precise” the part is regenerated. This method removes all nodes outside the contours of the part. To complete the repair process the part is finally “stitched”. This process removes the free edges by combining the nodes on the edges to single points creating a complete shell. Results can be shown in Figure 6-.

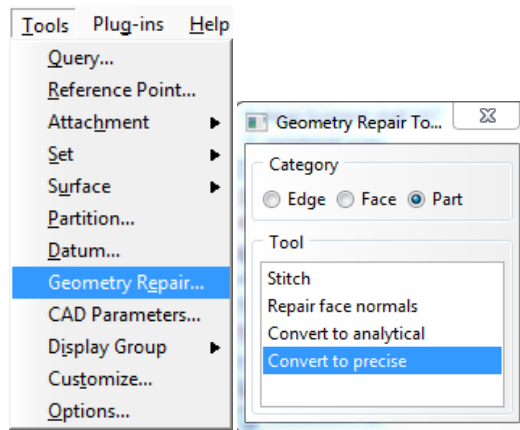


Figure 6-: Geometry repair tool

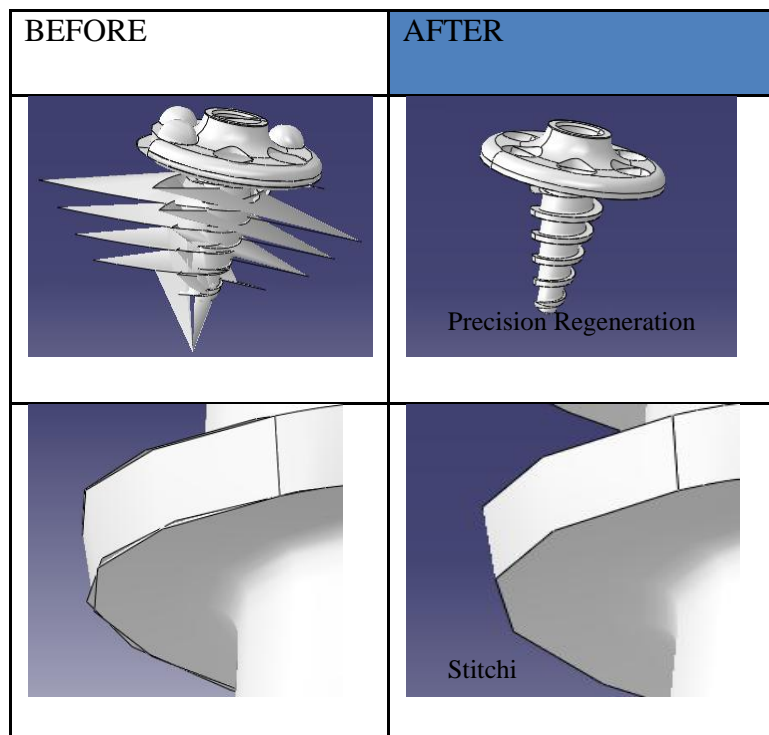


Figure 6-: Results after Geometry repair

Whilst still in the parts module the completed shell is converted into as Solid in order to be able to apply material properties as well as be able to further reconstruct the parts. This options is founds in “shape” as shown in Figure 6-.

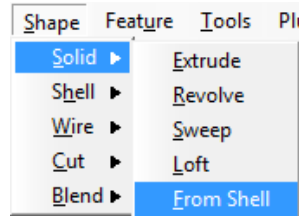


Figure 6-: Converting parts into Solid part

To apply material properties to the parts the materials themselves were first included individually as shown in Figure 6-. Selecting materials opens the “Edit Material” window which allows you to set general, mechanical, thermal and other material behaviour.

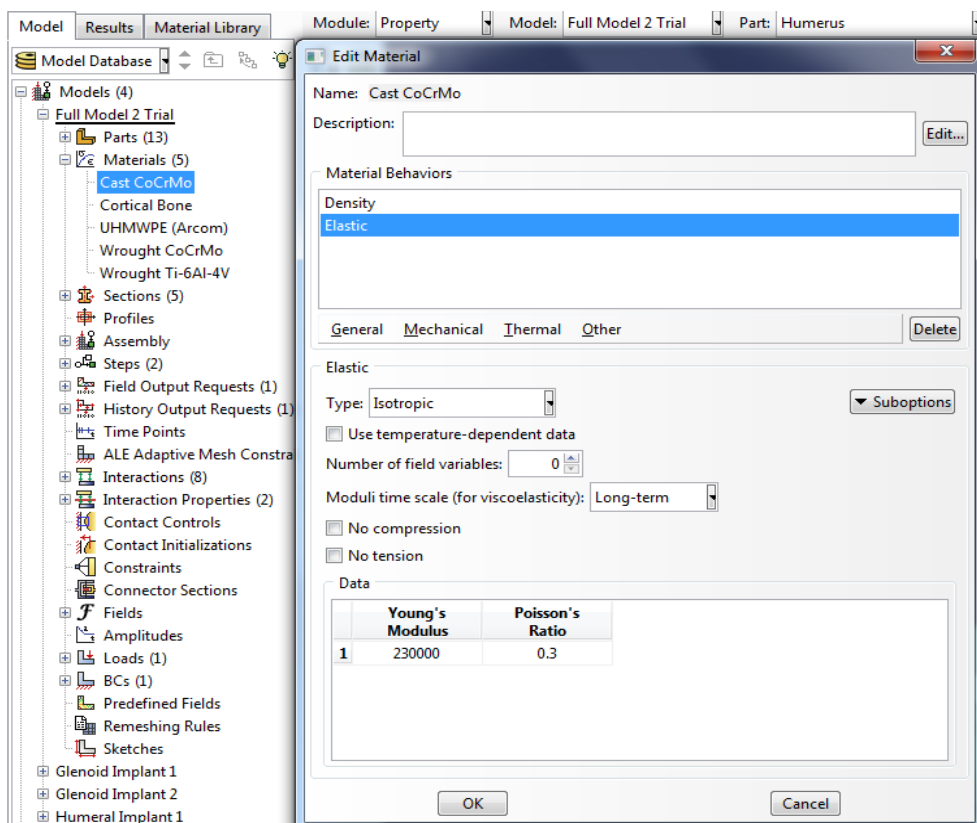


Figure 6-: Apply Material Properties to the parts

To simplify the problem the materials are all set to be isotropic. Using material properties obtained through research, the density and elastic behaviour is set for each material. Elastic behaviour includes Young’s Modulus and Poisson’s Ratio.

After materials were set, Sections are created in the Sections module as shown in Figure 6-. This module allows a definition of the model in terms of Solid, Shell, Beam and composition Homogenous, Generalized plane strain, Eulerian and composite. To simplify the problem the sections are set to Solid, and Homogenous and each renamed according to the materials they represent.

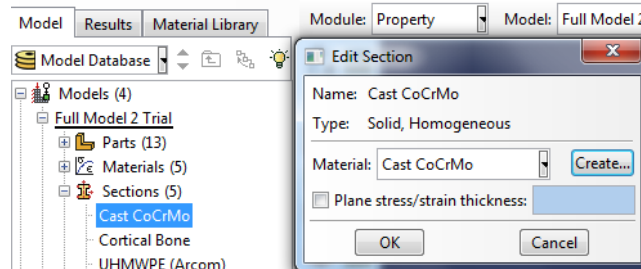


Figure 6-: Material Assignment

Going back to the parts module each part was allocated sections to apply the material properties and behaviour as shown in Figure 6-.

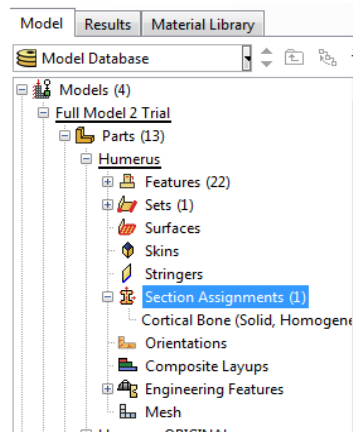
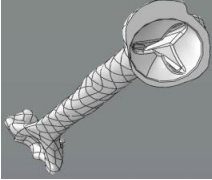

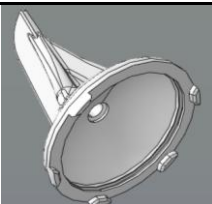
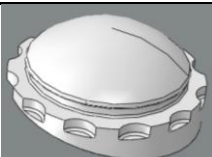
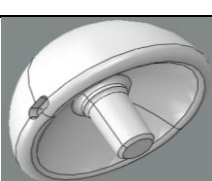
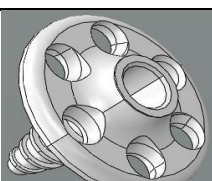



Figure 6-: Assign sections

The next step was to prepare the Humerus and Scapula to accommodate the humeral and glenoid implants. Initially the Humerus and the Scapula parts' data were received inconsistent with geometry errors (as mentioned in chapter 4, MIMICS was used to fix this). The cavities on both the humerus and the scapula parts were not cut. Using the Assembly module the parts were positioned together in an acceptable position using constraints as shown in the second column of Table 6-. This was achieved using translation, rotation, radial pattern, face-to-face, edge-to-edge, coincident point etc. All of which can be found in the “instance” and “constraint” menu. See Figure 6-.

Table 6- : Material Properties of each model part (Cortical bone+ implant parts)

PART		MATERIAL	YOUNG'S MODULUS	POISSON'S RATIO	DENSITY
	Humerus	3 RD Generation simulated cortical bone	12.4 GPa* *GPa (Giga Pascal)	0.27	1.7g/cm ³
	Scapula	3 RD Generation simulated cortical bone	12.4 GPa	0.27	1.7g/cm ³
	Large Humeral Shell	Cast CoCr (Cast Cobalt Chromium Alloy)	230GPa	0.3	8.2767g/cm ³
	36x3mm Liner	UHMWPE (Arcom) Ultra high molecular weight polyethylene	1.290GPa	0.38	0.9357g/cm ³
	36mm Glenoid Head	Wrought CoCr (Wrought Cobalt Chromium Alloy)	241GPa	0.3	8.2767g/cm ³
	Glenoid base plate	Wrought Ti6Al4V (Wrought Titanium Alloy)	114GPa	0.34	4.437g/cm ³
	Peripheral Screw (2)	Wrought Ti6Al4V	114GPa	0.34	4.437g/cm ³

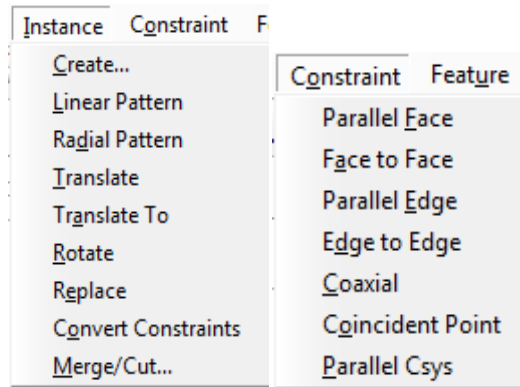


Figure 6-: Instance and Constraint menu

After achieving this, the “Merge/Cut Instances” function shown in Figure 6- is used to apply a cut to the master part in this case the Humerus and Scapula. The resulting part created is shown in the third column of Figure 6-.

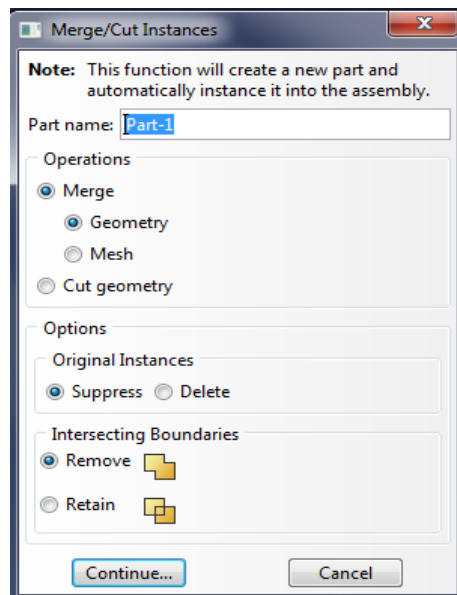


Figure 6-: Merge/Cut Instance Menu

The version of ABAQUS software used in this study can only allow a maximum number of nodes of 20,000 that can be analysed on a model. In FEA the larger number of nodes in the model the more time is needed to process the model. Therefore, to reduce the number of nodes prior to meshing the Humerus and Scapula were analysed individually; all unnecessary parts were removed from the assembly, and large sections of no interest removed completely from the part dimensions to reduce processing time.

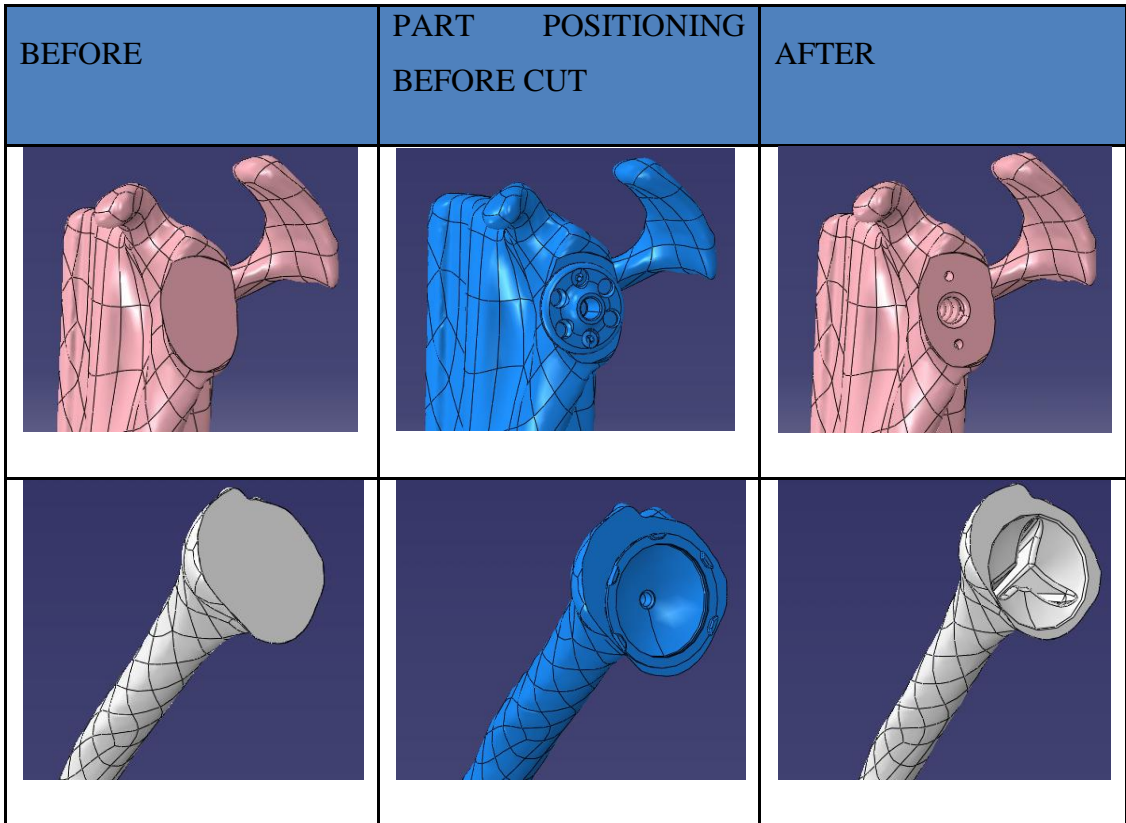


Figure 6-: Parts after merging and cutting

This is done using the Extrude Cut function in the “shape” menu as shown in Figure 6-.

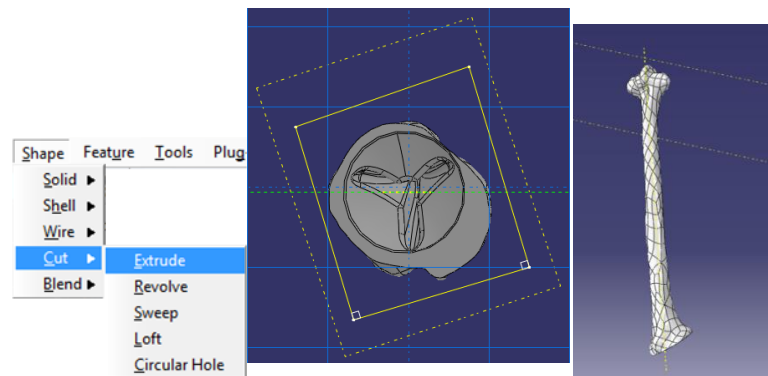


Figure 6-: Function cut-extrude to remove extra nodes from parts

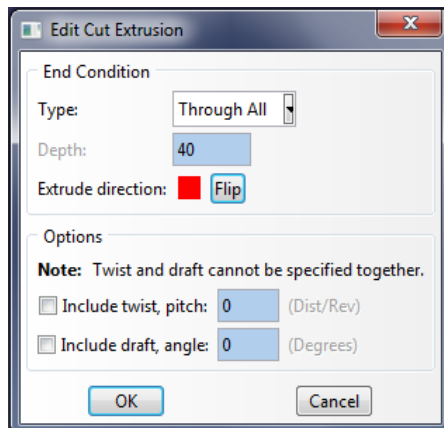


Figure 6-: Edit the cut extrusion in the required part

(Note: It is important to remember when using this method of cut to designate an axis of direction and plane.)

A plane is selected in which the extruding/cutting shape will be drawn and an axis is selected which indicates the direction of the extrusion. After the selection a shape is drawn on the plane that will cut the part using the sketch functions as seen in, an Edit cut extrusion window appears which is adjusted until the remaining part is sufficient for the analysis. To check that there are no extra nodes remained, a simulated test model was created and load was applied to check the value of the stress distribution; if it is equal to zero then the part is ready for analysis. The results from the test model created have allowed the removal of the remaining part that displayed no stress hence concentrate the remaining nodes in the foam-implant interface. The length of the cut was determined from this test.

The next procedure is *meshing* the parts according to the regions of significance or interest. For bio mechanics it is most common to use tetrahedrons. Due to complicated geometries hexahedral meshing is insufficient and so the tetrahedron meshing is selected in Mesh controls as shown in Figure 6-.

Selecting the mesh in the parts module displays all meshing functions such as nodes by size, node by number, etc. The functions open a “Seeds” window from which the node sizing or numbering is assigned. This can be seen in Figure 6- Figure 6-18 under seed menu. All functions are used to obtain a resulting node display on the part as seen in Figure 6-. Purple indicate local seeds while White indicate global seeds.

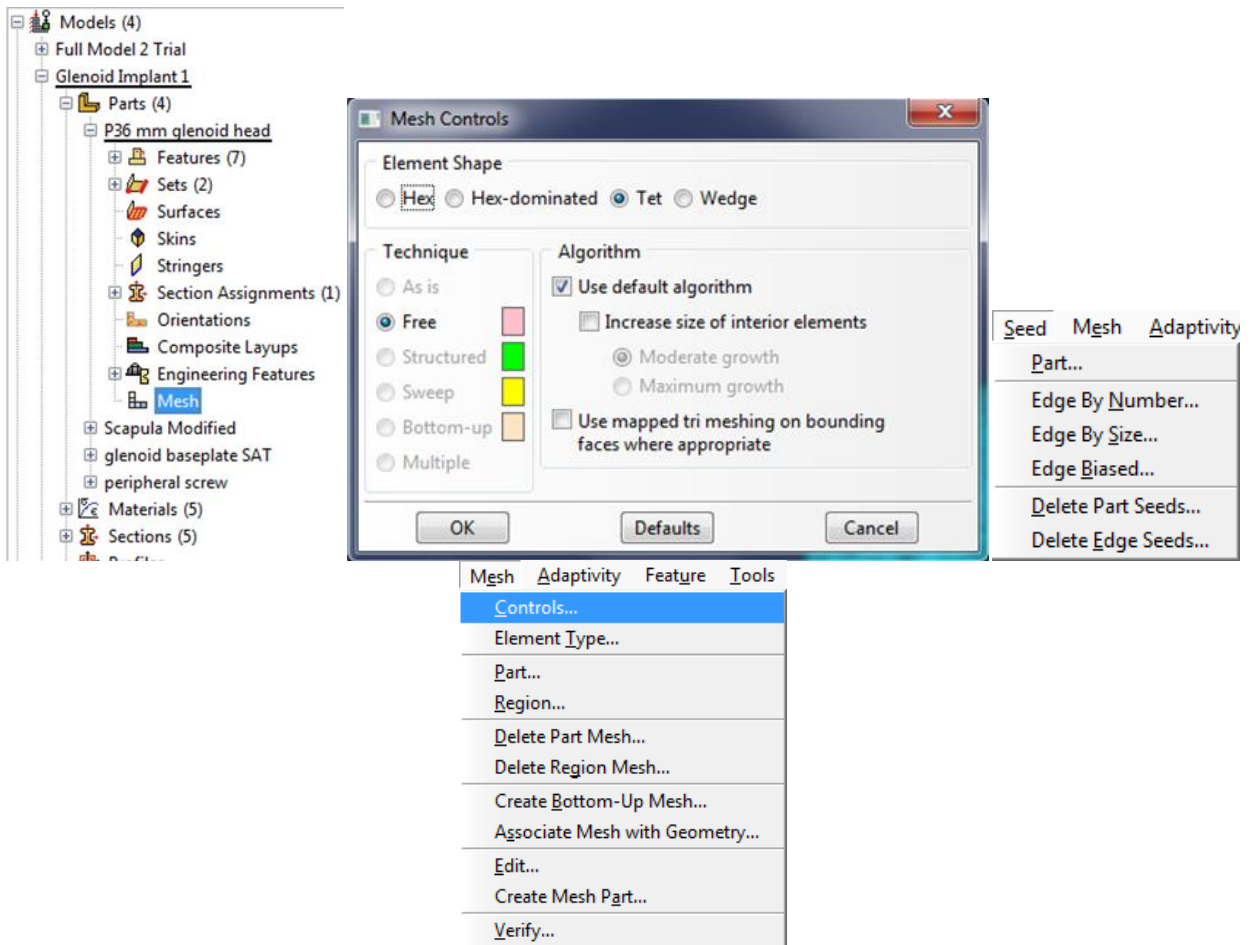


Figure 6-: Mesh Controls

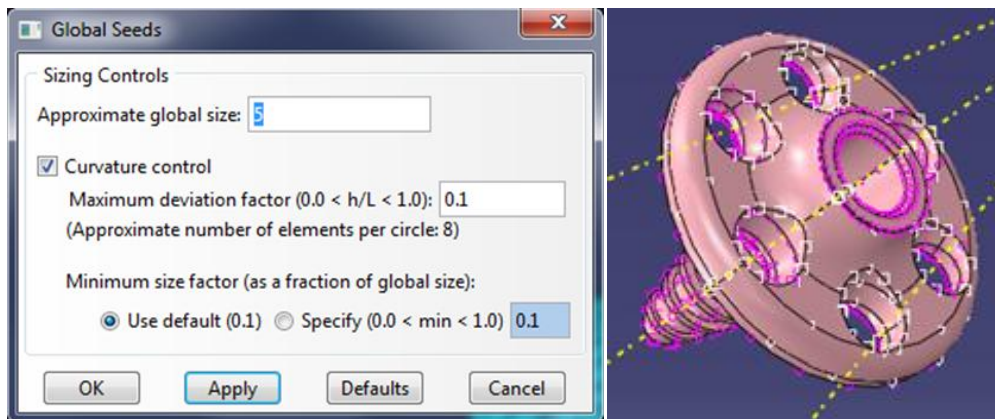


Figure 6-: Global Seed menu

The resulting meshes are as follows.

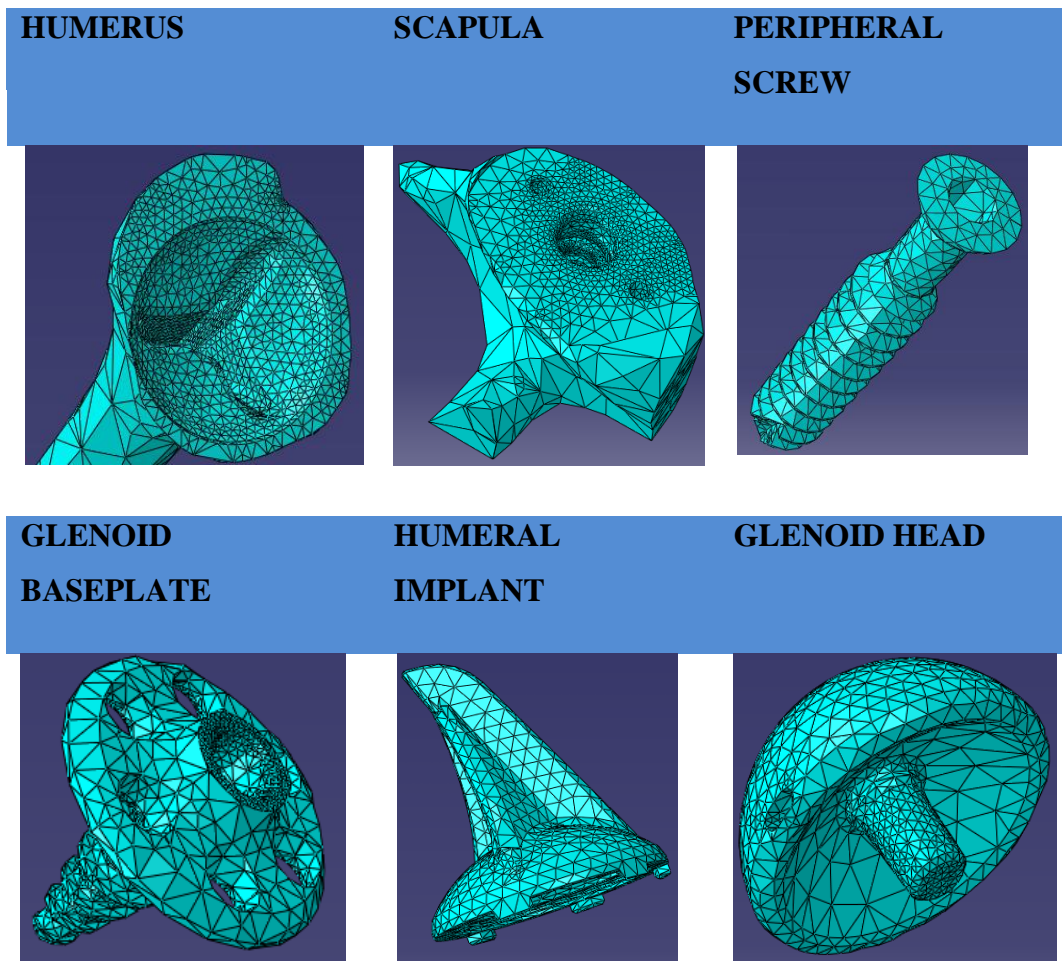


Figure 6-: Resulting Mesh Parts

Note: Due to license availability the total nodes were restricted to 20,000. The nodes were distributed cautiously to remain within this boundary whilst maximising accuracy.

The mesh displays a fine mesh within the regions of contact as these are expected to illustrate the highest levels of stresses therefore require the highest accuracy, and low elsewhere.. This can be seen in Figure 6-. Over excessive meshing is avoided as this increases computing time significantly.

Now the parts are fully prepped for simulation. In the next section the operating conditions are set.

At the beginning, the procedure type in the step module is defined. The selections include if the analysis is dynamic or static and the solution is explicit or implicit. Due to the complexity of the

simulation, the model is analysed dynamically, but with explicit method. This allows the force to be exerted in increments to allow more accurate calculation of 3D problems and also increases convergence therefore increasing probability of obtaining results.

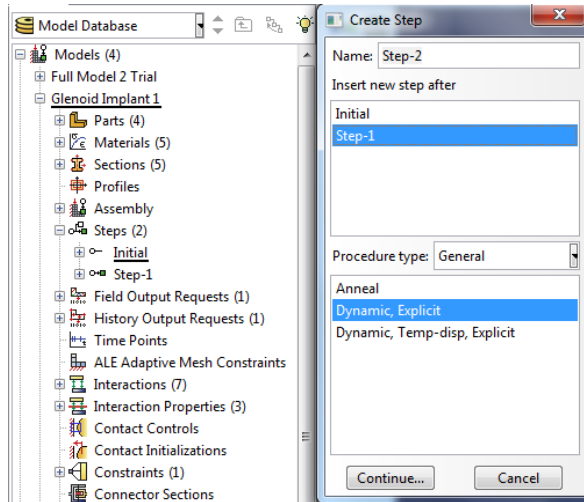


Figure 6-: Create Step Menu

Within the step modules the interactions is first set. To simplify the complicated interactions General contact is selected as shown in Figure 6-. This method finds all surface pairs and sets them to behave in the exact same manner. When this is selected the “Edit Interaction” window appears from which the parameters are set this can be seen in Figure 6-.

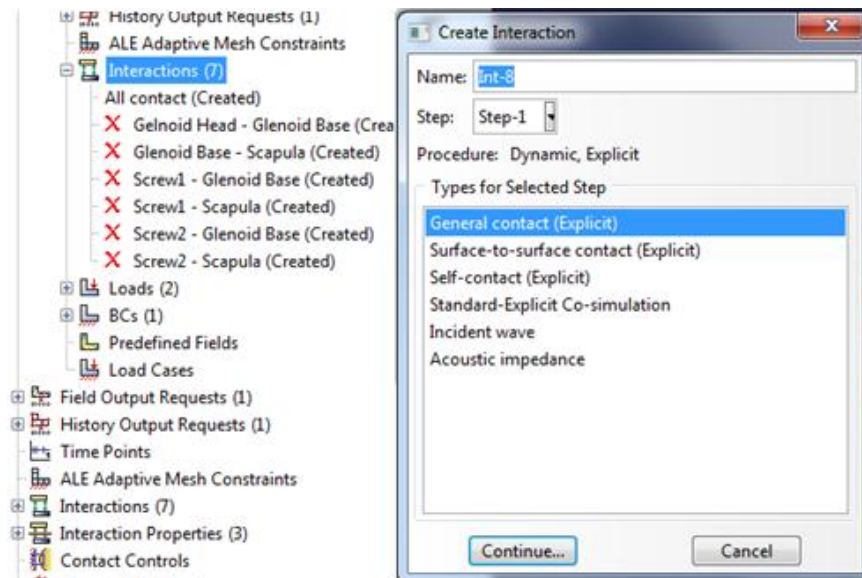


Figure 6-: Create Interaction Function

In the Edit Interaction window, “All with self” is selected to allow all surfaces to be selected and then the contact properties are set, Figure 6-. Selecting create open the “create interaction property” window from which contact is selected.

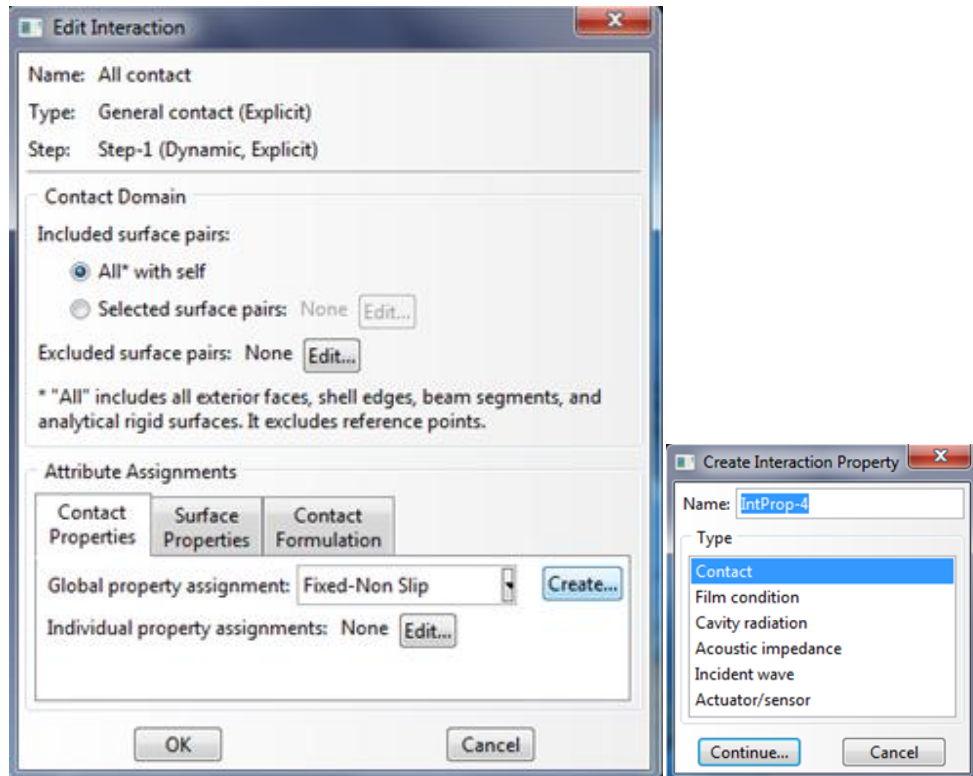


Figure 6-: Create interaction property

After contact is selected the “Edit contact properties” window appears from which mechanical and thermal behaviour can be set. To keep the problem simplified, thermal properties are excluded and only Tangential and Normal behaviours taken into account. For tangential the behaviour is set to (Rough), and this was done to help so at the moment of contact the parts do not separate and to allow distribution of stresses (i.e. to keep the part from separating). These can be seen in Figure 6-.

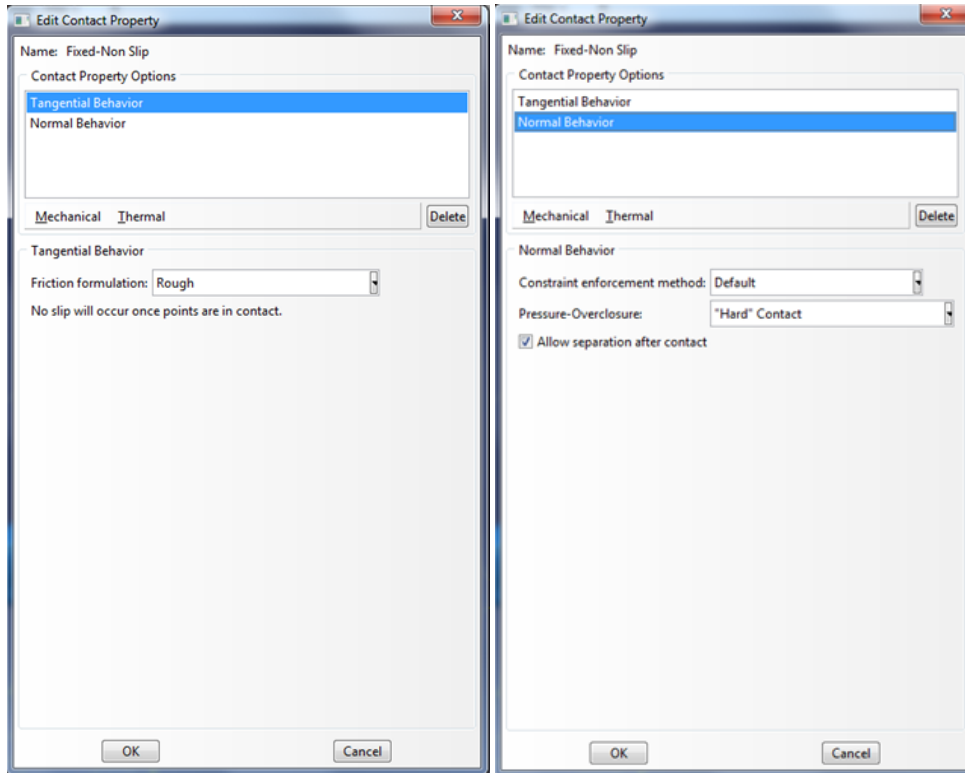


Figure 6-: Edit Contact Properties

Literature significantly shows variety of loadings of the shoulder in different conditions. The diagram below has been obtained from the journal (fixation of the reversed shoulder prosthesis (Hopkins et . al. 2008)) the magnitude of this loading was derived by Angling and Wyss who reviewed a series of shoulder motion analyses and derived what could be considered a high impact daily loading.

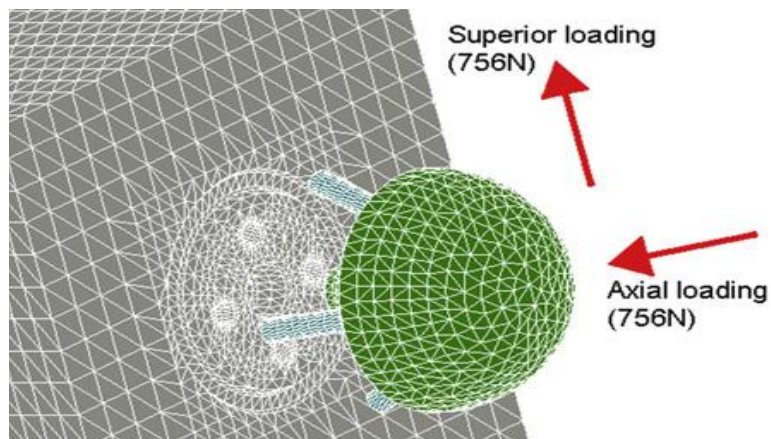


Figure 6-: Exploded view of an FE model of a glenoid implant inserted into a polyurethane block. Loadings are displayed.

Within the step module loads can be assigned as shown below in Figure 6-. “Create load” window from which concentrated force is selected to mimic the forces above, is opened.

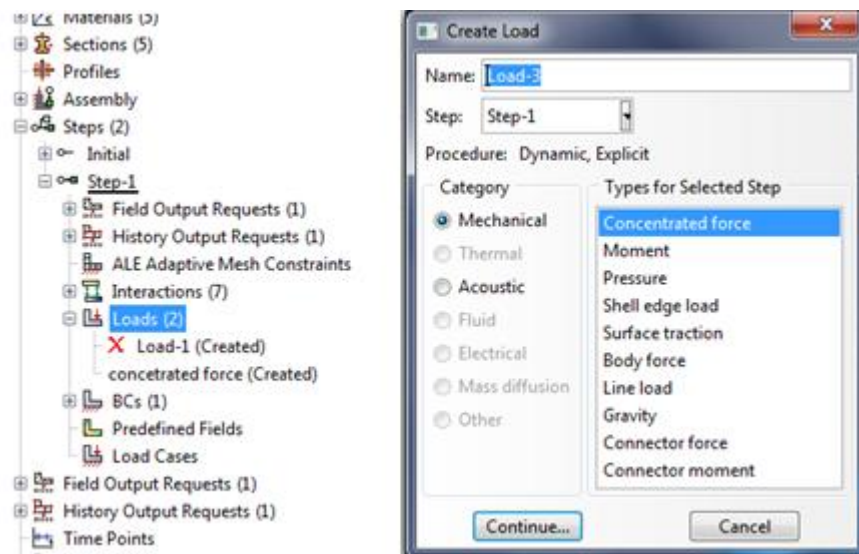


Figure 6-: Create Load to apply it on the model

To apply a specific load to the model, it is necessary to define the location, magnitude and direction of the force. In the “Edit Load” window a point is first selected where “csys datum” is previously created. The force directed through a selected axis x, y or z. This is done as shown in Figure 6-. The force is set to distribute uniformly and is set a magnitude.

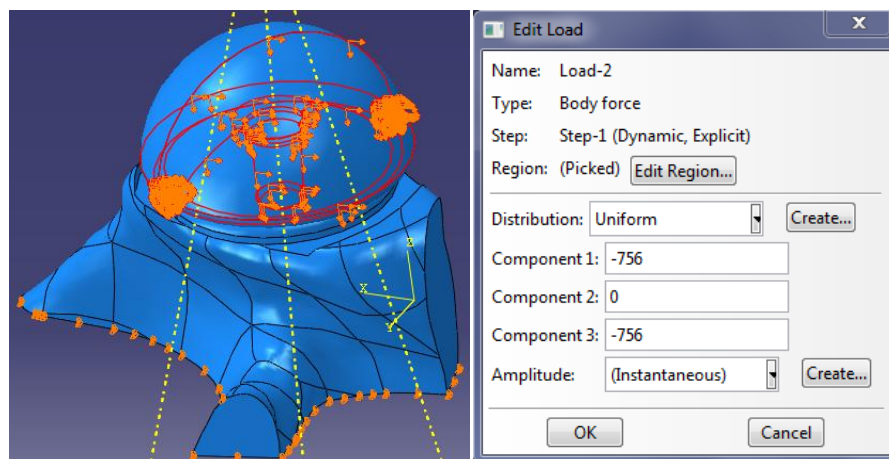


Figure 6-: Apply and edit load on the Implant

After the forces are applied the boundary conditions (constrains) are set. Defining constrains will help to remove/reduce the degree of freedom of the model to create a well define problem. Applying forces without defining the proper constrain will cause error in the simulation. This is

also found in the step module as seen in Figure 6-. When selecting BC, “Create boundary condition” window appears. In this window the conditions are set to “mechanical”, and “Symmetry/Anti symmetry/Encastre” type is selected.

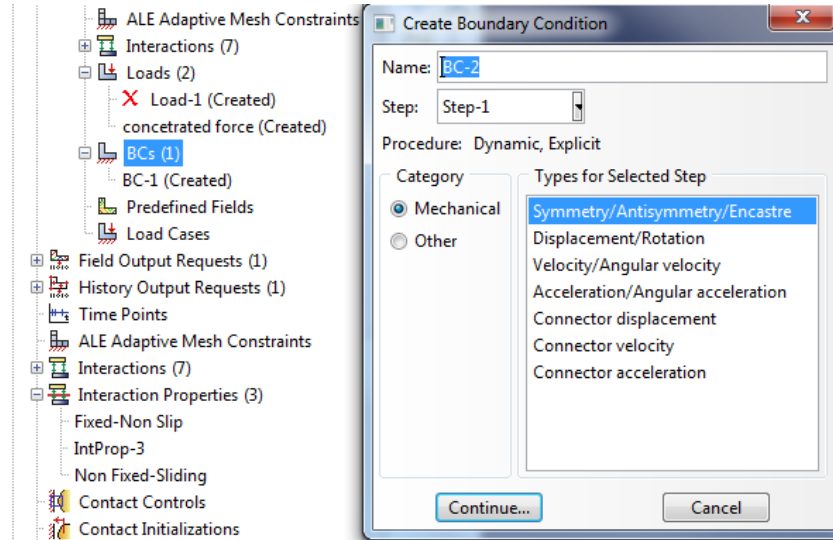


Figure 6-: Set the boundary condition to the Model

After selecting the type of the boundary conditions, the “Edit boundary condition” windows appear which allows variable Symmetry/Anti-symmetry/Encastre options. The boundary location is first highlighted in the viewport and then Pinned is selected which sets the movement of that points in x, y and z direction to zero. This can be shown in Figure 6- below.

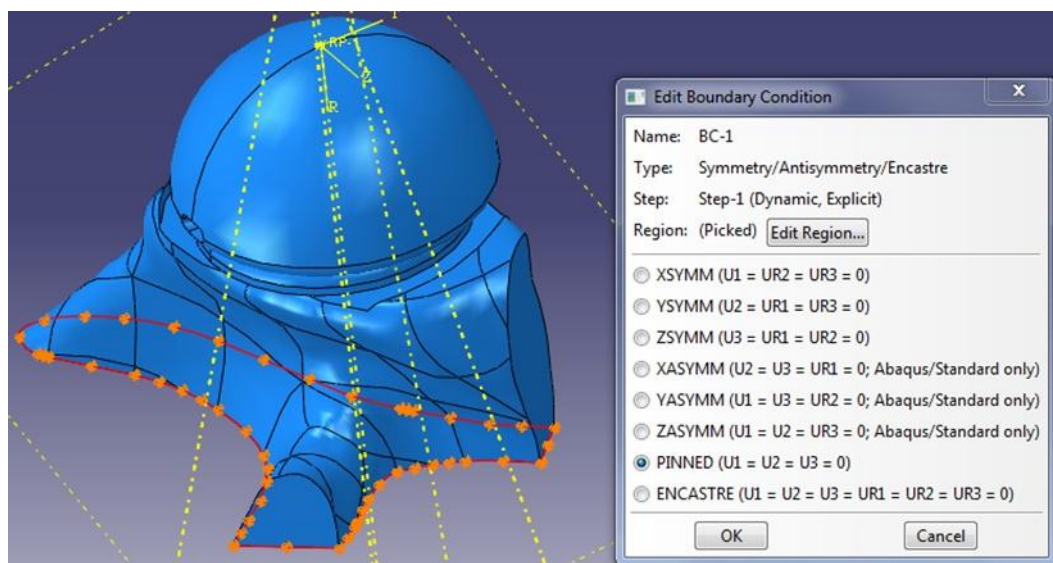


Figure 6-: Apply the BC to the model

All parts are either articulate or in direct contact with each other, therefore it is necessary to assign material contact behaviour such as tangential and normal behaviour between parts. The most important interaction is set between the Glenoid Head and Liner as these parts determine the centre of rotation of the shoulder, the movement of the arm and the load transfers from the humerus to scapula. The normal reactions has been set to behave as a “hard” contact under pressure and in the tangential direction the material will be frictionless (although in reality it is impossible for frictionless interaction) to simplify the problem.

After the parts have been assigned their material properties and boundary conditions the model is ready for assembly. Using the assembly function the parts were inserted onto the plane where constraints such as “Edge to Edge”, “Face to Face” and “Coincident Point” were used to reposition and constrain the parts into position.

The completed model is shown in Figure 6-.

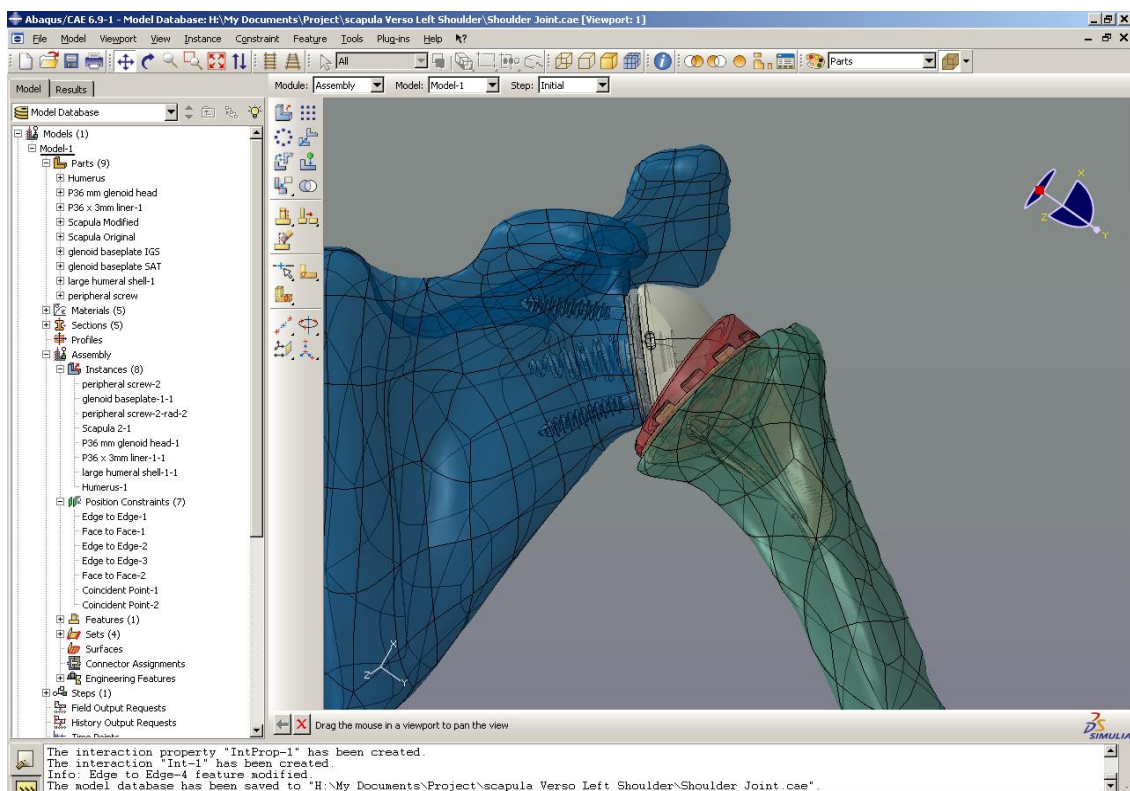


Figure 6-: Final Model after Assembly

From Figure 6- it is clearer to see the full scale meshing of the model. The areas where the mesh is concentrated as they appear darker due to the smaller elements and increased number of nodes used. For this investigation we will concentrate on interaction between the humerus and the humeral shell.

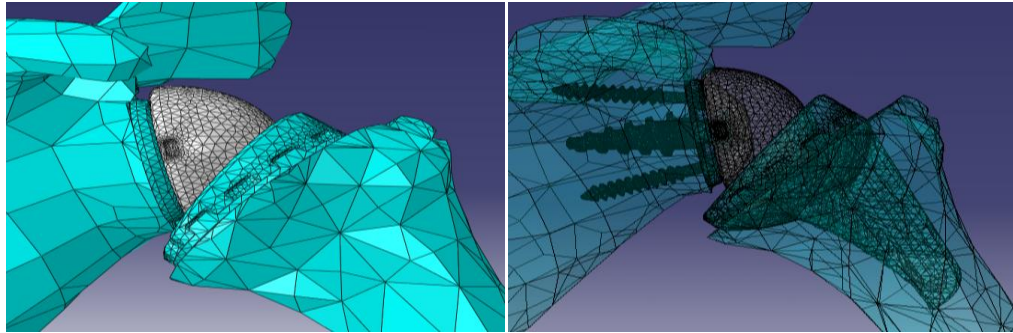


Figure 6-: Assembled shoulder with meshing

As seen from the Figure 6- the region where the humerus and the humeral implant come into contact the mesh is very fine in order to get a more detailed feedback in the stress distribution.

The final step of the program is to create a job so as to run a full analysis on the model. After selecting the jobs module the “create a job” window appears from which the desired model is chosen to be analysed. Figure 6- shows the create job step.

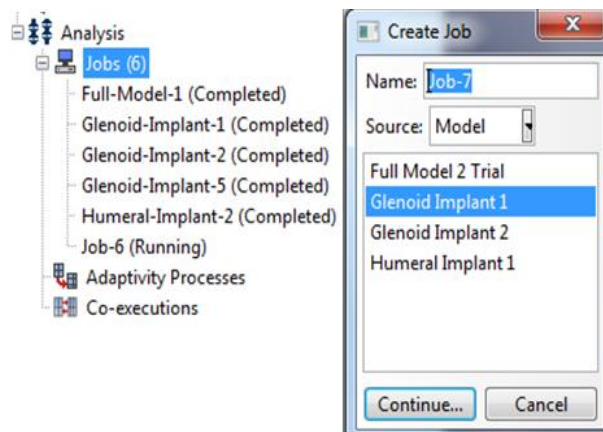


Figure 6-: Create Job step in the Model

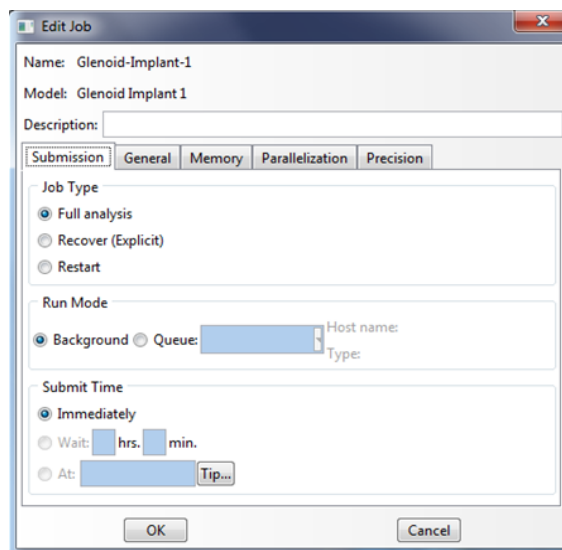


Figure 6-: Edit Job step

Consequently, it is essential to edit the job to perform a full-analysis to the desired model to apply the FEA and get the results. Figure 6-shows the step of Edit Job for the desired part of the model to apply the loads and BC to get the results.

6.4.2 Units System within ABAQUS Software:

It is essential that the units are consistent throughout the use of ABAQUS as there are no inherent units for ABAQUS. The model has length in units of mm therefore the remaining units follow the highlighted column shown below in Table 6-. By measuring the distance of the width of the base plate (being 31 units) it was possible to specify the units as being in mm. Once this had been found the material properties could then be assigned to each part as previously explained.

Table 6-: Unit Systems within ABAQUS /CAE

Quantity	SI	SI(mm)	US Unit (ft)	US Unit (inch)
Length	M	mm	ft	In
Force	N	N	lbf	Lbf
Mass	Kg	Tonne(10^3 kg)	Slug	lbf s ² /in
Time	s	s	s	S
Stress	Pa (N/m ²)	MPa (N/mm ²)	Lbf/ft ²	Psi (lbf/in ²)
Energy	J	mJ (10^{-3} J)	ft lbf	In lbf
Density	Kg/m ³	Tonne/mm ³	Slug/ft ³	Lbf s ² /in ⁴

6.4.3 Final Step - Finite Element Analysis Method



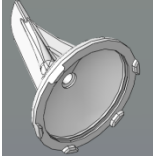
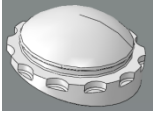

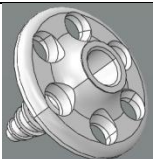
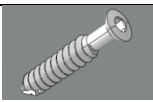
In order to obtain accurate results Dynamic Explicit method was used. A static implicit method is generally known to be more accurate when used for simple 2D models, however for more complex 3D models the static implicit method encounter problems with incremental forming processes such as ring-rolling in which several surfaces repeatedly make contact with and separate with parts. An Implicit model takes into account the integral forces and applies an equilibrium factor using Newton Raphson Iterations; therefore to obtain a result it is more difficult and relies heavily on the user to estimate the interactions values accurately.

FEA performed in three main groups. In all three groups Verso implant were used. In the first group of simulation a foam block model were used. The foam block was used from polyurethane as a standard material to simulate cancellous bone. The shape of the material was a simple block to facilitate the comparison with the experimental results in chapter 5, to validate or simulation. In the second and third groups of simulation, the real shape of the scapula and humerus were used, using the method explained in chapter 4 and beginning of chapter 5. However two different materials were used in these simulations for the bone, polyurethane and cortical.

6.5 Modelling and Simulation of a Foam Block as a bone:

This section, polyurethane as material properties for the bone has been selected. The reason for choosing this material is to make it possible to perform some mechanical testing to validate analytical simulation. In chapter 5 the mechanical test result of the implant, where it was mounted inside a foam block, under some mechanical measures will be discussed. The mechanical testing and simulation were done in addition to the FEA simulation. The simulation process has been done exactly with the same method as illustrated before, except the material properties were modified to mimic the same material properties as the foam block (the same material will be used in the mechanical testing later). Table 6- shows the mechanical properties of the materials of the implants and the bones. As it has been explained this material has to be define inside the program before simulation. The table shows high difference between the mechanical properties of the parts of implant and the bone. The head of the glenoid has the highest ultimate strength; i.e. It has been prepare even to tolerate high concentration of the stress.

Table 6:- Material properties in the FEA (Foam Block (Cancellous) + Cortical bone+ implant parts)

PART		MATERIAL	YOUNG'S MODULUS	POISSON'S RATIO	DENSITY	UTS/Yield strength
	Humerus	Solid Rigid Polyurethane Foam (20pcf) (Cancellous Bone)	Compressive 210MPa/ Tensile 284MPa	0.24	0.32g/cm ³	Compressive 8.4MPa /Tensile 5.6MPa
	Scapula	3 rd Generation simulated cortical bone	12.4GPa	0.27	1.7 g/cm ³	Compressive 120MPa Tensile 90MPa
	Large Humeral Shell	Cast CoCr	230GPa	0.30	8.27g/cm ³	896MPa
	36x3mm Liner	UHMWPE (Arcom)	1.29GPa	0.38	0.93g/cm ³	23.9MPa
	36mm Glenoid Head	Wrought CoCr	241GPa	0.30	8.27g/cm ³	1350MPa
	Glenoid base plate	Wrought Ti6Al4V	114GPa	0.34	4.43g/cm ³	950MPa
	Peripheral Screw	Wrought Ti6Al4V	114GPa	0.34	4.43g/cm ³	950MPa

6.5.1 Simplified Conditions for FEA Analysis using Mechanical testing Results:

This section discusses the conditions applied to obtain the FEA results. The conditions were obtained from the experimental results from the foam block model used in the mechanical testing discussed in chapter 5. The mechanical testing process was carried out in parallel with FEA process. The foam block model used in mechanical testing cannot be analysed until failure under compression/tension as the interactions between the implant and foam block model is recorded. To facilitate the failure detection, the foam block model used in mechanical testing has been analysed under tension where the first sign of the bone failing can be seen better and recorded. Similarly the model in ABAQUS has been assessed under the same condition; however this model will provide much better information on the performance as the internal interactions, forces, stresses can be viewed more clearly. Unlike the mechanical testing procedure; it is easier to observe the stress distribution in FE model and identify the stress locations.

The glenoid base has been modelled on artificial bone material. This method allows for mechanical failure testing and allows figures to be generated under loading and displacement in the vertical direction and identify the frequency of failure. In order to mimic these motions the following 3 models were generated in ABAQUS on an artificial bone block as seen in Figure 6- similar to the ones from the experimental testing (i.e. has the same foam block properties to compare the results). The 3 configurations are on par to the mechanical testing carried out.

Moreover, there will be two sets of testes applied on FEA model; tensile testing using the 5.6MPa limit UTS (Ultimate Tensile Strength) and Compressive testing with 8.4MPa limit as shown in Table 6-.

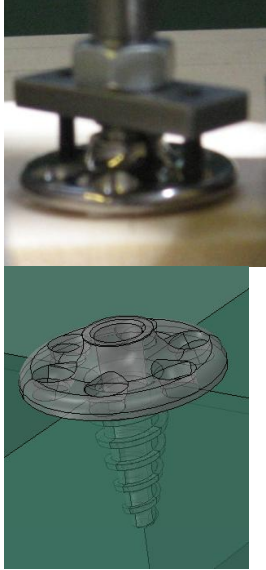
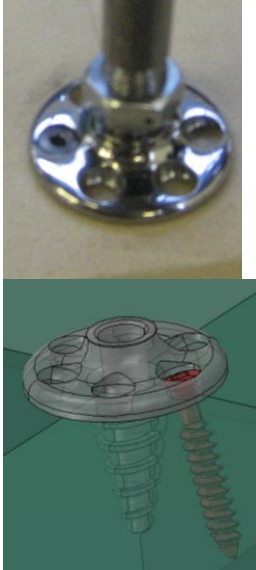
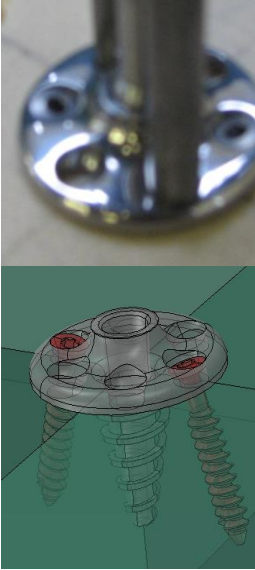
Glenoid Base	Glenoid Base + 1 peripheral screw	Glenoid Base + 2 peripheral screws
		

Figure 6-: Foam Block model configurations

6.5.2 Simplified Foam Block Modelling

The same steps mentioned previously in this chapter have been done in order to complete the FEA block model to be similar as the foam block model used in mechanical testing. The pulling load is applied to the base plate as a body force and an Encastre function (the function Encastre is used to ensure that the velocity vectors are all equal to zero so the block does not move) was used on the bottom of the simulated block (bone substitute) as boundary conditions, Figure 6-. The following CAD Model shown in Figure 6- was drawn using ABAQUS software to show that the FEA model used in the analysis will be same as the one used in the mechanical testing. The Foam Block used in Mechanical testing can be seen in Figure 5- : Foam Block from Saw Bone with 20 pcf, 13cm x 18cm x 4cm, in chapter 5.

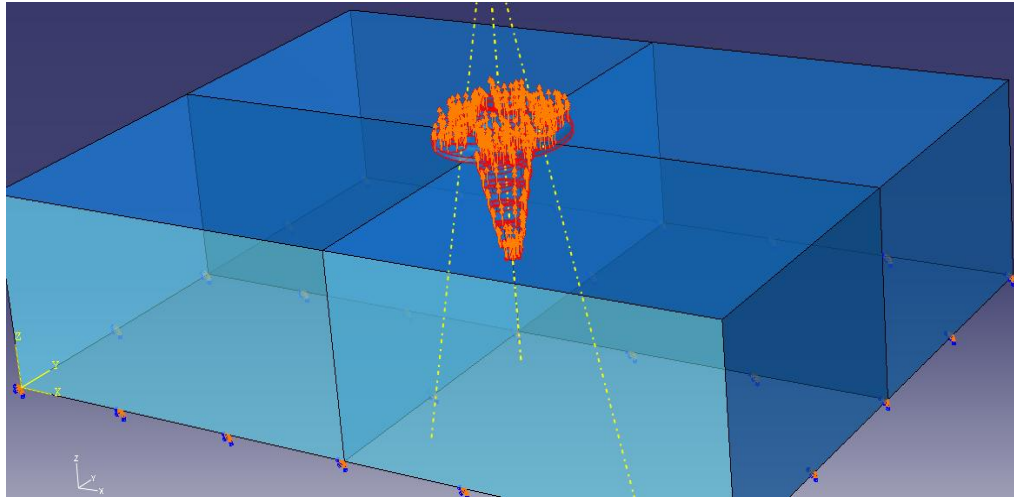


Figure 6-: Block Model

Table 6-: Average loads for the three set of tests carried out with no screws, with one screw and two screws attached to the GBP (Glenoid Base Plate)

Screws	0	0	0	1	1	1	2	2	2
Max Load (N)	1109	1172	1110	1461	1400	1548	2398	2250	2540
Max Stress (MPa)	11.68	12.33	11.69	15.38	14.73	16.29	25.23	23.68	26.74
Average Load	1130			1469			2396		

**Note: These are the results obtained from Mechanical Testing* see results in Chapter 5.*

6.5.3 Results and Discussion for Block Model

The following results are obtained are based on the block model shown in Figure 6-: Block Model. The analysis on ABAQUS generated the following results for all three configurations (No Screw, One Screw and Two Screws).

6.5.3.1 Stress Concentration:

In this section the stress concentration is shown in the figures below after applying the maximum loading during tension testing. This will help in identifying the failure mode properly using the UTS (Ultimate Tensile Strength) for each model. The results will be discussed under each figure.

Cancellous bone material properties were assigned to the following model (tested part) similar to the foam block material properties used in used in mechanical testing.

The model analyse the contact area between the implant and the simulated block model using fine elements or small areas (See meshing in methodology). This will help display the stress distribution around the bone-implant interface. This allows the model to display stresses accurately across the simulated foam-implant interaction (i.e. the increased number of nodes closer to the simulated foam-implant interface) provide accurate results, Figure 6-. In FEA it is easier to show where the exact region of failure is. The models show contours of Von Mises stresses across the region where the loads have been applied and failure was observed. The model is cut half way to show contact regions as in Figure 6-. The parts are also separated to show the stress distribution across the implant as well as the artificial bone. The legend indicates the stress concentration from blue (minimum) to red (maximum). The limits are set on each model to display grey areas of failure. The limits are altered according to materials analysed. This all can be seen in Figure 6-.

1. No Screw Model (GBP without screws)

In this model, only glenoid base plate (GBP) was installed in the modelled foam block without screws, and the pulling load of 1130N were applied (Average Loading), see Table 6-, on the glenoid base plate.

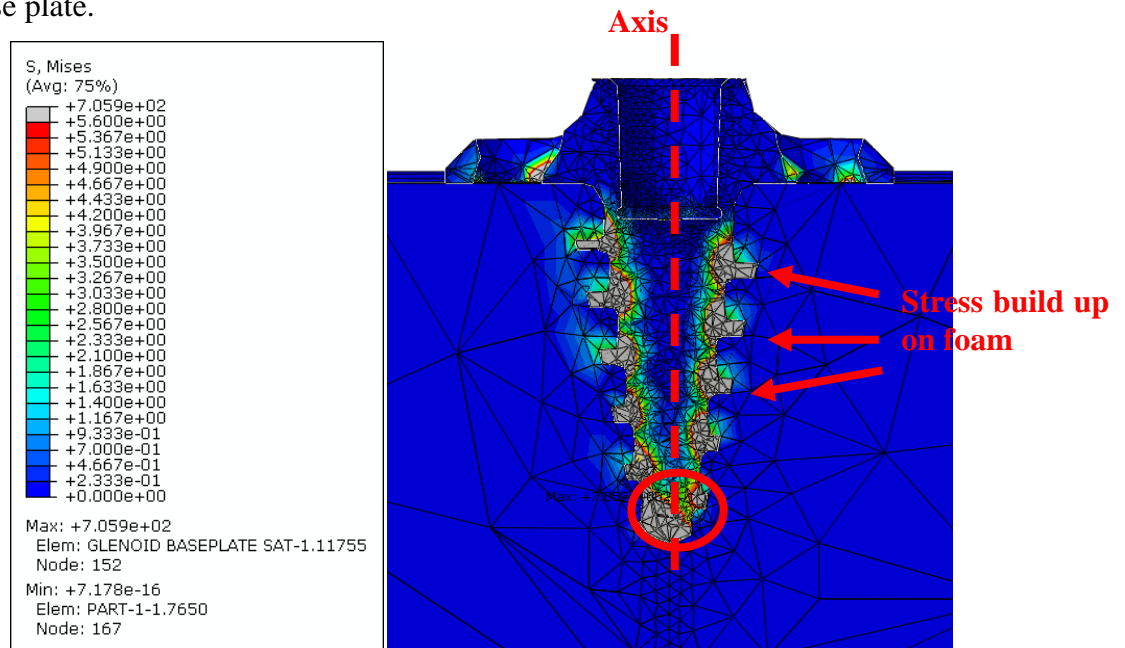


Figure 6-: Block Model Von Mises Stress GBP without screws Full Assembly (Average Loading 1130N)

From Figure 6- it can be seen that the stress concentrations are along the edges of the GBP conical shape screw attached to the bone (modelled artificial bone or bone substitute). This is due to the small cross sectional area of the GBP conical shape screw. As the screw is pulled vertically up it can be seen that the artificial bone reacts as the stress builds up. As the bone substitute behaviour is important, the limit has been set to the UTS of polyurethane foam (foam block) taken from Sawbone as shown in Table 5- (in this case 5.6MPa). The grey areas on the GBP do not indicate regions of failure on GBP in this figure as GBP is under much higher stresses. From this view the bone shows indication of failure represented in the grey areas. The cross section of the artificial bone shows in Figure 6- that there is failure at the set loading. Setting the maximum limit to 5.6MPa (see Table 5-) indicates grey regions of bone which begins to fail. As expected the stresses are high at the contact surfaces, however the largest failures are located at the bottom where the cross sectional areas is small and the top of the cavity where there is an unsupported Screw edge. Both these features amplify stress.

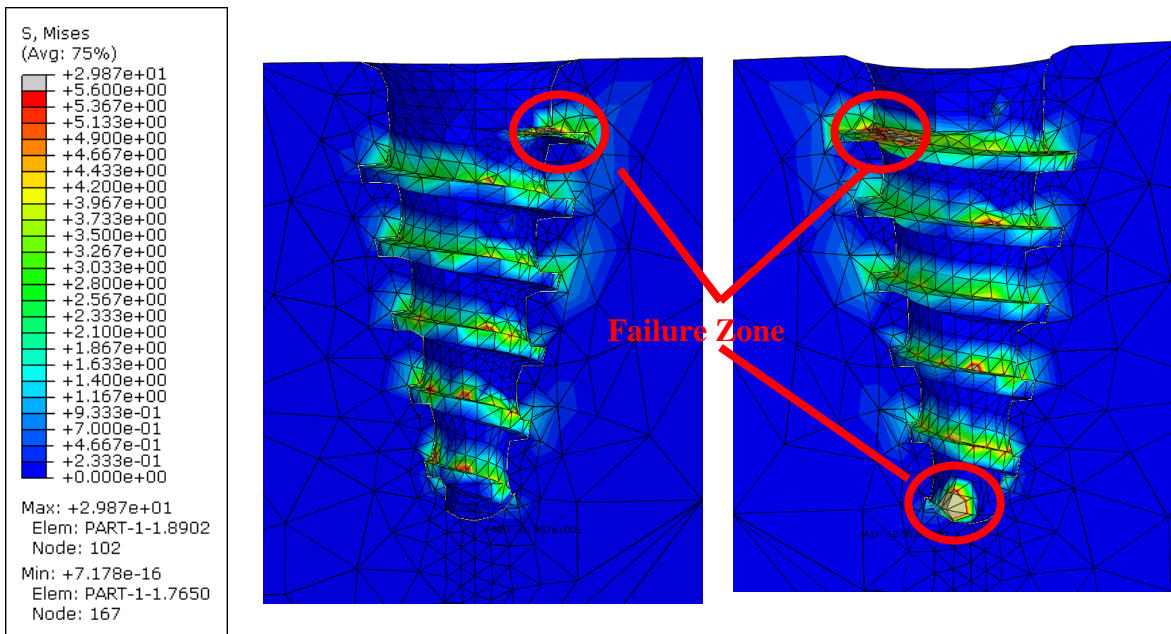


Figure 6-: Block Model Von Mises Stress GBP without screws Artificial Bone (Average Loading 1130N)

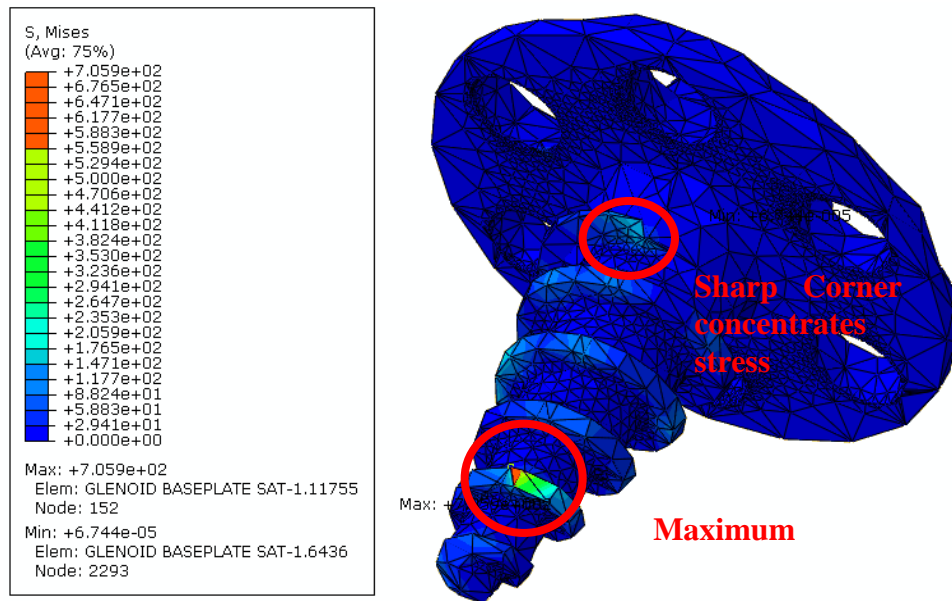


Figure 6-: Block Model Von Mises Stress GBP without screws Glenoid Base (Average Loading 1130N)

As the bone substitute indicates in Figure 6-, the stresses are mirrored on the Glenoid base as seen in Figure 6-. It is clear to see that the stresses develop around the screw edges, but most importantly they reach their peaks again at the bottom and top regions. Although the maximum reaches 705MPa found on a few elements (nodes) indicated in the figure they do not exceed the UTS (how much stress the object can take before it breaks) of 950MPa, therefore the GBP do not fail.

2. One Screw Model

In this model, glenoid and one peripheral screw was installed in the foam block, and the pulling load of 1469 N were applied, Table 6-, on the glenoid base plate.

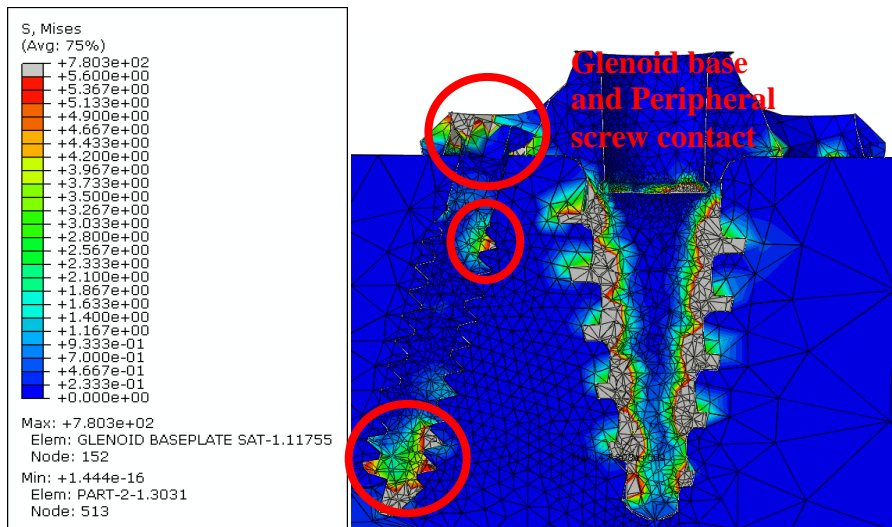


Figure 6-: Block Model Von Mises Stress 1 Screws Full Assembly (Average Loading 1469N)

When load is increased, the magnitude of the stress increases, Figure 6-. However as the GBP is pulled out, there is contact between the GBP and the peripheral screw as well, which requires higher loading and result in higher stress rate in the interface between GBP with one screw and the bone substitute. The stress concentration at the point of contact can be seen from the figure above. Nonetheless, the screw then experiences the load which is seemed to develop at the bottom region. There is also concentration in the upper middle portion this due to screw bending when pulled out; because the screw is not parallel to the direction of the force (it was simulated to be 10° angle away from the GBP main screw).

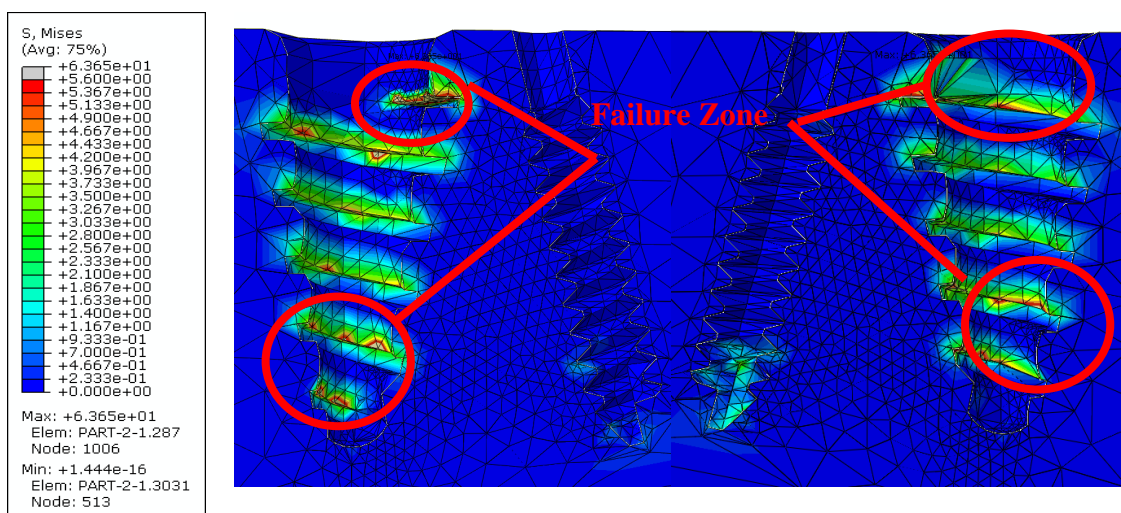


Figure 6-: Block Model Von Mises Stress 1 Screw Artificial Bone (Average Loading 1469N).**This is a mirror image of the same model result; there was no change of screw position*

The cross section of the bone substitute in Figure 6- shows that the interactions of the bone substitute have uniform patterns to the stress distribution. It can be seen that there is large build up of stress across the upper ridges of the glenoid cavity. Although there are signs of stress absorption by the screws, it is not great. After the UTS limit is set it can be seen the regions of failure are the same as configuration 1 (without peripheral screw). The first tooth and the last two teeth show the failures start in these regions. This is a mirror image to the same model result; there was no change of screw position.

Figure 6- shows a mirror image to the one screw model. From the GBP and screw profiles it can be seen that the stresses are high around the GBP, rather than the screws. But most importantly the base and screw have a maximum concentration of 780MPa which is below the UTS of 950MPa of the alloy. The maximum is located at the bottom of the glenoid.

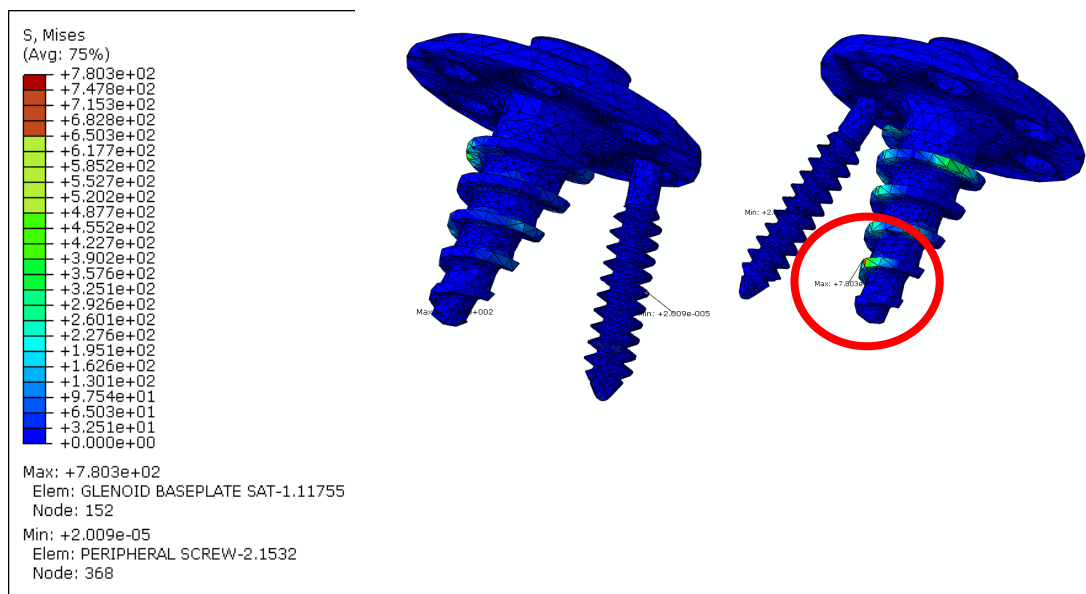


Figure 6-: Block Model Von Mises Stress 1 Screw Glenoid Base (Average Loading 1469N) shows a mirror image of the one screw model.

The same problem can be seen on the peripheral screw. Although they are made from the same material the screw experiences a large stress of 379MPa at the top. This is due to the contact made with the GBP; although the alloy will not fail, it may wear over time. This may be resolved by altering the angle of the screw to increase the contact surface area between the peripheral screw and the glenoid base.

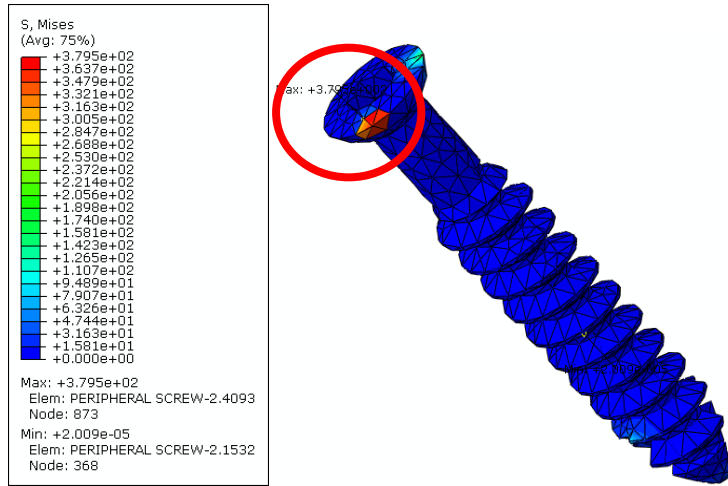


Figure 6-: Block Model Von Mises Stress 1 Screw Peripheral Screw (Average Loading 1469N)

3. Two Screws Model

In this model, glenoid and two peripheral screw was installed in the foam block, and the pulling load of 2396 N were applied, Table 6-, on the glenoid base plate.

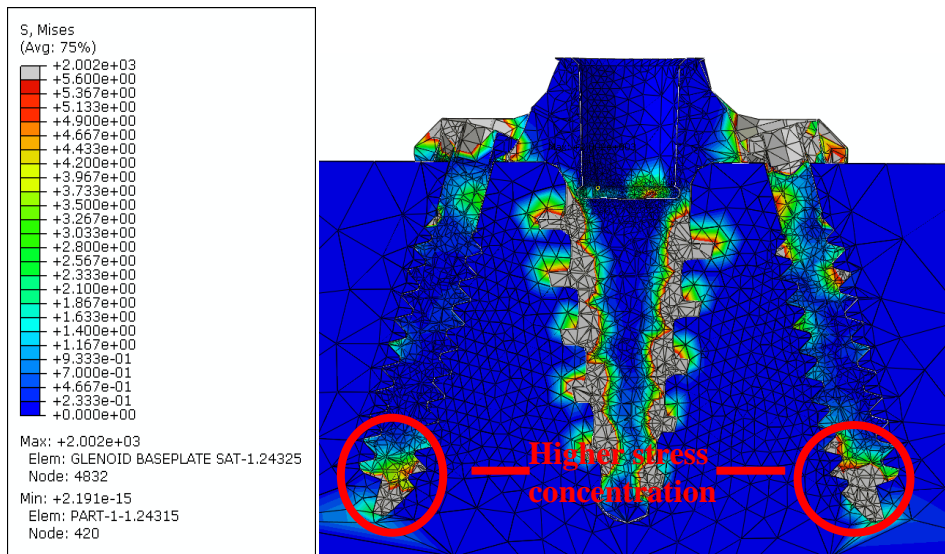


Figure 6-: Block Model Von Mises Stress 2 Screw Full Assembly (Average Loading 2396N)

The 3rd configuration (GBP +2 screws) shows that the screws are absorbing much more of the forces as the stresses are distributed more evenly across the interactions. Although the loads are much higher, the stresses are distributed along the upper surface of contacts of the glenoid cavity similar to configuration 1 and 2. However the stress is much higher than configuration 2 on the bottom tip of the peripheral screw cavities.

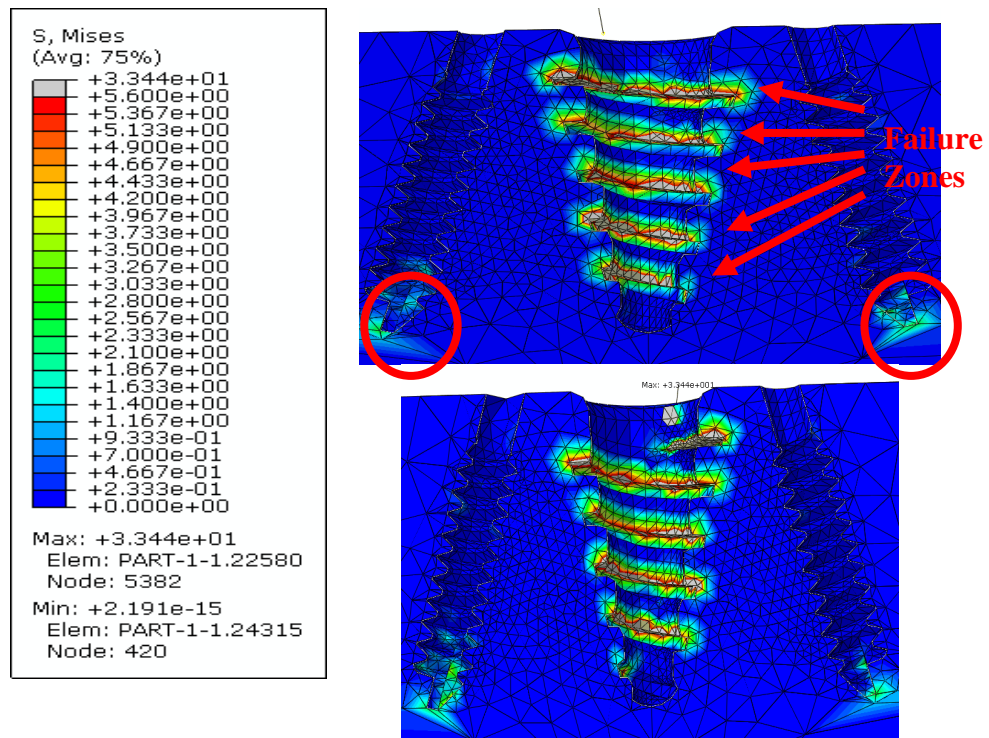


Figure 6-: Block Model Von Mises Stress 2 Screw Artificial Bone (Average Loading 2396N)

shows that the artificial bone at this load has high concentrated stress at the ridges. The failure areas are indicated by the grey region. The value of 33.4MPa showed in the failed region is beyond the 5.6MPa UTS (Ultimate Tensile Strength) limit of bone substitute. Although there is failure on the whole interface between the GBP +2 screws and the bone substitute of a value 2002MPa (Figure 6-) that exceeds the UTS of the GBP of 950MPa; the results show a more even distribution across the glenoid cavity ridges as more of the bone fails together. The interaction at the peripheral screw interface shows a build up of stress at the lower section.

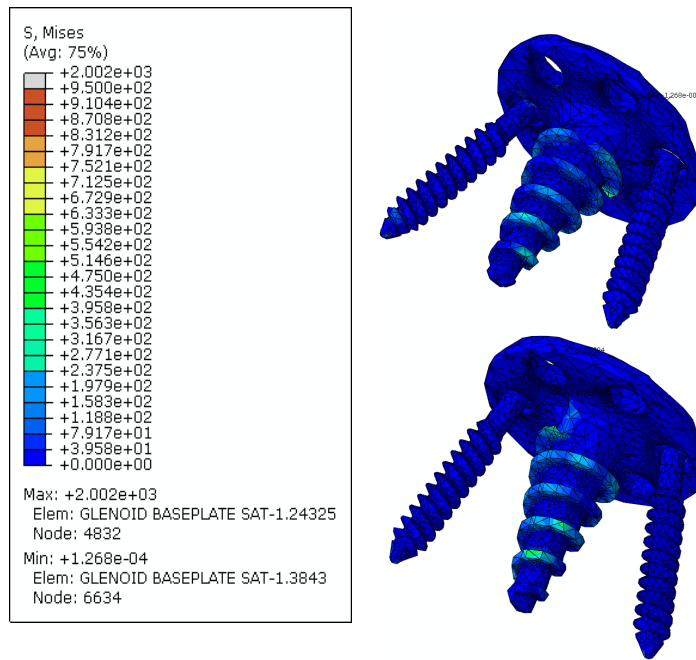


Figure 6-: Block Model Von Mises Stress 2 Screw Glenoid Base (Average Loading 2396N)

In Figure 6-44 it can be seen the stress is mainly on the GBP but the screws showing low stress value. The majority of the stress is built expectedly across the edges of the GBP screw and the lower part of screws and the top part of the screw showing the highest concentration similar to configuration 1. The upper limit is still set at 950MPa, however the scale dose now show the highest stress experienced by the bone. This is at a value of 2002MPa, far above the bone’s UTS and which would lead to the bone being highly damaged. This point is shown in Figure 6- and occurs toward the tip of the screw at the end of the thread in the top screw hole.

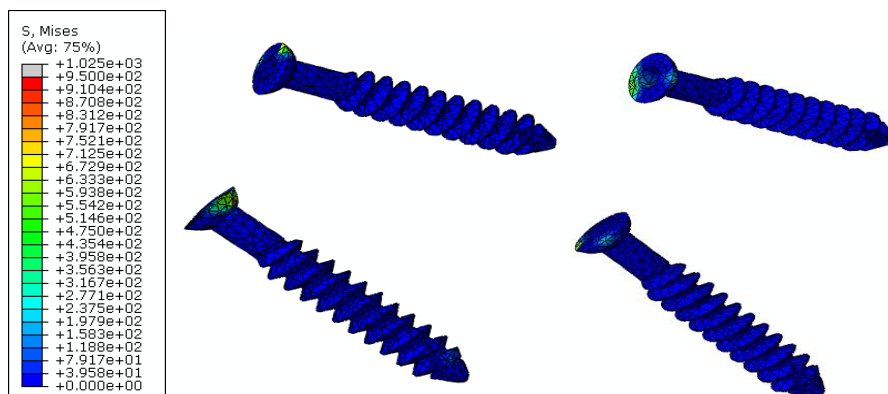


Figure 6-: Block Model Von Mises Stress 2 Screw Peripheral Screws (Average Loading 2396N)

From the Figure 6- it can be seen that the stress build up on the peripheral screws is not within the UTS limit and the screw do fail and the maximum stress reached was 1025MPa which is far

above the screws UTS of 950MPa. Nevertheless, the grey area represents the stress on the bone substitute site which is far above the bone's UTS (5.6MPa) and which would lead to the bone being highly damaged or fractured.

6.5.3.2 Micro-motion:

It is important to assess the micro-motion recorded when the implant-bone interface is subjected to a high load. In Figure 6- the motion of the bone is displayed under configuration 1 (without peripheral screws). When the GBP is pulled out under tension force the screw edges push against the bone substitute wall compressing the bone. The only direction the bone can move is up and outward. The regions that have the highest magnitude are the throat and the bottom tip. The remaining interactions are seen on the upper surfaces of the bone. Evidently it is possible to see in Figure 6- the maximum magnitude of 53.36 μ m due to high impact loading is within the allowable limit of micro-motion which is between 50-150 μ m (this limit is required to help bone re-growth).

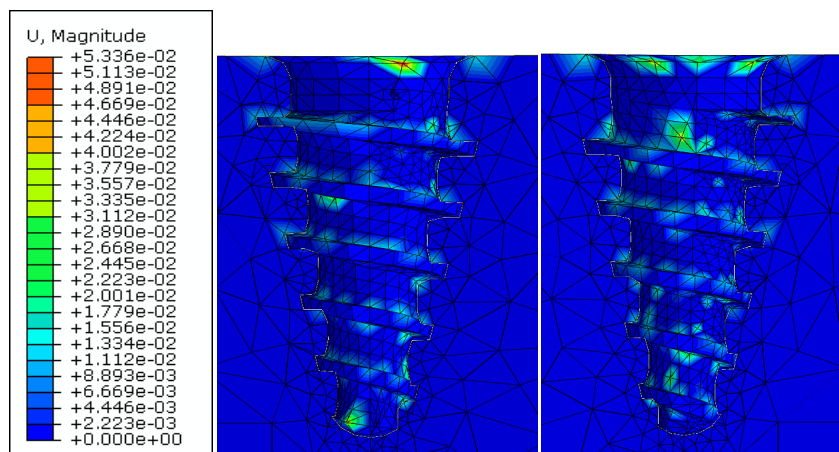


Figure 6-: Block Model Micro-motion No Screws Artificial Bone (Average Loading 1130N)

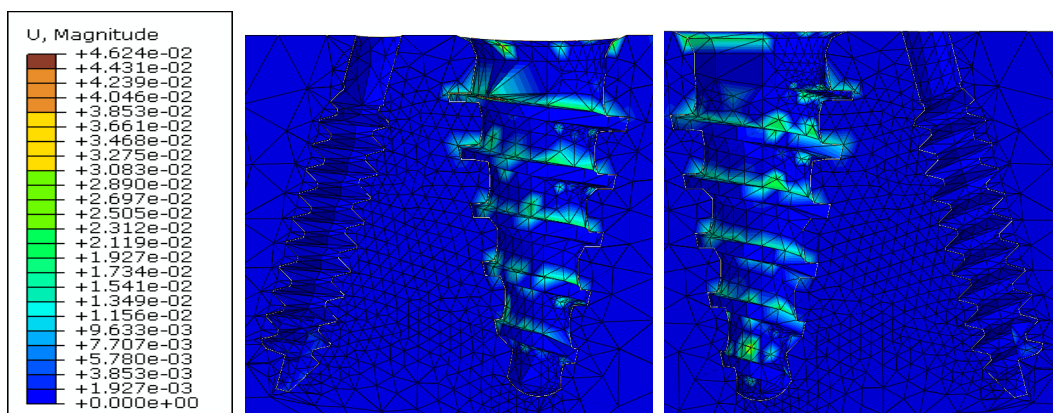


Figure 6-: Block Model Micro motion 1 Screw Artificial Bone (Average Loading 1469N)

Configuration 2 (GBP +1 side screw) showed identical distribution of displacement with the addition of minute motion on the tip of the peripheral screw cavity as seen in Figure 6-. The maximum again is found at the throat of the glenoid cavity. Although the maximum is not as high as configuration 1, the motion can be seen to be more evenly distributed across the upper surfaces of the cavity. The maximum micro-motion reached was 46.2 μ m; however the majority of the bone substitute experienced a lower magnitude level.

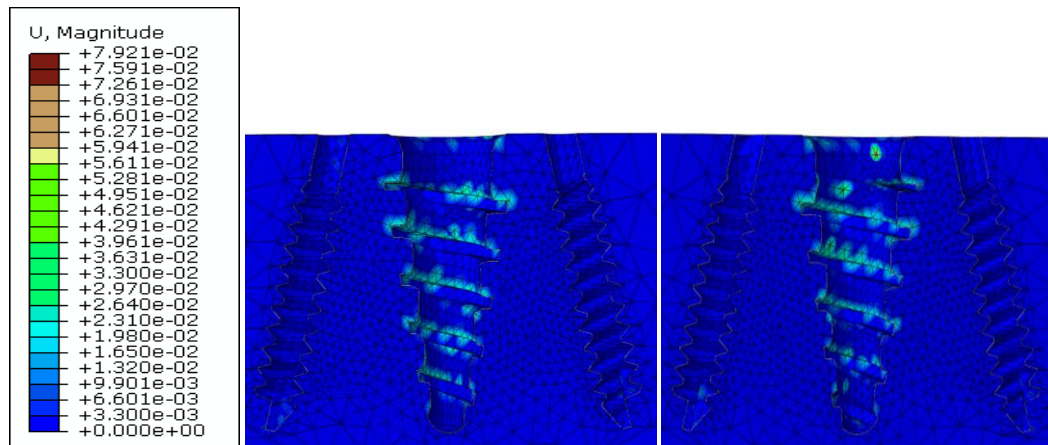


Figure 6-: Block Model Micro-motion 2 Screws Artificial Bone (Average Loading 2396N)

Configuration 3 showed a higher maximum displacement, this is due to a single element (node in the modelled part) distorting excessively found at the throat of the cavity. The majority of the part like the other configuration remains below 150 μ m. Similar to configuration 2 there is a slight level of motion on the tips of the peripheral screw cavities. However the use of 2 screws seems to have allowed a more even distribution across the throat and also concentrate most of the displacement to the upper surface of the cavities.

6.5.3.3 Maximum Principal Strain

In this section the maximum principal strain results for the same model (the interface between bone substitute with cancellous bone properties and GBP) can be shown in the following figures of mirror images of the analysed model.

As seen from Figure 6- to Figure 6- the strain levels are not too high. Although configuration 1, 2, and 3 showed maximum of 0.07, 0.09 and 0.1, it was seen that this occurred on single elements (nodes in the model). The remainder of part is far below ranging from 0.003-0.02, 0.004-0.03 and 0.007-0.01 respectively. Although the range is considerably small, and isn't clearly visible they correlate to the maximum displacement associated to each configuration. As

configuration 3 has an even distribution of low displacement and strain contours are small and difficult to see.

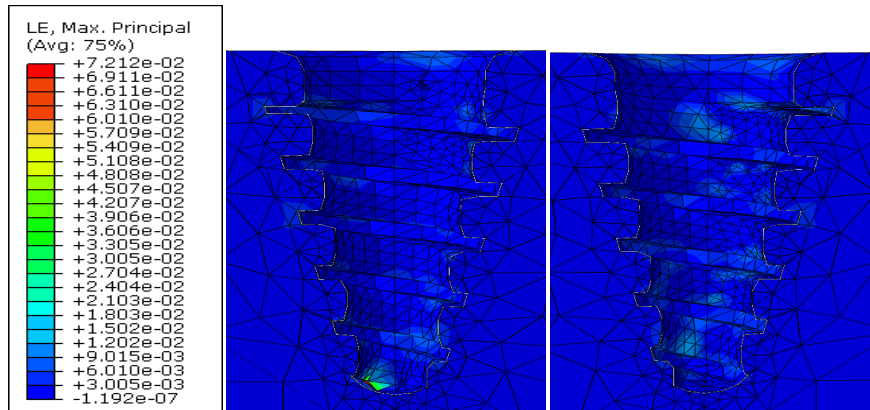


Figure 6-: Block Model Maximum Principal Strain No Screws Artificial Bone (Average Loading 1130N)

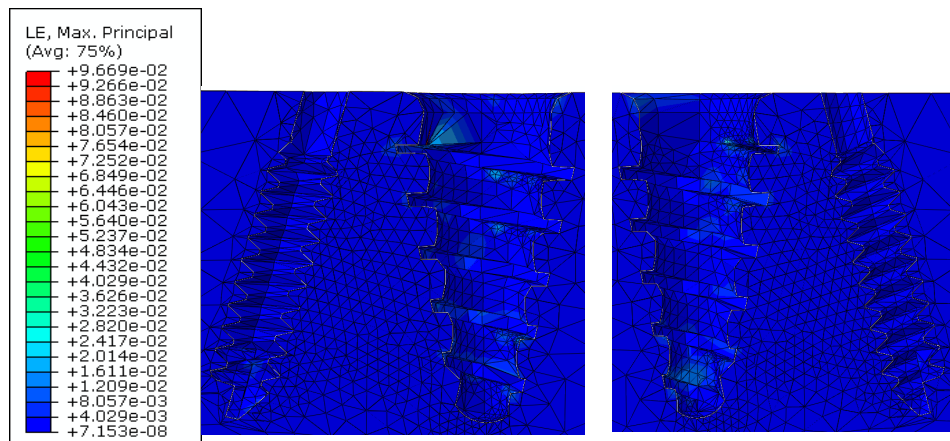


Figure 6-: Block Model Maximum Principal Strain 1 Screw Artificial Bone (Average Loading 1469N)

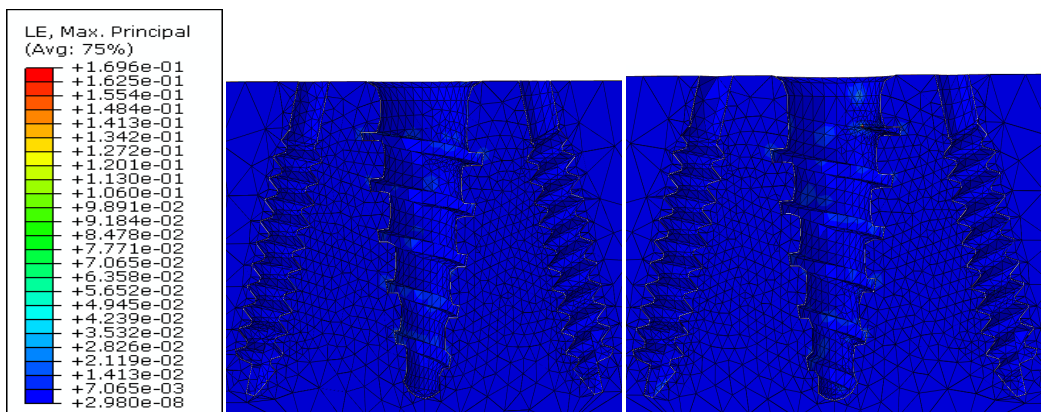


Figure 6-: Block Model Maximum Principal Strain 2 Screws Artificial Bone (Average Loading 2396N)

6.6 Humeral Interaction

In this section, the interaction between the implant and Humeral component has been simulated. The method previously stated was used to model the humerus part using two bone materials (cortical and cancellous (bone substitute)) and the model was tested under compression.

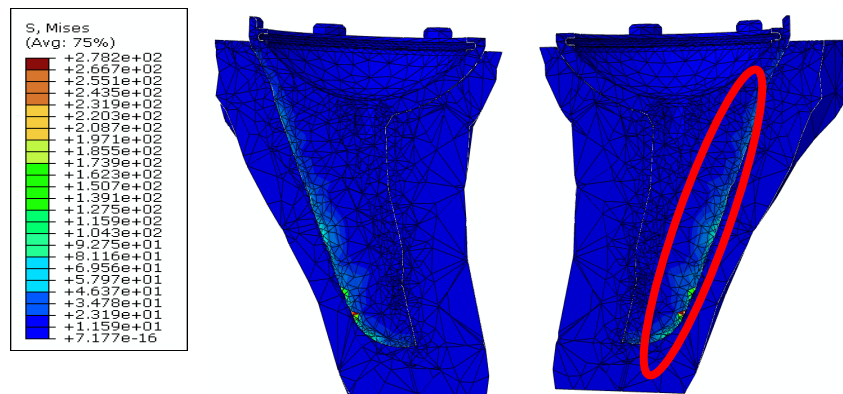


Figure 6-: Humeral Implant Model Von mises stress full assembly (1070N Magnitude)

6.6.1 CANCELLOUS BONE

The FEA simulation results for the humerus with cancellous bone model (bone substitute) explained from two different aspect; stress concentration and micro-motion.

6.6.1.1 Stress Concentration

Figure 6- represents the stress distribution across the humeral interaction. As seen the stresses develops against the longest stem of the humeral implant where this pushes against the bone. The stresses are evenly distributed against edge but as the edge is also pushed downwards the combination of the two forces applied increases the stresses further down the fin. The highest point is found at the curvature of the lower edge of the fin. The highest point is found at the curvature of the lower edge of the fin. The maximum is found to be 278MPa which is much lower than the Yield strength of 896MPa for the large humeral shell.

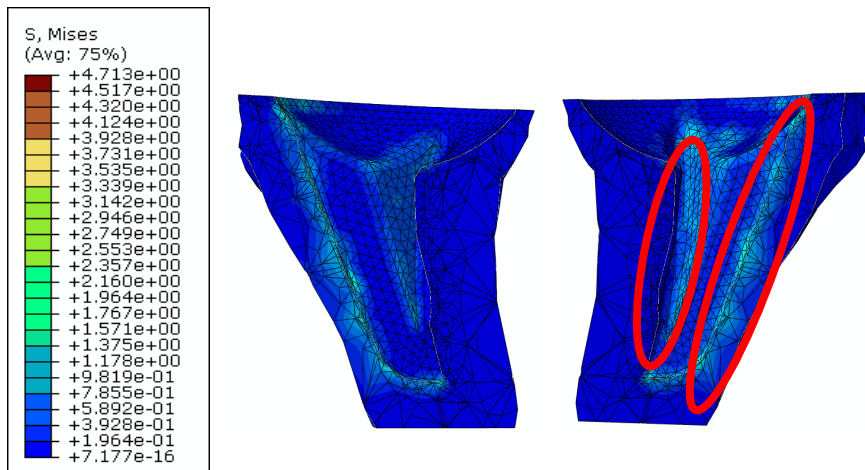


Figure 6-: Humeral Implant Model Von mises stress Artificial Bone side view (1070N Magnitude)

Figure 6- the stresses developed across the bone can be seen more clearly. The stress was evenly distributed across the back wall of the humerus. In addition, the region where the fin interacts with the bone shows slightly higher stresses distribution. The cross section between the interface of the humeral implant fin and the humerus bone wall displayed the stress distribution. However, the force and stress were concentrated in the direction of motion.

In compressive testing, it is evident that the distribution is biased across the back wall of the cavity with some stresses developing in the circular protrusion. The bottom end also shows high concentration however is not excessive as the inclination of the implant distributes the load in downward direction therefore absorbing the stress. Most importantly the maximum stress does not exceed the compressive yield strength of the bone of 8.4MPa as shown in Figure 6-.

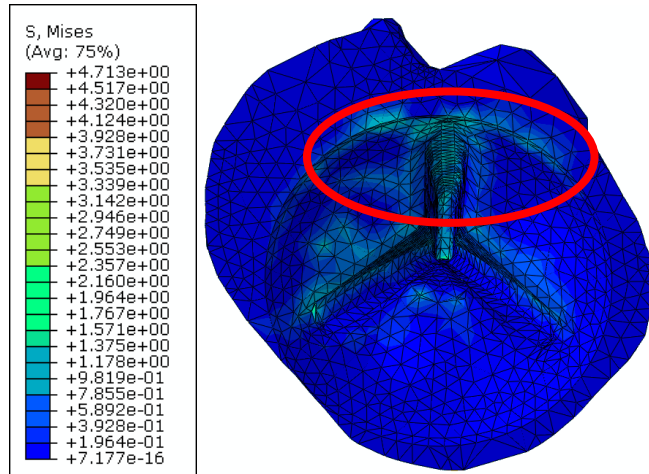


Figure 6-: Humeral Implant Model Von mises stress Artificial Bone top view (1070N Magnitude)

The concentration across the humeral implant is predictable similar to the pattern shown on the bone. However the implant shows much less diversity in distribution with higher concentration on the large fin of the stem. The maximum stress generated is 278MPa which is far below the yield strength of 896MPa. Therefore neither the bone nor implant fails under the conditions.

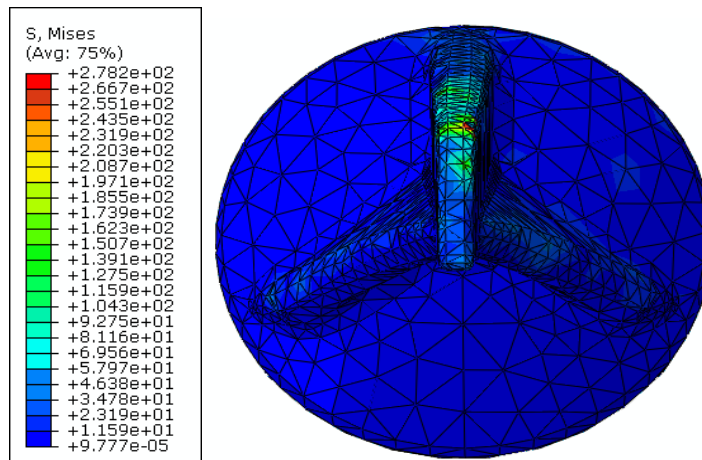


Figure 6-: Humeral Implant Model Von mises stress Implant (1070N Magnitude)

6.6.1.2 Micro-motion

The majority of displacement occurs in the regions with maximum stress distribution (see

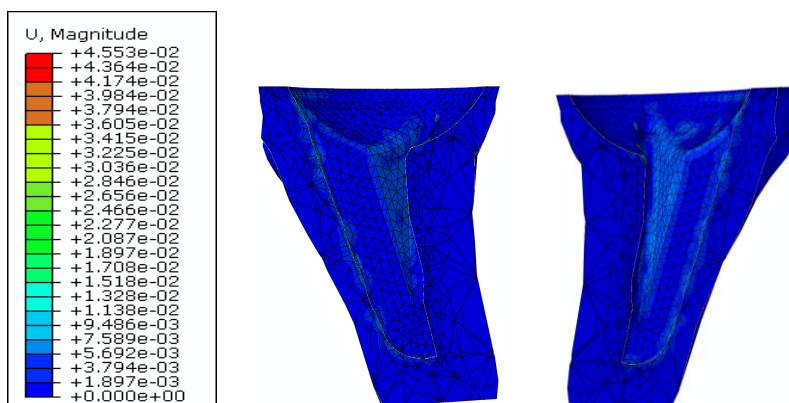


Figure 6-). The micro-motion was minimal and cannot be seen, Figure 6-. The maximum is shown at 45.5µm and this level is only reached at the highest stress levels and still below the allowable micro-motion level of 50-150 µm. The rest of the micro-motion around the bone remains between 0-22µm.

Figure 6-: Humeral Implant Model Micro-motion of Artificial Bone (side view, 1070N Magnitude)

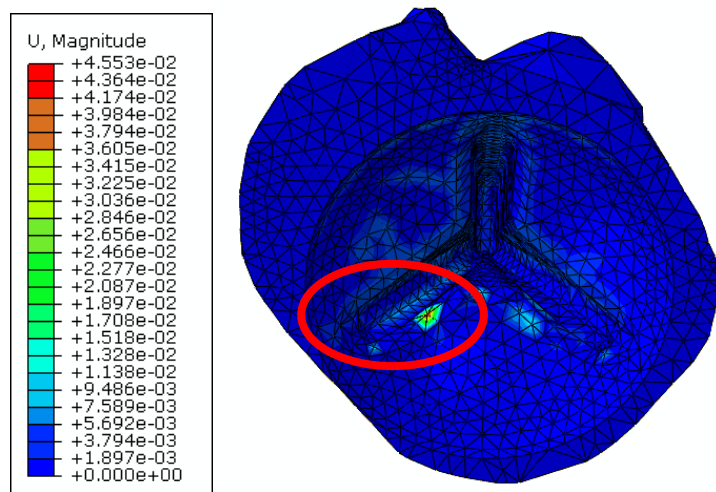


Figure 6-: Humeral Implant Model Micro-motion of Artificial Bone (top view, 1070N Magnitude)

The highest displacement is located at the top of the interaction on a surface where low force is exerted as seen in Figure 6-. There is low micro-motion across the upper surfaces with the range even lower than that stated previously.

6.6.1.3 Maximum Principal Strain

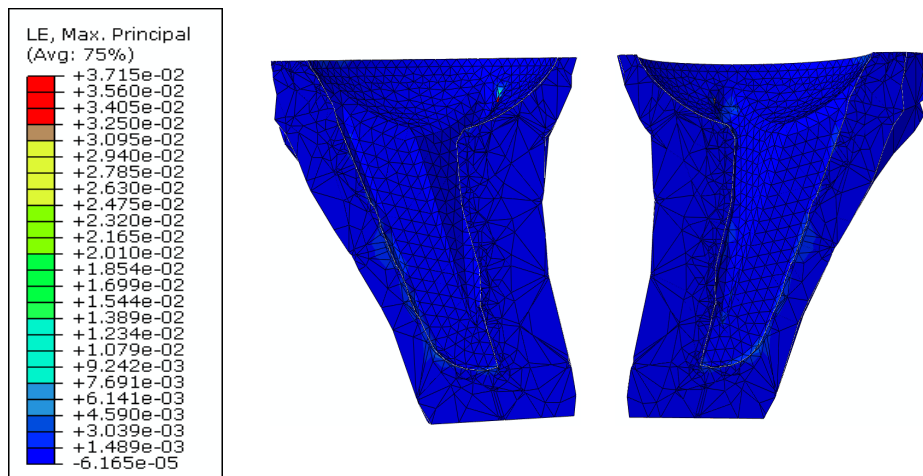


Figure 6-: Humeral Implant Model Maximum Principal Strain Artificial Bone (side view, 1070N magnitude)

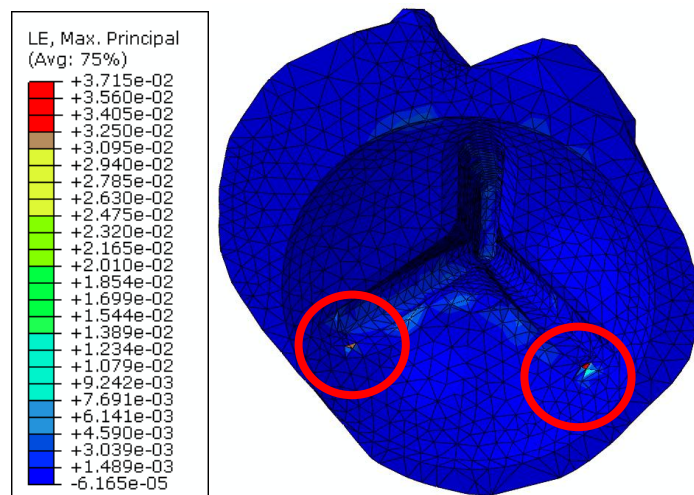


Figure 6-: Humeral Implant Model Maximum Principal Strain Artificial Bone (top view, 1070N magnitude)

As the micro-motion of the bone is small the maximum principal strain is also small. In Addition, the bone never reaches the yield stress or the corresponding yield strain therefore results show almost no signs of failure with a maximum ratio of 0.03. There are also no intermediate regions as seen, the maximums occur at the corners indicated in Figure 6-.

6.6.2 CORTICAL BONE

This section discusses the result of compression tests applied to the FEA model of the humeral stem implant and the humerus bone except using cortical bone material properties.

6.6.2.1 Stress Concentration

As expected, the stress distribution is identical to that seen in cancellous bone as the force direction and the shape of the bone remain the same. The maximum stress however was much higher with 792MPa as shown in Figure 6-.

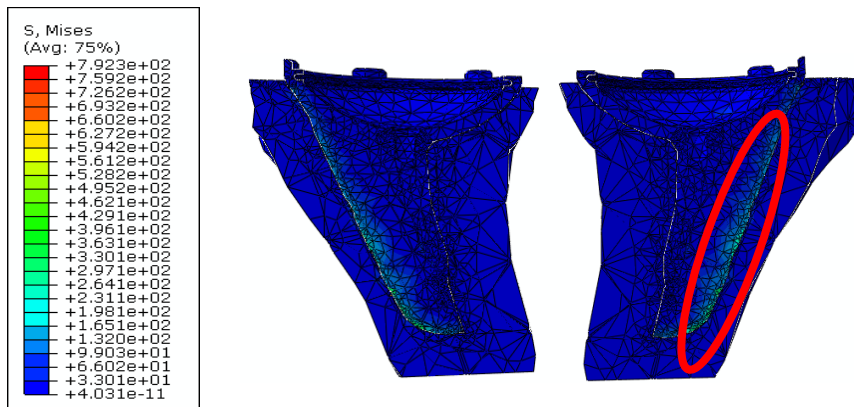


Figure 6-: Humeral Implant Model Von mises stress full assembly (side view, 1070N)

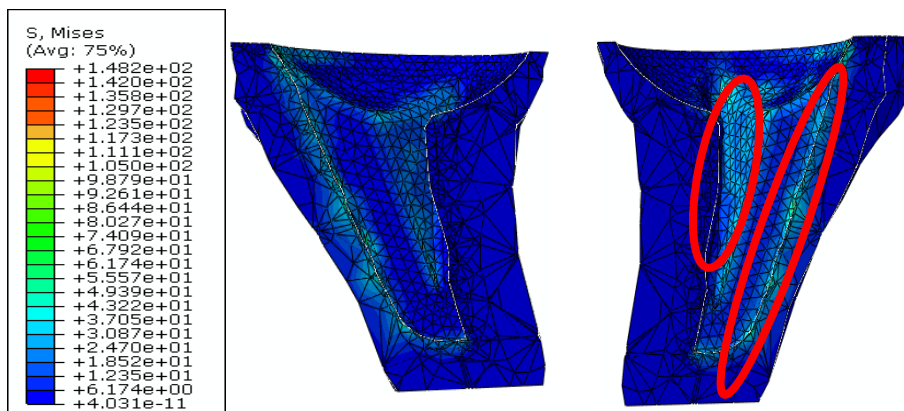


Figure 6-: Humeral Implant Model Von mises stress bone (side view, 1070N Magnitude)

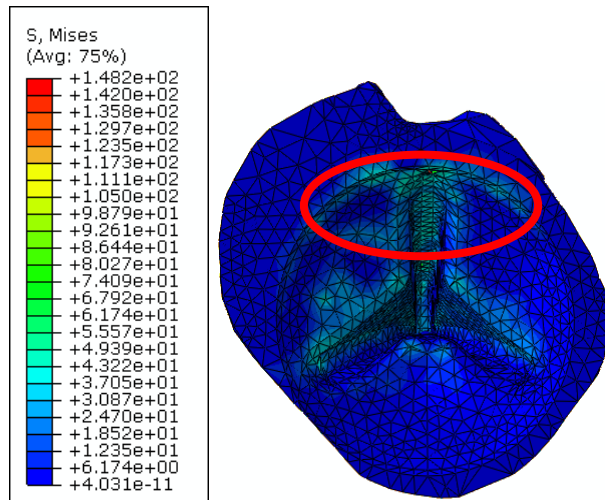


Figure 6-: Humeral Implant Model Von mises stress bone (top view, 1070N Magnitude)

In compression testing and when Isolating the humerus part, the stresses develop at the point of contact which can be seen clearly. As the implant moves towards the direction of the force the bone is compressed. The stiffer cortical bone shows the same distribution as cancellous however the maximum is much higher at 148MPa. As this value exceeds the yield strength (Table 6-) of the bone 120MPa on a closer look it can be seen this has occurred on a single element (node), with the majority of the part ranging between 0-60MPa. This can be seen in and Figure 6-.

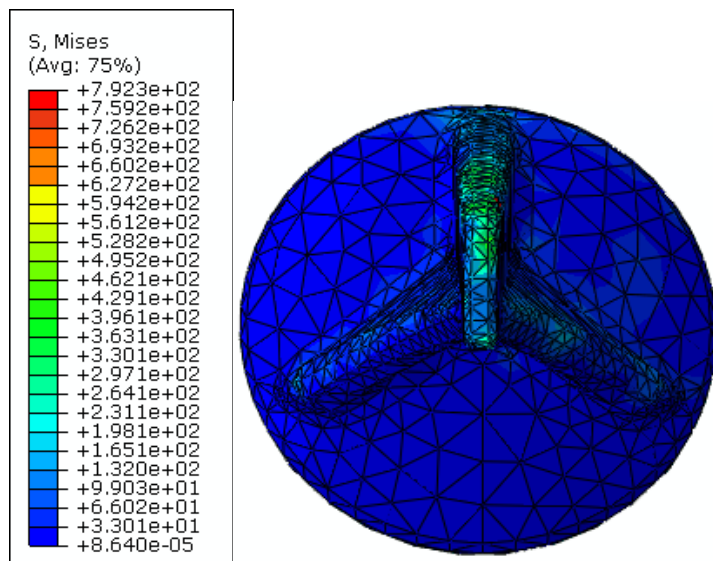


Figure 6-: Humeral Implant Model Von mises stress implant (top view, 1070N Magnitude)

The humeral implant shows distribution on par to the humerus. The maximum stresses are again found along the long edge side of the humeral stem. The maximum stress of 792MPa is found along the edge of a single element (node) in the model. The remaining part ranges between 0-380MPa far below the yield limit of 896MPa (Table 6-).

6.6.2.2 Micro-motion

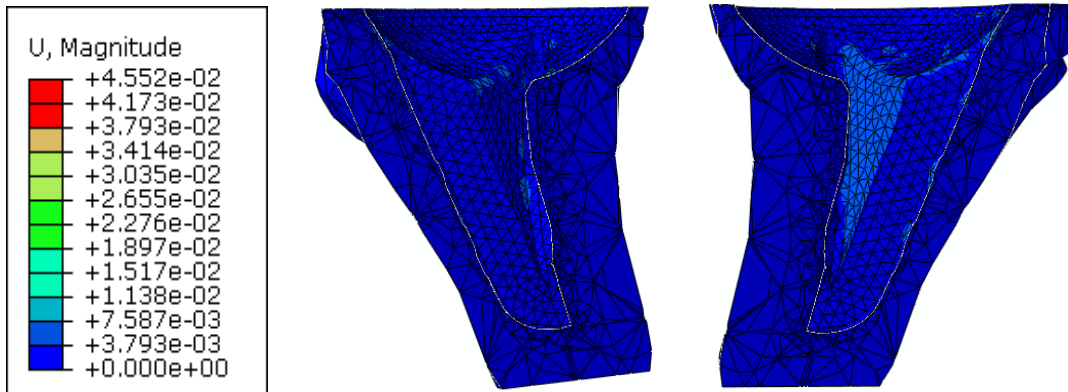


Figure 6-: Humeral Implant Model micro-motion bone (side view, 1070N Magnitude)

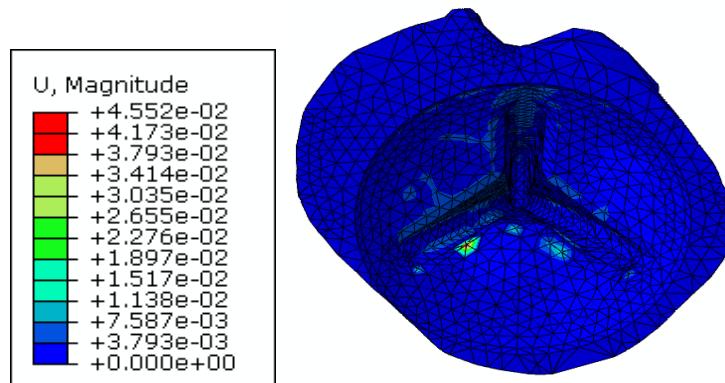


Figure 6-: Humeral Implant Model micro-motion bone (top view, 1070N Magnitude)

Figure 6- and Figure 6- show the bone does have a large magnitude of motion with the maximum at 45µm; however this occurred in only a few elements or nodes in the model, most of the part (bone) ranged from 0-22µm far lower than the maximum. The micro-motion on cancellous bone is found to be more dominant on with higher range of value.

6.7 Scapula Interaction

In this section, the interaction between the Glenoid head implant and scapula has been simulated. To prepare the model preparation for the simulation, same methodology stated before was used, i.e. two different materials have been selected; cancellous bone and cortical bone.

At this stage a concentrated vertical Loading of 1070N applied across glenoid head and peripheral screws. The concentration of the stress on the Glenoid head implant is shown in the Figure 6-, However to see the stress in different parts; it is necessary to cut the model in different planes.

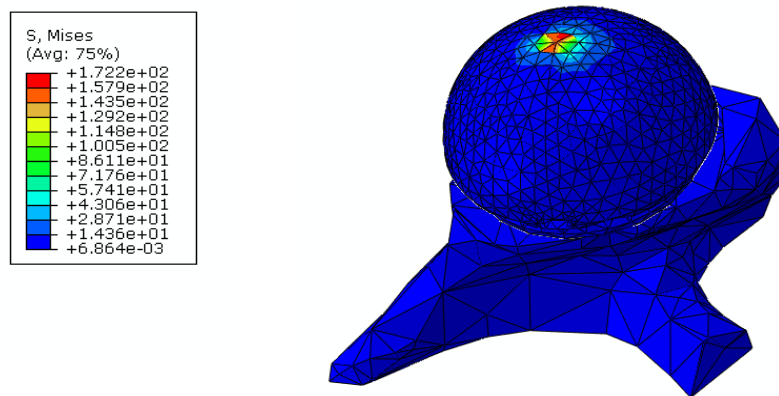


Figure 6-: Concentrated force on the implant head

6.7.1 CANCELLOUS BONE

In this section cancellous bone material were assigned to the scapula model.

Stress Concentration

shows the stress concentration on the scapula base which shows the highest stresses at the contact between the glenoid head and the glenoid base. The force from the head compresses against the inner wall of the base resulting in the distribution. The maximum is found on the glenoid head as the force is transferred from a larger surface to a smaller surface.

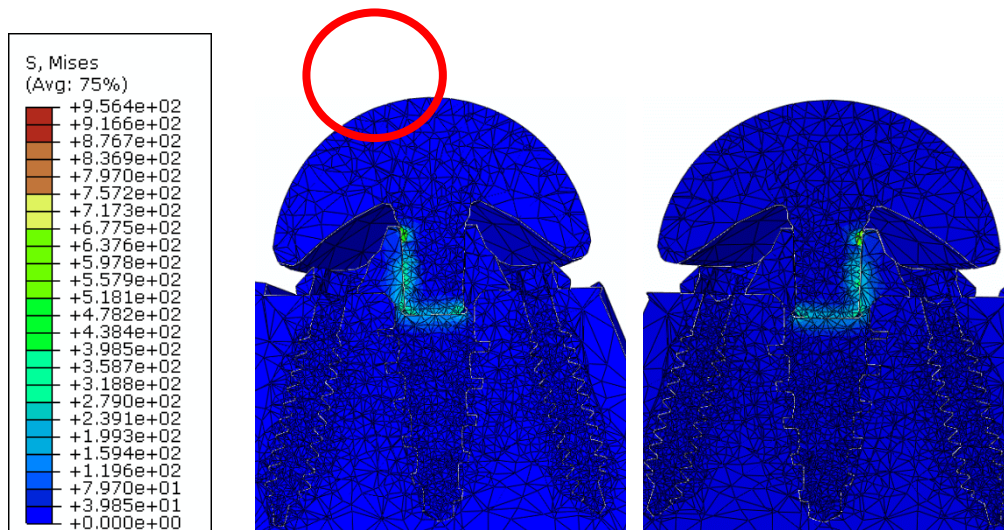


Figure 6-: Scapula Implant Model Von Mises stress full assembly (1070N Magnitude)

When looking at the bone individually the stress level was not clear as the maximum is far higher than the lower limits. When setting the limit to 0-0.1MPa the stress distribution displayed was small. The stress build-up occurs towards the direction of motion in the glenoid base cavity with the lower portion of the cavity showing minimal stress. The peripheral screws show that the compression of the bone from the clockwise moment of the base applies a force on the screws. The stress is concentrated largely on the bottom tip of the screw; where the maximum of 2.72MPa is also found on a single element. The bone remained far below the 8.4MPa yield strength therefore did not fail. This can be seen in Figure 6-.

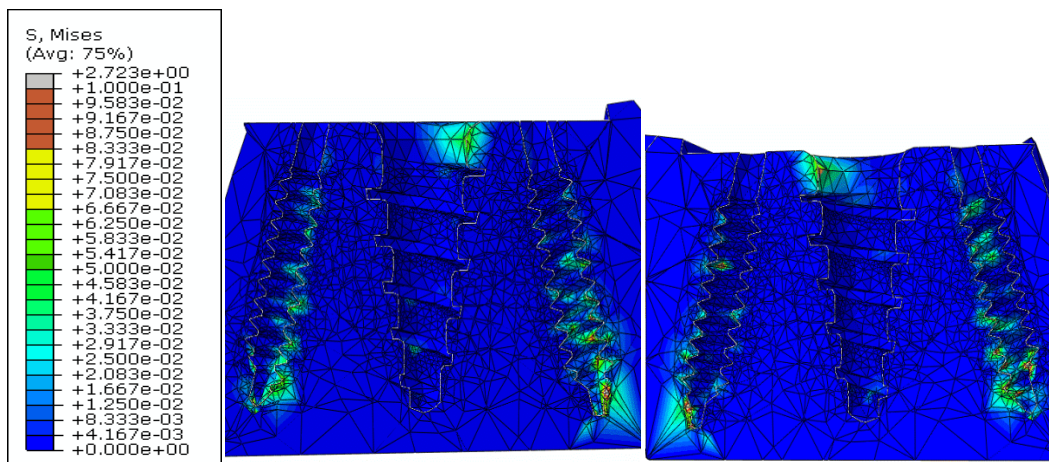
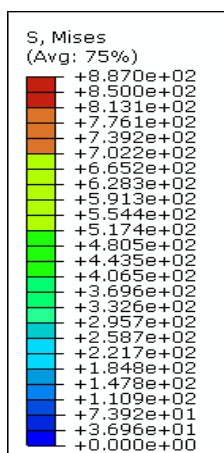


Figure 6-: Scapula Implant Model Von Mises stress Artificial Bone (1070N Magnitude)

The highest stress distribution was shown on the GBP head. The maximum stress is generated in the inner cylinder which of the glenoid head. There are also stresses around the edges of the flat head of the base. There is minimal stress build up on the peripheral screws. Although the



maximum is 887MPa the majority of the part remains between 0-480MPa and therefore doesn't exceed the yield strength of 950MPa. (Table 6-).

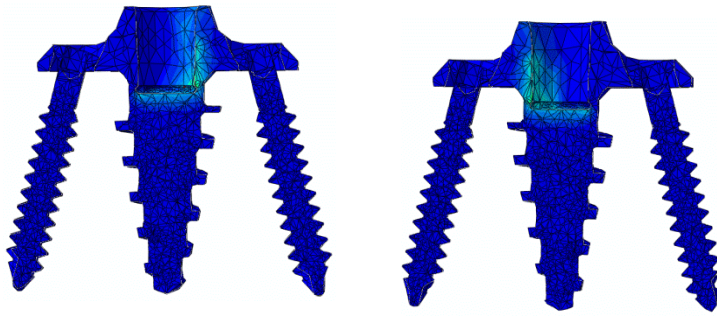


Figure 6-: Implant Model Von Mises stress Glenoid Base (1070N Magnitude)

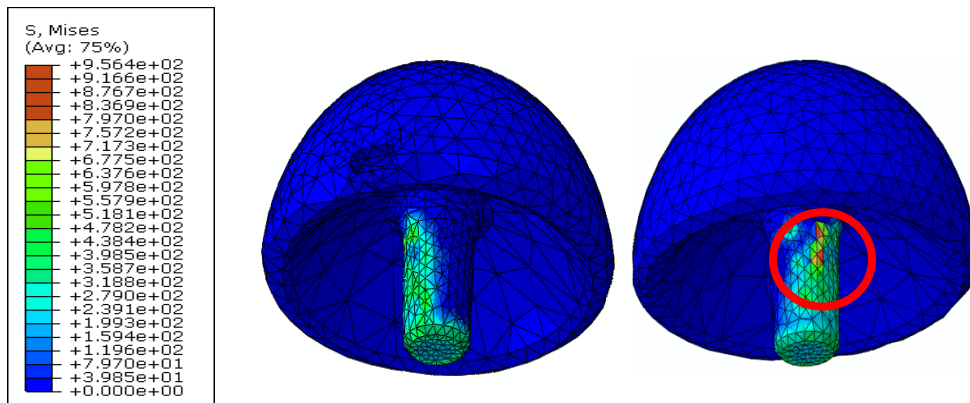


Figure 6-: Implant Model Von Mises stress Peripheral Screws (1070N Magnitude)

Isolating the glenoid head shows that the largest stresses are distributed across the interaction between the head and the base. The stresses develop across the attachment to the base in the direction of motion. The legend indicates that the maximum is 956MPa found on a single element indicated in Figure 6-; however the majority of the part ranges from 0-677MPa. The maximum yield strength of 1350MPa is not exceeded and there is no failure.

6.7.1.1 Micro-motion

From Figure 6- it can be seen that the displacement occurs across the glenoid cavity. As the base is compressing the bone the maximum displacement is found across the bottom edges of thread. The maximum displacement is found to be 33µm however as seen the majority falls much below between 0-13µm across the regions of interaction as the maximum is found only on a few elements (nodes).

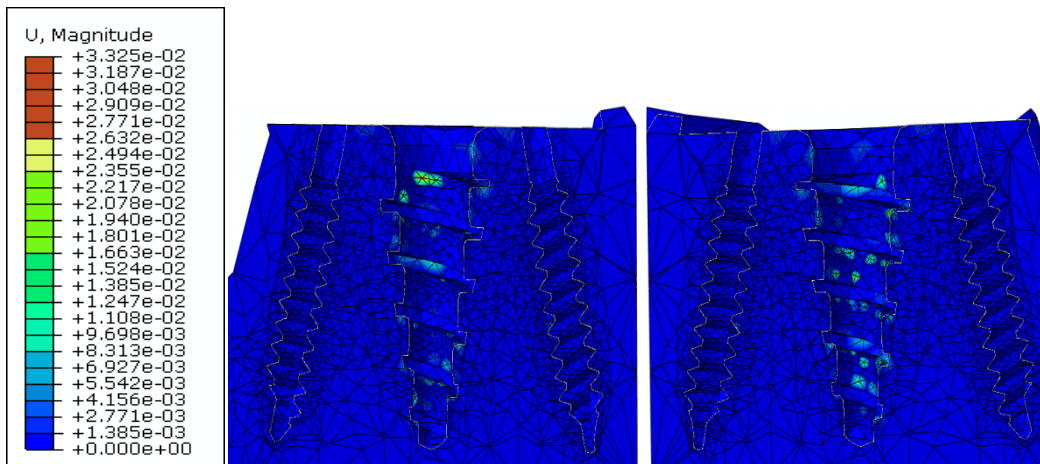


Figure 6-: Scapula Implant Model Micro-motion Artificial Bone (1070N Magnitude)

6.7.1.2 Maximum Principal Strain

As the displacement is small it is expected that the maximum principle strain is also low. The distribution is in the same region as shown Figure 6-, however the maximum strain is only seen in elements (nodes) that have the highest displacement only. The maximum strain is 0.05 however the majority of the regions of interaction are between 0-0.013.

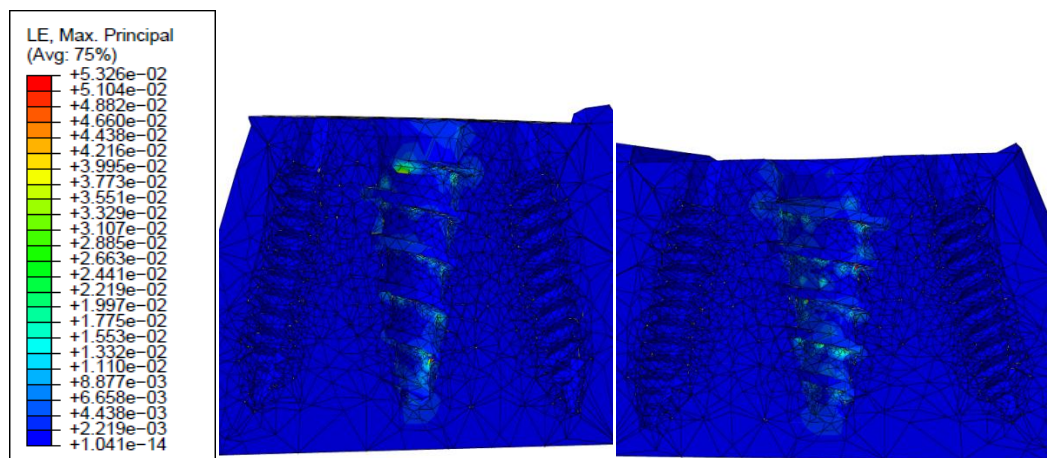


Figure 6-: Scapula Implant Model Maximum principal strain Artificial Bone (1070N Magnitude)

6.7.2 CORTICAL BONE

6.7.2.1 Stress Concentration

The stress distribution on this model is almost identical to the stress distribution on cancellous bone as seen in Figure 6-. The maximum is found on the glenoid head as the force is transferred from a larger surface to a smaller surface.

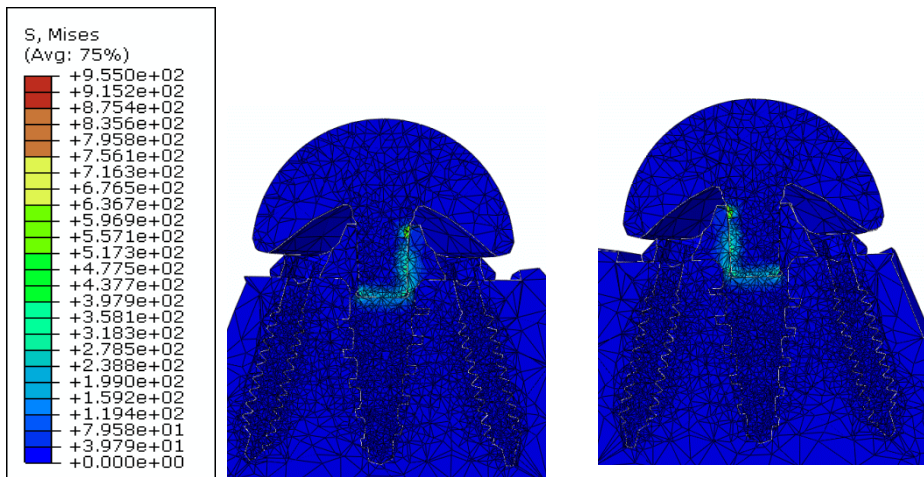


Figure 6-: Scapula Implant Model Von Mises stress full assembly (1070N Magnitude)

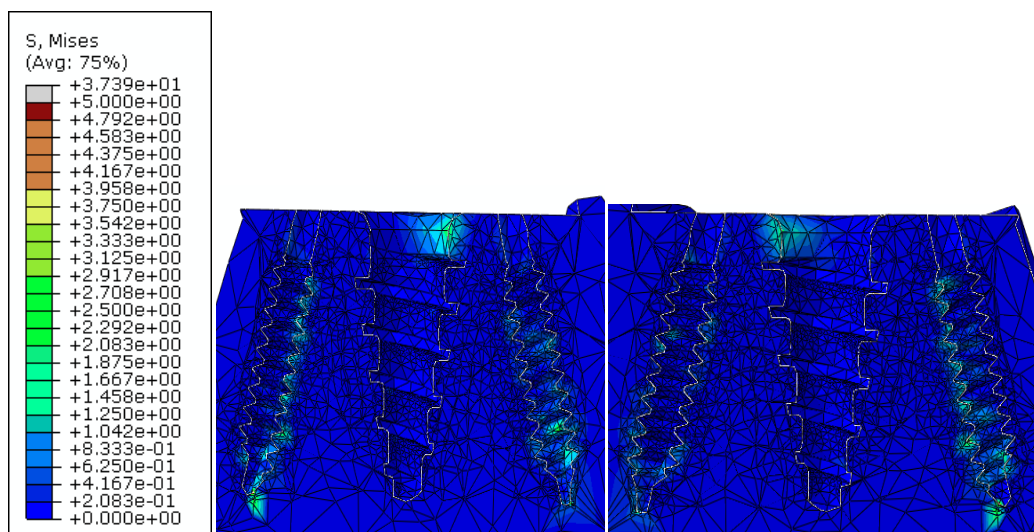


Figure 6-: Scapula Implant Model Von Mises stress Artificial Bone (1070N Magnitude)

When looking at the bone individually the stress level was not clear as the maximum is far higher than the lower limits. The stress level was set to range from 0-5MPa the stress distribution can then be seen more clearly in the model. The stress distribution is identical to cancellous bone model with stresses concentrated largely on the bottom tip of the screw; where the maximum of 37MPa is also found on a single element. The bone ranged between 0-2.5MPa and far below the 120MPa yield limit. This can be seen in Figure 6-.

The stress generated is identical to stress distribution across a cancellous bone. The maximum stresses were found in the cylinder which houses the head and minimal stress seen on the peripheral screws. Maximum is found to be slightly higher at 894MPa but the majority of the part remains between 0-484MPa and therefore doesn't exceed the yield strength of 950MPa.

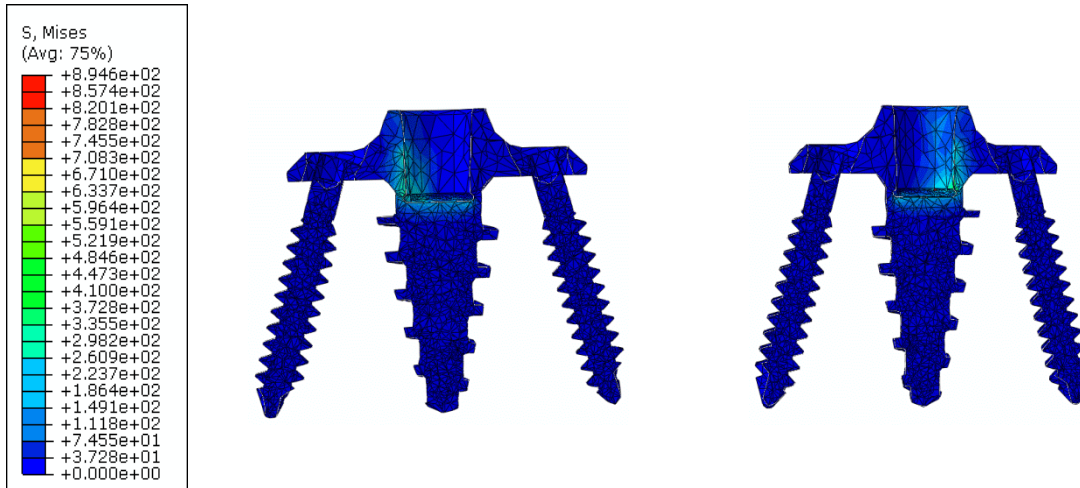


Figure 6-: Implant Model Von Mises stress Glenoid Base (1070N Magnitude)

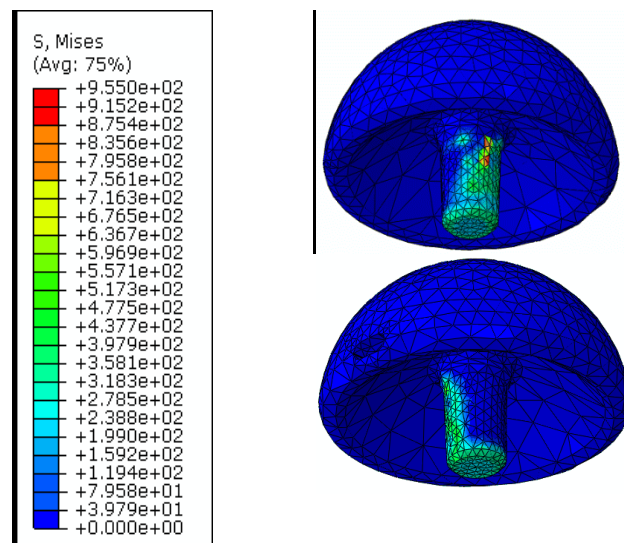


Figure 6-: Implant Model Von Mises stress Peripheral Screws (1070N Magnitude)

When isolating the glenoid head the stress distribution is similar to stress distribution seen in cancellous bone model. The largest stresses are distributed across the interaction between the glenoid head and the glenoid base. The maximum is found to be almost identical at 955MPa and also found on a single element (node) indicated in Figure 6- but most of the part remained between 0-557MPa. The part does not exceed the 1350MPa yield limit and therefore does not fail.

6.7.2.2 Micro-motion

Figure 6- shows the displacement occurs mainly across the glenoid cavity. As the glenoid base is compressing the bone, the maximum displacement is found across the bottom edges of glenoid conical screw thread. The maximum displacement is found to be 33 μ m. However, the majority of the part falls much below between 0-11 μ m. The values are very similar to those founds in cancellous bone model.

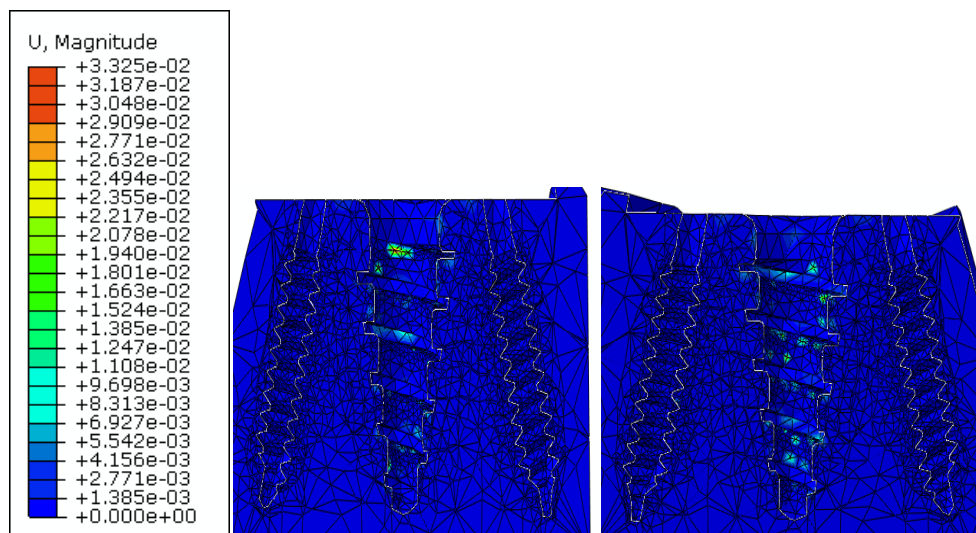


Figure 6-: Scapula Implant Model Micro-motion Artificial Bone (1070N Magnitude)

6.8 Discussion Summary

This section highlights the previous FEA models' results and assembles all the results in two tables to distinguish the differences in the results values from one model to the other. The FE models were tested in three different configurations for the GBP (0 screw, +1 side screw and +2 side screws). As stated before the FEA models created using two bone properties cortical bone properties and cancellous bone properties (provided by Biomet, UK, ltd). In section 6.6 the interaction between Humerus and implant were simulated and the stress and micro motions were studied. Moreover, the interaction of the Scapula and the implant were simulated in section 6.7. In all the cases the applied external forces were 1070 N in vertical direction.

Table 6-: Summary of the model's material and conditions of the FEA

Model	Part	Material	Load (N)	Compressive Yield Strength (MPa)	UTS Tensile (MPa)	Majority Range (MPa)	Max Stress (MPa)
Block-No Screw	Scapula	Polyurethane	1130	8.4	5.6	0 - 3.03	29.87
Block-No Screw	Glenoid Base	Wrought Ti6Al4V	1130	950	950	0 - 147	705.90
Block-1 Screw	Scapula	Polyurethane	1469	8.4	5.6	0 - 3.26	63.65
Block-1 Screw	Glenoid Base	Wrought Ti6Al4V	1469	950	950	0 - 260	780.30
Block-1 Screw	Peripheral Screws	Wrought Ti6Al4V	1469	950	950	0 - 15.81	379.50
Block-2 Screw	Scapula	Polyurethane	2396	8.4	5.6	0 - 3.97	33.44
Block-2 Screw	Glenoid Base	Wrought Ti6Al4V	2396	950	950	0 - 316.7	2002
Block-2 Screw	Peripheral Screws	Wrought Ti6Al4V	2396	950	950	0 - 277.1	1025
Humeral Interaction	Humerus	Polyurethane	1070	8.4	5.6	0 - 1.76	4.71
Humeral Interaction	Humeral Implant	Cast CoCr	1070	896	896	0 - 150	278.20
Humeral Interaction	Humerus	Cortical	1070	120	90	0 - 60	148
Humeral Interaction	Humeral Implant	Cast CoCr	1070	896	896	0 - 380	792
Scapula Interaction	Scapula	Polyurethane	1070	8.4	5.6	0 - 0.1	2.72
Scapula Interaction	Glenoid Head	Wrought CoCr	1070	1350	1350	0 - 597	956.40
Scapula Interaction	Glenoid Base	Wrought Ti6Al4V	1070	950	950	0 - 480	887.00
Scapula Interaction	Scapula	Cortical	1070	120	90	0 - 2.5	37.39
Scapula Interaction	Glenoid Head	Wrought CoCr	1070	1350	1350	0 - 557	955.00
Scapula Interaction	Glenoid Base	Wrought Ti6Al4V	1070	950	950	0 - 484	894.60

Table 6-: Summary of applied load and achieved micro motion

Model	Part	Material	Load (N)	Ideal Range (μm)	Majority Range (μm)	Max micro-motion (μm)
Block-No Screw	Scapula	Polyurethane	1130	50-150	0 - 3.03	53.36
Block-1 Screw	Scapula	Polyurethane	1469		0 - 3.26	46.65
Block-2 Screw	Scapula	Polyurethane	2396		0 - 3.97	79.2
Humeral Interaction	Humerus	Polyurethane	1070		0 - 22	45.53
Humeral Interaction	Humerus	Cortical	1070		0-22	45.52
Scapula Interaction	Scapula	Polyurethane	1070		0 - 13	33.00
Scapula Interaction	Scapula	Cortical	1070		0-11	33.00

6.9 Conclusion

It is possible to summarise the FEA results in three groups. In all three groups Verso implant were used. In the first group of simulation a simulated foam block model was used. The simulated foam block (bone substitute) was used from polyurethane as a standard material to simulate cancellous bone. The shape of the material was a simple block to facilitate the comparison with the experimental results in chapter 5, to validate the experiment results. In the second and third groups of simulation, the real shape of the scapula and humerus were used, using the method explained in chapter 4 and beginning of chapter 6. However, two different materials were used in the simulations of the bone, polyurethane (cancellous) and cortical.

6.9.1 Simulated Foam Block Model

Firstly the results from the simulated block model indicate that the failure obtained from experimental results is similar to the simulation results. The stress contours obtained in ABAQUS indicate the regions of failure which were in grey.

The grey areas represent the failure which occurs on the simulated block side (bone substitute) as the grey regions has exceeded the UTS of the bone which means bone damage or fracture.

An average maximum failure load was used in the models in order to indicate if they fail at the same loads shown in the experimental results. The results of all 3 configurations show that the bone fails at the stated loads indicated by the grey areas (exceeded the UTS), all of which propagate from the inner diameter of the glenoid cavity. In comparison the experimental data showed similar behaviour as the failure caused the entrapped parts of the bone to detach from the simulated block.

From the stress distribution it is seen that if side screws were added to the configuration the failure load increases significantly. This occurs as the peripheral screws act as anchors for the glenoid base under a tensile load, distributing the load across a much larger surface area. The screws main purpose is to disallow the unscrewing of the glenoid base during loading and also to absorb stresses generated from moments as the forces are never parallel to main shaft of the implants and in reality load applied on the glenoid head rather than the glenoid base to allow more stress distribution area.

The glenoid base showed stress distributions evenly across the screw all of which are far below the yield strength of the alloy. The highest concentration occurs at the point of contacts of the prosthesis parts. Most of which occurs across the glenoid screws and slightly on the peripheral screws. However, the yield strength of the screws is still not reached. The most important conclusion from loading to failure of the model is that it is clear that the bone will fail before the implant will; this is significant.

Measuring micro-motion of the interaction between the GBP and the simulated block showed interesting results. Under configuration 1 there is a maximum of 53.36 μm of motion, in configuration 2 this reduces to 46.2 μm and in configuration 3 this increases to 79.2 μm and they are all below the allowable limit of 50-150 μm .

Although these results are either within or some were below the recommended 50-150 μm from an engineering perspective this displacement occurs under a load in one direction only. In reality loads will be applied from every direction. Maximum displacement in a single direction can therefore be double in a single direction from a back and forth displacement, it can be significantly more if twisting effects are also taken into account.

The direction of force determines the load distribution; therefore the implant must be uni-axially functional. Although the number of screws increases the loading capacity, and the angle at which the peripheral screws are set determines the loading capacity in each direction therefore altering stress distribution.

6.9.2 Humerus Model

In this section the simulated humerus model and its results will be highlighted. Stresses are evenly distributed in the direction of the force. Although the humeral implant is subjected to such a heavy load the conditions are far higher than real life operating conditions.

The difference that the load is a compressive force means the maximum yield strength increases to 8.4MPa for polyurethane (cancellous bone) and 120MPa for 3rd generation cortical bone (Matweb). The cross section of the humerus shows that a load magnitude of 1070N generates a maximum of 4.7MPa stress on cancellous and 148MPa on cortical bone. Taking a closer look shows the maximum stress in the cortical bone model is found on a single element (node in the FE model); however the majority of the part (humerus) remained much lower between 0-60MPa; far lower than the yield stress indicating that the bone does not fail. The majority of stresses are distributed due to the triple fin design which allows distribution of loads from any direction over all three fins. The fins increase the surface area of the implant therefore increase the surface area of interaction. Therefore no matter which direction the load is applied the fins reduce the load from the fin tip, therefore reduce failure.

The stress concentrates across the edge of the largest fin of the humeral part of the implant. This occurs in the direction of motion and the small cross sectional area that funnels the load. Although much of the stress is distributed across the walls of the remaining two fins the maximum of 278MPa and 792MPa occurs on the largest fin for polyurethane and cortical bones respectively. The latter result indicates that the implant is close to its limit, but on closer inspection the maximum occurred on a single element; the majority of interaction surfaces ranged from 0-380MPa. This is significantly lower than the yield strength of 896MPa therefore the implant does not fail.

The magnitude of displacement is shown to be 45µm for both types of bones, changing the limit indicates that the majority of the interaction regions are also identical between 0-22µm. This is

lower than the allowable 50-150 μ m for promotion of bone growth. There was concentration of motion across the dome cavity of the humerus and this is because of the geometry where the fins begin, adding to this may be the meshing and also mass scaling (mass scaling was set to 10^3) which can localise stresses. Although the magnitudes are identical polyurethane (cancellous) had a larger portion of displacement above 10 μ m compared to cortical bone. This is due to the lower stiffness of the bone which allows higher compression; hence it can reach the allowable micro-motion.

As the displacement is minimal the strain was also minimal; showing a maximum of 0.03, most of the part remained far below this figure between 0.000006-0.003, in all cases the results indicate small displacement or compression across the interface.

Overall this indicates that a larger load can be applied to the humeral implant without the expectation of failure, which also would increase the displacement. However, this material shows that they are very durable in the condition and most importantly do not fail or compromise the bones integrity. Although the displacement is low in the humerus there is still some motion which is doubled if there is a reverse of load direction, adding twisting effects will also increase the magnitude of displacement, especially in cancellous bone.

6.9.3 Scapula Model

Under the same conditions as the humerus model scapula model showed similar results. The maximum stress concentration occurs at the bottom tip and at the first thread of the GBP. Looking at the cross section of the bone it shows the areas that have the highest load. The maximum reached is 2.72MPa for cancellous and 37.39MPa for cortical bone which is far below the yield strength of 8.4MPa and 120MPa respectively. When the limit was set (as in Table 6-) it can be seen the majority of the part is between 0-0.1MPa and 0-2.5MPa. This is due to the implant itself absorbing some of the stresses from the load source.

Looking at the implant itself it can be seen the glenoid implant has a lot of stress concentrations. The maximum stress distribution was shown at 956.4MPa for glenoid head and 887MPa for GBP in cancellous bone; and 955MPa for glenoid head and 894.6MPa for GBP in cortical bone scapula model. Those approximate similar results indicate that the bone material itself has slight effect on the stress distribution across the implant parts.

The stresses on the glenoid head were high for both bone types (cortical and cancellous). However, on a close inspection they showed a majority range between 0-597MPa (cancellous) and 0-557MPa (cortical) indicating the glenoid head does not fail in both models. The GBP showed similar pattern as the bulk of stresses ranged between 0-480MPa (cancellous) and 0-484MPa (cortical). This means that the GBP does not fail.

Analysing the peripheral screws individually it can be seen that the screws do have some stresses. These are due to the tangential direction of the force which slides the glenoid therefore causing contact with the screws as well as the twisting effect of the glenoid base which compresses the bone on one side. The results show that the stresses are small; most of the screw is far below the limit. This indicates although some force is absorbed the contact is not sufficient enough to absorb a significant amount under compressive forces. The stresses are insufficient to cause any problems under compression.

Under compressive forces the micro-motion was small. The magnitude of the scapula bone showed the maximum was 33 μ m for both bone types (cortical and cancellous). But most of the part (scapula) remains below this limit between 0-13 μ m for cancellous and 0-11 μ m for cortical. This again showed that the displacement is not large even under a heavy load. The model only takes into account the motion in a single direction therefore the magnitude can double if back and forth motion is taken into account and increase further if twisting effects are included. As the displacement is small the maximum principle strain is small. The maximum is seen to be 0.05 which is small.

Although increasing the number of peripheral screws increases the load tolerability of the implant it also compromises the integrity of the bone due to more bone removal. The GBP alone can tolerate over 1070N of load. A single screw configuration compromises the stability of the motion by stabilising forces on one side only but it allow the GBP with the screw to tolerate more load.

Under compressive loads the peripheral screws do not absorb any stresses therefore the load is entirely on the GBP. The flat section of GBP under compression is effective in reducing the stresses exerted onto the base thread, and in turn becomes as effective in comparison to a tensile load.

In general, the micro-motion results were shown to be low. In any model the results shows magnitude of displacement under a single load in a single direction whereas in reality the part will be subjected to many forces from many directions simultaneously. Therefore the magnitude of displacement can double in a single direction if considering a compressive and tensile load.

The distance between the peripheral screws can play an effective and crucial role in reducing stress or micro-motion in the reverse prosthesis. Determining the proper angle of the screws and creating a perfect fit will distribute load much more evenly and disallow contact concentration. Round edges of the threads of the GBP main screw and peripheral screws will be effective in reducing the concentrations across the bone and the implant.

Chapter 7. Discussion

7.1 Introduction

This chapter highlights and discuss the results produced previously in chapter 5 (mechanical testing) and chapter 6 (FEA simulation and modelling).

This study aims to describe the mechanical behaviour of Scapula and Humerus bones at the implant sites. The study uses a finite element method to examine the mechanical parameter such as stress and strain at the interface between the Verso implant and the modelled bone. The possible micro-motion at the interface under loading was evaluated. A series of mechanical testing including load to failure tests and cyclic testing were carried out on the Glenoid base plate (GBP) attached to a foam block. The foam block used in the mechanical testing has same material properties as a cancellous bone (provided by Sawbone).

The mechanical testing procedure is essential so that Implant mechanical behaviour investigations and/or recognition techniques can be successfully implemented and monitored non-invasively in the shoulder joint. The studies reported in this thesis represent a step forward in understanding the nature of the shoulder joint and the development of techniques for the simulation of the implant using finite element analysis. Furthermore, the FEA model generated provides geometric dataset which can be used to enhance other computational models of the Verso implant within the shoulder joint.

This chapter will conclude and summarise the results achieved from both simulation and mechanical testing.

7.2 Mechanical tests

A series of mechanical test were applied to find out the durability of this Implant under various loads similar to the real conditions. The experimental test could be categorized in two different parts.

In the first set of the test a pull out test (tensile test) were performed on the composite of the GBP and the foam block with or without side screws at a 5mm/min sample rate.

In the second set of the experiment to examine the durability of the GBP and the peripheral screws; a series of cyclic loading were applied prior another pulling out tests.

Table 5- shows preconditioning test were performed before pulling out test.

The entire tests were carried out in three different conditions: GBP without screw, with one screw and with two screws. The outcome of the mechanical testing can be categorized as follow:

7.2.1 Visual observation for pull-out test

All the pulling-out results have shown neither irregular nor unexpected mechanical behaviour; nor any failure in the GBP with or without peripheral screw.

7.2.2 Maximum tolerated load on the interface between GBP and foam block

Pulling out test showed high strength of composite of the GBP and the foam block and the effect of adding the peripheral screws has increased this.

The mean of reached maximum load for the three pull out tests in each case was shown previously in chapter 5:

GBP without peripheral screws: 1130 N.

GBP with one peripheral screw: 1470 N.

GBP with two peripheral screws: 2540 N.

From the results it can be seen, adding one and two screws to the GBP increases the strength of the composite by 30% and 124% respectively compared to the GBP without any peripheral screw.

The composite strength has increased when the peripheral screws were added. This could be because of the symmetry in the GBP with two side screws case and also the opposite ends of 10° angle for these two side screws to the vertical line which makes the GBP more stable. According to the results shown, increasing the number of screws will increase the strength of the composite.

7.2.3 Stiffness

From the Force-Displacement figure illustrated in chapter 5, it can be seen that the composite of the GBP and foam block could tolerate the tensile load till yield point (Table 5-), which this point correspond to the specific movement or displacement inside the composite.

In the other words, if the implant in the body received such forces, the implant can have this acceptable movement before the foam block fail. This acceptable movement can be defined as micro-motions. On the other hand, in the literature the acceptable micro motion has been defined between 50 to 150 μ m (0.05 to 0.15mm), which is lower than displacement related to the yield point of the composite. To measure the stiffness, slope of the linear part of the figure in limits of 50 μ m to 150 μ m has been measured.

Stiffness of GBP without screws: 2800N/mm.

Stiffness of GBP with one screw: 4500N/mm.

Stiffness of GBP with one screw: 1700N/mm.

The results showed the stiffness of the composite (interface between GBP and foam block) increased by adding one peripheral screw to the glenoid base plate.

Adding two screws to the GBP indeed has increased the strength of the composite. On the other hand, it has developed more resistance of a higher value that led to an increase in the time required for the composite to be pulled out completely from the foam block (bone substitute). As it is explained before the fracture is by the shear forces and by having more screws, automatically the area supporting the force has been increased, hence stress reduces in the bone with the same force.

Nevertheless, the two fitted peripheral screws with 10° angle inclined from the GBP conical shape screw, has played a role in increasing the time required for the composite to be pulled out. In addition, the conical shape GBP screw might have moved sideways when pulled out with the two side screws attached, and that led to an increase in the resistance and time taken to reach the maximum loading. Therefore, the deflection has increased causing the stiffness of the composite to decrease.

7.2.4 Cyclic test as a measure of fatigue of the joint

Table 5- shows preconditioning test were performed before pulling out test. For example one set of preconditioning test is: Applying 10N to 50N force for 10 cycles at 1.0Hz (pre-cyclic test). It will be followed by a cyclical loading of 50N to 250N for 500 cycles. Then a load to failure tensile testing performed.

The cyclic loading in three different case of the GBP without, with one and with two peripheral screws were applied according to the setting force in Table 5- as explained previously.

In addition, Figure 5- and Figure 5- showed that the micro motion slightly increased by the time and this can lead to implant loosening, which is one of the most important problems. Moreover, it can be seen from the Figure 5-, the test performed in the border of acceptable range of micro motion. However Figure 5- is clearly shows this phenomenon, which means the load, is higher than elastic behaviour of the composite. In other words the composite will fail if the cyclic load test was repeated.

7.2.5 Pull out test at different loading rate

It was observed that applying load in a higher rate will increase the possibility of foam block fracture. This fact has shown that impact loading under different loading rate could be one of the important reasons for fracture of the bone in the implant area.

7.3 Finite element analysis

The finite element analysis created in this study was to investigate the interaction between the Verso implant and humerus, scapula bones. The aim was to compare and validate the finite element analysis results to those obtained from the mechanical testing. A series of compression and tension tests were applied to the FEA models created. This study has used third generation cortical and cancellous bone substitute properties to show the different interaction, stress distribution between the bone substitute and the Implant parts.

FEA performed in three groups. In all three groups Verso implant were used. In the first group of simulation, a foam block model was used. In the second and third groups of simulation, the real

shape of the scapula and humerus were used. However, two different materials were used in the simulations for the bone the polyurethane (cancellous bone) and cortical.

7.3.1 Simulated Block Model

A simulated model using FEA was created to replicate the same structure of the foam block used in the mechanical testing. Then a simulated GBP was attached to the simulated block model (bone substitute). The average loads reached in the mechanical testing were used as a maximum load to be applied to the simulated FEA block model (bone substitute). The simulated block model has used same configurations of the GBP (no screw, one screw and two screws) used in the mechanical experiment.

The results of all 3 configurations showed that the simulated block (bone) fails at the stated loads indicated by the grey areas, all of which propagate from the inner diameter of the glenoid cavity.

The important conclusion from loading to failure FEA model is that; it is clear that the bone will fail before the implant; this is significant as a broken part lodged in the bone and will most likely require removal of more bone to retrieve.

7.3.2 Humerus Model

Stresses are evenly distributed in the direction of the force. A compressive force was applied and the maximum yield strength increases to 8.4MPa for polyurethane (simulated block) and 120MPa for 3rd generation cortical bone (Matweb website).

The majority of stresses were distributed evenly due to the triple fin design (humeral component part) which allows distribution of loads from any direction over all three fins. The fins increase the surface area of the implant therefore increase the surface area of interaction. In addition, no matter which direction the load is applied the fins reduces the load from the fin tip, therefore reduce failure. Overall this indicates that a larger load can be applied to the humeral implant without the expectation of failure, which also will increase the displacement of the bone.

7.3.3 Scapula Model

Under the same conditions as the humerus model scapula model shows similar results. The maximum stress concentration occurs at the bottom tip and at the first thread the GBP conical shape screw. The maximum reached was 2.72MPa and 37.39MPa which is far below the yield strength of 8.4MPa and 120MPa. When the limit (i.e. to 5.6MPa) is set it can be seen the majority of the bone substitute FEA modelled part was between 0-0.1MPa and 0-2.5MPa. This is due to the implant itself absorbing some of the stresses from the load source.

The glenoid head FE model have showed a high stress value for both bones substitute types (cancellous and cortical) during the analysis; stress range between 0-597MPa and 0-557MPa indicating the glenoid head does not fail in both models. The glenoid base also showed same result as the bulk of the stress ranged between 0-480MPa and 0-484MPa for polyurethane (cancellous) and cortical bones respectively. This also shows that the GBP does not fail.

The analysis of the peripheral screws individually has shown a stress distribution across them. Therefore some force is distributed across them as well. These are due to the tangential direction of the force which slides the glenoid causing contact with the screws and the glenoid base which compresses the bone on one side. The results show that the stresses are small over most of the screw and were far below the limit.

Under compressive loads the peripheral screws do absorb stresses as well as glenoid base plate (GBP). The flat section of the GBP under compression is effective in reducing the stresses exerted onto the base thread, and in turn becomes as effective in comparison to a tensile load.

The micro-motion results were shown to be low. In any model the results showed the magnitude of displacement under a single load in a single direction whereas in reality the part will be subjected to many forces from many directions simultaneously. Therefore the magnitude of displacement can double in a single direction if considering a compressive and tensile load. Including moments and twisting in the model will also increase the overall motion. Therefore it is possible to achieve the required micro-motion or get much closer.

The experimental studies reported in this thesis have achieved the intended aims and provide information which helps to improve our current understanding of the biomechanical behaviour of the Verso Implant, Load displacement relation and stress, strain relation.

7.4 Comparison between the Mechanical tests and FEA

There are many factors that may affect the outcome of the mechanical testing such as the humidity, pressure, implant positioning on the foam block, applied force, material properties, unisotropy and other factors that were not observed or considered. On the contrary, FEA does not have any of these problems/factors listed previously; hence the results will rely totally on the number of nodes included when the load/force applied. Considering these main difference in mind, it is possible to compare the results more realistically.

The simulation results have showed similar results to the experimental results. The stress contours obtained in ABAQUS indicate the regions of failure on the bone.

From the stress distribution it is seen that as the number of screws are added to the configuration the failure load increases significantly. This occurs as the peripheral screws act as anchors for the glenoid base under a tensile load, distributing the load across a much larger surface area. The screws main purpose is to disallow the unscrewing of the glenoid base and also to absorb stresses generated from moments as the forces are never parallel to main shaft of the implants and in reality load applied on the glenoid head rather than the glenoid base.

The glenoid base showed stress distributions evenly across the screw all of which are far below the yield strength of the alloy. The highest concentration occurs at the point of contacts of the prosthesis parts. Most of which occurs across the glenoid screws and very little on the peripheral screws. The most important conclusion from loading to failure of the model is that it is clear that the bone will fail before the implant will; this is significant as a broken part lodged in the bone will most likely require removal of more bone.

Measuring micro-motion of the interaction showed interesting results. Under configuration 1 there is a maximum of 53 μ m of motion, in configuration 2 this reduces to 46 μ m and in configuration 3 this increases to 79 μ m.

The direction of force greatly determines the load dispersion therefore the implant must be uni-axially functional. Although the number of screws increases the loading capacity, the angle at which the peripheral screws are set determines the loading capacity in each direction therefore altering stress distribution.

7.5 Error analysis

Error in a scientific measurement does not usually mean a mistake or blunder. Instead, the terms “error” and “uncertainty” both refer to unavoidable imprecision in measurement. Since we will not be able to measure things with arbitrarily high precision, it is useful to know how to quantify the imprecision of the results. Even if it is assumed that we know the error associated with each individual quantity, the problem is to find the errors of the combined quantity. Sometimes one of the errors is dominant in comparison with the rest of errors; at other times, the errors compensate for each other.

There are in general two types of error, random and systematic. In this part, we first define these kinds of error in general and then bring out the source of our errors and try to categorise these on the basis of the definitions. Finally we try to calculate the errors of the present system.

7.5.1 Random errors

Random errors in experimental measurements are caused by unknown and unpredictable changes in the experiment. These changes may occur in the measuring instruments or in the environmental. The best way to tackle such errors is to repeat the test several times and take an average of the results to have more reliable findings.

7.5.2 Systematic Errors

Systematic errors are errors associated with a flaw in the equipment or in the design of the experiment. Systematic errors cannot be estimated by repeating the experiment with the same equipment. This will lead to underestimation or overestimation of all results. Systematic errors, unlike random errors, always shift the results in one direction.

Systematic errors are much harder to estimate than random errors. In order to identify systematic errors, we should understand the nature of the experiment and the instruments involved. When we encounter significant systematic errors in our experiments, we may suspect that our measurements are biased; if so, we should try to identify the possible sources of systematic error.

There are a few areas especially in pull out experiments that the error could cause problems: in Drawing Force & displacement Figure, finding micro motion, calculating the stress & strain and in definition & calculating the stiffness.

7.5.3 Manufacturing errors

As it has been discussed, the glenoid base plate (GBP) has been attached to the tensile test machine by an in-house fixture. This fixture connected the implant to the Instron (tensile test machine) in a serial way; this means that the displacement (looseness in the connection) and elongation of the fixture is included in the reading from the machine. This kind of errors is a systematic error and cannot be resolved just by repeating the tests. To compensate this error, the fixture just has been tested and the related errors have been calculated about 15% of our reading. It means the displacement which machine shows is about 15% higher than real displacement inside the composite.

7.5.4 Measurement errors

These errors are mostly related to the Instron machine, as both force and displacement are measured with this machine. According to the manufacture manual the maximum error for the load cell of the machine to measure the forces in the range 1N-3000N is 0.5%. Also the maximum error for the LVDT to measure the displacement in the range of 0-10 mm is the 0.5% of the measurement. These errors are random errors. The effects of these errors have been minimized by repeating each test (at least three times) and using the average of the results.

7.5.5 Reading errors

The results are recorded and transferred to the computers by Blue hill software.

7.5.6 Calculating and definition errors

There are some errors which are just because of the definition of the parameters. For instance, although the definition of the stress either normal or shear is clear (force over area), the area which we can use in this problem is not clear. To define the area there are different options, however for this pull out test, our suggestion is using the area of the root of the thread in the foam block part, as the failure will start from these areas. As it has been shown in the

Figure 5- and Figure 5- the failure clearly happened at the root of the thread and these parts came out thoroughly from the foam block.

The other problem is the definition of the strain and micro motion. In a simple word, strain is the elongation over original length. Then we have to discuss the displacement which the machine recorded, and how it was divided between different parts of the composite. It is possible to have three values, the first one is the elongation of the implant itself, and the second one is the elongation in the foam block and the third one can be the most important part which is the relative movement between the foam block and implant. The last value is known as micro motion.

Stiffness can be defined the stiffness of the implant, the stiffness of the foam block or the stiffness of the connection between the implant the foam block. When the relative displacement between the implant and foam block is in the range of micro motion, it is related to the stiffness of the connection of the implant and foam block.

7.6 Summary

Glenoid loosening is one of the most common and important problems that may arise post-operatively. In this research we have used experimental and analytical approach to study this problem for Verso implant. The pre cyclic test results represent the implant had successful performance in the long term situation. However, having a high strength composite is not always ideal for the implant-shoulder as it may lead to breakage in the bone side.

Chapter 8. Conclusion and Future Work

Verso reverse shoulder implant is a special bone conserving reverse total shoulder replacement. It follows the basic principles of reverse replacements. It is bone preserving and causes less bone erosion over the longer period.

The reversed geometry of total shoulder replacement is designed for use in shoulders that have a deficient rotator cuff, arthritis or complex fractures. It changes the orientation of the shoulder such that the normal socket (glenoid) is replaced with an artificial ball, and the normal ball (humeral head) is replaced with an implant that has a socket into which the ball rests. The design changes the mechanics of the shoulder allowing pain relief and an improvement in function and stability (Hatzidakis, Norris, Boileau, 2005).

This chapter will highlight the novelty of the findings of the research study. The Verso shoulder Implant was developed at the Reading Shoulder Unit, over a period of 10 years. It has been implanted in patients since 2005 with very promising early results. Consequently, FEA modes were created using ABAQUS 6.9 software to study the implant mechanical behaviour. In addition, a series of repetitive mechanical testing was carried out in Brunel University mechanical lab using a foam block of 20 pcf. This research is the first of its kind done on the Verso implant using the FEA and the mechanical testing methods together.

The next section summarises the findings of this research.

8.1 Research Findings:

The Verso (reverse) shoulder implant reverses the normal shoulder anatomy. Previous study by Kontaxis (Kontaxis et. al., 2007) has shown that there are mechanical benefits with an increased

moment arm allowing for weaker rotator cuff muscular forces along with the deltoid to act more efficiently on the joint. The main concern is that the device reverses the natural joint leading to the speculation of possible physical and mechanical anomalies which would not have previously occurred. Holcomb (Holcomb et. al., 2009) showed that the main area of failure in reverse shoulder arthroplasty was the screws and insets at the interface of the implant and scapula with the continual movement of the arm leading to an ever increasing degree of damage.

Failure in this area tends to be down to two factors. The first is that the implant parts are overloaded, either due to incorrect geometry or positioning of the sphere of the implant causing the natural muscular forces to apply forces which the implant has not been designed to take, or from experiencing a considerably high impact load through the arm. The former is down to the fitting of the implant while the latter is down to the design of the implant, which can be analysed in order to see, theoretically, how the joint will react.

The second main factor for failure is down to how the bone surrounding the implant repairs itself. Bone is a living material and needs to be put under stresses and small displacements in order to strengthen. In order for the bone to grow denser around the implant, it requires a micro-motion range of between 50 and 150 μm . Any less and the bone will not be encourage to strengthen, any more and the bone will be damaged.

This research was aiming to answer the following questions: *Is Verso Shoulder implant reliable under high impact loading? Will it break? Will it jeopardize the bone integrity with the implant?*. The Implant has been tested in various positions and under different conditions, to observe the Implant behaviour from the Glenoid side of the shoulder blade.

The failure cases reported in mechanical testing were minimal and subject to the position of the Implant on the foam block. Nonetheless, all the failure cases were reported on the foam block not on the actual implant. The Verso implant neither failed during FEA process nor in experimental process. However, it can be seen from the results obtained *the stronger the implant can get the weaker the bone can get*. The interpretation to this result is the number of screws is crucial to determine the strength of the bone; the number of screws definitely jeopardise the bone strength.

The important type of measurement that identifies how good or bad the prosthesis is the load vs. displacement. Under compressive load the micro motion is seen to be small. The magnitude of the scapula bone shows that the maximum is 33 μ m on both bones (cancellous and cortical). But most of the part remains below this limit between 0-13 μ m for polyurethane (cancellous) and 0-11 μ m for cortical.

Although increasing the number of peripheral screws increases the load capacity of the implant it also compromises the integrity of the bone due to more removal of the bone. The glenoid base alone can withstand over 1000N of load. Due to the complicated motion of the shoulder joint it is more important to provide stability and have a large safety factor, therefore two side screws is ideal for its purpose.

Under compressive loads the peripheral screws do not absorb any stresses therefore the load is entirely on the glenoid base. Given this it is still seen to withstand this load effectively. The flat section of the glenoid base under compression is very effective in reducing the stresses exerted onto the base thread, and in turn becomes as effective in comparison to a tensile load.

Nonetheless, the mechanical testing results have shown that speed, amount and position to where the loading was applied on the implant has played a crucial factor in identifying the failure. During tension testing the Implant did not fail but the foam block did. Meanwhile, applying the same amount of load in cyclic testing at different loading rate has shown more displacement that was recorded.

Similarly, the followed cyclic tests for the GBP with one and two screws have shown different results and a micro-motion was recorded. The micro-motion was observed mainly when a loading rate of 20mm/min was applied after a cyclic testing carried out for 500 cycles. The results and the micro-motion were explained in more details in the cyclic testing tables. The full results were documented in Table 5-.

Finally, although the results were merely similar in between both methods, but the FEA did not have the effects of room temperature, humidity, and the stiffness of the foam block together with the positioning of the implant as opposed to the experimental process. The FEA has relied on the number of nodes, which has shown that the force is applied on any node in the model evenly.

The research findings can be itemised in the following points:

- 1- The Verso shoulder implant did not fail in both methods (FEA and experimental process).
- 2- The failure occurs at the bone substitute side.
- 3- In case of an accident such as falling; the Verso Implant has shown its strength and ability to maintain the shoulder joint with least amount of micro-motion.
- 4- The Verso Implant peripheral screws fitted at 10° angle showed an extra stability for the implant. However, the use of the screws has to be kept at minimum to avoid any future complication or bone fractures.
- 5- The micro-motion reported in this study was considered minimum or insignificant; thus the use of this implant as a reverse total shoulder replacement is safe and can be recommended.

8.2 Future Suggestions:

There is a large scope for possible future study on the reverse shoulder implant. As it is possible to see from the results there are excessively high levels of stress found around the screws at the interface of the scapula which with more in-depth study of the current design could warrant a redesign of the method of attaching the implant to the bone. These studies could include further finite element analysis. The research has only focused on using a foam block, but further studies may look into using human bones. In addition, the experimental testing was done on the GBP part of Verso. Moreover, modifying the conical screw angle in the GBP can prolong the deflection and increase the stiffness of the interface between the implant and the bone substitute. This can be considered for future work.

Finally, moving away from the Verso would allow for comparison between different makes of implant to see which design reacts better to loading and which ingratiates itself with bone better. This could be combined with analysing the movement of the humeral cup over the head leading to kinematic studies of the centre of rotation and moment arm of various implants, leading to designing a more efficient arrangement.

References:

- ABAQUS Version 6.9 2009, “Getting Started with ABAQUS”, ABAQUS Inc., United States of America.
- Ahir SP, Walker PS, Squire-Taylor CJ, Blunn GW, Bayley JI. Analysis of glenoid fixation for a reverse anatomy fixed fulcrum shoulder replacement. *J Biomech* 2004;37:1699-708.
- Anatomic variation of the mechanical properties of the glenoid. Mansat, P., Barea, C., Hobatha, M.C., Darmana, R., Mansat, M. 2, Toulouse : *Journal of Shoulder and Elbow Surgery*, 1998, Vol. 7.
- Fixation of the reversed shoulder prosthesis. Andrew R. Hopkins, Ulrich N. Hansen, Anthony M. J. Bull, Roger Emery, Andrew A. Amis. London : *J Shoulder Elbow Surg*, 2008.
- Armodios M., Hatzidakis, Tom R. Norris, Pascal Boileau. “Reverse Shoulder Arthroplasty Indications, Techniques and Results”. *Techniques in shoulder and elbow surgery*.2005;6(3):135-149.
- Ashman RB, Rho JY. Elastic modulus of trabecular bone material. *J Biomech* 1988;21:177–81.
- Baptist Orthopaedic Surgeon Rhett Hobgood, MD, 2009. <http://www.orangeorthopaedics.com>
- Barnett CH, Davies DV, MacConnail MA. Synovial joints: their structure and mechanics. *Synovial joints*: 1961.
- Biewener A.A., *Biomechanics – Structures and Systems, a practical approach*, 1992, *Oxford University Press*, New York, USA
- Biomet Ltd, UK, “Biomet Shoulder Joint Replacement Prosthese”.2010: 01-50-0944.
- Biomet Ltd, UK, Comprehensive surgical technique. 2006: 01-50-0944.
- Biomet UK Ltd. “Verso Operation Techniques”, 2008.
- Blauth W, Donner K. Notes on the history of arthroplasty (author’s transl) [in German]. *Z Orthop Ihre Grenzgeb*. 1979;117: 997–1006.
- Bodey W, Yeoman P. Arthroplasty of the shoulder. *Acta Orthop Scand* 1983;54:900-3.
- Boileau P, Watkinson DJ, Hatzidakis AM, Balg F. Grammont reverse prosthesis: Design rationale and biomechanics. *J Shoulder Elbow Surg* 2005;14:147S-61S
- Boudreau S., Boudreau Ed, Higgins LD, Wilcox III, “Rehabilitation Following reverse total Shoulder Arthroplasty”. *Journal of Orthopaedic and sport therapy* 2007: Vol 37, 12(734-743).
- Boulahia A, Edwards TB, Walch G, Baratta RV. “Early results of a reverse design prosthesis in the treatment of arthritis of the shoulder in elderly patients with a large rotator cuff tear”. *Orthopedics*. 2002;25(2):129-133.

- Bradley Edwards T., Joanne E. Labriola, Rodney J. Stanley, Daniel P. O'Connor, PhD, Hussein A. Elkousy, Gary M. Gartsman, Radiographic comparison of pegged and keeled glenoid components using modern cementing techniques: A prospective randomized study, *Journal of Shoulder Elbow Surgery* (2010) 19, 251-257.
- Brostrom LA, Wallenstein R, Olsson E, Anderson D. The Kessel prosthesis in total shoulder arthroplasty. *Clin Orthop Relat Res* 1992;277:155-60.
- Buchler, P., Ramaniraka, N. A., Rakotomanana, L. R., Iannotti, J. P., Farron, A., 2002. A finite element model of the shoulder: application to the comparison of normal and osteoarthritic joints. *Clin Biomech (Bristol, Avon)* 17, 630-9.
- Buechel F, Pappas M, Depalma A. Floating socket total shoulder replacement, anatomical, biomechanical and surgical rationale. *J Biomed Mater Res* 1997;12:89-114.
- Burkhead W. History and development of shoulder arthroplasty. *In* : Friedman R, editor. *Arthroplasty of the shoulder*. Thieme: New York; 1994.
- Chadwick, E.K., van Noort, A., van der Helm, F.C., Biomechanical analysis of scapular neck malunion- a simulation study. *Clinical Biomechanics*, Bristol, Avon, 2004, 19(9), 906-912.
- Charnley J. *Low friction arthroplasty of the hip. Theory & practice*. London: Springer, 1979.
- Chizari M., Snow M., Wang B. Post-operative assessment of an implant fixation in anterior cruciate ligament reconstructive surgery. *J Med Syst*. March 2010. DOI 10.1007/s10916-010-9514-z.
- Cofield RH, Stauffer RN. The Bickel glenohumeral arthroplasty. *In*: Morrey BF, ed. *Conference on Joint Replacement in the Upper Limb*. London, UK: Institute of Mechanical Engineering; 1977:15-25.
- Copeland S., Levy O., Sforza G., "Physiotherapy Protocols". Reading shoulder unit 2010.
- Coughlin MJ, Morris JM, West WF. The semiconstrained total shoulder arthroplasty. *J Bone Joint Surg Am*. 1979;61:574-581
- Delloye C, Joris D, Colette A, Eudier A, Dubuc JE. Complications mechanical prosthesis reversed the shoulder. *Rev Chir Orthop Reparatrice Appar Mot* 2002;88:410-4.
- De Wilde LF, Audenaert EA, Berghs BM. Shoulder prostheses treating cuff tear arthropathy: A comparative biomechanical study. *J Orthop Res* 2004;22:1222-30.
- Evan L. Flatow MD, Alicia K. Harrison MD., A history of Reverse total Shoulder Arthroplasty, *Clin Orthop Relat Res*, 2011 469: 2432-2439
- Fagan M.J., *Finite Element Analysis, Theory and Practice, 1992, Longman Group UK Limited*
- Fenlin JM Jr. Total glenohumeral joint replacement. *Orthop Clin North Am* 1975;6:565-83
- Fenlin J. Semi-constrained prosthesis for the rotator cuff deficient patient. *Ortho Trans* 1985;9:55.

- Figgie MP, Inglis AE, Figgie HE, 3rd, Sobel M, Burstein AH, Kraay MJ. "Custom total shoulder arthroplasty in inflammatory arthritis. Preliminary results". *J Arthroplasty*. 1992;7:1-6.
- Frederick A. Matsen, III, Pascal Boileau, Gilles Walch, Christian Gerber and Ryan T. "The Reverse Total Shoulder Arthroplasty" *Bicknell J Bone Joint Surg Am*. 2007;89:660-667.
- Frankle M, Siegal S, Pupello D, Saleem A, Migheli M, Vasey M. The reverse shoulder prosthesis for glenohumeral arthritis associated with severe rotator cuff deficiency: A minimum two year follow up study of sixty patients. *J Bone Joint Surg Am* 2005;87:1697-705.
- Fu, H.F, Seel, M.J., Berger, R.A., Relevant Shoulder Biomechanics, Operative Techniques in Orthopaedics, Vol. 1, No 2 (April), 1991: PP 134-146
- Gerard Y, Leblanc J, Rousseau B. A total shoulder prosthesis. *Chirurgie* 1973;99:655-63.
- Gerard Y. A total prosthesis shoulder retentive is possible? *Acta Orthop Belg* 1985;51:616-24.
- Grammont PM, Baulot E. "Delta shoulder prosthesis for rotator cuff rupture". *Orthopedics*. 1993;16(1):65-68.
- Grammont P, Trouilloud P, Laffay J, Deries X. Concept study and realization of a new total shoulder prosthesis. *Rhumatologie*. 1987;39:407-418.
- Gristina AG, Webb LX. The Trispherical total shoulder replacement. In: Bayley I, Kessel L, eds. *Shoulder Surgery*. New York, NY: Springer-Verlag; 1982:153-57.
- Guery J, Favard L, Sirveaux F, Oudet D, Mole D, Walch G. Reverse total shoulder arthroplasty: survivorship analysis of eighty replacements followed for five to ten years. *J Bone Joint Surg Am*. 2006;88:1742-1747.
- Gupta S, van der Helm FC, van Keulen F. The possibilities of uncemented glenoid component--a finite element study. *Clin Biomech (Bristol, Avon)*. 2004 Mar;19(3):292-302. PubMed PMID: 15003345.
- Hamill, J., Knutzen, K.M., *Biomechanical Basis of Human Movement*, London, Williams and Wilkins, 1995.
- Harman M, Frankle M, Vasey M, Banks S. Initial glenoid component fixation in "Reverse" total shoulder arthroplasty: A biomechanical evaluation. *J Shoulder Elbow Surg* 2005;14:162S-7S
- Hay, J.G., Reid, J.G., *Anatomy, Mechanics, and human motion*, 3rd edition, New Jersey: Prentice-Hall, 1999
- Jason O. Holcomb, Derek Cuff, Steve A. Petersen, Derek R. Pupello, Mark A. Frankle. *Revision reverse shoulder arthroplasty for glenoid baseplate failure after primary reverse shoulder arthroplasty*. Tampa, FL : Elsevier, 2009.
- Hopkins A. R., Hansen U. N., Bull A. MJ, Emery R., Amis A.: *Fixation of the reversed shoulder prosthesis.. London : J Shoulder Elbow Surg*, 2008.

- Katz D, O'Toole G, Cogswell L, Sauzieres P, Valenti P. A history of the reverse shoulder prosthesis. *Int J Shoulder Surg* 2007;1:108-13
- Kolbel R, Friedebold G. Shoulder joint replacement. *Arch Orthop Unfallchir* 1973;76:31-9.
- Kolbel R. Stabilization of shoulders with bone and muscle defects in Shoulder replacement. *In* : Kolbel, Helbig, Blauth, editors. Springer-Verlag Berlin: Heidelberg; 1987. p. 189-95
- Kontaxis A., Banerjee S., Bull A. MJ, Johnson G. R.. Kinematics Performance on Activities of Daily Living After Reverse Shoulder Joint Replacement. Newcastle : Newcastle University, 2007.
- Labriola, J. E., Lee, T. Q., Debski, R. E., McMahon, P. J., Stability and instability of the glenohumeral, 2005.
- Lacroix D, Murphy LA, Prendergast PJ. Three-dimensional finite element analysis of glenoid replacement prostheses: a comparison of keeled and pegged anchorage systems. *J Biomech Eng.* 2000 Aug;122(4):430-6. PubMed PMID: 11036568
- Lettin AW, Scales JT. Total replacement of the shoulder joint (two cases). *Proc R Soc Med.* 1972;65:373–374.
- Lettin AW, Copeland SA, Scales JT. The Stanmore total shoulder replacement. *J Bone Joint Surg Br.* 1982;64:47–51.
- Levigne C, Boileau P, Favard L, Garaud P, Mole D, Sirveaux F, Walch G. scapular notching in reverse shoulder arthroplasty. *J Shoulder Elbow Surg.* 2008;17:925–935.
- Levy O., Narvani A., Hous N., Abraham R., Relwani J., Atoun E., Van Tongle A., Even T., Sforza G., Copeland S., “2-5 years results of stemless-metaphyseal reversed prosthesis for arthropathy with sever cuff deficiency”. 2011: 1-26. Reading shoulder unit.
- Linscheid RL, Colfield RH. Total shoulder arthroplasty: experimental but promising. *Geriatrics.* 1976;31:64–69.
- Lubliner, Jacob (2008). *Plasticity Theory (Revised Edition)*. Dover Publications. ISBN 0486462900.
- Lugli T. Artificial shoulder joint by PEAN 89: The fact of an exceptional intervention and the prosthetic method. *Clin Orthop Relat Res* 1978;133:215-8.
- Magarey ME, Jones MA. “Dynamic evaluation and early management of altered motor control around the shoulder complex”. 2003 *Man Ther* 8:195–206.
- Mansat P, Briot J, Mansat M, Swider P. Evaluation of the glenoid implant survival using a biomechanical finite element analysis: influence of the implant design, bone properties, and loading location. *J Shoulder Elbow Surg.* 2007 May-Jun;16(3 Suppl):S79-83. Epub 2006 Aug 7. PubMed PMID: 17493558.
- Marieb, E.N, *Human Anatomy and physiology*, 3rd edition, California Benjamin Cummings Publication Company, Inc 1995.
- Martini, F.H., Ober, W.C., Garrison, C.W., Welch, K, Hutchings, R.T, *Fundamentals of Anatomy and Physiology*, 5th edition, New Jersey: Prentice-Hall, Inc, 2001.

- Mase, G. Thomas; George E. Mase (1999). *Continuum Mechanics for Engineers* (Second ed.). CRC Press. pp. 47–102. ISBN 0-8493-1855-6. http://books.google.ca/books?id=uI1110A8B_UC&lpg=PP1&rview=1&pg=PA47#v=onepage&q=&f=false.
- Masten III, F.A., Chebli, C., Lippitt, S., Principles for the Evaluation and Management of shoulder Instability, *The Journal of Bone & Joint Surgery*, 2006; 88:647-659
- McFarland E.G, Sanguanjit P, Tasaki A, Keyurapan E, Fishman E.K, Fayad L.M, The reverse shoulder prosthesis: a review of imaging features and complications, *Skeletal Radiol* (2006) 35:488-496 DOI 10.1007/s00256-006-0109-1
- Mimics 13.1 reference guide manual, www.Materialise.com (MIMICS Software).
- Nazeem A. Virani MDa, Melinda Harman MScb, Ke Li PhDc, Jonathan Levy MDd, Derek R. Pupello MBAA, Mark A. Frankle MDe, In vitro and finite element analysis of glenoid bone/baseplate interaction in the reverse shoulder design, *Journal of Shoulder and Elbow Surgery*, Volume 17, Issue 3, May-June 2008, Pages 509-521
- Neer C.S.and Morrison D.S., Glenoid bone-grafting in total shoulder arthroplasty. *J. Bone Joint Surg. Am.*, 70 (1988), pp. 1154–1162.
- Neer CS 2nd, Watson KC, Stanton FJ. Recent experience in total shoulder replacement. *J Bone Joint Surg Am* 1982;64:319-37.
- Nyffeler RW, Werner CM, Simmen BR, Gerber C. Analysis of a retrieved Delta III total shoulder prosthesis. *J Bone Joint Surg Br* 2004;86:1187-91.
- Popham F, Vanat Q, Chizari M, Esat I, “Finite Element Analysis of the Scapula at the Interface of the Glenoid in a Reverse Shoulder Implant”. International Conference of Orthopaedic Surgery June 2010 Brunel University.
- Popham, F., Chizari M., Rahman M., AbulkhairN., Esat I., *FEA Assignment*. 2008.
- Post M, Jablon M, Miller H, Singh M. Constrained total shoulder joint replacement: a critical review. *Clin Orthop Relat Res*. 1979;144:135–150.
- Rees, David (2006). *Basic Engineering Plasticity - An Introduction with Engineering and Manufacturing Applications*. Butterworth-Heinemann. ISBN 0750680253.
- Reeves B, Jobbins B, Dowson D, Wright V. A total shoulder endoprosthesis. *Eng Med*. 1974;1: 64–67.
- Reeves B, Jobbins B, Flowers F, Dowson D, Wright V. Biomechanical problems in the development of a total shoulder endo-prosthesis. *Ann Rheum Dis*. 1972;31:425–426.
- Roetert, E. P., Shouldering the Load, *Strength and Conditioning Journal* 25(1):20-21, 2003.
- Sawbones Third-Generation Simulated Cancellous Bone (Solid). *MatWeb*. [Online] [Cited: 15 03 2010.] <http://www.matweb.com/search/DataSheet.aspx?MatGUID=01f9890437db401d90e120d5d97c4272>.

- Schiffern S.C., Rozencwaig R, Antoniou J, Richardson M.L., Matsen F.A., 3rd, Anteroposterior centring of the humeral head on the glenoid in vivo. *Am. J. Sports Med.* 2002; 30: 382-7.
- Seebauer L, Walter W, Keyl W. “Reverse total shoulder arthroplasty for the treatment of defect arthropathy”. *Oper Orthop Traumatol.*2005;17:1-24.
- Sirveaux F., Favard L., Oudet D., Huquet D., Walch G, Mole D., Grammont inverted total shoulder arthroplasty in the treatment of glenohumeral osteoarthritis with massive rupture of the cuff. Results of a multicentre study of 80 shoulders. *Journal of Bone Joint Surgery* 2004; 86:388-395.
- Simovitch RW, Zumstein MA, Lohri E, Helmy N, Gerber C. Predictors of scapular notching in patients managed with the Delta III reverse total shoulder replacement. *J Bone Joint Surg Am.* 2007;89:588–600.
- Sirveaux F, Favard L, Oudet D, Huquet D, Walch G, Mole D. Grammont inverted total shoulder arthroplasty in the treatment of glenohumeral osteoarthritis with massive rupture of the cuff: Results of a multi centre study of 80 shoulders. *J Bone Joint Surg Br* 2004;86:388-95.
- Sperling JW, Cofield RH, Rowland CM. Minimum fifteen-year followup of Neer hemiarthroplasty and total shoulder arthroplasty in patients aged fifty years or younger. *J Shoulder Elbow Surg* 2004;13:604-13. doi:10.1016/j.jse.2004.03.013
- Steven M. Kurtz, Dan Mazzucco, Clare M. Rimnac, Dave Schroeder. “Anisotropy and oxidative resistance of highly crosslinked UHMWPE after deformation processing by solid-state ram extrusion”. *Philadelphia, PA : Elsevier*, 2006.
- Titanium Alloy Ti 6Al-4V ELI. *Carpenter Technology*. [Online] 07 01 2000. [Cited: 15 03 2010.] <http://cartech.ides.com/datasheet.aspx?i=101&E=268>.
- Titanium Ti-6Al-4V (Grade 5), Annealed . *MatWeb*. [Online] [Cited: 24 02 2010.] <http://www.matweb.com/search/DataSheet.aspx?MatGUID=a0655d261898456b958e5f825ae85390>.
- Ungethüm M, Bl Omer W. Endoprosthetic replacement of the shoulder joint. Possibilities and their analysis. *Z Ortho Ihre Grenzgeb* 1986;124:50-6.
- Valenti P, Boutens D, Nerot C. DELTA III reversed prosthesis for osteoarthritis with massive rotator cuff tear: Long term results (>5 years). *In* : Walch G, Mole D, editors. 2000 shoulder prostheses. Two to Ten years follow. Sauramp Medical: Montpellier; 2001. p. 253-9
- Valenti P, Katz D, Sauzieres P. What is less midialiser a prosthesis reversed? Results compared radiological and clinical prosthesis Delta and the prosthesis arrow. Presented at the French Society of Orthopaedic surgeons (SOFOT) annual congress: Paris; November 2006.
- Wall B, Nove-Josserand L, O’Connor DP, Edwards TB, Walch G. Reverse total shoulder arthroplasty: a review of results according to etiology. *J Bone Joint Surg Am.* 2007;89:1476-1485.
- Wattanaprakornkul D., Halaki M., Boettcher C., Cathers I., Ginn K. “A Comprehensive Analysis of Muscle Recruitment Patterns During Shoulder Flexion: An Electromyographic Study”. *Clinical anatomy* 2011, Vol 24: 619-626.

- Werner CM, Steinmann PA, Gilbert M, Gerber C. Treatment of painful pseudoparesis due to irreparable rotator cuff dysfunction with the Delta III reverse-ball-and-socket total shoulder prosthesis. *J Bone Joint Surg Am.* 2005;87:1476–1486.
- Wierks C, Skolasky RL, Ji JH, McFarland EG. Reverse total shoulder replacement: intraoperative and early postoperative complications. *Clin Orthop Relat Res.* 2009;467:225–234.
- Wirth M, Rockwood CA Jr. Current concept review: Complications of total shoulder replacement arthroplasty. *J Bone Joint Surg Am* 1996;78:603-16.
- Wretenberg MD, Wallensten R. The Kessel total shoulder arthroplasty: A 13 to 16 year retrospective follow-up. *Clin Orthop Relat Res* 1999;365:100-3
- Wu Sh., Qiu We. Nonlinear transient dynamic analysis by explicit finite element with iterative consistent mass matrix. *Commun. Numer. Meth. Engng* (2008), Published online in Wiley Interscience (www.interscience.wiley.com). DOI: 10.1002/cnm.1110
- Yokochi, C., Rohen, J.W., Weinreb, E.L., *Photographic Anatomy of the Human Body*, 3rd edition, Tokyo: Igaku-Shoin.
- Sites:
 - <http://www.thesouldercentre.com/Reverse-Total-Shoulder-Replacement.htm>
 - http://www.readingshoulderunit.com/education_arthropathy.php
 - <http://www1.apsu.edu/thompsonj/Anatomy%20&%20Physiology/2010/2010%20Exam%20Reviews/Exam%201%20Review/Ch01%20Gen%20Terms%20and%20Gen%20Anat%20Terms.htm> “Body Planes”.
 - <http://en.wikipedia.org/wiki/Stiffness>
 - http://www.instron.us/wa/applications/test_types/tension/default.aspx
 - http://www.kneesource.com/shldr_dislocation.aspx
 - <http://en.wikipedia.org/wiki/Kinematics>
 - http://www.listen-up.org/med/ct_mri.htm

Appendix A:

Nomenclature:

Abduction: A movement away from the midline of the body.

Absolute Reference Frame: A reference frame in which the origin is at the joint center.

Adduction: A movement toward the midline of the body.

Anatomical Position: The standardized reference position used in the medical profession.

Anatomy: The science of the structure of the body.

Angular Motion: Motion around an axis of rotation in which different regions of the same object do not move through the same distance.

Anterior: A position in front of a designated reference point.

Anteroposterior Axis: The axis through the center of mass of the body running from posterior to anterior.

Appendicular Skeleton: The bones of the extremities.

Axis: The imaginary line of a reference system along which position is measured.

Axial Skeleton: The bones of the head, neck, and trunk.

Axis of Rotation: The imaginary line about which an object rotates.

Biomechanics: The study of motion and the effect of forces on biological systems.

Cardinal Planes: The planes of the body that intersect at the total body center of mass.

Circumduction: A movement that is a combination of flexion, adduction, extension, and abduction.

Contralateral: On the opposite side.

Degree of Freedom: The movement of a joint in a plane.

Depression: The lowering movement of a body part such as the scapula.

Distal: A position relatively far from a designated reference point.

Dorsal: See Posterior.

Dorsiflexion: The motion in which the relative angle between the foot and the leg decreases.

Downward Rotation: The action whereby the scapula swings toward the midline of the body.

Dynamics: The branch of mechanics in which the system being studied undergoes acceleration.

Eversion: The movement in which the lateral border of the foot lifts so that the sole of the foot faces away from the midline of the body.

Extension: The action in which the relative angle between two adjacent segments gets larger.

Frontal (Coronal) Plane: The plane that bisects the body into front and back halves.

Fundamental Position: A standardized reference position similar to the anatomical position.

Functional Anatomy: The study of the body components needed to achieve a human movement or function.

Horizontal Abduction: A combination of extension and abduction of the arm or thigh.

Horizontal Adduction: A combination of flexion and adduction of the arm or thigh.

Hyperabduction: Abduction movement beyond the normal range of abduction.

Hyperadduction: Adduction movement beyond the normal range of adduction.

Hyperextension: Extension movement beyond the normal range of extension.

Hyperflexion: Flexion movement goes beyond the normal range of flexion.

Inferior: A position below a designated reference point.

Inversion: The movement in which the medial border of the foot lifts so that the sole of the foot faces away from the midline of the body.

Ipsilateral: On the same side.

Kinematics: Area of study that examines the spatial and temporal components of motion (position, velocity, acceleration).

Kinesiology: Study of human movement.

Kinetics: Study of the forces that act on a system.

Lateral: A position relatively far from the midline of the body.

Lateral Flexion: A flexion movement of the head or trunk.

Linear Motion: Motion in a straight or curved line in which different regions of the same object move the same distance.

Longitudinal Axis: The axis through the center of mass of the body running from top to bottom.

Medial: A position relatively closer to the midline of the body.

Mediolateral Axis: The axis through the center of mass of the body running from right to left.

Movement or Motion: A change in place, position, or posture occurring over time and relative to some point in the environment.

Origin: The intersection of the axes of a reference system and the reference point from which measures are taken.

Plane of Motion: A two-dimensional surface running through an object. Motion occurs in the plane or parallel to the plane.

Plantarflexion: The motion in which the relative angle between the foot and the leg increases.

Posterior: A position behind a designated reference point.

Pronation: Movement in which the front or ventral surface rotates to face downward, as seen in the forearm and foot.

Protraction: The motion describing the separating action of the scapula.

Proximal: A position relatively closer to a designated reference point.

Qualitative Analysis: A nonnumeric description or evaluation of movement based on direct observation.

Quantitative Analysis: A numeric description or evaluation of movement based on data collected during the performance of the movement.

Radial Flexion: The flexion movement of the hand toward the forearm on the thumb side of the hand.

Reference System: A system to locate a point in space.

Relative Angle (Joint Angle): The included angle between two adjacent segments.

Relative Reference Frame: A reference frame in which the origin is at the joint center and one of the axes is placed along one of the segments.

Retraction: The motion describing the coming together action of the scapula.

Rotation: A movement about an axis of rotation in which not every point of the segment or body covers the same distance in the same time.

Sagittal Plane: The plane that bisects the body into right and left sides.

Statics: A branch of mechanics in which the system being studied undergoes no acceleration.

Transverse (Horizontal) Plane: The plane that bisects the body into top and bottom halves.

Superior: A position above a designated reference point.

Supination: Movement in which the back or dorsal surface rotates upward, as seen in the forearm and foot.

Ulnar Flexion: The flexion movement of the hand toward the forearm on the little finger side of the hand.

Upward Rotation: The action whereby the scapula swings out from the midline of the body.

Upper limb (also upper extremity): in human anatomy, refers to the region distal to the deltoid. In formal usage, the term "arm" only refers to the structures from the shoulder to the elbow, explicitly excluding the forearm, and thus "upper limb" and "arm" are not synonymous. The upper limb includes the following structures: Shoulder Arm - in anatomy, the region between the shoulder and the elbow - Elbow, Forearm, Wrist, Hand

Ventral: See Anterior.

Appendix B

The Surgery:

Traditional Reverse Shoulder Implant using [Delta]:

Understanding the precise problem the patient is suffering from, explore the patients' options and then make the right advice is the first step the surgeons do. Determining the right type of Shoulder Implant is the second step. Finally, the surgeon performs the operation depending on the patient condition severity.

This procedure is not recommended for people who have infections, deficiencies in the scapula, or for patients without functioning deltoid muscles. It is also not recommended for younger patients. On the contrary, this procedure can be used in revision surgery, for failed shoulder replacement and shoulder fractures. It's also commonly used for patients who don't have a rotator cuff (pseudo-paralytic shoulder) (Grammont, Baulot, 1993).

The Reverse Shoulder System consists of five basic parts, or components as shown in Figure 3.2. The upper portion of the humeral stem is called the epiphysis and it lies even with the top of the humerus. It is made of metal (titanium, cobalt chrome, stainless steel). The bottom portion of the humeral stem is called the diaphysis and it is inserted down into the centre of the humerus. The epiphysis holds the third component, a polyethylene cup that forms the socket part of the new joint (Grammont, Baulot, 1993).

On the scapular side, the fourth component, the metaglène, is a specially coated metal plate that is firmly attached to the scapula with screws.

The fifth component is the ball portion of the joint called the glenosphere. It is a half-globe shaped metal piece that fits onto the metaglène. The glenosphere fits inside the polyethylene cup on the humeral side to form a new shoulder joint. Both the glenosphere and the polyethylene cup come in different sizes so the implant may be tailored to different body sizes.

A reverse shoulder replacement is an inpatient procedure (patient need to be admitted and stay in the hospital). To begin, surgeon will make an incision on the front of the patient's shoulder. Surgeon will remove the damaged head of the humerus. The bone socket is exposed, and the damaged cartilage is removed. A base plate is secured to the glenoid with surgical screws. The artificial socket is inserted and secured on the humerus. The ball is inserted and

secured on the glenoid. The wound is closed, and a soft dressing is applied (Biomet Ltd. UK, 2006).

Shoulder replacement surgery usually lasts about two hours. The incision for the surgery is usually about four to six inches long and the incision is made along the front of the shoulder joint. The surgery is most commonly done under general anesthetic.

The surgery starts by placing the patient under general anaesthetic. Elevate the patient body on the operative chair from 45°-60° as shown in Figure Appendix B-1. Some cautions must be taken such as to avoid placing the patient's neck in hyperextension or hyperflexion, and to avoid creating pressure points (Biomet Ltd. UK, 2006).



Appendix B-1: Patients Positioning

The reverse prosthesis was approved by FDA in USA in 2004. It is relatively new prosthesis. The following lists of figures were taken from Baptist orthopaedic surgeons (USA). This operation has been done for a female patient 75 years old who had large rotator cuff tear and subsequently had large degeneration ball and socket joint. This condition can only be treated with using a reverse prosthesis post removing the patient's degenerated humeral head (Baptist Orthopaedic Surgeon Rhett Hobgood, MD, 2009)⁷.

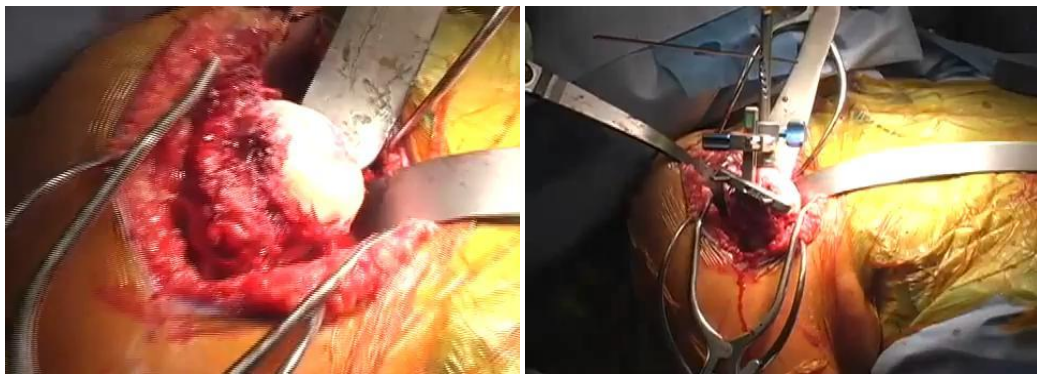
⁷ <http://www.youtube.com/watch?v=0TBO6sP4zvQ>



Appendix B-2: Patient preparation after been put under general anaesthetic, Surgeon chooses the proper size according to the patient shoulder size



Appendix B-3: Surgeon starts operating and exposing the arthritic shoulder



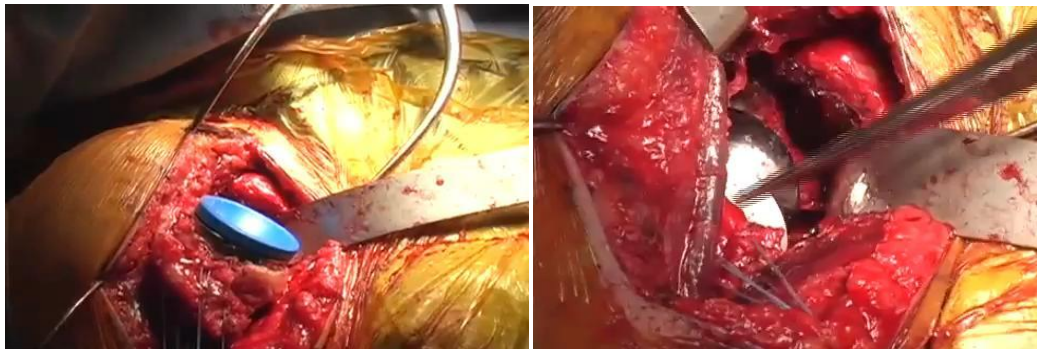
Appendix B-4: arthritic and degenerative humeral head exposed then removed. Fixing the rod to choose a cutting angle for the humeral head



Appendix B-5: screwing into the humeral head and preparing the canal for the implant



Appendix B-6: cementing the humeral canal, fitting the implant through the humerus



Appendix B-7: choosing the proper type and fit it, screwing the base plate into the glenoid with the required number of screws making sure that the ball is centred in the right place



Appendix B-8: Checking the implant angles and position, pushing back the joint into place and close and clean up the wound

In this operation: The surgeon starts with incision of 11cm across the shoulder, making an opening whole into the shoulder exposing the humerus head. Then make a whole into the humerus head to reach the canal then the surgeon will ream the canal. After that, the surgeon cut the degenerated humeral head. The alignment rod is 20° retroversion of the humeral head along with the forearm. Then the surgeon prepares the humerus by cementing the canal of the humerus to enable him to fit the stem the diaphysis. Then fit the upper portion of the humeral stem which is called the epiphysis transforming the humerus into the socket. The glenoid of the scapula then will prepared by screwing into the base plate with the required number of screws to fit the ball

side of the implant. Finally, surgeon pushes back the joint into place and sew the wound (Baptist Orthopaedic Surgeon Rhett Hobgood, MD, 2009).

Verso Implant by Biomet (the Surgery):

The operation lasts approximately up to 90 minutes. The patient usually will be in hospital for about 2 – 3 days after the surgery. This surgery was last reported to be done in Reading Shoulder Unit at Royal Berkshire Hospital, England. Because it was not possible to get the actual surgery images for replacing the arthritic shoulder joint with Verso Implant in this research. Therefore, the previous reverse shoulder surgery images stated to give the reader the basic knowledge of how the reverse shoulder replacement surgery is done.

Verso Shoulder surgery can be summarised in the following steps:

- 1- The surgeon starts by positioning the patient as in Appendix B-9.

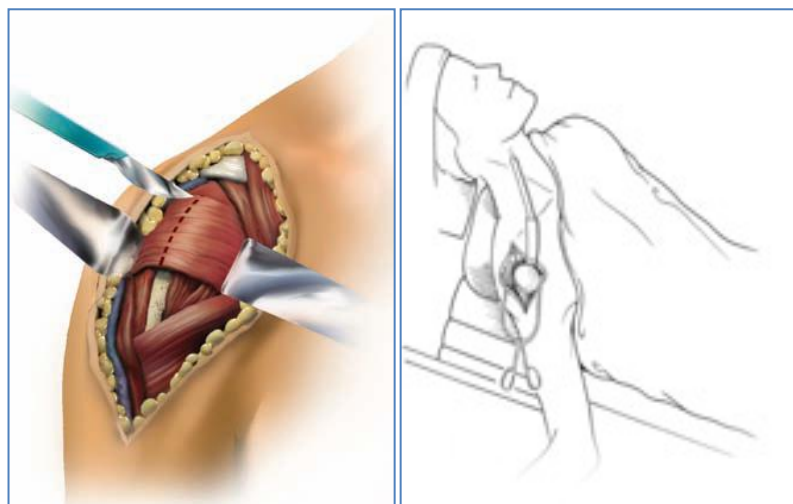
The patient should be placed in a semi sitting or beach chair position at about 45 degrees of head-up tilt with the head on a neurosurgical headpiece and the arm on a short arm board attached to the side of the operating table.

- 2- An incision of approximately 6 to 9 inches will be done as in Appendix B-9.



Appendix B-9: Surgical Incision

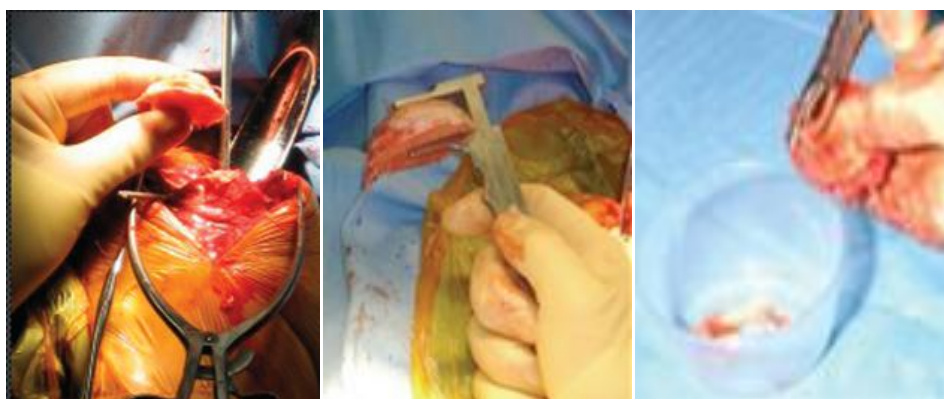
“Utilize an extended deltopectoral anterior incision with an optional biceps tenodesis beginning immediately above the coracoid process and extending distally and laterally, following the deltopectoral groove along the anterior border of the deltoid laterally retracts the deltoid muscle, avoiding release of the deltoid from the clavicle. The deltoid may be partially released from its distal insertion by subperiosteal dissection. Make a partial relaxing incision through the proximal coracoid tendon and medially retract the conjoined tendon.” (Biomet Ltd, UK, 2008), (Levy, Hous, Copeland, others, 2011).



Appendix B-10: Location of the cut in the operated shoulder

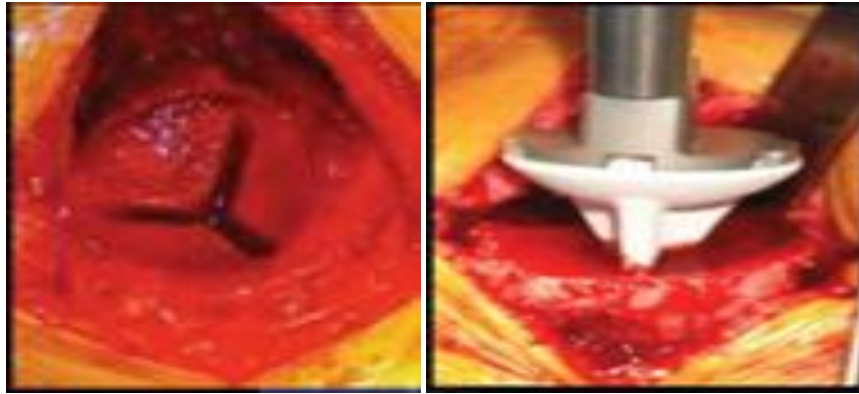
“Identify anterior structures and externally rotate the humerus. Make a longitudinal incision through the tendinous portion of the subscapularis muscle and capsule, just medial to the lesser tuberosity (). In cases of severe contracture, subscapularis lengthening may be required. Tag the subscapularis tendon with non-absorbent sutures. Externally rotate and extend the humerus to expose the humeral head, while protecting the axillary nerve.”

- 3- Starting with the affected humeral head by removing the humeral shell with 20mm slice thickness (the removed part will then be used for bone grafting).



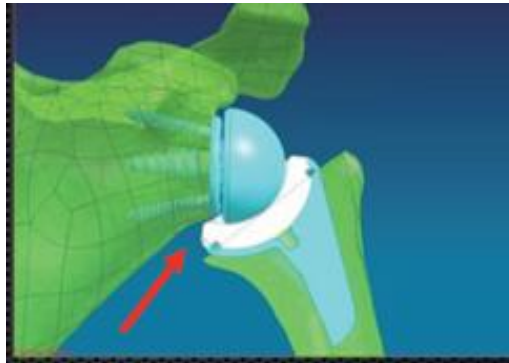
Appendix B-11: Removing the arthritic humeral head and do a bone grafting for later use in the patient shoulder

- 4- A cut will then be made according to the required size to fit the Stemless Humeral part which has three thin fins as shown in .



Appendix B-12: Inserting stemless cementless metaphyseal fixation for the humeral part

- 5- Insertion of humeral shell in 30° retroversion.
- 6- Placing the Dial-able Arcom which is 10° angled to avoid future glenoid notching as shown in Appendix B-13 (Levy, Hous, Copeland, others, 2011).



Appendix B-13: The Dial-able' Arcom Poly liners, Provide Low Medial Edge, Reducing Likelihood of Notching

- 7- Moving to the glenoid part the surgeon starts with screwing into the base plate into the glenoid part as shown in Appendix B-14 below.

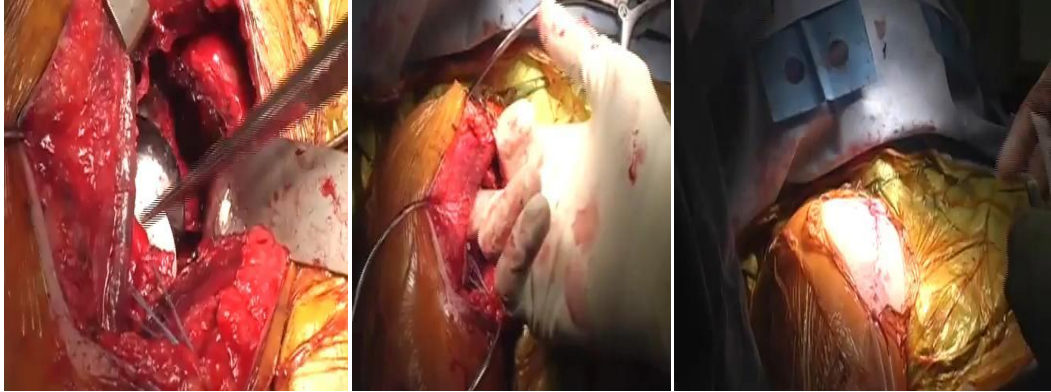


Appendix B-14: The Glenoid Base Plate fitted in the glenoid part

- 8- Screw in the number of screws needed to keep the implant in place.

9- Press and fit the glenoid head into the glenoid base plate.

10- Make sure the implant angles are aligned and then push back the operated into place and close up the lesion as shown in Appendix B-15 (Levy, Hous, Copeland, others, 2011).

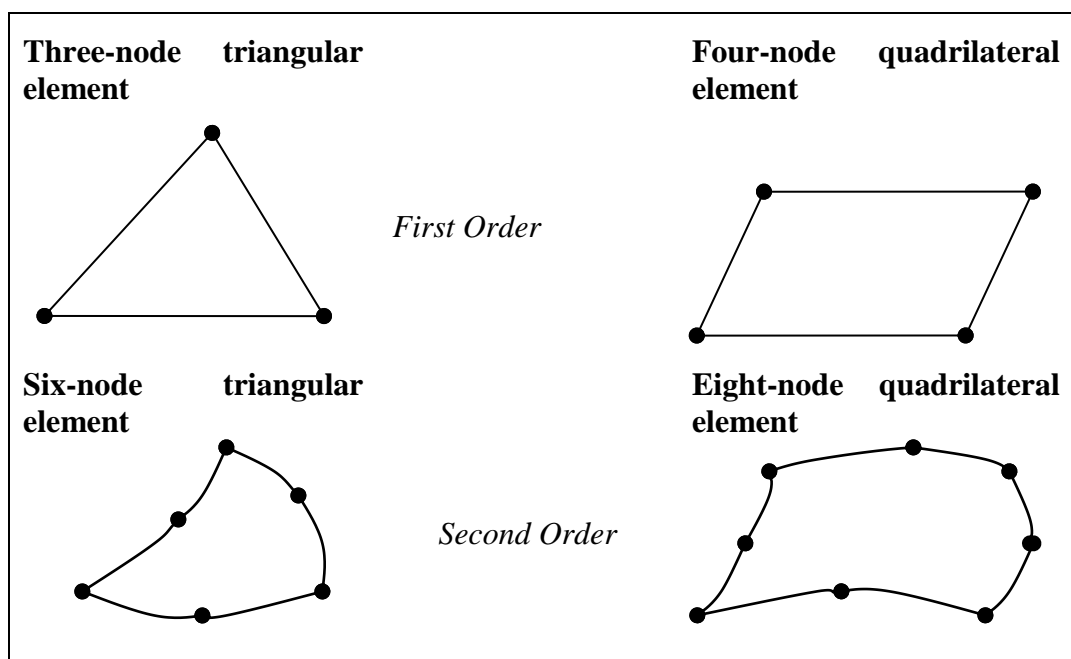


Appendix B-15: Close the Surgery Cut and clean up

Appendix C

ABAQUS Manual:

Second order elements contain twice the nodes as first order elements, and therefore have twice as many degrees of freedom per element. They are often used for more complex geometry than first order elements as their links are allowed to bend around the shapes, however it does mean that computational time is increased as the program will need to solve the properties at each node and their quadratic relationships.



Appendix C-1: Element Types

The relationships between the nodes are found by deriving a stiffness matrix for each element. The information for each element is then substituted into a global stiffness matrix, which when computed will show the stresses and displacements across the entire body. The matrices of each element are then added together to form the global matrix known as the stiffness matrix. As each node contains two degrees of freedom the final matrix will have twice the number of rows and columns as there are nodes. The stiffness matrix can then be rearranged and solved in order to find the unknown stresses and displacements (ABAQUS 6.9 user manual, 2009).

Appendix D

Published papers by the author:

1. *A Investigation Into Inverse Dynamics in Cycling Motion* by I. Esat, N. Abualkhair, Department of Mechanical Engineering, Brunel University West London, Uxbridge, London, UK. *Society for Design and Process Science, San Diego, USA, 2006.*
2. *Advances and Problems in Shoulder Implants.* Ofer Levy, Stephen Copeland, Ibrahim Esat, Nesreen Abualkhair Department of Mechanical Engineering Brunel University West London Uxbridge, London, UK, *Society for Design and Process Science, San Diego, Turkey, 2007.*
3. *Stress Analysis of a Reverse Shoulder Implant at the Interface between the Implant and Bones.* N. Abulkhair¹, Y. Shah, I.I. Esat, M. Chizari. Brunel University West London, UK; ²Royal Berkshire Hospital, UK. *Oral and Poster Presentations / Journal of Biomechanics 43S1 (2010) S23–S74.*
4. *A Review of Metaphyseal Fixing Reversed Shoulder Replacement Implant.* N.Abulkhair¹, Y. Shah, I. Esat¹, M. Chizari. Department Of Mechanical Engineering, Brunel University West London, UK. Royal Berkshire Hospital, UK. *The ATLAS T3 Bi-Annual Meeting Proceedings Printed in the United States of America, Texas, May, 2010.*